THEORY AND APPLICATION OF EXPERIMENTAL MODEL ANALYSIS IN EARTHQUAKE ENGINEERING

by

Piotr D. Moncarz

and

Helmut Krawinkler

The John A. Blume Earthquake Engineering Center

Department of Civil Engineering

Stanford University

Stanford, California 94305

A Report on a Research Project Sponsored by the

NATIONAL SCIENCE FOUNDATION

Grants ENV75-20036 and ENV77-14444

June 1981

ABSTRACT

This report summarizes part of a four year study on the feasibility and limitations of small-scale model studies in earthquake engineering research and practice. The emphasis is placed on dynamic modeling theory, a study of the mechanical properties of model materials, the development of suitable model construction techniques and an evaluation of the accuracy of prototype response prediction through model case studies on components and simple structures. Steel and reinforced concrete structures are considered in this study.

The basics of similitude theory and its application to the modeling of dynamically excited structures are reviewed and similitude laws for various types of models are developed. These models include true replica models in which all physical quantities are properly simulated, and various kinds of adequate models in which the violation of specific similitude laws does not affect appreciably the response prediction.

Adequate simulation of material properties was found to be the most important aspect of model research, particularly under dynamic excitations. Materials for modeling of steel structures (structural steel and copper alloy 510) and reinforced concrete structures (wire-reinforced microconcrete) are investigated under low and high strain rates and with due regard to cyclic load effects. A comprehensive set of material data is assembled for direct use in model studies, and systematic material testing procedures are developed for the investigation of alternative model materials.

Problems encountered in the construction of models are identified and recommendations are made for the fabrication and joining of model

elements for steel structures as well as for microconcrete mix design practices, fabrication of model reinforcement and fabrication and curing of reinforced microconcrete elements.

The adequacy of the simulation of prototype response is evaluated on hand of a series of tests on models for which prototype test data are available. The correlation between model and prototype response is judged as good to excellent, depending on the type of structure. Whenever discrepancies in the response are observed, the causes are identified and evaluated to assess the limitations of model research in earthquake engineering. The test specimens used for this purpose are cantilever beams made of steel, phosphor bronze and microconcrete, and simple single degree of freedom structures made of steel and phosphor bronze which are tested on a shake table.

The research has demonstrated that model analysis can be used in many cases to obtain quantitiative information on the seismic behavior of complex structures which cannot be analyzed confidently by conventional techniques. Methodologies for model testing and response evaluation are developed in the project and applications of model analysis in seismic response studies on various types of civil engineering structures (buildings, bridges, dams, etc.) are evaluated.

ACKNOWLEDGEMENTS

The research reported herein is part of the project "Scale Modeling and Testing of Structures for Reproducing Response to Earthquake Excitation" conducted under the sponsorship of the National Science Foundation. The authors are grateful for the financial support of NSF which made this project possible. The continued encouragement of Dr. S. C. Liu of NSF is especially acknowledged.

The authors gratefully acknowledge the continuous participation of the principal investigator of this project, Professor James M. Gere, as well as the advice provided by Professor Holt Ashley on modeling theory and by Professor Cedric W. Richards on materials research. The skillful help of the graduate students Maher A. Bader, Nathaniel G. Cofie, Bahman Lashkari-Irvani, Russell S. Mills and Mahmud Zohrei in various phases of the experimental research is much appreciated.

The use of experimental and computer facilities was provided by the John A. Blume Earthquake Engineering Center, Professors James M. Gere and Haresh C. Shah, Directors. The technical staff of the Center is acknowledged for an excellent job done in the fabrication of test specimens and instrumentation.

TABLE OF CONTENTS

CHAPTER

CHAPTER

CHAPTER 1

INTRODUCTION

Experimental techniques have always been a vital part of advanced engineering design. Whenever the current theoretical knowledge reaches its limit, an experiment provides an alternative in the evaluation of the adequacy of the proposed design. The final design of innumerable advanced structures is based on the results of experimental analysis. At present, mathematical methods are capable of predicting the response of a structure to environmental effect, providing the complete functions of material characteristics, geometric delineation and boundary conditions are available. The time and temperature dependance of such functions often results in a complexity surpassing the feasibilities of mathematical approach. Consequently, the experiment remains the only alternative. The interrelation between the complexity of the analyzed structure, the ratio of the cost of design to the value of the structure (relative cost) and the applicable analysis techniques is presented schematically in Fig. 1.1 (after Hossdorf, Ref. 1). With the improvements in numerical techniques and theoretical knowledge, the line of analytical capability moves to the right, thus including a larger number of structures in the left portion of the figure. This progress does not indicate a decrease in the number of structures located to the right of that line, as the demands posed on the design are increasing with the technological progress.

Considering the high cost of experimentation as compared to conventional or computer analysis, the scope of experimental work is usually limited to fundamental research and the study of complex input and response phenomena which cannot be modeled mathematically with confidence.

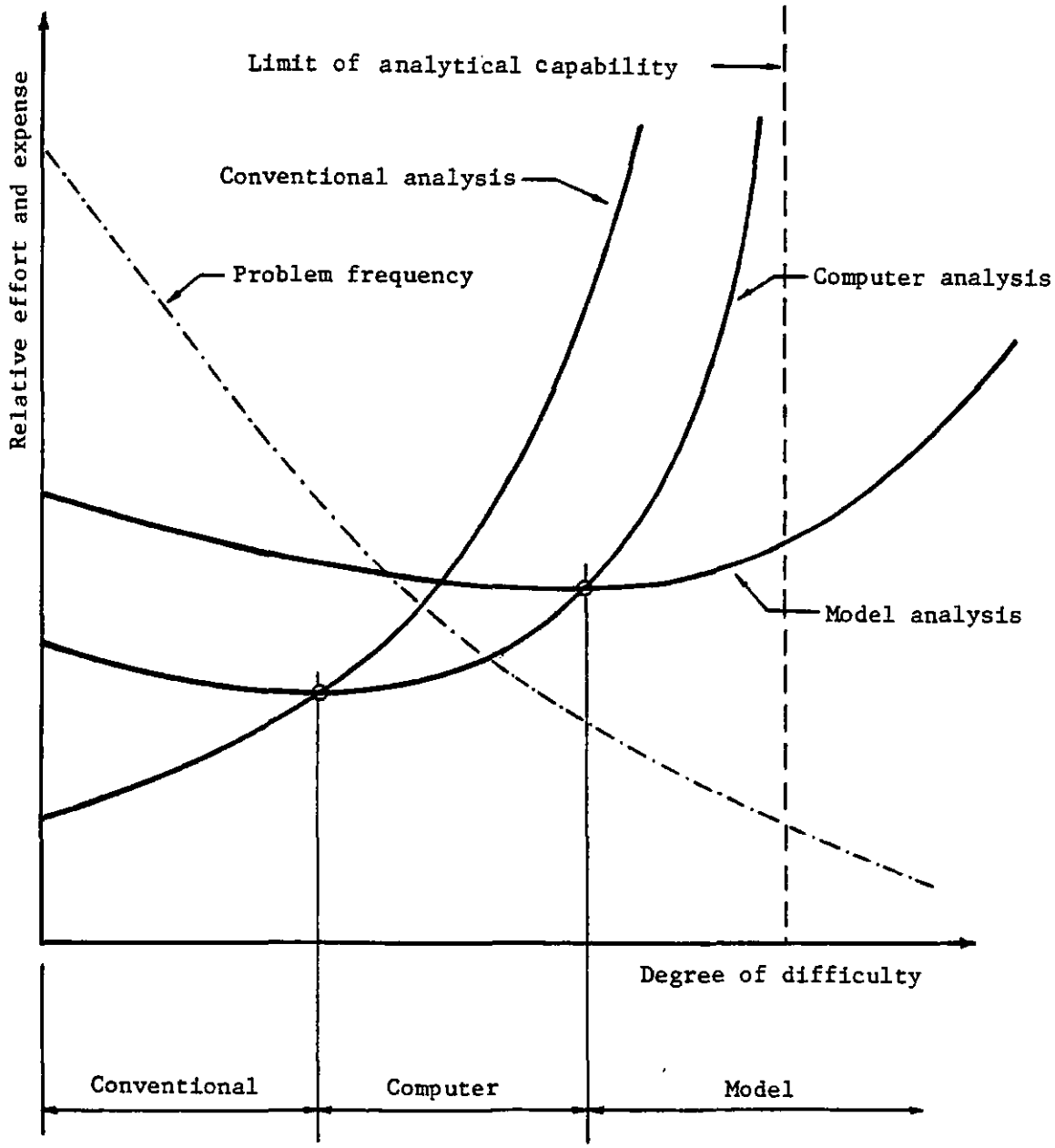

Figure 1.1 Application of Various Methods of Structural Analysis (Ref. 1)

In most cases, experimentation is carried out to fulfill one of the following three basic objectives:

(1) Develop or verify analytical models of force-deformation characteristics of materials, individual elements and structural subassemblies.

(2) Establish realistic loading criteria for complex environmental effects such as wind or earthquakes.

(3) Study the behavior of structural systems or specific structures under simulated loading conditions. The purpose of such experimentation may be the verification of analytical studies, the demonstration of the integrity and safety of structural systems under various levels of environmental disturbances, or a general study of the response characteristics of structural systems with controlled variation of input and response parameters.

Experimental work can be carried out on either unscaled prototypes or scale models of elements, subassemblies and complete structures. The confidence the profession places in the results of experimental studies appears to be proportional to the selected scale factor. Very few doubts are raised regarding the reliability of experimental results of prototype tests or one-half to one-third scale model tests. On the other hand, small scale model tests (in the order of 1:5 and smaller) are often viewed with considerable skepticism. This skepticism is often unwarranted when scale effects in the materials and the load application are properly accounted for and the instrumentation system is adapted to the size of the test specimen. Nevertheless, it is desirable to keep the scale factor close to one whenever feasible.

In earthquake engineering, where post-elastic response characte-

ristics and safety against failure are of primary interest, the analysis of many structures requires the application of experimental methods. Experimentation may be performed in the field or in a controlled laboratory environment. Cost limitations, test versatility and control precision make laboratory testing most applicable to experimental analysis. In earthquake engineering, laboratory experimentation on complete structures is, in most cases, limited to testing of scale models, often at rather small scales.

A powerful tool was provided to experimental analysis in earthquake engineering through the development of closed-loop shake tables and high speed data acquisition systems. In the U.S. there are available a small number of medium size tables (larger than 10 ft. x 10 ft.). With few exceptions, such as component and equipment testing and testing of very small prototype structures, experimentation on such tables is limited to one-half or smaller scale models. There are obvious advantages to the use of large scale models (one-half to one-third scale). For instance, small rolled sections can be used for models of steel structures, and prototype material (reinforcing bars and concrete) can be used for reinforced concrete models. Nevertheless, such structures are models and do not fully simulate the behavior of an actual structure unless model similitude laws for ground motion, material, and force simulation are taken into consideration.

The majority of shake tables available in the U.S. have to be classified as small tables (10 ft. x 10 ft. and smaller). Most of these tables are used primarily for demonstration pruposes, qualitative studies, or component testing. It appears that they are not fully utilized for replica modeling of actual structures at small scales. The reason for

this limited utilization is that modeling problems increase with a decrease in scale and that insufficient information is available in the literature on the possibilities and limitations of small scale replica modeling.

To fully utilize available laboratory facilities for mitigation of hazards of eqrthquakes, it is necessary to develop a general capability for constructing, at different scales, replicas of actual buildings, bridges, dams, etc., and for reproducing adequately the manner in which they respond, absorb and dissipate energy, and ultimately fail under prescribed earthquake excitation. If such a capability can be developed it should be possible to use small shake tables in a cost efficient manner as a viable and reliable research tool in the field of earthquake engineering. Among the many topics on which model tests on shake tables should provide useful information are the following:

1. High-quality, small-scale models can be used as complement for and/or an alternative to analytical investigations. This need is especially urgent in connection with complex structures, where mathematical models are difficult to construct and to verify.
2. Models are especially useful for comparative studies or controlled parameter variations, since it is relatively easy to alter their configurations systematically.
3. Replica models enable the investigation of earthquake-related phenomena which cannot be studied on actual prototype structures. Such phenomena include rate of loading effects, dynamic response characteristics under realistic seismic excitation ranging from low amplitude vibrations to excitations producing inelastic response and failure, failure mechanisms, effects of mass and

stiffness irregularities, torsional effects, overturning effects, dynamic instability and idealized soil-structure interaction effects.

4. The demonstration of integrity and safety under various levels of earthquake inputs--if it is ever to be accomplished prior to the erection of an actual structure--could be achieved with a fine replica model.

At this time of rapid advancement in knowledge of all aspects of earthquake engineering it is necessary to examine carefully the place dynamic model testing could occupy in the field of earthquake engineering research. It can be said that experimental research with dynamic load application is in its infancy compared to quasi-static experimentation and analytical studies, and there is little doubt that it will play a more significant role in the years to come.

A study of the feasibility and limitations of small-scale model testing in earhtquake engineering was the subject of a four-year NSF sponsored study which in part is summarized in this report. In the first report on this study, Mills et. al. (Ref. 58) present a comprehensive discussion of shake table performances and of modern data acquisition system. A model study of a three-story steel frame structures is also described in Ref. 58.

This report emphasizes general aspects of dynamic modeling theory, model material behavior and the accuracy of prototype response prediction through small-scale model tests. In conjunction with Ref. 58 this report is intended to provide a state-of-the-art assessment to researchers and practicing engineers who want to utilize small-scale model tests in earthquake engineering research and practice.

CHAPTER 2

OBJECTIVES AND SCOPE

The main objective of this work is to asses the feasibility of model testing in earthquake engineering and to provide systematic and detailed information on procedures involved in the design, execution, and modus operandi of dynamic model experiments. This goal is approached by placing the emphasis on dynamic modeling theory, model material studies, model fabrication techniques, and case studies performed on components and simple structures. The research concentrates on models of steel and reinforced concrete structures.

The scope of the work presented in this report is summarized in the following paragraphs.

1. Dynamic Modeling Theory. The emphasis is placed on the synthesis and extension of modeling theory into the domain of time-dependent, nonlinear response of structures and materials. Various types of models are explored which can be constructed within the constraints of material, mass, and earthquake simulation but still permit an adequate prediction of prototype behavior.

2. Model Material Studies. The emphasis is placed on the identification of material properties affecting the reliability of prototype response prediction based on small scale model tests. A systematic approach to material studies is developed. Various types of material tests and of necessary testing equipment are explored. Material studies on steel, phosphor bronze, microconcrete and model reinforcement are carried out including studies of the uniaxial stress-strain behavior of the materials under various strain rates and of the cyclic behavior of steel and phosphor bronze.

3. Model Tests of Components and Simple Structures. Small-scale models of structural elements and simple structures are fabricated and tested to develop suitable model construction techniques and to study the accuracy of prototype response prediction. Cyclic loading tests are carried out on cantilever specimens made of steel, phosphor bronze and microconcrete. The simulation of prototype response is evaluated with due regard to the effect of the speed of loading (cycling frequency). For the microconcrete specimens, tests are performed with cycling frequencies from 0.0025 Hz to 10 Hz and, with beams of different span-to-depth ratios to investigate the simualtion of different failure modes from flexure to pure shear. The results of a shake table study on a simple steel structure and its phosphor bronze model are evaluated by comparing displacements, accelerations and story shears in the prototype domain.

One of the major concerns of this work is to present the information in as complete a form as possible, incorporating throughout the text results of studies reported by other researchers. In addition, an extensive list of U.S. and foreigh literature is compiled.

CHAPTER 3

LITERATURE REVIEW

The purpose of this chapter is to acquaint the reader and prospective model builder with the state of the art in model analysis and with relevant reference material that contains the background information necessary for successful modeling of structures in seismic environments. Since for many years replica models have been used in civil engineering as a complement and alternative to design and analysis, it is recognized that this literature review is incomplete and limited to those publications which were found particularly helpful in the development of this research project. Emphasis is placed on identifying past studies on building structures and materials, especially those which either are concerned with dynamic modeling or contain information which can be utilized for dynamic model studies.

General Information: From the many books written on the subject of model analysis, that by Hossdorf (Ref. 1) provides an excellent introduction to the subject. It does not go deeply into any one aspect of model analysis but touches many aspects and gives a healthy perspective of the place of model analysis in structural engineering. The book by Muller (Ref. 2) treats the topics of model materials and instrumentation in a thorough manner, and that by Fumagalli (Ref. 3) contains a large number of interesting model case studies, particularly those concerning buildings and dams.

One of the first comprehensive series of papers on structural models was presented at a RILEM symposium in 1959 in Madrid, Spain. References 4 and 5 contain some of the papers of this symposium relevant to this

research project. References 6 to 11 are summary papers on general problems of modeling of structures in the elastic and inelastic range.

Many studies are reported in the literature on modeling of reinforced concrete structures. Much of the progress on this subject is presented in papers compiled in Refs. 12 to 14 and is summarized in Ref. 15. Specific topics in static modeling of reinforced concrete structures and structural elements are discussed in Refs. 16 to 29.

Scale modeling of structures made of materials other than reinforced or plain concrete has received surprisingly little attention in the past. Reference 30 presents the results of a research project on modeling of concrete masonry blocks and structural elements. Detailed information on fabrication and testing (under static loading conditions) of small scale models of steel structures and their components, using steel as a model material, is presented in Ref. 31.

Dynamic Model Studies: The references mentioned so far are not specifically concerned with dynamic modeling problems but contain comprehensive background information on the subject of model analysis in structural engineering. The literature search disclosed that quite a few model experiments on structures under simulated dynamic loads and earthquake motions have been carried out in the past (Refs. 32 to 61). However, much of this work was concerned with elastic behavior only. The case studies reported in the literature on modeling of structures to failure generally lack a thorough discussion of the consequences of inadequate material simulation and often do not take full advantage of the potential of dimensional analysis in deriving appropriate modeling laws.

Physical models for elastic earthquake response prediction were used

as much as fifty years ago. Ruge (Ref. 32) presented a comprehensive paper on elastic dynamic modeling theory in 1934, and in Ref. 33 he described a detailed model study on the earthquake resistance of elevated water-tanks which included a feasibility study of various model materials (mercury to simulate water and brass to simulate steel) and a discussion of feasible model distortions. Even earlier, dynamic studies on models of wood panels, cylindrical tanks, and multistory buildings had been carried out on a shake table at Stanford University (Refs. 34, 35). The masses in the building models were lumped at story levels and represented by steel plates kept apart by vertical ball-supports, while the building frame and wall rigidities of the prototype were represented by horizontal coiled springs.

A thorough and comprehensive study on dynamic modeling of steel and reinforced concrete structures was carried out in the early sixties at MIT (Refs. 36 to 39). The purpose of this study was primarily the investigation of structural response to blast loading. As such, the source of excitation and many of the relevant response characteristics are quite different from earthquake loading, but much of the modeling theory, material studies and fabrication techniques presented in these research reports can be directly utilized for model studies in earthquake engineering. Other useful information from model studies of structures subjected to blast loading can be found in Refs. 40 to 43.

In the United States, the use of large and small scale models for seismic response investigations in the inelastic material domain became an acceptable alternative to analytical studies only in the early seventies. In most cases these studies were directed towards verification of analytical models for specific structural systems (e.g.,

reinforced concrete shear walls) or earthquake response phenomena (e.g., overturning and uplift problems). In such cases, distortions of seismic input or of structural configurations (to suit available shake table capabilities or permit the use of established material and model construction techniques) can often be accepted since the physical model results are compared to analytical results and not to prototype behavior.

The shake tables in the research laboratories at the University of Illinois and the University of California at Berkeley have been used extensively for such model studies. The University of Illinois facility has been used primarily for small scale model studies of reinforced concrete building structures. Much of this research work is summarized in a paper by Sozen (Ref. 44); more detailed results can be found in Refs. 45 to 49.

Reference 50 provides an example of small scale model studies performed at Cornell University on the behavior of reinforced concrete structures under seismic excitation.

The U.C. Berkeley facility which is built around a 6x6 m (20x20 ft) shake table is used primarily for testing of structures which may be considered to be large-scale pseudo-models. The structural elements are usually made of prototype structural material (small hot rolled steel section or concrete reinforced with small reinforcing bars) and floor masses are simulated with a sufficient number of concrete blocks to simulate gravity-induced stresses. In size, the structures may be roughly one half that of actual structures. The seismic input motion usually is not scaled according to model similitude laws, and intentionally so since the test structures are not meant to be replica models of actual structures

but physical representations of mathematical models. The drawback of this kind of experimentation is that a one-to-one correspondence with a prototype structure cannot be established; the advantage is that structural detailing can be simulated without much difficulty and material behavior is well known which increases the confidence in test results and permits reliable analytical correlation. References 51 to 56 discuss specific studies of this type carried out at the U.C. Berkeley shake table.

Actual replica models are also tested at the U.C. Berkeley facility. An excellent example is the 1:30 scale model of a reinforced concrete high curved overcrossing (Ref. 57). This model was built of micro-concrete and closely follows dynamic similitude laws. Great care was taken in precise simulation of all details at expansion joints which were known a priori to be subjected to severe damage caused by multiple impacting in both torsional and translational modes. To maintain body forces similitude, the mass of the model was increased to 30 times the self-weight by adding lead blocks.

More recently, a shake table study on a 1:12 scale steel model of a three story, one bay steel frame structure was completed by Mills et. al., (Ref. 58) on the Stanford University shake table. The 1:6 scale model of a 1:2 scale pseudo-prototype tested at Berkeley (Ref. 51) was used to compare directly the results obtained from the tests of the pseudo--prototype and its model. Reference 58 includes a comprehensive description of the evaluation of the shake table performance, of the instrumentation, and of data acquisition and reduction systems. The report discusses in detail the modeling techniques for steel structures and presents guidelines for a rational comparison of experimental data from model and

prototype tests.

It should be noted that much valuable information on dynamic modeling can be drawn from publications in fields other than structural engineering. References 59 to 61 are examples of collections of informative papers. Although much of the theory and dimensional analysis developed herein will prove useful, it has to be recognized that the references tend to focus on response within the elastic range of material behavior.

The use of physical models in earthquake engineering has been much more extensive in Europe than in the United States and Canada. For instance, the Istituto Sperimentale Modelli e Strutture in Bergamo, Italy, the Laboratorio Nacional de Engenharia Civil in Lisbon, Portugal, and the Institute for Research and Testing in Materials and Structures in Ljubljana, Yugoslavia, have elaborate and well-equipped model laboratories which are used for research work in earthquake engineering. References 62 to 84 describe some of the dynamic model studies carried out at these and other laboratories and contain information on modeling of buildings, bridges, dams, nuclear reactor components and containment vessels.

Several model studies on seismic behavior of building structures and containment vessels were also carried out in industrial and university laboratories in Japan. Some of these models were pseudo-models (as described previously) and some were actual scale models. References 85 to 88 are examples of this work.

Dynamic Modeling Theory: Applications of dynamic modeling theory are discussed in many of the aforementioned references. The basis for the development of model similitude laws can be found in many books concerned with the theory of similitude and dimensional analysis, of which Refs. 89

to 98 are a representative sample. Dimensional analysis as an analytical tool for the derivation of model similitude laws is largely attributed to the work of Buckingham (Ref. 99) and Rayleigh (Ref. 100). Specific aspects of modeling theory as applied to civil engineering problems are discussed in Refs. 101 to 105. A comprehensive discussion of the physical quantities entering a structural problem and of their dimensional dependence is present in Ref. 38.

Model Materials and Model Fabrication: The interrelated subjects of material selection, scaling effects in material simulation, and model fabrication have been the subject of many studies and are widely reported upon in the literature. Nevertheless, there remains a large number of unanswered questions some of which are the subject of this study.

Good summaries on available model materials and problems associated with material simulation and model fabrication can be found in Refs. 106 to 111, concerned with elastic and ultimate strength models made of plastics, cementitious and metallic materials.

Specific and detailed information on the use of microconcrete and gypsum mortar and the simulation of reinforcement in models of reinforced conrete structures are presented in Refs. 12, 14, 25, 29, 36, 39 and 106 to 123. References 14, 39, 43 and 114 to 119 provide guidelines on the design of microconcrete mixes for various strength and mechanical properties. Appropriate aggregate grading, mix proportions, mixing and curing techniques are discussed. Maisel (Ref. 118) points out the possibility of changing the mechanical properties of microconcrete (E-moduli, f'_t/f'_c-ratio) through the use of different aggregate types, additives, and by coating of the aggregate with a thin layer of hard and

smooth silicone resin. References 18, 39, 117, and 122 discuss the effects of speed of testing on the compressive strength of microconcrete. Reference 123 provides state-of-the-art report on size effects in model concretes. References 18, 21, 39, 117, 118 and 124 present results of individual case studies concerned with size effects. References 125 to 144 provide information on mix design, testing, mechanical properties, and load rate effect on prototype concrete. References 18, 43, 117, 118, 140 and 145 present techniques used in model reinforcement fabrication. Ref. 146 presents results of a study on strain rate effect on the tensile behavior of model reinforcement. Ref. 147 discusses the problem of crack and deformation similitude in reinforced concrete which was investigated by means of bending tests of similar beams at different scales. References 147 to 150 provide information on reinforced concrete behavior (prototype and model) under dynamic loading conditions.

Much less information than on reinforced concrete is available on the feasibility of using steel or other metallic materials to simulate prototype structural steel. The study summarized in Ref. 31 and the recent study by Mills et. al., (Ref. 58) treat in detail the problems of element fabrication and member joining encountered when steel is used as a model material for steel structures. Strain rate effects in low carbon steel are discussed in Refs. 151 to 153. Size effects on tensile and flexural behavior of structural steel are investigated by Richards in Refs. 154 and 155. The properties of phosphor bronze and its feasibility as a model material for steel structures under dynamic loads are discussed in Ref. 38. Ref. 157 is an excellent text on basic material behavior.

Model Instrumentation and Dynamic Test Facilities: It is evident

that the instrumentation system for measurement of pertinent response parameters must be adapted to the size of the models to be tested. Requirements on the instrumentation system and feasible measuring devices are discussed in Refs. 58, 158, and 159. The use of minicomputers in measurement, analysis and control of experimentation is summarized in Refs. 58, 160, and 161 and specific problems associated with recording and interpretation of dynamic test results are discussed in Ref. 162.

The problem of simulating an earthquake environment in the field and in the laboratory was the subject of an NSF sponsored workshop in San Francisco. The proceedings of this workshop (Ref. 163) contain valuable information on the role of experimental research in earthquake engineering, on experimental needs, and on existing experimental facilities. Several other publications that discuss earthquake simulation systems and specific simulation problems are listed in Refs. 164 to 169.

CHAPTER 4

DYNAMIC MODELING THEORY

4.1 DEFINITIONS

The physical quantities of importance in an experiment can be divided into variables and parameters, these being either dependent or independent.

The independent quantities are automatically assigned by the physical characteristics of the problem.

The dependent quantities are those measured during the experiment.

A variable is a quantity which spans a continuous range of values in a single problem (e.g., time in a dynamic problem).

An independent parameter is what Bridgman (Ref. 89) calls a dimensional constant.

A dependent parameter is a result, usually global in nature, that typically represents a single experimental measurement.

A physical quantity can be measured by comparing a sample with a known amount of the same quantity. This known reference amount is called a unit. For the complete specification of any physical quantity, both the unit used and the number of units contained in the sample must be given.

The unit of any physical quantity can be expressed as a combination of units of basic or fundamental quantities (e.g., the unit of stress can be expressed in terms of units of such basic quantities as force and length).

The units of basic quantities are called basic or fundamental units.

Dimensions are products of powers of basic quantities (described in basic units), and as such relate the units of measurement of any physical

quantity to the selected basic units.

A dimensionally homogeneous equation is an equation which does not depend on the fundamental units of measurement. Such an equation consists of the sum of products of powers of physical quantities and each term in the sum has the same dimension.

π-Factors are dimensionless products of powers of physical quantities. A complete set of dimensionless products describes a physical phenomenon in a dimensionless form and as such renders it independent on selected units.

A dimensional matrix is an arrangement of numbers containing dimensional exponents of physical quantities expressed in terms of basic quantities. It comprises as many columns as physical quantities in the functional relationship of a problem and as many rows as basic quantities. For instance, if the functional description for the displacement of an elastic problem is given by $u = u(x,y,z;E,\nu,P)$, the dimensional matrix has the following form:

	dependent variable	independent variables			independent parameters		
	u	x	y	z	E	ν	P
Force F	0	0	0	0	1	0	1
Length ℓ	1	1	1	1	-2	0	0

4.2 GENERAL DISCUSSION

The purpose of model analysis in earthquake engineering is the prediction of the dynamic response of prototype structures from laboratory tests on physical models. This prediction may include all pertinent response parameters or it may be limited to selected parameters such as

natural frequencies and mode shapes. The desired range of prediction may be limited to the linear elastic response or it may comprise the complete response history to failure including material and geometric nonlinearities. In the cases of single parameter and elastic response prediction several model design requirements can often be relaxed which makes model analysis a simpler but also less powerful tool.

In this chapter modeling theory is discussed in a general sense which makes it suitable for all types of model studies and is then applied to specific cases which are most useful in seismic investigation. Modeling theory establishes the rules according to which the geometry, mateial properties, initial conditions, boundary conditions and environmental effects (loading) of the model and the prototype have to be related so that the behavior of one can be expressed as a function of the behavior of the other. The theory which leads to the development of a complete set of correlation functions (sometimes referred to as scaling laws) defining the model-prototype correspondence is that of similitude.

The Oxford English Dictionary defines similitude as: "the quality of state of being like resemblance, similarity, likeness. Now somewhat rare." Among the ideas associated with similitude are: analogies, dimensional analysis, dimensionless numbers, group invariance, homogeneity, inspectional analysis, local similarity, local solutions, modeling, scaling laws, self-similarity, separation of variables, similarity rules, symmetry, transformations.

The theory of similitude, upon which model design and analysis is based, may be developed by dimensional analysis. Dimensional analysis as a powerful analytical tool is developed from a consideration of the di-

mensions in which each of the pertinent quantities involved in a physical phenomenon is expressed. The principles of dimensional analysis are well established in the literature and are summarized in Section 4.3 as far as needed for the development of a general modeling theory. For more detailed information the reader is referred to the books listed as Refs. 1 and 89 to 98 and the technical publications listed as Refs. 38 and 99 to 105.

To develop the necessary mathematical relationships between the characteristics of a prototype and its model, let us start from the premise that every physical phenomenon can be expressed by a dimensionally homogeneous equation of the type

$$q_1 = F(q_2, q_3, \ldots . q_n) \tag{4-1}$$

where n is the total number of physical quantities involved in the phenomenon. In this expression q_1 is a dependent quantity and q_2 to q_n are the variables and parameters on which q_1 depends. According to Buckingham's Pi theorem (Section 4.3), every dimensionally homogeneous equation can be written in the form

$$\pi_1 = f(\pi_2, \pi_3, \ldots . \pi_{n-N}) \tag{4-2}$$

where π_1 to π_{n-N} are dimensionless products of powers of the physical quantities q_1 to q_n. The number N is the rank of the dimensional matrix which is usually equal to the number of basic units needed to describe the physical quantities.

Since Eq. (4-2) is identical to Eq. (4-1), it describes the same physical phenomenon and, because of its dimensionless form, must be equally valid for prototype and model if similitude is to be achieved. A sufficient condition for complete similitude is therefore

$$(\pi_1)_p = (\pi_1)_m \tag{4-3}$$

and

$$\begin{aligned} (\pi_2)_p &= (\pi_2)_m \\ &\vdots \\ (\pi_{n-N})_p &= (\pi_{n-N})_m \end{aligned} \tag{4-4}$$

Equation (4-3) is often referred to as the prediction equation and Eq's. (4-4) constitute the design conditions for the model. Methods for deriving the dimensionless products are summarized in Section 4.3

There are two major difficulties the model analyst has to face. First he has to exercise extreme care in specifying the right number of physical quantities which enter Eq. (4-1). Quantities which have insignificant effect on the response parameters of interest will impose unnecessary restraints on the model, while neglecting a significant quantity can yield incorrect results. Secondly, the experimenter is often faced with almost unsurmountable problems when he tries to reproduce at model scales the design conditions posed by Eq's. (4-4). In particular, the simulation of material properties and loading conditions may be an extremely difficult or impossible task. The latter often leads to the design of distorted models in which one or more of the design conditions are violated. Nevertheless, such models may still be adequate if the prediction can be corrected to account for the violations in the design conditions.

The specification of all important quantities on the right hand side of Eq. (4-1) does require some insight into the physical problem under study. In general, the more that is known about the behavior of the

prototype and of the laws which describe it, the easier it is to design the model, but the less necessary the model is. Considering the level of confidence in model results and the effort invested in design, testing and data analysis, models are most useful when the general features of the prototype behavior are known but specifics such as complex geometry or material nonlinearities render it difficult to obtain quantitative information by analytical means.

The physical quantities which may enter a structural problem are difficult to enumerate in their entirety but are for most cases contained in one of the following four groups (Refs. 38, 90).

Geometric Properties: Geometry includes all the space relationships which may influence the results. All distances or lengths and all angles that are pertinent must be represented. For geometrically similar models a location vector is sufficient to describe any point in the structure. In dynamic problems the vector will depend not only on the space coordinates but also on the time t. Alternatively, the location vector may be specified at a time t_o and the geometry at time t may be defined by the location vector $\vec{r}_o$ and a time dependent displacement vector $\vec{u}(t)$.

Material Properties: In general, these properties may vary from point to point in space and with time and temperature. A material has thermal, mechanical, electrical and magnetic properties, although the latter two can usually be neglected in structural problems. Thermal properties of interest may be specific heat, coefficients of thermal conductivity and linear expansion, and emissivity. The mechanical properties are the specific mass, and the material properties defining the state of stress and strain in the material. These properties may be time

and temperature dependent (e.g., creep and relaxation), vary from point to point (inhomogeneity), and be direction dependent (anisotropy). They also describe the interaction between different directions (Poisson's ratio) and the interaction between neighboring points (e.g., strain gradient effects). A complete discussion of these properties is beyond the scope of this report, but to show the complexities involved in a thorough material state description, the uniaxial stress-strain relation proposed by Harris et al. (Ref. 38) is reproduced below:

$$\sigma\left(\vec{r},t,T,\frac{\partial\varepsilon}{\partial t}\right) = \sigma_o\left(\vec{r},t_o,T_o\frac{\partial\varepsilon}{\partial t}\bigg|_o\right)+$$

$$\sum_{n=1}^{\infty}\frac{(\varepsilon-\varepsilon_o)^n}{n!}\left\{\frac{\partial^n\sigma}{\partial\varepsilon^n}\left(t_o,T_o,\frac{\partial\varepsilon}{\partial t}\bigg|_o\right)+\sum_{j=1}^{\infty}\frac{(t-t_o)^j}{j!}\frac{\partial^{n+j}\sigma}{\partial\varepsilon^n\partial t^j}\bigg|_{t=t_o}+\right. \tag{4-5}$$

$$\left.\sum_{\ell=1}^{\infty}\frac{(T-T_o)^\ell}{\ell!}\frac{\partial^{n+\ell}\sigma}{\partial\varepsilon^n\partial T^\ell}\bigg|_{T=T_o}+\sum_{k=1}^{\infty}\frac{\left(\frac{\partial\varepsilon}{\partial t}-\frac{\partial\varepsilon}{\partial t}\big|_o\right)^k}{k!}\frac{\partial^k}{\partial\left(\frac{\partial\varepsilon}{\partial t}\right)^k}\left[\frac{\partial^n\sigma}{\partial\varepsilon^n}\right]\right\}\bigg|_{\sigma=\sigma_o}$$

where t and T are the time and temperature variables, respectively, and the subscript o denotes a reference value. It should be noted that material damping, which is of importance in seismic studies, is included in this state equation, although for low level excitations it is often isolated and specified separately as a coefficient of damping.

It is evident from Eq. (4-5) that compromises in material simulation must be accepted in model studies since no two materials are alike in the time and temperature domain. Even the use of prototype material is a compromise because of size scaling and the dependence of material properties on time rate effects. Material simulation is discussed in

more detail in Chapter 5.

Initial Conditions: These conditions can be described by initial stress and temperature functions, σ_o and T_o, at time t_o. In many cases, the specification and simulation of σ_o and T_o will be an extremely difficult task due to their dependence on fabrication and construction procedures and previous loading histories. In the design of models this will necessitate a faithful reproduction of fabrication and construction procedures whenever those have a significant effect on the initial conditions. In reinforced concrete structures initial conditions may be strongly affected by creep and shrinkage effects, while in steel structures residual stresses due to welding and erection stresses have to be considered. For steel as a prototype material it may be necessary to trace the history back to member fabrication which is usually the source of significant residual stresses.

External Influences (Environmental Effects): Such influences may be prescribed displacements wich may be time dependent as in the case of seismic ground motions, prescribed temperature variations, surface forces on the boundaries of the structure, and body forces caused by the gravitational field of the earth or generated by artificial means such as magnetic fields.

For most structural problems the pertinent physical quantities can be selected from these four groups. Based on a physical understanding of the problem, it is the task of the model analyst to choose those quantities which will significantly affect the response quantities to be measured during the model experiment. The experimenter may be interested in tracing the complete response history which may be described by

stress, strain or displacement functions, or only in specific quantities such as the failure load which may be characterized by material failure or buckling phenomena.

To aid the model analyst in selecting model design and response quantities, an extensive but certainly incomplete list of physical quantities and their dimensional description is presented in Table 4.1.

Before we can utilize Eq's. (4-1) and (4-2) to derive appropriate similitude realtionships for dynamic model studies, it is necessary to briefly summarize the fundamentals of dimensional analysis which is done in the next section.

Before entering this discussion, a different approach to modeling theory than that of dimensional analysis should be mentioned, namely, model analysis based on system response equations. In several cases the differential equation representing the response of a stucture is known, although the solution of it cannot be obtained analytically. By transforming the variables of such an equation and also of its boundary and initial conditions into a dimensionless form one obtains a set of dimensionless parameters defining the relation between the model and the prototype. Although some authors call this method a forcing of the model to be an analog computer for solution of the equation, a careful use of it can help in elimination of certain otherwise very rigid requirements obtained from the dimensional studies.

4.3 DIMENSIONAL ANALYSIS

Dimensional analysis is an analytical method by which a dimensionally homogeneous equation, containing physical quantities and describing

a physical phenomenon, is converted into an equivalent equation containing only dimensionless products (π-factors) of powers of the physical quantities. Since these dimensionless products describe the same physical phenomenon and are independent of the units of measurement, they must be equal in prototype and model if complete similitude is to be achieved.

Dimensional analysis is based on the Buckingham Pi Theorem (Ref. 99) which states that a dimensionally homogeneous equation can be reduced to a functional relationship between a complete set of independent dimensionless products (π-factors). The number of independent dimensionless products is equal to the total number of physical quantities involved minus the number of fundamental quantities needed to describe the dimensions of all physical quantities.

The simple rule for the determination of the number of independent dimensionless products has been shown to fail occasionally (Ref. 89) and has been reformulated in more formal mathematical terms (Ref's. 91, 94) as: the number of dimensionless products in a complete set is equal to the total number of physical quantities involved minus the rank of their dimensional matrix. (The rank of a matrix is the order of the largest submatrix whose determinant is nonzero).

In order to determine a complete set of dimensionless products it should be noted that the units of any physical quantity can be expressed as a combination of units of basic or fundamental quantities. The choice of basic quantities is largely an arbitrary one but is governed by practical considerations of physical phenomena and simplicity of measurement. Different fields of science may choose different basic quantities. In

engineering, the most common sets of basic quantities are those of mass M, length L, time T and temperature Θ (called the MLTΘ system) or force F, L, T and Θ (called the FLTΘ system). Several authors (Refs. 38, 105) use for convenience heat as a basic quantity, disregarding its equivalence to energy. Rocha (Ref. 103) and Beaujoint (Ref. 105) discuss the usefullness of strain as a basic quantity and assign it a basic unit. This idea is discussed in Section 4.5.3.

Table 4.1 presents a set of commonly used physical quantities in engineering mechanics and their dimensional description in the MLTΘ and FLTΘ systems. It should be noted that several quantities in this table are dimensionally equivalent, such as pressure, stress and modulus of elasticity. Also, it is often necessary to distinguish between certain quantities through their physical meaning although they may be dimensionally and quantitatively equivalent. As an example we can use energy terms where each one of them, kinetic, potential, damping, hysteretic or recoverable strain energy may have a distinctly different meaning to the investigator. Thus, commonly used physical derivations of quantities are included in the table where feasible.

The basic quantities can be used as building blocks since the dimensions of all other physical quantities can be expressed as products of powers of basic quantities. When the dimensions of physical quantities are properly arranged in a dimensional matrix it is reasonably simple to extract dimensionless products by comparing individual quantities as to their dimensional dependence. Although systematic methods for generating a complete set of dimensionless products are presented in most text books, it can equally well be achieved by inspection if the following rules and guidelines are considered:

TABLE 4.1

PHYSICAL QUANTITIES AND THEIR DIMENSIONS

Physical Quantity	Symbol	Description in terms of other physical quantities	Dimensions in FLTθ Systems				Dimensions in MLTθ Systems			
			F	L	T	θ	M	L	T	θ
Angle	ϕ		0	0	0	0	0	0	0	0
Strain	ε	σ/E	0	0	0	0	0	0	0	0
Poisson's Ratio	ν		0	0	0	0	0	0	0	0
Coefficient of Friction	μ_F	F_F/F	0	0	0	0	0	0	0	0
Length	ℓ		0	1	0	0	0	1	0	0
Time	t		0	0	1	0	0	0	1	0
Frequency	ω	$(K/m)^{\frac{1}{2}}$	0	0	-1	0	0	0	-1	0
Elastic Restoring Force	F_E	$K\delta$, $\sigma\ell^2$, $\varepsilon E\ell^2$								
Gravitational Force	F_G	$\gamma\ell^3$, $\rho g\ell^3$								
Inertia Forces	F_I	ma, $\rho\ell^3 a$	1	0	0	0	1	1	-2	0
Viscous Damping Force	F_D	cv								
Coulomb Friction Force	F_F	$\mu_F F$								
Modulus of Elasticity	E	σ/ε, $F_E/\varepsilon\ell^2$								
Shear Modulus	G	$E/2(1+\nu)$								
Stress	σ	εE, F_E/ℓ^2	1	-2	0	0	1	-1	-2	0
Pressure	p	F/ℓ^2								
Displacement	δ	$\varepsilon\ell$, $F_E/E\ell$	0	1	0	0	0	1	0	0
First Moment of Area	Q		0	3	0	0	0	3	0	0
Second Moment of Area	I		0	4	0	0	0	4	0	0
Elastic Stiffness	K	$\varepsilon E\ell$, F_E/δ								
Axial Stiffness	K_a	AE/ℓ	1	-1	0	0	1	0	-2	0
Shear Stiffness	K_s	$A_s G/\ell$								
Flexural Stiffness	K_f	EI/ℓ^3								
Moment	M	$F\ell$	1	1	0	0	1	2	-2	0

TABLE 4.1 (continued)

Physical Quantity	Symbol	Description in terms of other physical quantities	Dimensions in FLTθ Systems				Dimensions in MLTθ Systems			
			F	L	T	θ	M	L	T	θ
Specific Weight	γ	ρg, F_G/ℓ^3	1	-3	0	0	1	-2	-2	0
Mass density	ρ	γ/g, $F_G/g\ell^3$	1	-4	2	0	1	-3	0	0
Mass	m	$\rho\ell^3$, $F_G/\hat{g}$	1	-1	2	0	1	0	0	0
Mass Moment of Inertia	I_m	$m\ell^2$	1	1	2	0	1	2	0	0
Velocity	v									
S-Wave Velocity	v_s	$[E/2(1+\nu)\rho]^{\frac{1}{2}}$	0	1	-1	0	0	1	-1	0
P-Wave Velocity	v_p	$[(1-\nu)E/(1-\nu-2\nu^2)\rho]^{\frac{1}{2}}$								
Angular Velocity	$\dot{\phi}$		0	0	-1	0	0	0	-1	0
Acceleration	a		0	1	-2	0	0	1	-2	0
Acceleration of Gravity	g									
Angular Acceleration	$\ddot{\phi}$		0	0	-2	0	0	0	-2	0
Coefficient of Viscous Damping	c	F_D/v	1	-1	1	0	1	0	-1	0
Dynamic Viscosity	μ	$\tau/(dv/dy)$	1	-2	1	0	1	-1	-1	0
Kinematic Viscosity	ν	μ/ρ	0	2	-1	0	0	2	-1	0
Kinetic Energy	KE	mv^2								
Potential Energy	PE	$F\delta$								
Damping Energy	DE	cv^2t	1	1	0	0	1	2	-2	0
Hysteretic Energy	HE	$\sigma\varepsilon\ell^3$								
Recoverable Strain Energy	RSE	$\sigma\varepsilon\ell^3$, $K\delta^2$								
Heat	H	$Cm\theta$, $k\ell T\theta$								
Momentum	M	mv	1	0	1	0	1	1	-1	0
Power	P	Fv	1	1	-1	0	1	2	-3	0
Temperature	θ		0	0	0	1	0	0	0	1
Coefficient of Thermal Expansion	α	$\delta/\ell\theta$	0	0	0	-1	0	0	0	-1
Thermal Conductivity	k	$H/T\ell\theta$	1	0	-1	-1	1	1	-3	-1
Specific Heat	C	$H/m\theta$	0	2	-2	-1	0	2	-2	-1
Coefficient of Heat Transfer	h	$H/T\ell^2\theta$	1	-1	-1	-1	1	0	-3	-1

1. The dimensionless products are composed of products of powers of the physical quantities and should involve not more than N-1 quantities in any one product, where N is the number of basic quantities.

2. The dimensionless products must be independent, i.e., none of the products can be obtained as a product of powers of other products.

3. Independence is easy to verify if the dimensionless products are generated such that each product involves a quantity which does not appear in any other product.

4. The dimensional matrix should be arranged such that the response quantity of interest (dependent variable) is listed first, followed by independent variables and then parameters.

5. Dimensionless products should be generated such that quantities are eliminated from left to right in the dimensional matrix.

Guidelines 4 and 5 are important for the design and control of the experiment. Since complete sets of dimensionless parameters are not unique, one will be more useful than others in model analysis. Buckingham has pointed out that we obtain maximum amount of experimental control over the dimensionless products if the original physical quantities that can be regulated in the experiment each occur in only one dimensionless product (Ref. 91). Thus, a warning must be issued against a superficial use of dimensional analysis. It is a powerful tool but its usefulness for specific model analysis problems is entirely in the hand of the user. Here, it may not be out of place to cite two of the "fathers" of dimensional analysis:

> Dimensional analysis yields an amount of information dependent on the skill and experience of the analyst.
>
> -P. W. Buckingham
> Encyclopedia Britannica
> 1964 ed.

> Dimensional analysis proves to be an exceedingly powerful weapon, although I should add the warning, based on bitter experience of my own as well as a critical study of other people's work, that it is also a blind, indiscriminating weapon and that it is fatally easy to prove too much and to get more out of a problem than was put into it.
>
> -G. K. Batchelor
> Quart. J. Roy. Meteor. Soc.,
>
> 1959

The generation of a complete set of independent dimensionless parameters by inspectional analysis is illustrated in the following simple example. Let us consider the problem of elastic bending of a rectangular cantilever beam which is affected by the following physical qantities:

geometric properties: b, h, ℓ

material properties: E, ν

applied load: P

The response quantity of interest is the deflection δ under the load, i.e., $\delta = (b,h,\ell,E,\nu,P)$. All quantities can be expressed in terms of the basic quantities F and L which leads to the following dimensional matrix:

	δ	b	h	ℓ	E	ν	P
F	0	0	0	0	1	0	1
L	1	1	1	1	-2	0	0

The rank of the matrix is 2, hence we have 7 - 2 = 5 independent dimensionless products. It is convenient to form one product that contains the response quantity to the first power and relate it to what seems to be the most relevant independent quantities. Additional products that can be written down immediately are those which are given by dimen-

sionless quantities, in this case ν, and those which are formed by ratios of quantiities having like dimensions. The remaining products can be formed by trial and following the aforementioned guidelines. For the beam this procedure gives

$$\frac{\delta}{\ell} = f\left(\nu, \frac{b}{\ell}, \frac{h}{\ell}, \frac{P}{E\ell^2}\right) \tag{4-6}$$

It is easy to see that these factors are independent since each one contains a quantity which is not involved in any other factor.

Insight into the physical problem may reveal that the solution is independent on certain parameters that would at first sight appear significant (i.e., for slender beam the dependence on ν could be dropped). The knowledge that the problem is linear with respect to certain parameters can further simplify the functional relation. For example, using linear theory of elasticity one can state that the deflection is directly proportional to the load applied and inversely proportional to the breadth of the beam, hence the corresponding factors can be taken outside the function:

$$\frac{\delta}{\ell} = \frac{P}{E\ell b} f_1\left(\frac{h}{\ell}, \nu\right) \tag{4-7}$$

This linear dependence upon certain dimensionless parameters is very helpful when model distortions have to be considered (see Section 4.4).

In some cases the complete set of dimensionless products obtained by inspectional analysis may not satisfy the experimenter's desire for optimum experimental control. In such cases a different set of products can be generated by means of simple transformation techniques. These techniques are presented in most textbooks on dimensional analysis and need not be repeated here.

Several dimensionless products have gained traditional status in engineering and are commonly used in defining physical problems. Table 4.2 presents a set of such "popular" dimensionless products.

4.4 SIMILITUDE RELATIONSHIPS AND TYPES OF MODELS

The necessary conditions for complete similitude between model and prototype can be derived through the following procedure:

1. Write down all physical quantities on which the solution of the phenomenon under study depends significantly.

2. Develop a suitable and complete set of independent dimensionless products from these physical quantities (Eq. 4-2).

3. Establish equality between prototype and model for each of the independent dimensionless products (Eq's. 4-2 and 4-4).

The third step defines the design conditions for the model and the prediction equation (or equations) for the dependent response quantity (or quantities) which relates the measured model response to the prototype behavior. As such, this step establishes the scaling laws for all physical quantities or products of physical quantities. Usually, these scaling laws are expressed as ratios of the numbers of units needed to describe identical quantities in model versus prototype. In this report these ratios are designated with a subscript r added to the description of the physical quantity, i.e., $\ell_r = \ell_m / \ell_p = 0.1$ means that one unit of length measurement (e.g., in.) in the model corresponds to ten equal units of length measurement in the prototype.

One important observation can be made from the fact that all physical quantities can be expressed in terms of basic or fundamental quanti-

TABLE 4.2

DIMENSIONLESS PRODUCTS

(a) Named Dimensionless Products

Biot Number	$h\ell/k$	
Bond Number	$\rho g\ell^2/\gamma$	γ - surface tension $[FL^{-1}]$
Cauchy Number	$\rho v^2/E$	
Einstein Number	v/c	
Euler Number	$\Delta p/\rho v^2$	
Fanning Number	$\tau_w/(\frac{1}{2}\rho v^2)$	τ_w - shear at the wall
Fourier Number	$kt/\rho c\ell^2$	
Froude Number	$v^2/\ell g$	
Grashof Number	$\frac{\alpha\theta\ell^3 g}{\nu^2}$	ν - kinematic viscosity
Mach Number	v/c	c - speed of sound
Newton Number	$R/\rho\ell^2 v^2$	R - aerodyn. reaction experienced by a body
Nusselt's Number	$h\ell/k$	
Prandtl's Number	$C\mu/k$	
Pressure Coefficient	$p/\rho v^2$	
Reech Number	$v^2/\ell f$	f - force per unit mass
Reynolds Number	$\ell v/\nu$ or $\ell v\rho/\mu$	
Strouhal Number	$\omega\ell/v$	
Weber Number	$\rho v^2\ell/\gamma$	γ - surface tension

(b) Dimensionless Products Commonly Encountered in Structural Engineering Problems

$$\frac{\rho v^2}{E},\ \frac{v^2}{\ell g},\ \frac{\sigma\ell^2}{P},\ \frac{E\ell^2}{P},\ t\sqrt{\frac{a}{\ell}},\ \frac{\rho a\ell^3}{P},\ \alpha T,\ \frac{t}{\ell}\sqrt{\frac{E}{\rho}},\ \frac{\rho g\ell}{E},\ \frac{g}{E},\ \frac{\lambda\omega^2}{g},\ \frac{\delta}{\ell},\ \frac{a}{g}$$

ties (e.g., FLTΘ or MLTΘ). Since these basic quantities are independent on each other, it is evident that as many scales can be selected arbitrarily (within physical constraints) as there are basic quantities needed to describe the problem. For instance, in a static problem which has F and L as basic quantities, two scales can be selected arbitrarily. In a dynamic problem which may be described by M, L and T, three scales can be selected arbitrarily. However, in this case it is usually necessary to select $g_r = 1$ (g is the acceleration of gravity) which reduces the choice of arbitrary scales to two. The scales of all other physical quantities are then expressed in terms of the arbitrarily selected ones and can be obtained from the dimensionless products.

It should be noted that the choice of arbitrary scales is not limited to basic quantities; any set of independent quantities may be selected for this purpose. The number of independent quantities is always equal to the number of basic ones, and their independence can be checked through the formation of the Jacobian whose determinant must be nonzero (Ref. 38), i.e.,

$$\left| \frac{\partial(q_1, q_2, \ldots . q_r)}{\partial(k_1, k_2, \ldots . k_r)} \right| \neq 0 \qquad (4\text{-}8)$$

where r is the number of independent quantities, q_1 to q_r are the selected quantities whose independence is to be checked, and k_1 to k_r are the basic quantities.

To illustrate the determination of scaling laws, let us take the beam example of Section 4.3 whose dimensionless products were written as

$$\frac{\delta}{\ell} = f\left(\nu, \frac{b}{\ell}, \frac{h}{\ell}, \frac{P}{E\ell^2}\right) \qquad \begin{matrix}(4\text{-}6)\\ \text{repeated}\end{matrix}$$

If we freely select a length scale ℓ_r and a scale for the modulus of

elasticity E_r, complete similitude requires that $b_r = h_r = \ell_r$ (which is evident from geometric similarity) and $P_r = E_r(\ell_r)^2$. Clearly, ν as a dimensionless quantity must be equal for model and prototype. The prediction equation states that $\delta_r = \ell_r$. Such a model that fulfills all similitude requirements is called in this report a true replica model.

In many practical situations the fulfillment of all design conditons will be an impossible task. Under those circumstances it is a matter of judgement and experience to isolate those features which may be altered such that model construction becomes feasible but the response prediction is not encumbered with an excessive amount of error.

In these kinds of models, Murphy (Ref. 90) distinguishes between adequate and distorted models. Adequate models are those where the prediction equation is not affected (except for the error introduced by the disregard or violation of a design condition) and design conditions may be violated when insight into the physical problem reveals that the results will not depend significantly on the violated design condition. For instance, in the above example, cross-sectional similarity may not be critical if shear deformations do not contribute significantly to the deflection δ. In this case, the moment of inertia is adequate to describe the cross section and b and h can be distorted accordingly. As another example, in certain dynamic problems the effects of gravitational forces may be small compared to those of inertia forces and consequently certain design conditions may be disregarded (see Section 4.5.2).

Actual distorted models are those where the distortion in one dimensionless product either leads to a distortion of the prediction equation or is accounted for by introducing compensating distortions in

other dimensionless products. In the first case the prediction equation needs to be modified by a prediction factor δ defined as

$$\delta = \frac{(\pi_1)_p}{(\pi_1)_m} \tag{4-9}$$

where π_1 is the dimensionless product defining the prediction equation. The prediction factor can be determined through physical insight into the problem or by means of a series of auxiliary experiments. For instance, in the example problem defined by Eq. (4-6) it is evident that δ is inversely proportional to b thus if b is distorted by a factor α, the prediction factor is given by $\delta = 1/\alpha$.

For more information on the determination of δ and compensating distortions the reader is referred to the book by Murphy (Ref. 90). An alternative method for the evaluation of compensating distortions is presented in Section 4.5.3. There, the distorted physical quantity is introduced as an artificial basic quantity.

4.5 PHYSICAL MODELS FOR SHAKE TABLE STUDIES

4.5.1 True Replica Models

Suppose the task is to reproduce, at model scale, the time history of stress components $\sigma_{ij}(\vec{r},t)$ in a replica model subjected to a time history of vector imposed acceleration a (t). Recognizing that the distributions of stress and of material in the prototype and model must be identical, dimensional analysis can be applied by calling σ a typical stress, ρ a typical density, and E some representative stiffness property. Then the stress distribution may be written as

$$\sigma_{ij} = \sigma S_{ij}(\vec{r},t) \qquad i,j = 1,2,3$$

where S_{ij} is dimensionless.

With the greatest degree of simplification, the typical stress can be expressed through a functional relationship of the form

$$\sigma = F(\vec{r},t;\rho,E,a,g,\ell,\sigma_o,\vec{r}_o) \tag{4-10}$$

where σ_o and $\vec{r}_o$ refer to initial conditons. Evidently, the omission of all material properties with the exception of E implies that similarity of material properties is tacitly assumed.

Utilizing dimensional analysis, a complete set of dimensionless products can be generated from the dimensional matrix of the quantities in Eq. (4-10). The products presented in Table 4-2 should be useful for this task. The resulting dimensionless relationship could be of the following form

$$\frac{\sigma}{E} = f\left(\frac{\vec{r}}{\ell}, \frac{t}{\ell}\sqrt{\frac{E}{\rho}}; \frac{a}{g}, \frac{g\ell\rho}{E}, \frac{\sigma_o}{E}, \frac{\vec{r}_o}{\ell}\right) \tag{4-11}$$

If gravitational contributions to stress histories must be accounted for, the two terms containing the gravitational acceleration g very much so restrict the model analyst's freedom in selecting model materials and scale factors. Since there is almost no practical way that g can be changed between model and prototye, the value of g_r usually must be taken equal to one. Consequntly, from the dimensionless product a/g (Froude's Number, usually written as $v^2/\ell g$) it follows that

$$a_r = g_r = 1 \tag{4-12}$$

If this relationship is substituted into the design condition

$(g\ell\rho/E)_r = 1$, it follows that

$$\left(\frac{E}{\rho}\right)_r = \ell_r \qquad (4\text{-}13)$$

This scaling law places a severe limitation on the choice of suitable model materials.

Equation (4-13) is sometimes expressed in terms of one-dimensional wave propagation velocities, as follows:

$$v_r = \sqrt{\left(\frac{E}{\rho}\right)_r} = \sqrt{\ell_r} \qquad (4\text{-}14)$$

and is then referred to as the Couchy condition (based on Couchy's Number $\rho v^2/E$).

There are alternatives to the use of dimensional analysis as a way of arriving at the Froude and Cauchy criteria. For instance, one can examine the internal and external forces to which a structure of a given geometry is exposed. The most important of these are inertia, gravitational, and restoring forces (F_I, F_G, and F_R, respectively). Their relationships to material density, stiffness, length, and applied acceleration may be expressed as

$$F_I \sim \rho\ell^3 a$$

$$F_G \sim \rho\ell^3 g$$

$$F_R \sim \sigma\ell^2 = \varepsilon E\ell^2$$

In these expressions σ and ε are representative measures of stress and strain.

Independent of scale, F_I and F_G must bear instantaneously a fixed

ratio, as also must F_I and F_R. In a one-g field, the following parameters result from this requirement:

$$\frac{F_I}{F_G} \sim \frac{\rho \ell^3 a}{\rho \ell^3 g} \sim \begin{cases} \frac{a}{g} \\ \frac{v^2}{\ell g} \end{cases} \qquad \text{Froude's Number}$$

$$\frac{F_I}{F_R} \sim \frac{\rho \ell^3 a}{\varepsilon E \ell^2} \sim \begin{cases} \frac{\rho \ell a}{E} \\ \frac{\rho v^2}{E} \end{cases} \qquad \text{Cauchy's Number}$$

The ratio between Froude's and Cauchy's numbers produces a parameter $E/\ell\rho g$. If it is required that a replica model reproduce the full-scale values of those numbers, for fixed g, Eqs. (4-12) and (4-13) can be derived. Thus, Eq. (4-13) is a necessary condition for simultaneous replication of restoring forces, inertia forces and gravitational forces.

Additional design conditions are obtained from the other dimensionless terms of Eq. (4-11). For instance, it follows from the second term on the right-hand side that

$$t_r = \frac{\ell_r}{\sqrt{\left(\frac{E}{\rho}\right)_r}} = \sqrt{\ell_r} \qquad (4\text{-}15)$$

Since elastic and plastic strains are dimensionless, they must be instantaneously equal in the prototype and model structures. From this observation it follows that typical structural displacements are related by

$$\delta_r = \ell_r$$

This relation ensures that geometric nonlinearity in structural behavior is property simulated.

Table 4.3 shows in column (1) the scaling laws for several physical quantities for a true replica model. In this case the independent quantities are chosen to be ℓ, E and g, and g_r is taken equal to one.

Only one--but almost unsurmountable--difficulty exists in this true replica modeling, namely, the selection of a suitable model material. Exact material simulation goes far beyond simulation of modulus of elasticity, Poisson's ratio and strain; theoretically it should include all pertinent material properties discussed in Section 4.2, such as those defined by Eq. (4-5). Since no two materials in nature are exactly alike, material simulation will always introduce errors in the prediction values. The importance of these errors, or in many cases their insignificance, are the subject of a material study which is discussed in Chapter 5.

In the simplest case, similarity is necessary for the uniaxial stress- strain curve for the range of strains of interest. Since true replica modeling requires that $\varepsilon_r = 1$ (since ε is dimensionless), the stress-strain curves of model and prototype materials should be identical except for a constant stretching by the ratio E_p/E_m in the ε-direction (see Fig. 4.1).

Materials with shape-similar σ-ε diagrams are difficult to find, particularly if no distortion in the ε-direction ($\varepsilon_r = 1$) is permitted. Under certain conditions, strain distortion ($\varepsilon_r \neq 1$) may provide an interesting alternative to true replica modeling, an idea which is discussed in Section 4.5.3.

True replica models are extremely difficult to realize because of problems in material simulation. Nevertheless, for certain length scale

TABLE 4.3. SIMILITUDE LAWS

Scaling Parameters \ Model Type		True Replica	Artificial Mass Simulation	Gravity Forces Neglected*		Strain Distortion
				any material	prototype mat.	
		(1)	(2)	(3)	(4)	(5)
length	ℓ_r	$\underline{\ell_r}$	$\underline{\ell_r}$	$\underline{\ell_r}$	$\underline{\ell_r}$	$\underline{\ell_r}$
time	t_r	$\ell_r^{1/2}$	$\ell_r^{1/2}$	$\ell_r(E/\rho)_r^{-1/2}$	ℓ_r	$(\varepsilon_r\ell_r)^{1/2}$
frequency	ω_r	$\ell_r^{-1/2}$	$\ell_r^{-1/2}$	$\ell_r^{-1}(E/\rho)_r^{1/2}$	ℓ_r^{-1}	$(\varepsilon_r\ell_r)^{-1/2}$
velocity	v_r	$\ell_r^{1/2}$	$\ell_r^{1/2}$	$(E/\rho)^{1/2}$	1	$(\varepsilon_r\ell_r)^{1/2}$
gravitational acceleration	g_r	$\underline{1}$	$\underline{1}$	neglected	neglected	$\underline{1}$
acceleration	a_r	1	1	$\ell_r^{-1}(E/\rho)_r$	ℓ_r^{-1}	1
mass density	ρ_r	E_r/ℓ_r	**	$\underline{\rho_r}$	$\underline{1}$	$\varepsilon_r E_r \ell_r^{-1}$
strain	ε_r	1	1	1	1	$\underline{\varepsilon_r}$
stress	σ_r	E_r	E_r	E_r	1	$E_r\varepsilon_r$
modulus of elasticity	E_r	$\underline{E_r}$	$\underline{E_r}$	$\underline{E_r}$	$\underline{1}$	$\underline{E_r}$
specific stiffness	$(E/\rho)_r$	ℓ_r	**	$(E/\rho)_r$	1	$\ell_r\varepsilon_r^{-1}$
displacement	δ_r	ℓ_r	ℓ_r	ℓ_r	ℓ_r	$\ell_r\varepsilon_r$
force	F_r	$E_r\ell_r^2$	$E_r\ell_r^2$	$E_r\ell_r^2$	ℓ_r^2	$E_r\ell_r^2\varepsilon_r$
energy	$(EN)_r$	$E_r\ell_r^3$	$E_r\ell_r^3$	$E_r\ell_r^3$	ℓ_r^3	$E_r\ell_r^3\varepsilon_r^2$

*Can always be used for linear elastic models.
**See Section 4.5.2.
The scale ratios underlined are chosen by the investigator.

factors ($\ell_r = E_r/\rho_r$), suitable materials for the modeling of metallic structures can be found (see Chapter 5) and a pilot testing program on simple models of this type is discussed in Chapter 9.

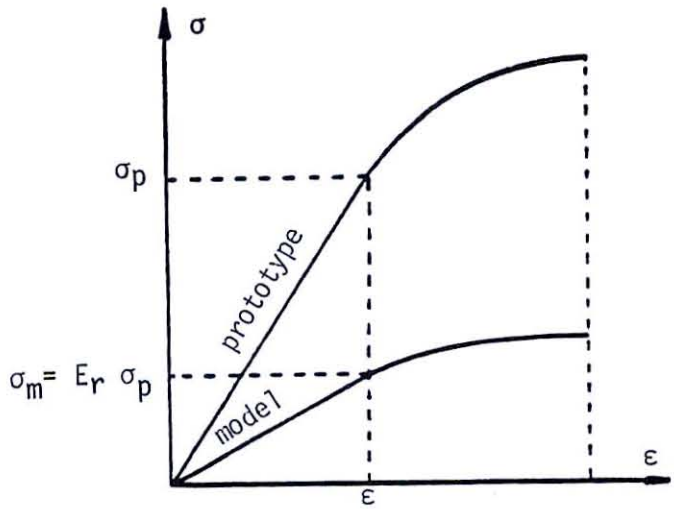

Figure 4.1 Stress-Strain Similitude Requirements

In many cases it is possible to find acceptable alternatives to true replica modeling which are based on compromises that minimize the errors in response prediction. Several of these alternatives are discussed in Sections 4.5.2 and 4.5.3; none of them will solve all the problems encountered in dynamic modeling but all are believed to be suitable for certain types of model studies concerned with particular parameters and structural configurations.

Model Testing in a Centrifuge: To overcome the difficulty of simultaneously reproducing restoring forces, inertia forces and gravitational forces, one could try to increase the effective value of g_m in the model test. It might be possible to achieve this by mounting a shake table in a suitable orientation on the cab of a large centrifuge. Also, it would have to be possible to bring leads from the cab so that required data can be recorded and processed on the outside. Let it further be hypothesized

that a uniform, parallel acceleration field is created over the entire model and, during centrifuge operation, that there would be no difficulty in applying the required earthquake acceleration a_m to the model. Thus, given "controllable gravity", it follows from $(g\ell\rho/E)_r = 1$ that

$$g_r \ell_r = \left(\frac{E}{\rho}\right)_r$$

As an example, one could choose the same materials for model and prototype; thus:

$$g_r = \frac{1}{\ell_r}$$

For small models, this last requirement might prove impractical. It would call for both very high rates of rotation in the centrifuge and for very high imposed acceleration levels a_m since $a_r = g_r = 1/\ell_r$.

In order to put this results in perspective, let us look at the NASA Ames Research Center twenty-g centrifuge described in the "Ames Research Facilities Summary, 1974". This facility can provide long-time exposure of up to 20g for a payload of up to 1200 (earth) pounds. No smaller than a twentieth-scale model of the same material could therefore be accomodated. With a roughly 1000 lbs. limit on the weight of this model, the weight of a prototype structure that could be modeled is limited to $1000 \times (20)^3$ lbs., or about 8,000 kips.

Alternatively, it is possible that a centrifuge might be employed with reduced E/ρ models. Thus, one might choose phosphor bronze, which has roughly half the E/ρ of steel. On the 20-g facility, one could then model, at 1/40 scale, structures of steel that weight up to 64,000 kips.

4.5.2 Adequate Models

All physical models which violate any of the design conditions discussed in the previous section could be called distorted models. However, if the effect of a distortion in one dimensionless product is such that it does not require an adjustment of other dimensionless products or of the prediction equation, then it appears appropriate to separate such models from truly distorted models. In this report such models are called adequate models.

The need for such models is based on the desire to use the same materials as in prototypes. However, the types of models discussed in this section are not limited to the use of prototype materials; in certain cases the use of different materials may make such models even more powerful tools.

There are two distinct "distortions" leading to two types of models which should prove very useful for model studies of certain classes of structures on shake tables.

1. Model Tests with "Artificial" Mass Simulation

Equation (4-13) for true replica modeling requires that model materials have a small modulus or large mass density or both. Since such materials are difficult to find, it appears attractive to augment the density of the structurally effective material with additional material which is structurally not effective. This can easily be achieved in lumped mass systems but may also be feasible for distributed mass systems as is discussed below.

(a) Lumped Mass Systems: For many types of typical building

structures it is acceptable to represent the seismically effective mass by a series of masses concentrated at the floor levels (lumped masses). In this case the seismically effective mass can be decoupled from the density of the structurally effective material which relaxes the dimensional requirement that $(E/\rho)_r$ must be equal to ℓ_r.

Cauchy's requirement for proper simulation of inertial forces and restoring forces can then be written as

$$\left(\frac{gM}{\ell^2 E}\right)_m = \left(\frac{gM}{\ell^2 E}\right)_p \qquad (4\text{-}16)$$

which for $g_r = 1$ becomes

$$M_r = E_r \ell_r^2$$

In this equation, M represents the lumped masses at the floor levels.

A word of caution has to be added to the seemingly trivial term "lumped mass." Such masses are those which are seismically but not structurally effective. In reality, any mass which is attached to structural components will affect the structural response. Masses at floor levels, such as a concrete slab system, will certainly affect the stress distribution in the structural elements and in many cases will be part of the structural system. Great care must be taken in positioning such "lumped masses" in models to simulate realistically the effects of gravitational and inertia forces. In may cases the distributed mass simulation discussed in (b) is preferable.

Nevertheless, when the structurally effective mass is small and a representation of the seismically effective mass by lumped masses is feasible, the structural model may be made of prototype material ($E_r = 1$) and lumped masses are then scaled in the ratio $M_r = \ell_r^2$. For small scale

model tests this often requires excessive weights which may render such tests impractical. The weight requirements may be reduced when model materials with small stiffness properties (E) are used (see Eq. 4-16).

(b) Distributed Mass Systems: For many types of structures a correct simulation of the mass distribution in space is essential and a simplified lumped mass system cannot be accepted. A simple way of testing adequate models of such structures would be to decouple the mass density ρ_o of the structurally effective material from an additive ρ_1, which is to be built into the model but has no counterpart in the prototype. Thus the full-scale density and stiffness would be represented by $(\rho_o)_p$ and E_p, whereas those for the model would be $(\rho_o)_m + \rho_1$ and E_m, respectively.

This modification would alter Cauchy's requirement as follows:

$$\left[\frac{g\ell(\rho_o + \rho_1)}{E}\right]_m = \left[\frac{g\ell\rho_o}{E}\right]_p$$

With one-g testing this relation leads to

$$(\rho_o)_r + \frac{\rho_1}{(\rho_o)_p} = \frac{E_r}{\ell_r}$$

or

$$\rho_1 = \left[\frac{E_r}{\ell_r} - (\rho_o)_r\right](\rho_o)_p \qquad (4\text{-}17)$$

For instance, for a 1/20 scale model using prototype material ($E_r = (\rho_o)_r = 1$) the density will have to be increased by a factor of 19. In a small-scale model, it takes considerable imagination to see how the material that increases the density by ρ_1 might be incorporated.

Much work needs to be done on this subject, since it is very

difficult to effectively separate the seismically effective mass from the structurally effective material. There are, however, instances where it seems quite practical. For instance, in structures consisting of slender load-carrying members, the scheme for adding mass could be to attach to each member suitable amounts of lead or other soft high density material, arranged in such a way that it contributes negligibly to the strength and stiffness but augments the weight and inertia. The spacing of these added masses should be maximized, so as to facilitate the manufacture while still adequately approximating a distributed inertia.

The modeling law for such distributed masses can be obtained by replacing the mass per unit volume ρ_o with some representative mass per unit length μ_o. When lead or other material with running mass μ_1 is attached to the model members, Cauchy's requirement then is altered to

$$\left[\frac{g(\mu_o + \mu_1)}{E\ell}\right]_m = \left[\frac{g\mu_o}{E\ell}\right]_p$$

With one-g testing this leads to

$$(\mu_o)_r + \frac{\mu_1}{(\mu_o)_p} = E_r \ell_r$$

or

$$\mu_1 = \left[E_r \ell_r - (\mu_o)_r\right](\mu_o)_p \qquad (4\text{-}18)$$

Using the same material in model and prototype would make $E_r = 1$ and $(\mu_o)_r = \ell_r^2$ (from $\rho_o = \mu_o/\ell^2$). This leads to the requirement

$$\mu_1 = (\ell_r - \ell_r^2)(\mu_o)_p \qquad (4\text{-}19)$$

This law may or may not be practicable, because it calls for adding a lot of mass. For instance, for linear elements of a 1/20 scale model of identical structurally-effective material, $(\mu_o)_m$ is 1/400 of $(\mu_o)_p$

whereas μ_1 is 1/21 of $(\mu_o)_p$ hence 19-times as massive per unit lengths as the basic model structure.

It appears that the practical realization of this scheme for small scale models in many cases will call for using reduced E/ρ_o model materials. The use of such materials (which need not obey the requirement $(E/\rho)_r = \ell_r$) will require a lesser amount of added μ_1 which might enable the model designer to reach much more desirable compromises in the choice of materials and added weights.

As an example, the combination of lumped masses and model materials other than those of the prototype could prove to be useful in case of truss type structures such as transmission towers, drilling towers, radar stations, etc. For instance, in the case of a radar station it would be improper to neglect the weight of the members and account only for the radar screen weight; on the other hand lumping of the masses at the joints or at the best at a few points along each member seems to be sufficiently precise. Use of a model material of lower E/ρ than that of the prototype material will help to keep those masses down to manageable sizes. Construction of this kind of model seems to be relatively simple provided the joint area is not of critical importance.

The modeling laws summarized in column (1) of Table 4.3 apply to the cases discussed in (a) and (b) with the exception of the requirement $(E/\rho)_r = \ell_r$. For the case of identical prototype and model material $(E_r = 1)$ the modeling laws are shown in column (2) of the table.

Models with "artifical" mass simulation have been used extensively in the past for static and dynamic model studies. References 45 to 58 are examples of the application of such models in the field of earthquake

engineering. Particularly, multistory buildings and bridge structures appear to be well suited for these types of studies. Such model studies are expected to result in a good prediction of prototype behavior provided that mass distribution is properly simulated, the ground motion is reproduced according to the laws of similitude, model design and construction is done according to prototype procedures, and last but perhaps most important, a thorough material study has proven the adequacy of material simulation. It is expected that model tests with "artificial" mass simulation will remain a very important source of information on structures whose stress and displacement histories have to be simulated in the elastic and inelastic range and whose materials are difficult or impossible to simulate by other than prototype-like materials, such as in the case of reinforced concrete structures.

2. Model Tests Without Simulation of Gravity Forces

Considering at this time only building structures, it appears that for certain types of structural configurations the stresses induced by gravity loads are small and maybe negligible compared to stress histories generated by seismic motions. In this case $(a/g)_r$ need not be equal to one, which allows considerably more freedom in selecting model materials and scaling parameters.

The scaling laws can be derived from the remaining dimensionless products of Eq. (4-11), with g in $g\ell\rho/E$ replaced by a. If ℓ and E as well as ρ of a specific model material are selected as the independent quantities, the scale factors shown in column (3) of Table 4.3 can be derived. If prototype material is used (i.e., $E_r = \rho_r = 1$), all scale factors can be expressed in terms of ℓ_r, see column (4) in Table 4.3.

It is important to note that the scale factors for many physical

quantities are different from those for true replica models which will affect the shake table input, the model design and the response prediction. For instance, when prototype material is used (column (4) in Table 4.3), with $t_r = \ell_r$ and $a_r = \ell_r^{-1}$, a reproduction of actual seismic motions on commercially available shake tables may cause problems. This again invites the use of other than prototype materials with $(E/\rho)_r$ smaller than one. For instance, if brass is used for the simulation of steel, $(E/\rho)_r$ is approximately 0.5 which results in $t_r = 1.41\ell_r$, $v_r = 0.71$, and $a_r = 0.5\ell_r^{-1}$. With these values, seismic motions become more easily reproducible on shake tables.

A building system which may be suitable for this type of model testing is a $K = 0.80$ building, i.e., a structural system where the lateral load resisting system consists primarily of shear walls which carry little vertical loads except through boundary elements. In slender shear walls the level of stress due to vertical loads in the boundary elements will usually be small and will not affect the response of a shear wall to a significant degree. Clearly, even a $K = 0.80$ building will not be replicated "precisely" through a model of this type since the stress level in the moment resisting space frame surrounding the shear walls is not properly simulated. However, considering the low stiffness of this frame compared to the shear wall, from such model tests one can expect reliable information on shear walls far into the inelastic range.

Considering steel structures, let us look at a multistory braced frame without moment resisting connections. In most types of bracing systems the stresses in the bracing members due to vertical loads will be negligible compared to those induced by lateral loads. Thus, the response of bracing members will be replicated through model tests of the type discussed herein. However, a simulation of the load-deformational

response of the structure will require proper modeling of, at least, the vertical elements of braced bays.

Let us investigate a braced frame of the type shown in Fig. 4.2.

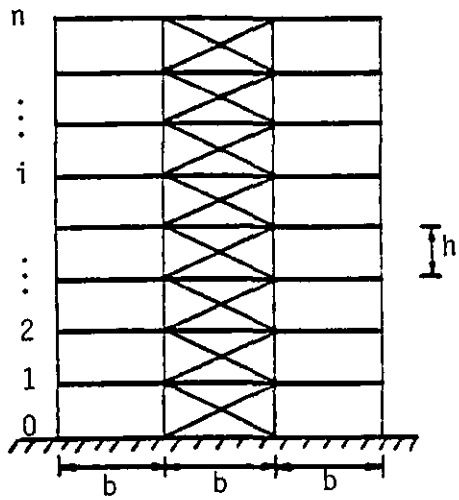

Figure 4.2 Braced Frame

Assuming uniform distribution of dead load w_D(psf) and live load w_L(psf) and a triangular lateral load distribution, an approximate analysis shows that the ratio of axial column loads due to seismic and gravity forces above level i is given as

$$\left(\frac{P_{EQ}}{P_G}\right)_i = \alpha \frac{W_D}{W_D + W_L} \frac{3hn}{b(n-i)} \frac{\sum_{j=i+1}^{n} j(j-i)}{\sum_{j=1}^{n} j}$$

where α is a seismic coefficient defined by base shear $V = \alpha W_D$.

For the ground floor (i = 0), this equation reduces to

$$\left(\frac{P_{EQ}}{P_G}\right)_0 = \alpha \frac{W_D}{W_D + W_L} \frac{3h}{b} \frac{\sum_{j=1}^{n} j^2}{\sum_{j=1}^{n} j}$$

For braced frames with b = 2h and w_L = 0 (a rational assumption for model tests) one obtains the force ratios given in Table 4.4

Table 4.4

i \ n	P_{EQ}/P_G			
	5	10	20	30
0	5.5α	10.5α	20.5α	30.5α
5		7.1α		
10			13.4α	24.4α
20				14.4α

Assuming the seismic coefficient α to be of the order of 0.1 to 0.3, it can be seen that the effect of gravity loads becomes less significant with an increasing number of stories. This leads one to believe that a replication of gravity loads may sometimes not be necessary for this type of frame.

Model tests of the kind described here appear attractive since they permit the use of prototype material. Nuclear reactor containment vessels are another type of structure where such tests appear quite feasible since the effects of gravity loads are small compared to the effects of internal pressurization and severe ground motions. It usually is up to the model designer's judgement to decide whether or not the errors introduced by neglecting gravity effects are acceptable. If the errors are too large, true model distortion is evident and either the prediction equation or other dimensionless products have to be modified to compensate for the error. When material or geometric nonlinearities are involved in the problem, this will be an extremely difficult task.

However, when the model test is only concerned with linear elastic behavior, gravitatinal effects can be decoupled from seismic effects and

can always be neglected in the derivation of similitude law. Thus, the scaling laws in columns (3) and (4) of Table 4.3 can always be used for linear elastic problems, regardless of the importance of gravity effects. This makes model design for linear elastic tests very simple since the only material contraints are that of a linear elastic range characterized by E and, where needed, similitude of Poisson's ratio ν and material damping properties.

4.5.3 Distorted Models

The use of truly distorted models for seismic studies of nonlinear problems is rather limited since it rarely will be possible to find adequate corrections to the prediction equation or other physical quantities, to account properly for the violation of an important design condition.

One could attempt, for instance, to design a model where gravity effects are only partially simulated through the addition of "artificial" masses to reduce the error introduced when all gravity effects are neglected. Such a "mixed" model would be governed by similitude laws which are a compromise of those listed in columns (2) and (3) of Table 4.3. Thus, the scale factors for the quantities governing the seismic input to the model (t_r, v_r, a_r) will need to be re-evaluated through physical insight or an auxiliary testing program.

Alternatively, one could try to properly simulate spatial geometry of the structure but distort the geometry of the cross section such that gravitational and inertial forces produce the correct level of stress in each member as well as correct displacement similtitude ($\sigma_r = \ell_r$). Using prototype material for the model one arrives, from $\varepsilon_r E_r \ell_r^2 = \rho_r \ell_r^3$, at

the following similitude laws:

$$A_r = \ell_r^3, \qquad A_r^s = \ell_r^3$$

$$I_r = \ell_r^5, \qquad J_r = \ell_r^5$$

This shows that simultaneous replication of axial load, shear, bending and torsional effects will not be possible. However, the possibility exists to change the shape of the cross section such that close similarity between A, A^s, I and J may be achievable.

Both of these alternatives will have limited applicability and are not pursued further in this project. However, another type of distortion, namely strain distortion, shows certain promise for small scale model studies provided that no geometrical nonlinearities are expected.

The requirement of identical strains in model and prototype ($\varepsilon_r = 1$, see Fig. 4.1) is often difficult to fulfill from the standpoint of availability of suitable model materials. It is much easier to find shape-similar materials if a stretching by $\varepsilon_r \neq 1$ in the ε-direction is permitted as is illustrated in Fig. 4.3.

To account for strain distortion in cases where small displacement theory holds true throughout the experiment (i.e., no secondary effects are involved), Rocha (Ref. 103) proposed the introduction of an artificial fundamental quantity D for strain measurement. When this term is included in the dimensional matrix in the addition to M, L and T, and a dimensional exponent of 1 is assigned to the quantities dependent on ε, the following dimensionless functional relationship can be obtained:

$$\frac{\sigma}{E\varepsilon} = \overline{f}\left(\frac{\vec{r}}{\ell\varepsilon}, \frac{t}{\ell}\sqrt{\frac{E}{\rho}}; \quad \frac{a}{g}, \frac{g\ell\rho}{E\varepsilon}, \frac{\sigma_o}{E\varepsilon}, \frac{\vec{r}_o}{\ell\varepsilon}\right) \tag{4-20}$$

For $a_r = g_r = 1$, the following similitude laws can then be derived:

$$\left(\frac{E}{\rho}\right)_r = \frac{\ell_r}{\varepsilon_r} \tag{4-21}$$

$$t_r = \sqrt{\ell_r \varepsilon_r}$$

and

$$\delta_r = \ell_r \varepsilon_r$$

These and other similitude laws derived from Eq. (4-20) are shown in column (5) of Table 4.3.

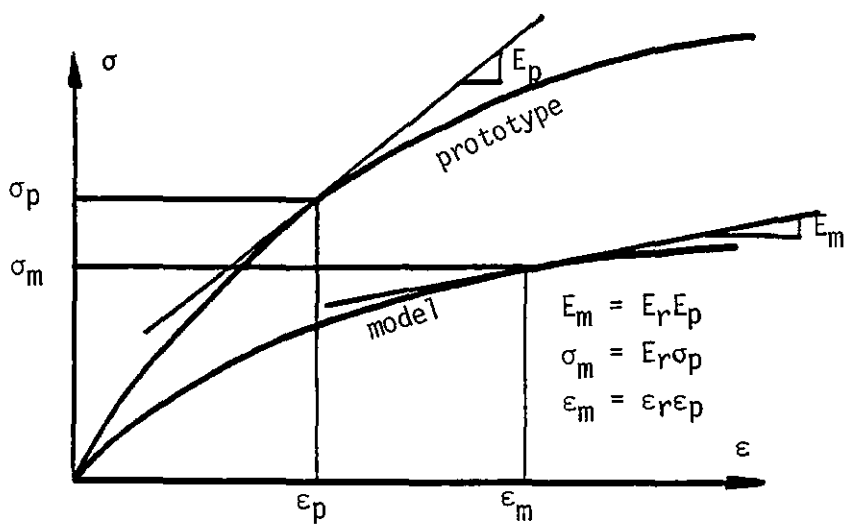

Figure 4.3 Stress-Strain Diagram -- Strain Distortion

As the development of these similitude laws is based on the somewhat philosophical idea of a fundamental strain quantity and assumes linear dependence of selected physical quantities on this fundamental quantity, further study is needed to prove the feasibility of this distortion for inelastic model studies. Assuming that the similitude laws of column (5) of Table 4.3 adequately account for strain distortions, it may prove to be very useful for modeling of problems where geometric nonlinearities

are known to be insignificant. The restrictive requirement $(E/\rho)_r = \ell_r$ for materials for true replica models can then be relaxed to $(E/\rho)_r = \ell_r/\varepsilon_r$ which permits considerably more freedom in the choice of suitable model materials. For instance, it may be possible to fabricate small scale models of steel structures made of certain copper alloys ($E_r \simeq 0.5$, $\rho_r \simeq 1$) without artificial mass simulation, presuming that it is possible to anneal the alloys such that they have a yield strength of $(\sigma_y)_m = (\sigma_y)_p E_r \varepsilon_r = (\sigma_y)_p E_r \ell_r/(E/\rho)_r \simeq \ell_r$ for $\rho_r \simeq 1$. However, this also implies that $\varepsilon_r \simeq 2\ell_r$ (for $E_r \simeq 0.5$) and $\delta_r \simeq 2\ell_r^2$ which will require very sensitive instrumentation.

Other types of inadvertently caused model distortions often have to be considered, primarily those caused by inadequate material simulation such as distortions in Poisson's ratio, hysteretic energy dissipation, strain rate effects, etc. Such unintentional distortions are sources of errors and can rarely be accounted for through modifications in the dimensionless functional relationship of the problem. These errors are discussed in more detail in Chapter 5.

4.5.4 Summary

Dimensional analysis has been used to derive modeling laws for various types of model tests of structures subjected to seismic motion. At the outset it has to be realized that an exact replication of all parameters affecting the response of structures under dynamic actions can rarely ever be achieved. The emphasis in this study is directed towards identification of important parameters and possible types of model tests which allow, as exact as possible, replication of these important parameters.

Although most of the modeling laws presented herein are generally applicable, emphasis was placed primarily on model studies of prototypes of homogeneous isotropic material such as steel. The model test results obtained in this study are encouraging and lead one to believe that many types of steel structures can be modeled with sufficient accuracy. A final answer can only be obtained through a series of model tests, which can directly be compared with prototype studies. It needs to be pointed out that, in this study, only primary structural elements have been considered and no interaction between structural and nonstructural elements is included.

The choice of the right type of model for the intended purpose and the degree of approximation that must be accepted are of primary concern to the model analyst. In the most general case of a complex three-dimensional structure, where gravity and inertia effects are equally important, a true replica model is the ideal choice provided that a suitable model material can be found. If this is not possible, adequate accuracy in model tests can often be achieved by means of model tests with "artificial" mass-simulation. In cases where prior knowledge shows that gravitational effects are sufficiently small compared to seismic effects, model tests without simulation of gravity forces are feasible alternatives. These three types of model studies are believed to be the most suitable ones for the replication of seismic response phenomena by means of small shake tables.

CHAPTER 5

EVALUATION OF MODEL MATERIALS

5.1 INTRODUCTION

Providing the right model material whose properties are well documented in the literature and which properly simulates the behavior of the prototype material has always been a major obstacle to the acceptance of model tests as a verification of prototype response, and has raised continuous suspicion as to the reliability of model test results. This holds particularly true for dynamic tests to failure which are of primary interest in experimental work in earthquake engineering.

The demands placed on a model material can easily be defined but the search for a suitable material and a verification of its suitability are a formidable task. Ideally, a model material should provide similarity of all material properties discussed in Section 4.2, i.e., the listed thermal and mechanical properties should be identical to those of the prototype material after the application of scaling laws. In the simple case of a unixial stress-strain relationship (see Eq. 4-5) this requires similarity of the derivatives of stress with respect to strain, time, and temperature, and of strain with respect to time. Fortunately, in practical modeling problems, similarity is only required for those material properties which affect significantly the response quantities of interest in the study. An a priori knowledge of these relevant material properties, derived from physical understanding of the problem, is important for every model study since it may simplify the search for a suitable model material.

Even then, satisfactory model material will be difficult to find, particularly for dynamic studies in the inelastic response domain.

Firstly, a model material must be readily available, reasonably inexpensive and, above all, must be easily adaptable to structural shapes and must allow a simulation of prototype fabrication of member connections. Secondly, one must realize that no two materials are alike and compromises in material simulation must be accepted. Even a prototype material will not simulate mechanical properties properly in the time and length domain due to strain rate and size effects. It is imperative, therefore, in a model study, to isolate the material properties which must be simulated and those which can be compromised. Also, the errors encountered due to improper simulation of material properties must be evaluated as to their importance in response prediction.

Since this study is concerned primarily with dynamic models of steel and reinforced concrete structures, emphasis in material modeling is placed on the simulation of structural steel, concrete and steel reinforcement.

Successful studies on ultimate strength models of steel prototype structures have been reported by several researchers who used either prototype material (i.e., Refs. 31, 58, 85, 86) or non-ferrous metals (i.e., Ref. 38). Results of material tests on structural steel and on copper alloys performed in this study are reported in Chapter 6.

For modeling of concrete structures subjected to inelastic deformations it is hardly ever possible to use anything but concrete-like materials such as microconcrete, cement mortar or gypsum mortar. The static properties of model concrete and model reinforcement are well documented in the literature (Refs. 18, 36, 39, 115 to 117, 120, 145, 147), while much less is known about the properties under dynamic test conditions (Refs. 39, 122, 146, 149). A significant portion of this study is devoted to modeling of reinforced concrete. Techniques adopted

in the fabbrication and testing of microconcrete and reinforcing wire are discussed in Chapter 7 together with the results of static and dynamic tests of these materials. Chapter 8 provides a discussion on the fabrication, testing and test results of reinforced microconcrete beams. Both static and dynamic behavior are considered.

In this chapter, the properties which are expected to affect the dynamic response in the elastic and inelastic range are identified and their simulation requirements are briefly summarized. A material testing program is discussed which should provide the information necessary for the evaluation of the pertinent material characteristics. The chapter includes also a section on laboratory equipment and instrumentation needed for the implementation of such a program.

5.2 MECHANICAL PROPERTIES OF INTEREST

When it is necessary to simulate the complete load-deformation response of a structure from zero load to failure, ideally the following material properties should be simulated:

1. Stress-Strain Diagram from Unixial Load Tests: If no strain distortion is allowed this will require point by point equality of the ratio σ/E, in prototype and model material, where E is the modulus of elasticity or some other representative stiffness property, and σ is any elastic or post-elastic stress value on the σ-ε diagram. In other words, the stress-strain curves of model and prototype materials should be identical except for a stretching by the ratio E_p/E_m in the σ - direction (see Fig. 4.1). This requirement is often difficult to fulfill as will be shown in the case of individual materials. However, exact simulation of the monotonic stress-strain behavior may not be of the utmost importance

in cases where the material (whether single or composite) is known to be subjected to inelastic stress reversals. In seismic response studies the requirement that the amount of energy dissipated by the material be properly simulated is of primary importance. Ideal simulation would mean that at all strain amplitudes the shape and area of hysteresis loops should follow the modeling law. Again, this may be difficult to achieve entirely, but prototype and model materials should have similar strain hardening or softening tendencies and shape similar hysteresis loops in the strain range of interest.

It should be observed that a simple tension test or a cyclic load test of the prototype and model material is a model study by itself, and hence should fulfill similitude laws such as strain rate scaling and scaling of the geometry of the specimens. The importance of this observation will become apparent in the next few points.

2. Poisson's Ratio : In the discussion of modeling theory it was stressed that all dimensionless quantities should be equal for model and prototype. This applies also to Poisson's ratio unless the error introduced by a distortion of ν is negligible or can be accounted for through modification of other physical quantities. Approaching the modeling theory through the equation of state defining the response of the prototype enables the investigator to approximate the error involved in the misscaling of ν. For instance, Hossdorf (Ref. 1) shows that for a bar subjected to a considerable amount of torsion, the π quantity ν could be replaced by a different dimensionless product of the form:

$$\pi = \frac{EI}{GJ_T} = \frac{I}{(1 + \nu)J_T}$$

Thus, the prediction error for torsional response will not be propor-

tional to the respective ν values, but will be proportional to the $1 + \nu$ values. For example, if $\nu_p = 0.3$ and $\nu_m = 0.2$, the difference between $1 + \nu_p$ and $1 + \nu_m$ is only about 8 percent.

The possibility of accounting for distortions in ν through modifications of related physical quantities can be illustrated in the example of the vibration of a simply supported plate (Ref. 96). The governing equation for small transverse bending vibration of a thin plate is

$$\frac{\partial^4 w}{\partial x^4} + \frac{\partial^4 w}{\partial y^4} + 2\frac{\partial^4 w}{\partial x^2 \partial y^2} = -\frac{\rho}{E}\frac{3(1-\nu^2)}{h^2}\frac{\partial^2 w}{\partial t^2}$$

For true dynamic replica modeling it must hold that $(E/\rho)_r = l_r$ and $t_r^2 = l_r$, thus, dimensional homogeneity will require that $((1-\nu^2)/h^2)_r = 1/l_r^2$ This condition permits the derivation of a separate scale for the half thickness h of the plate as $h_r = l_r\sqrt{(1-\nu^2)_r}$.

Hence, in many practical cases it is possible to evaluate the influence of Poissons's ratio on the load-deformation response of the structure. When found to be of a minor importance (probably in a majority of building structures), a compromise in the modeling of ν is acceptable.

3. Material Damping: The importance of this parameter in material simulation depends on the definition given to this term. Damping in structures subjected to severe earthquakes will be caused, amongst other factors, by anelastic material damping (the energy dissipated by a material within a hysteresis loop without permanent strain offset), actual hysteretic damping (associated with a permanent strain offset), and friction type damping at interfaces between structural materials (e.g., at bolted connections) and between structural and nonstructural elements.

The anelastic material damping depends greatly upon the stress or strain amplitude (Refs. 170, 171) and although its value can be of signi-

ficance in the elastic cycles, once the linear range of material behavior is exceeded, it is small compared to other damping contributions and is not investigated further in this study. Hysteretic damping at strain amplitudes beyond the yield level is a matter of shape and size of the hysteresis loops which can be compared directly between prototype and the model material. As such, this covers material damping in steel but not necessarily material damping in materials and composites which exhibit a nonlinear range between the proportional limit and the designated yield strength. This range may be a source of significant difference in damping between the prototype and model materials. It will be necessary, therefore, to evaluate this damping in model materials, at various stress levels, by means of the damping tests discussed in the next section.

Simulation of friction-type damping is a problem which may greatly affect the response of structures but is not included in this material study. Actual model tests are necessary to evaluate structural damping as a whole and to provide answers regarding the adequacy of the simulation of this type of damping.

4. Strain Rate Effects: It is well known that high strain rates will affect the σ-ε diagram. For structural steel they will cause a distinct increase in the yield strength, a negligible increase in the tensile strength, and a decrease in the ductility of the material. For concrete, they will cause a significant increase in compressive strength (f'_c), a noteworthy increase in initial stiffness (E), and a decrease in the strain at f'_c.

The understanding of such phenomena is of importance for two main reasons: first, to estimate the dynamic properties of the prototype material based on the values obtained in static tests, and second, to account for different strain rates in the prototype and in the model. To

illustrate the second problem, the empirical formula derived by Nagaraja (Ref. 151) for mild steel is presented:

$$(\sigma_y)_d \; / \; (\sigma_y)_s = 1 + 0.762 \; \dot{\varepsilon}^{0.26}$$

where $\dot{\varepsilon}$ represents the strain rate in sec^{-1}.

Since the strain rate in the model test will be scaled by the factor $1/t_r$, the increase in yield strength due to strain rate effects for an ideal model material should follow the rule

$$(\sigma_y)_d \; / \; (\sigma_y)_s = 1 + 0.762 \; (t_r \dot{\varepsilon})^{0.26}$$

This expression shows that the use of prototype material is not ideal for model tests; it will exhibit too large a yield strength, although only by a small amount except for very high strain rates.

5. Long-Time Effects: In theory, simulation of initial conditions will require the tracing of all time-history events affecting the prototype from the time of construction to the time at which the dynamic event takes place. These events will include, amongst others, time-dependent material effects such as creep, shrinkage and increase of compressive strength of concrete. A study of these phenomena was not part of the reported research and only a short discussion follows in subsequent sections.

6. Size Effects: The increase in strength with decreasing size of specimens has been studied by various researchers for both steel and concrete materials. Nevertheless, only fragmentary data can be found in the literature on size effects of mild steel and even less precise information is available on these effects for concrete. In part, the size effects can be accounted for by carrying out the material studies on specimens comparable in size to the smallest dimension of model structural elements. Specific size effects, such as strain gradient effects and effects related to fabrication (e.g., weldments), can hardly ever be a-

voided and deserve attention in the evaluation of model test results. In particular, a simulation of crack initiation and propagation at weldments cannot be achieved at reduced scales and should not be attempted in model tests.

7. Ductility: Sufficient evidence is available to prove that high strain rates will decrease the ductility of materials. Size effects will also change the ductility characteristics. Within structural elements the changes in ductility characteristics of metal model materials should be of negligible consequence; however, the fracture characteristics at connections (in particular at welds) are size dependent (see previous paragraph) which in turn may affect the inelastic deformation capacity of model elements. In model elements of reinforced concrete structures the element ductility will depend not only on the ductility of the component materials but also on the bond characteristics and fabrication details as is discussed in Chapter 8.

8. Means of Fabricating Elements: Elements of models of steel structures may be fabricated from model material by means of machining, casting, extruding, rolling, welding, soldering, or glueing. Possible changes in material characteristics through any of these processes must be closely controlled. Suitable fabrication techniques are discussed in detail in Ref. 58.

5.3 MATERIAL TESTS - EXPERIMENTAL FACILITIES

In order to perform a successful model material study, a specialized testing system must be developed which consists of suitable testing facilities, instrumentation and a data acquisition system. The following paragraphs summarize the experience gained and the observations made during

this study with regard to the three components of a suitable testing system.

5.3.1 Testing Equipment

Under this heading such elements as testing machines, support frames and gripping devices are included. The main objectives in the design of testing equipment are to provide the necessary load application capacity and control over the applied force and reliable and simple gripping of the specimen. The desired characteristics of the system will depend greatly on the type of tests to be performed and also on the geometry and strength of the specimens.

5.3.1.1 Uniaxial Load Test Facilities

This group includes facilities for monotonic tensile, monotonic compressive and cyclic tests. The tests can be performed either at static or at dynamic rates.

One of the major problems in this type of tests is the relative stiffness of the testing system compared to the stiffness of the specimen, and simultaneously the ability of the system to respond fast enough to the information provided by the control device (strain, stroke or force control device). This is of particular importance when a rapid change in specimen stiffness is expected (upper yield in mild steel, compressive strength in concrete) and specimen behavior beyond that point is of interest. High rate loading places particularly high demands on the resolution capacities of the testing facilities. To overcome the problem caused by relatively stiff concrete specimens with a rapid strength loss at f'_c, methods of artificial stiffening of the testing system have been

employed by various researchers (Ref. 126 to 130). Wang, et. al., (Ref. 126) used a case hardened steel tube which was compressed elastically together with the concrete specimen and which prevented a rapid change in the resistance capacity to the applied load after the ultimate capacity of the concrete specimen had been reached. This approach requires a testing machine of load capacity much higher than that of the specimen tested and is limited to strains below the proportional limit strain of the steel sleeve.

A solution to the problem of insufficient stiffness of the testing machine could be provided by an "ideal" closed-loop system (soft system) which would respond instantaneously to the signal of the controlling device. These conditions are becoming increasingly attainable with the increasing sophistication of electronically controlled testing equipment. It should be stressed that even the simplest material test cannot be designed without a close correlation with the capacities of the testing equipment.

In this study, the uniaxial load tests were carried out on an MTS 10,000kG (98kN, 22 kips, model 810.015) closed-loop testing system. The load in this uniaxial system is applied through the movement of an hydraulic actuator. This movement is controlled electronically either through an LVDT monitoring displacement of the actuator (stroke control), a load cell monitoring load applied to the specimen, or a clip extensometer monitoring average strain (displacement between two points) in the specimen (strain control). Each of the controlling devices is suitable for different types of tests. Load control is used in cases in which no sudden change in the stiffness of the specimen occurs, thus usually for elastic tests. Stroke control can be used for displacement control tests

on relatively soft specimens. This control is unsuitable for relatively stiff specimens, as the monitored displacements include the deformations within the testing system (machine frame and actuator displacement, load cell and gripping device deformation). In those cases and in cases in which strain control is desired, an extensometer can be used for the control of the test.

All the tests on metal specimens were strain controlled, and compression tests on microconcrete cylinders were controlled by the extensometer monitoring the change in distance between the plattens.

For simple tension tests of steel specimens, standard MTS hydraulic tension-compression grips were used for gripping the test specimens since small preloads and misalignment inherent in the use of this grip proved to be of no significant influence. However, the problem of testing materials of lower strength than that of steel, the use of small specimens necessitated by scaling of length, and the need for cyclic testing with excursions into the compressive range required better alignment than could be achieved with the standard MTS grips. This problem was solved through the fabrication of a special "self aligning" Woods metal grip similar to that developed by Morrow (129). A sketch of this grip is presented in Fig. 5.1 and a test specimen embedded in the grip and mounted on the MTS system is shown in Fig. 5.2.

The gripping procedure was as follows:

1. Thread and lock the specimen into the load cell attached to the MTS crosshead and into the inner part of the grip.
2. Heat the fusible alloy in the grip by running saturated steam through the heating-cooling spiral in the outer sleave of the grip. (Fusible alloys = easily meltable alloys whose eutectic temperatures are below

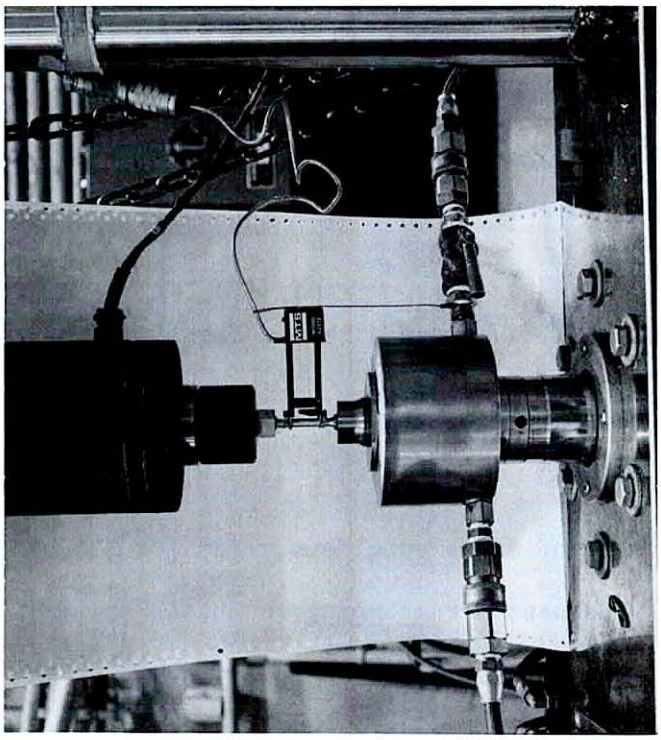

Figure 5.2 View of Setup for Uniaxial Test of Metal Specimen

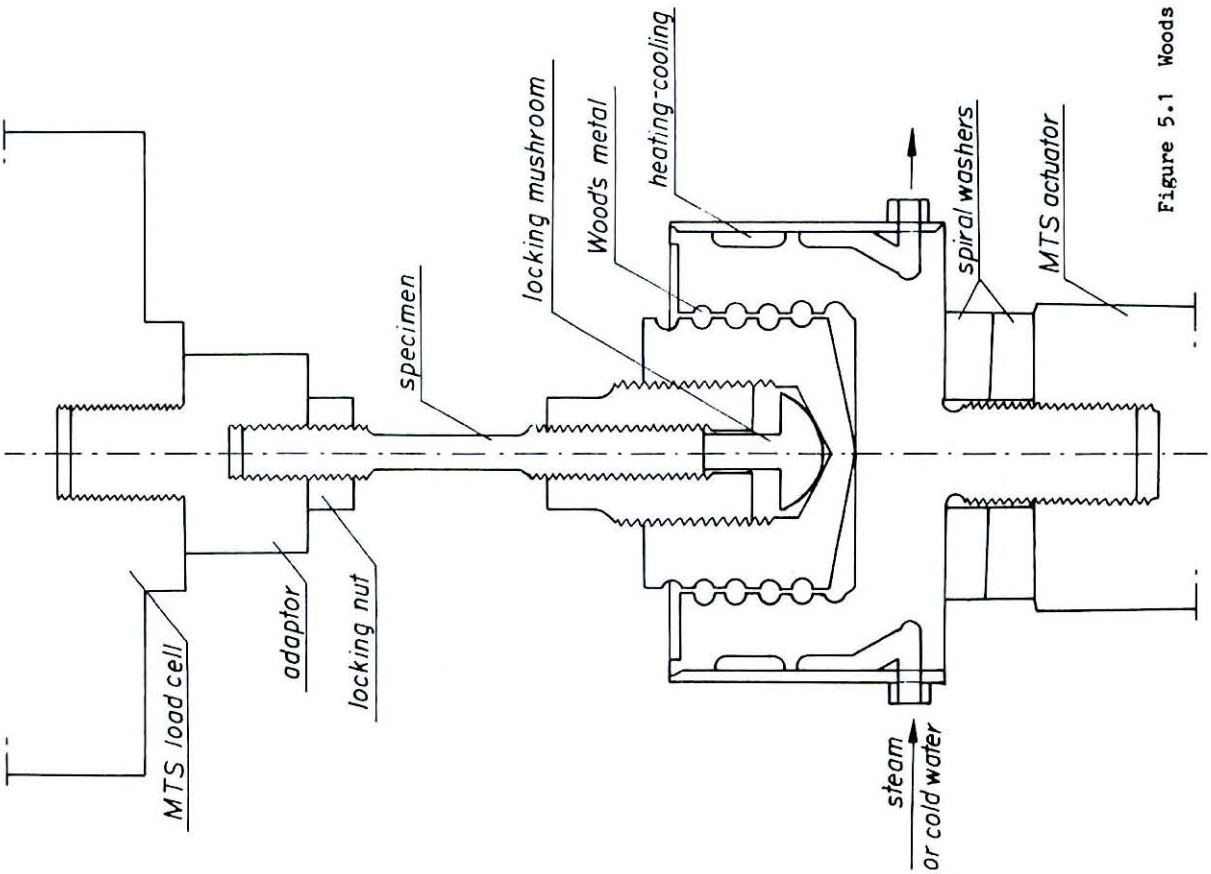

Figure 5.1 Woods Metal Grip

the melting temperatures of the alloying constituents; Woods metal used is the product of alloying 50% of bismuth, 25% of lead, 12.5% of tin and 12.5% of cadmium with the resulting melting temperature of about 70°C, and with positive volume change in the cooling process).

3. Lower the crosshead till contact develops between the parts of the grip.
4. Activate the MTS actuator under load control to produce a minimal compressive load.
5. Cool the alloy by running cold water through the spiral.
6. Switch the control to the extensometer attached to the specimen.

5.3.1.2 Component Test Facilities

As will be discussed later, component tests are often necessary to permit a reliable correlation between prototype and model response, and to aid in an evaluation of the feasibility of specific model materials.

In this study, the pseudo-static and dynamic behavior of components was studied by means of subassembly tests of the type shown in Fig. 5.3. These tests were carried out on the MTS testing machine utilizing a specially designed erector-type rigid test frame which is shown in Figs. 5.3 and 5.4. The frame was constructed in such a way as to permit its translation and rotation respect to the MTS machine and to allow the testing of specimens of different configurations. For the specimen shown in Fig. 5.3, ball bearing hinges were fabricated to provide low friction support for the column of the subassembly. Monotonic or cyclic loads can be applied to the tip of the cantilever beam by means of the MTS actuator. Lateral support of the beam is provided by pairs of teflon padded vertical rails attached to the test frame at specified locations.

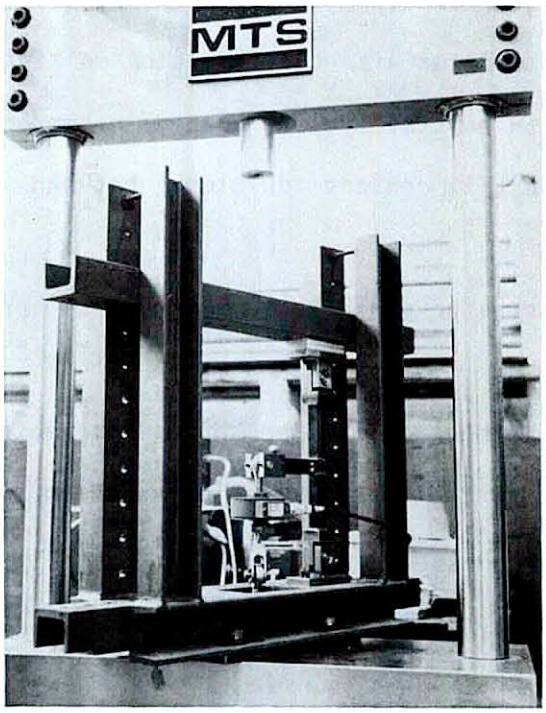

Figure 5.3 View of Component Test Setup

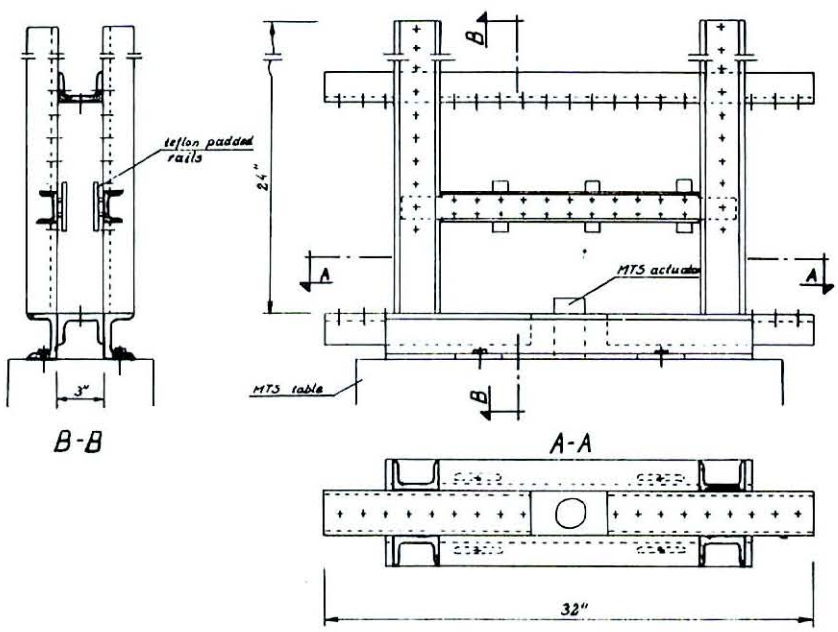

Figure 5.4 Test Frame for Component Testing

A different type of subassembly which was tested in this support frame is shown later in Fig. 8.2.

5.3.1.3 Load History Control

The capability for the reproduction of various load histories is of basic importance in material test studies. Mills, et. al., (Ref. 58) discuss wave forms which may be used to control material tests. The subsequent paragraphs present a summary of the major points of that discussion.

Three basic functions are commonly used for the test history control, namely ramp function, triangular wave and sinusoidal wave. Each of these waves can be used with shifted origin thus resulting in cycles with positive or negative mean load, displacement or strain. Numerical, computer-generated random histories can be converted to analog form (continuous voltage output) and used for test control.

As rate of loading is of considerable importance in material testing for dynamically loaded models, it is necessary to evaluate this parameter for consistent correlation between the tests. Ramp loading and triangular wave forms provide constant testing rate throughout the entire time history. Sinusoidal waves result in a rate varying from a maximum near the axis of symmetry to zero at the peak of the wave, and thus only a mean rate can be estimated. Despite this disadvantage, a sinusoidal wave form proved to be very suitable for cyclic studies. It provides a smooth change of the direction of the loading and also resembles more closely the loading history which the specimen undergoes within the structure during a dynamic motion.

In this study, ramp functions were used for the control of monotonic

testss and sinusoidal functions were used for the control of cyclic material and component tests.

5.3.2 Instrumentation

Standard instrumentation for experimental model analysis is discussed by Mills, et. al., (Ref. 58). In this section, only a brief review of the instrumentation used in this study is given with the emphasis on the instrumentation developed for special measurements in material and component tests.

In addition to the previously mentioned instrumentation belonging to the standard equipment of the MTS testing machine, e.g., linear variable differential transducers (LVDT) for displacement control, load cells of various sensitivity depending upon the load applied, and clip extensometers for the measurement of small length changes which permit an assessment of average strain, the following instruments were used in this study:

- o LVDTs used to measure deflections in component tests
- o strain gages used to calibrate the instrumentation and to measure localized strains in flexural metal elements
- o mercury gage extensometers used for the measurement of average strain in compressed concrete cylinders
- o mercury gage extensometers for the measurement of average curvature in component study of reinforced microconcrete cantilever beams.

The necessity for instrumentation capable of measuring accurately very small displacements (of the order of 0.005 mm, 2×10^{-4} in.) is evident in material studies. In the studies on model materials and compo-

nents an additional demand is imposed, namely that the instrumentation be of a minimal size. Mills, et. al., (Ref. 58), used mercury gages (Fig. 5.5) for the measurement of panel distortion in the tests of small scale beam-to-column subassemblages. The gages exhibit a very low resistance (0.3 ohm) and therefore have to be used either with a balancing mercury gage in the opposite arm of the bridge or with precision resistors. For standard signal conditioners, the resistance of the gages is too low and therefore the use of a four arm bridge is recommended, with the remaining two arms supplied by higher resistance (e.g., 120 ohm) precision resistors. The gages should be used in a pretensioned condition in order to ensure their linear behavior. Each gage must be calibrated individually to provide the calibration constant. For instance, for 20 mm (0.75 in) long mercury gages and the signal conditioner set at 1 mV/V, the calibration constant was 1.2 to 1.5 V/mm. The calibration was done using an MTS testing machine with an extensometer used for the control of the displacement.

The measurement of strains in compressed concrete cylinders presents a major difficulty. Glued-on strain gages provide only localized information which may become meaningless if a crack develops under the gage. In addition, this method is inefficient in studies in which a large number of specimens is to be tested, due to the high cost and large amount of preparatory work involved. In this study, four clip gages were used to measure the average strain over a gage length of 50 mm (2 in.) at 90^{o} intervals around the specimen. The gages (Fig. 5.6) were developed in the laboratory, with mercury gages used to monitor the change in the gage length.

The mercury gages proved also to be very useful for the measurement

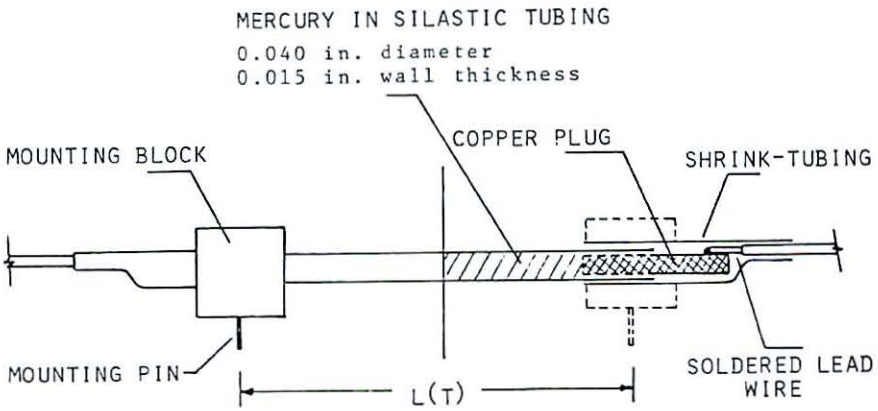

Figure 5.5 Silastic Mercury Gage (Ref. 58)

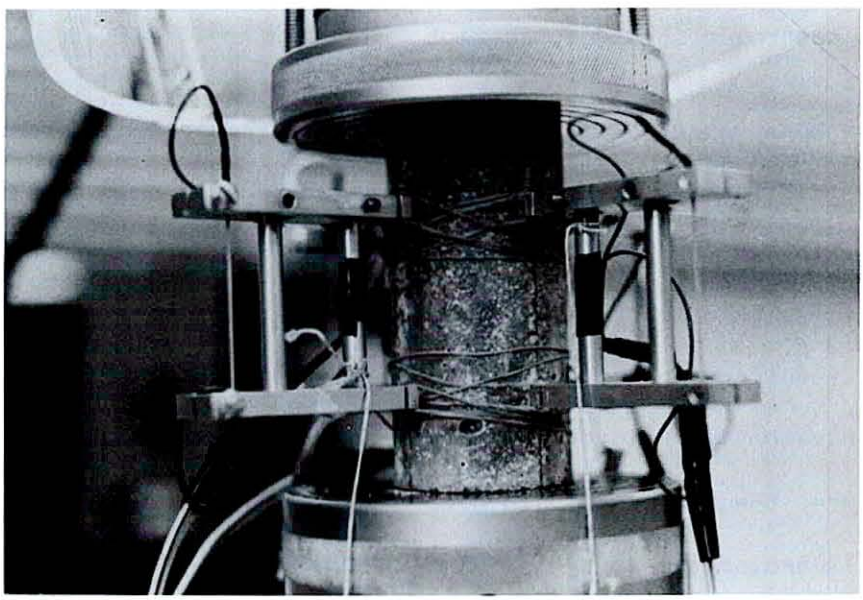

Figure 5.6 View of Setup for Microconcrete Compression Test

of relative displacements between two points in a structural element. For instance, in the study of reinforced concrete components the measurement of the rotation of a specific cross-section of the beam with respect to the column face was necessary. This was done by measuring the change in distance between the column face and a frame attached to the beam at the cross-section in question (Fig. 8.5). The measurements were done using mercury gages.

5.3.3 Data Acquisition and Reduction System

All the aforementioned instrumentation is of electronic nature and the measurements are obtained in terms of voltage, thus allowing a continuous record of the data. Although graphical recording is of importance primarily for an immediate test evaluation, digital registration of the data is needed for final data reduction. A properly designed data acquisittion system permits a rapid and continuous recording of data from a large number of channels (instruments) simultaneously. Once the data is recorded, its reduction in terms of numerical analysis can be performed. The data acquisition system used in this study allows a recording of data from up to 32 channels at the rate of 42000 data points/second. An extensive data reduction package is available in the computer library of the laboratory. Figs. 5.7 and 5.8 present schematically the experimental facilities and data reduction package available at Stanford. A detailed description of the data acquisition and reduction system is presented in Ref. 58.

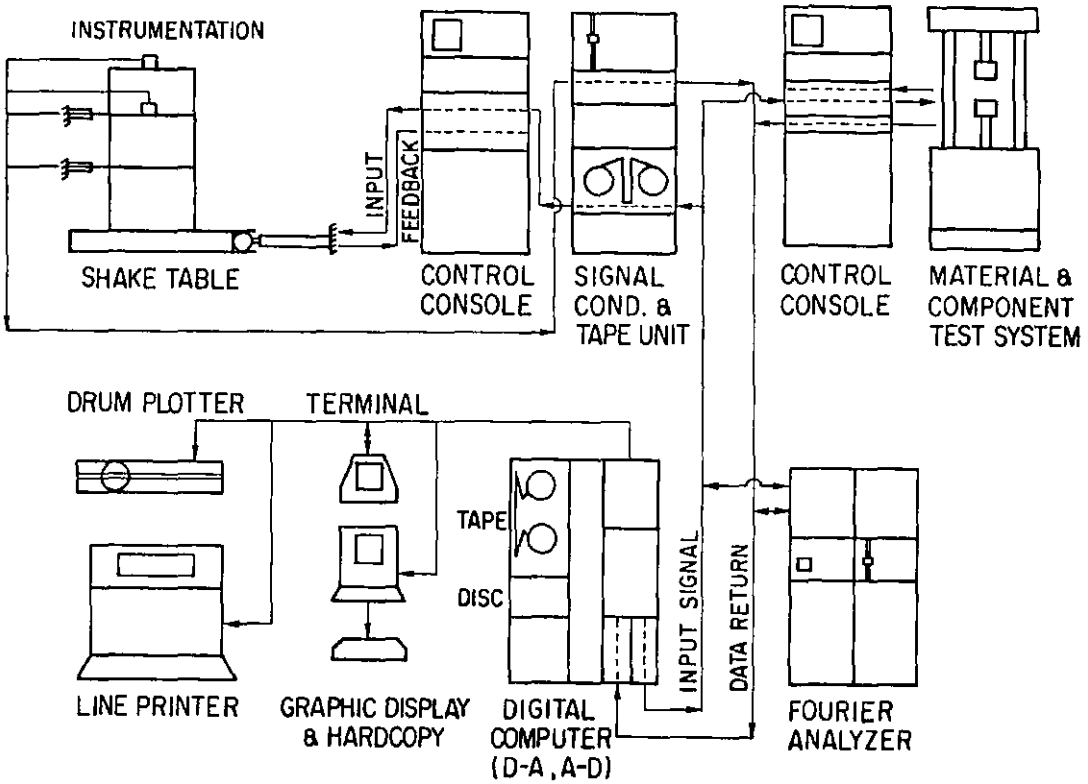

Figure 5.7 Testing Facilities at Stanford Structural Laboratory

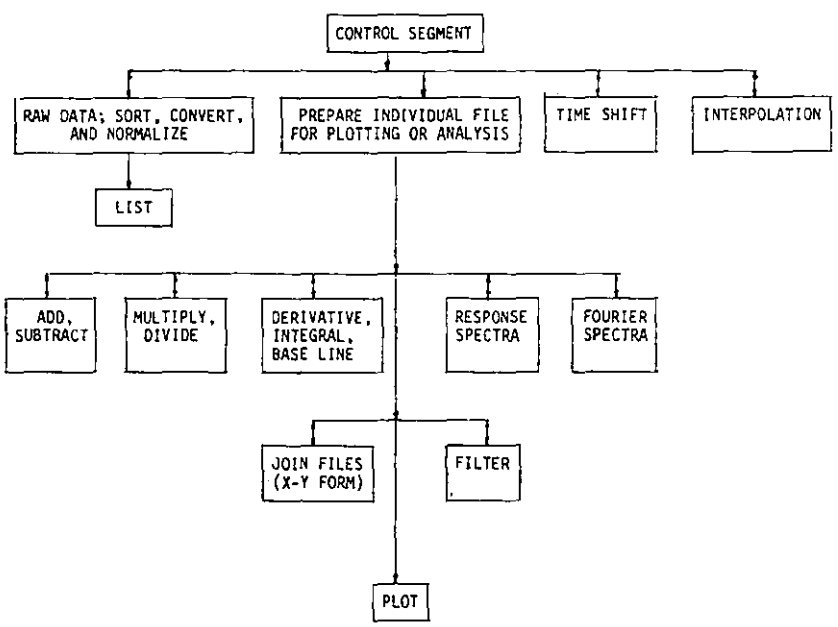

Figure 5.8 Basic Data Reduction Package (Ref. 58)

5.4 Testing Program

The testing program carried out in this study included the following tests for prototype and model materials:

1. Low Strain Rate Monotonic Tests: Standard ASTM tension tests were carried out on steel prototype material and on reduced size specimens (geometrically scaled in proportion to the model length scale l_r) of model materials. In most cases the tests were carried to failure to investigate similitude at all ranges of deformations. Various sources suggest different strain rates as being representative for a static loading test. Since a perfectly isothermal test (Ref. 173) is not within the range of engineering investigations, a low yet feasible strain rate of 2×10^{-4}/sec. has been selected as a static strain rate. Compression tests on steel specimens were also performed to provide a comparison for the compressive branch of the skeleton curve obtained from cyclic load tests.

In the material study of model concretes, compression tests were carried out on 50x100 mm (2x4 in.) microconcrete cylinders to investigate the strength of microconcretes obtained from various mix proportions and cured for various lengths of time.

2. High Strain Rate Monotonic Tests: This series of tests with various strain rates was carried out to supplement the data on strain rate effects available in the literature for steel and microconcrete and to investigate strain rate effects in phosphor bronze and its adequacy in satisfying Eq. (5-1). The tests were carried out with constant average strain rates over the mid-section of the metal specimens (extensometer attached to the specimen), and over the entire height of the microconcrete cylinders (extensometer controlling the distance between

the plattens). Ramp functions were used for the control signal of the extensometer.

3. Cyclic Load Tests: Low strain rate cyclic load tests were carried out on metal specimens with a gage length equal to twice the section diameter. These stocky specimens were required to prevent buckling in the strain range of interest. The selected load histories consisted of symmetric cycles with increasing strain amplitude $_a$ as shown in Fig. 5.9. The three selected loading histories permit an evaluation of strain hardening or strain softening tendencies, a comparison of shape-similarity and area of hysteresis loops and an assessment of the stability of hysteresis loops of equal strain amplitudes (see loading history #3). The tests were carried out under strain control with sinusoidal input wave. Cyclic loading tests with random loading histories and high strain rates would be desirable but were not within the scope of this study.

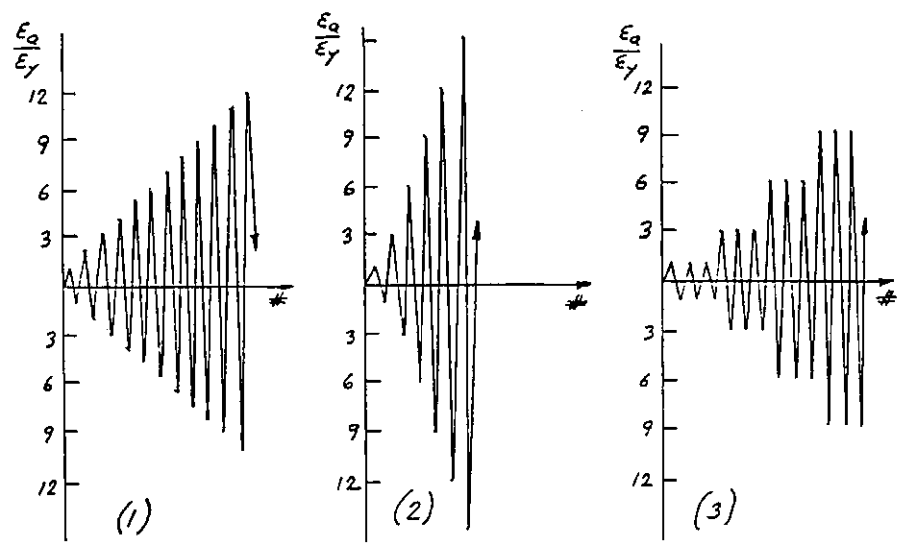

Figure 5.9 Cyclic Load Histories Used in Metal Specimen Tests

4. Material Damping: The anelastic material damping can be evaluated at various stress levels from free vibration tests in torsion or bending by means of standard laboratory equipment. This was done for the

metal materials studied. The actual hysteresis damping in the metal materials can be deduced from cyclic load tests for loops with various strain amplitudes. An equivalent viscous damping can be calculated from the expression proposed by Jacobsen (Ref. 174), i.e.,

$$\beta_{eq} = \frac{1}{2\pi} \frac{\Delta W}{W}$$

where β_{eq} = equivalent viscous damping coefficient

ΔW = dissipated work per cycle

W = work capacity per cycle

There are alternative ways to measure material damping (Refs. 170, 175) which are not pursued further in this project since the knowledge of damping of the integrated structural system is of more importance that that of an isolated material segment. Thus, the emphasis in this study was on measurement of the damping in complete models through free and forced vibration tests on the shake table, with the damping characteristics extracted from the decay of free vibration or from spectral analysis of forced vibration records (Ref. 176).

5. Component Tests: It must be emphasized that material tests alone are not sufficient to permit a reliable correlation between prototype and model response and an evaluation of the feasibility of specific model materials. Such important phenomena as size effects, strain gradient effects, and simulations of local instabilities and stress concentrations at bolted or welded connections can only be studied through component test with known quasi-static load application. Also, simple component tests have shown that apparent dissimilarities in material behavior may often have little effect on the response of structural elements. Consequently, certain dissimilarities such as the absence of an upper yield point and of a yield plateau in model materials for steel structures may

sometimes be acceptable.

The tests described in this chapter are time consuming but, once a methodology has been developed, they can be carried out in most well-equipped structural laboratories. They form an integral part of every successful dynamic model study, for the purpose of providing the information necessary to select a suitable model material and to assess the reliability of the prototype response predicted from model tests.

CHAPTER 6

MATERIALS FOR MODELS OF STEEL STRUCTURES

6.1 INTRODUCTION

Despite the extensive use of steel in structural design the number of model studies performed on steel structures is remarkably small compared to the number of model studies performed on reinforced concrete structures. The reason for the scarcity of model studies on steel structures may be that larger confidence is placed in mathematical techniques applied to this type of structures. Structural analysis methods based on the theory of elasticity are widely accepted in steel design. Local nonlinearities (connections, local instabilities) can be accounted for by applying experience gained in innumerous laboratory tests performed on full scale structural components and subassemblages. This is not so in the case of reinforced concrete structures. Early nonlinearities appearing in the behavior of this composite material always imposed serious questions on the reliability of standard structural analysis methods. The complex nature of force transfer within the material and between the members required extensive study, not only of the components but also of entire structural systems, and hence perpetuated model studies on concrete structures.

Under earthquake excitations and other dynamic loading events (blast loading, extreme wind, impact loading, etc.), energy dissipation through inelastic deformation may become of primary importance. In these cases, available mathematical modeling techniques may be inadequate and experimental model analysis may provide much additional information. Harris, et. al., (Ref. 38), have performed an experimental study on model mate-

rials for dynamic models of steel prototype structures. In Refs. 31, 85, 86 and 143, case studies on models of steel prototypes are reported.

6.2 Stress-Strain Characteristics of Structural Steel

A one-to-one simulation of the scaled stress-strain diagram is demanded by similitude laws (Section 4.5.1) for monotonic as well as cyclic load application. Therefore, a brief review of the uniaxial stress--strain characteristics of structural steel is presented in the following paragraphs.

Fig. 6.1 presents a schematic diagram of an engineering stress vs. strain curve for structural steel (low carbon steel) subjected to monotonic tension till failure. The yielding phenomenon is associated with the initial yielding of metal at a stress concentration point (upper yield), and the propagation of plastically deformed metal bands (Luder's bands) along the lower yield plateau. The initiation and development of the yield bands depends upon the amount of interstitial atoms preventing the dislocations (impurity pinning) from a free propagation. Carbon atoms present in the structural steel crystalline exemplify interstitial atoms. Under normal testing conditions, the drop in strength from upper to lower yield is of the order of 10 to 20% for structural steel. An explanation of the physical phenomena associated with strain hardening, necking and rupture is presented, for instance, in Ref. 157.

A typical stress-strain diagram for structural steel under cyclic load application is shown in Fig. 6.2. Compared to the monotonic stress--strain diagram, a description of the cyclic characteristics is complicated considerably by the occurence of cyclic work hardening, Bauschinger effects, mean stress relaxation and other memory effects. Many empirical

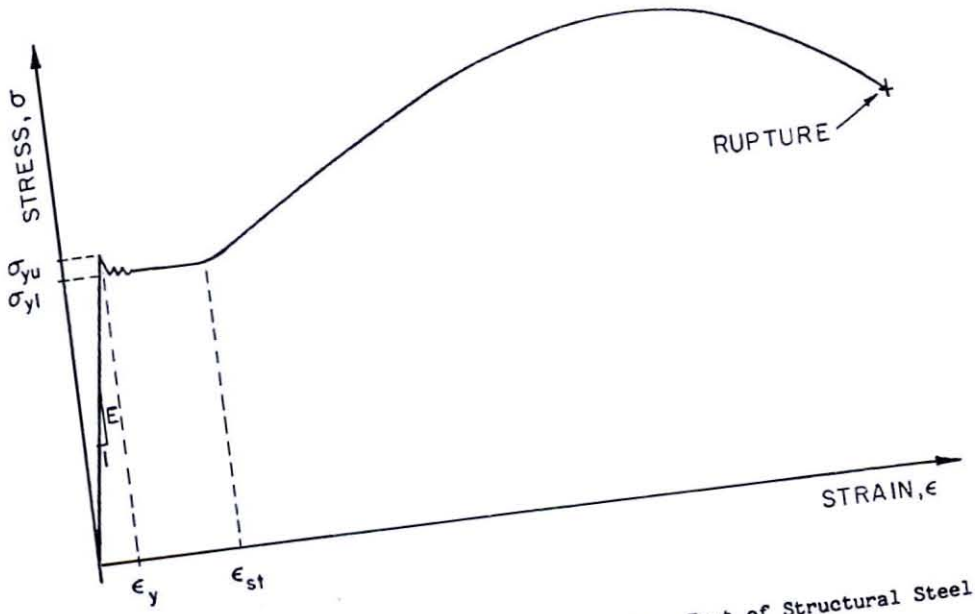

Figure 6.1 Stress-Strain Diagram from Tension Test of Structural Steel

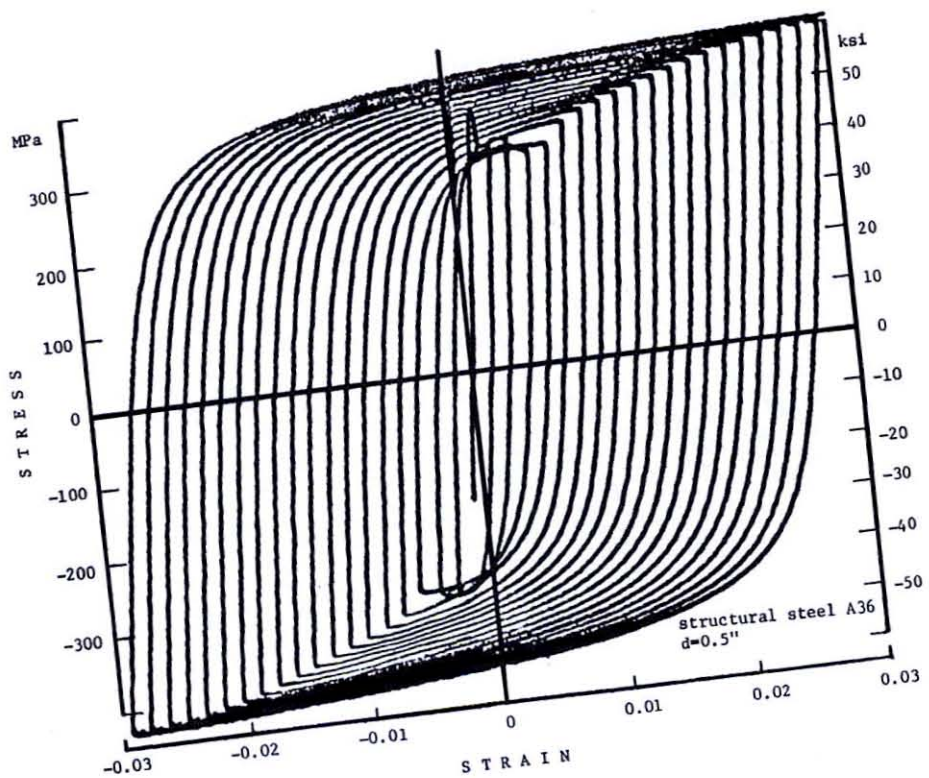

Figure 6.2 Cyclic Stress-Strain Diagram for Structural Steel

models have been proposed in the literature for a mathematical evaluation of these phenomena, but none have been applied with great success to fully random load histories. Under load histories with symmetric strain amplitudes it can be observed that the peak stresses and hysteresis loops stabilize after a few cycles of equal strain amplitude. The line connecting the peaks of stabilized loops at various strain amplitudes is often referred to as the cyclic stress-strain curve. This curve and the shape of the symmetric hysteresis loops are used in this study to characterize the cyclic stress-strain behavior.

An experimental study on the cyclic behavior of structural steel, which has been recently completed at the Structures Laboratory at Stanford (Ref. 156), provides valuable data for a comparison with the cyclic behavior of other than steel model materials. The three basic symmetric strain histories with zero mean strain adopted from Ref. 156 are listed in Table 6.1. The test with load history #4 was added in this study to establish whether three cycles per amplitude provide information on the final (stable) hysteresis loops.

Table 6.1

Cyclic Load Histories

Cyclic Load History No.	Amplitude		Cycles per Amplitude
	First	Incremental	
—	ε_y steel		—
1	2	1	1
2	2	1	3
3	4	3	3
4	2	1	12

6.3 SUITABLE MODEL MATERIALS

6.3.1 Introduction

One of the major difficulties in the modeling of steel structures is the choice of a satisfactory model material. Ideally (true replica models), the material should satisfy the similitude requirement stating that the specific stiffness scale ratio should be equal to the geometrical scale, i.e, $(E/\rho)_r = l_r$ (see Section 4.5.1). This rule eliminates the use of prototype material for true replica models. Due to the specific nature of the stress-strain diagram of structural steel, it is very difficult to find non-ferrous materials with behavior similar to that of steel.

A preliminary search for a suitable model material may be based on the monotonic stress-strain characteristics but must then be supplemented with information on the cyclic stress-strain behavior. Table 6.2, which is taken from the Material Selector Issue of Material Engineering, provides a convenient tabulation of specific stiffnesses of a wide variety of materials. Besides the required E/ρ ratio, the material must satisfy the condition that the yield strength to modulus ratio, σ_y/E, be the same as that of the prototype material (uniqueness of strain scaling, see Section 4.5.1). For A36 structural steel, σ_y/E is approximately equal to 0.0012. This requirement poses severe problems for thermoplastics because of their inherently low elastic moduli. Most thermoplastics studied were found to have much higher yield strengths compared to their E values than steel (for example, for polypropylene $\sigma_y/E = 0.02$). Consequently, to make use of these plastics ways would have to be found of drastically reducing their yield strengths while not affecting the

Table 6.2

Specific Stiffnesses E/ρ

E/ρ, 10^6 in

Material	Ratio	Material	Ratio
Beryllium	657	Beryllium Copper	64
Silicon Carbide	607	Zirconium and Its Alloys	59
Boron Carbide	483	Yellow Brasses (cast)	58
Beryllia	413	Nickel Silvers	57
Alumina Ceramics	420	Phenolics, Shock Resistant	56
Mica, Natural	337	Silicon Bronzes	56
Mica, Synthetic	281	Red Brass, 85%	54
Titanium Carbide Cermet	248	Commercial Bronze, 90%	54
Polycrystalline Glass	219	Leaded Brasses	53
Tungsten-Titanium Carbide Cermet	192	Gilding, 95%	53
Zircon	188	Phosphor Bronzes	53
Tungsten Carbide Cermet	185	Copper	53
Boron Nitride	163	Tin and Aluminum Brasses	53
Standard Electrical Ceramics	143	Cartridge Brass, 70%	52
Glass, Alumino-Silicate	140	Low Brass, 80%	51
Ruthenium	136	Leaded Tin Bronzes (cast)	51
Glass, Fused Silica	129	Tellurium Copper	50
Mica, Glass-Bonded	129	Muntz Metal	50
Molybdenum and Its Alloys	127	Yellow Brass	49
Glass, 96% Silica	124	Columbium	48
Glass, Borosilicate	123	Leaded Red Brass (cast)	47
Steatite	120	Tantalum	45
Cobalt-Base Superalloys	120	Uranium	43
Nickel-Base Superalloys	112	Hafnium	43
Titanium and Its Alloys	111	Melamines	42
Glass, Soda Lime	111	Carbon	41
High Temperature Steels	111	Palladium	39
Ultra High Strength Steels	107	Ureas	34
Ingot Irons	106	Polystyrenes, Glass-Filled	33
Carbon Steels (cast)	106	Reinforced Plastics, Polyester	33
Wrought Iron	106	Graphite	31
Pearlitic Malleable Irons	106	Pewter	29
Carbon Steels	106	Silver	29
Alloy Steels	106	Phenylene Oxide, 30% Glass-Filled	29
Nitriding Steels	106	Tin-Lead-Antimony Alloys	29
Stainless Steels (cast)	106	Platinum	27
Aluminum and Its Alloys	105	Diallyl Phthalate	25
Age Hardenable Stainless Steels	104	Grade A Tin	25
Heat Resistant Alloys (cast)	104	Thorium	24
Ferritic Stainless Steels	104	Phenolics, GP	23
Martensitic Stainless Steels	104	Polyvinyl Formal	19
Iron-Base Superalloys (Cr-Ni-Co)	103	Modified Polystyrenes	18
Free-Cutting Steels	102	Gold	17
Iron-Base Superalloys (Cr-Ni)	102	Polyesters (cast)	16
Magnesium Alloys	102	Polystyrenes, GP	16
Austenitic Stainless Steels	100	Acrylics, GP	14
Nodular Irons (cast)	100	Phenolics (cast)	12
Osmium	98	Polyvinyl Butyral	12
Reinforced Plastics, Phenolic	96	Nylon 66	12
Malleable Irons (cast)	96	Ethyl Cellulose, GP	10
Rhodium	94	Nylon 6	10
Cobalt	94	Phenylene Oxide, SE-100	9.5
Nickel and Its Alloys	93	Acrylics, High Impact	9
Cordierite	93	Acetal	9
Iridium	91	ABS Resins	9
Vanadium	87	Ethyl Cellulose, High Impact	9
Nickel and Its Alloys (cast)	86	Polycarbonate	9
Phenolics, Electrical	85	Nylon 610	8
Tungsten	84	Polypropylene	6
Glass, Lead Silicate	82	Nylon 11	6
Monel	82	Cellulose Nitrate	5
Low Expansion Nickel Alloys	81	Lead and Its Alloys	5
Gray Irons (cast)	77	CFE Fluorocarbons	5
Columbium Alloys	74	Polyethylenes, Low Density	1
Cupro-Nickels	68	TFE Fluorocarbons	1
Aluminum Bronzes (cast)	66	Polyvinyl Chloride, Nonrigid	0.07

* Specific stiffness, or stiffness-weight ratios, were obtained by dividing modulus of elasticity in tension (psi) by density (lb/cu in.). Specifically, the highest value of a range of typical values was divided by that material's density.

elastic properties. Fig. 6.3 (after Ref. 38) presents the stress-strain curve for ethyl cellulose (ethyl ether of cellulose), and Fig. 6.4 shows the comparison of the idealized stress - strain curve to that of structural steel. The specific stiffness ratio is equal to about 1/63, the modulus of elasticity ratio is equal to about 1/160 and the ratio of yield stresses is equal to about 1/10. The two last ratios indicate, that in order to satisfy the true replica model requirements, the yield strength of this material would have to be lowered by the factor of 16, which is impractical. Another possible difficulty with the thermoplastics is their high Poisson's ratios compared to steel and other metals. Metallic materials with E/ρ ratios higher than that of structural steel, such as lead alloys and copper alloys, on the other hand, can be heat-treated to develop appropriate σ_y/E ratios.

In view of the above considerations in the preliminary study, the effort was concentrated initially on both lead and copper alloys and on one specific copper alloy, namely phosphor bronze (CA 510) in the final study.

For adequate models (see Section 4.5.2) the requirement that $(E/\rho)_r = 1_r$ need not be fulfilled. Thus any material that fulfills the material similitude requirements can be used for such model studies. The obvious choice is clearly the prototype material, i.e., structural steel. Suitable copper alloys are often desirable alternatives due to their smaller stiffness which reduces the weight requirements for artificial mass simulation.

Whatever the choice of a model material, it must be emphasized that certain material characteristics cannot be simulated at model scales.

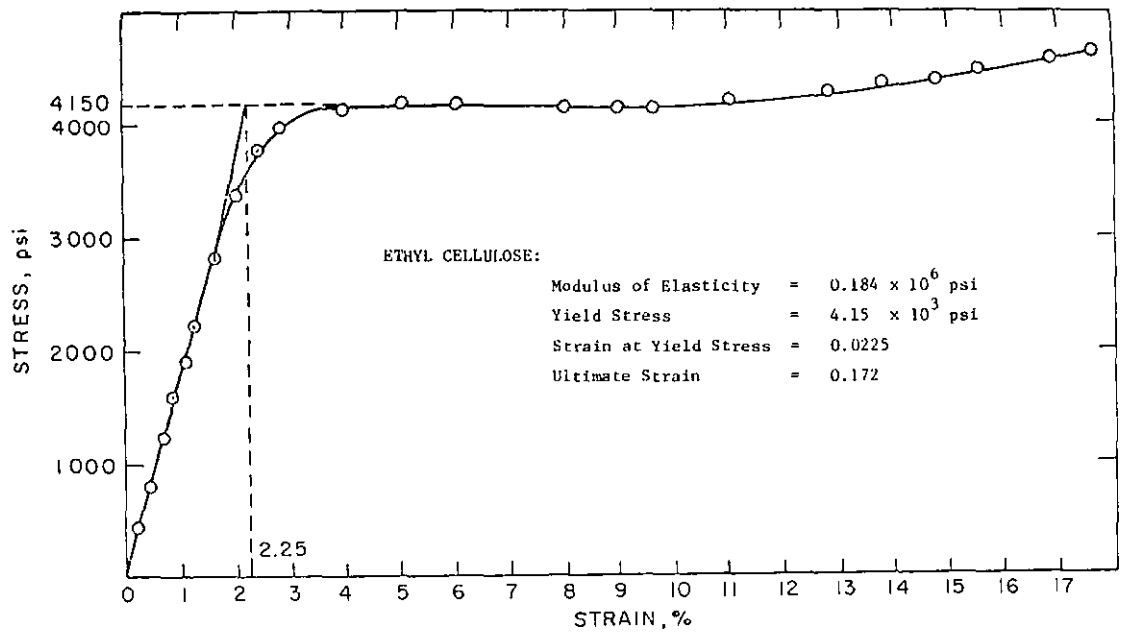

Figure 6.3 Stress-Strain Diagram from Tension Test of Ethyl Cellulose (Ref. 38)

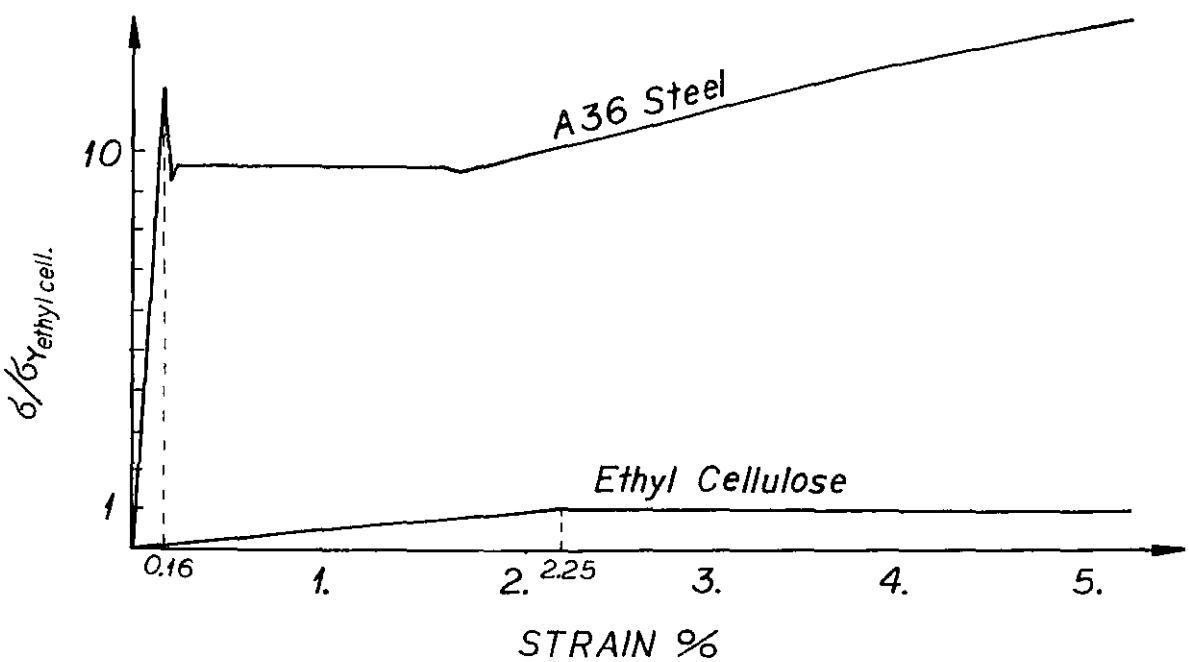

Figure 6.4 Comparison of Tensile Stress-Strain Diagrams of Strucural Steel and Ethyl Cellulose

This holds true particularly for fatigue and fracture properties, whether the model material is nonferrous or structural steel as in the prototype. Even in the latter case the size and distribution of initial flaws and the fracture properties as well as crack propagation rates cannot be simulated due to size effects.

6.3.2 Structural Steel as a Model Material

Within certain limitations, structural steel is the best suited material for models of steel structures with artificial mass simulation or without simulation of gravity forces. The identical shapes of the stress-strain diagrams of the model and prototype materials, and the ability to closely simulate prototype connections (bolted or welded) are the major advantages. Nevertheless, the question remains as to the significance of the increase in the strength of the model material caused by the higher strain rates (t_r) as compared to prototype material. Thus, much emphasis is placed in this study on a thorough evaluation of strain rate effects in structural steel. The importance of size effects is discussed in a subsequent section. When strain rate and size effects are quantitatively known for the selected length and time scale, it is reasonably simple to account for specific aspects of these effects by either modifying the gravity loads and seismic input or, perhaps more appropriately, by suitable heat treatment reducing the yield strength to the desired value. In this study, A36 structural steel was used for all the experiments. The modulus of elasticity of the material used in the tests is $E = 212.3 \times 10^3$ MPa (30.5×10^6 psi) and the specific gravity is 7.6930.

6.3.2.1 Strain Rate Effects

Considerable research has been devoted to the influence of the speed of testing on the yield stress and the ultimate strength of mild steel.

Manjoine (Ref. 152, 1944) reports a study in which mild steel was tested in tension at strain rates from 10^{-8}/sec. to 10^{3}/sec. The reported increase in yield stress for this range is 83% and for the range from 10^{-5}/sec. to 10^{-1}/sec. the increase is 31%. These high values might have an inherent error due to the inadequate strain rate control. Manjoine also observed that the yield stress increases with the increase in strain rate until the limit when the ultimate stress (which is independent of strain rate) is reached without yielding.

Garner (Ref. 153) presents a compilation of data from 9 sources for yield strength obtained at strain rates varying from 10^{-4}/sec. to 10^{3}/sec.

More recently (1966) Nagaraja (Ref. 151) performed a study on strain rate effects on the yield strength of structural steel. The empirical formula derived in this study for rates till $1.4\text{x}10^{-3}$/sec. is

$$(\sigma_y)_d/(\sigma_y)_s = 1 + 0.762\ \dot{\varepsilon}^{0.26}$$

or, using the yield stress obtained at a strain rate of $\dot{\varepsilon} = 2\text{x}10^{-4}$/sec. as the normalizing value:

$$\sigma_y/(\sigma_y)_{2\text{x}10^{-4}} = 0.923 + 0.703\ \dot{\varepsilon}^{0.26} \qquad (6\text{-}1)$$

Pirotin and East (Ref. 189) presented the following relationship for strain rate effect on the yield strength of stainless steel (after normalization for $\dot{\varepsilon} = 2\text{x}10^{-4}$/sec.) :

$$\sigma_y/(\sigma_y)_{2\text{x}10^{-4}} = 0.920 + 0.44\ \dot{\varepsilon}^{0.2} \qquad (6\text{-}2)$$

In this study, tensile tests were performed on structural steel at strain rates from 10^{-5}/sec. to 10^{-1}/sec. A set of 24 specimens was ma-

chined out of A36 steel square bar stock and stress relieved at 600°C for one hour after machining. The central section of the specimens was 45 mm (1.75 in.) long with a diameter of 9.52 mm (0.375 in.) and with smooth transition from the square ends. The specimens were mounted in the testing machine with the help of hydraulic grips.

The tests were performed under constant strain rate controlled by a 25 mm (1 in.) gage length MTS extensometer attached to the central portion of the specimen. Ramp function (constant strain rate) was used as the controlling signal. The tension tests were terminated when the averaged strain reached 3 percent. The measurements made during the test (load, average strain) were recorded continuously by the computer data acquisition system (Section 5.3.3).

Fig. 6.5 displays two typical stress-strain diagrams obtained for low and high strain rates. The high strain rate curve exhibits two anomalies. First, the lack of sharp transition from upper to lower yield, and second, the strong stress fluctuation along the lower yield plateau. Both the phenomena are believed to be independent of real material behavior and to be caused by the inability of the testing system to control such rapid load changes (0.09 sec. till yielding).

All the lower yield stress values were normalized with respect to the average value obtained for the strain rate of 2×10^{-4}/sec. (300 MPa, 43.5 ksi). The results of the testing program are summarized in Table 6.3 and the normalized data points with a fitted curve are displayed in Fig. 6.6. The mathematical representation of this curve is of the following form :

$$\sigma_y/(\sigma_y)_{2x10^{-4}} = 0.973 + 0.45\ \dot{\varepsilon}^{0.33} \qquad (6\text{-}3)$$

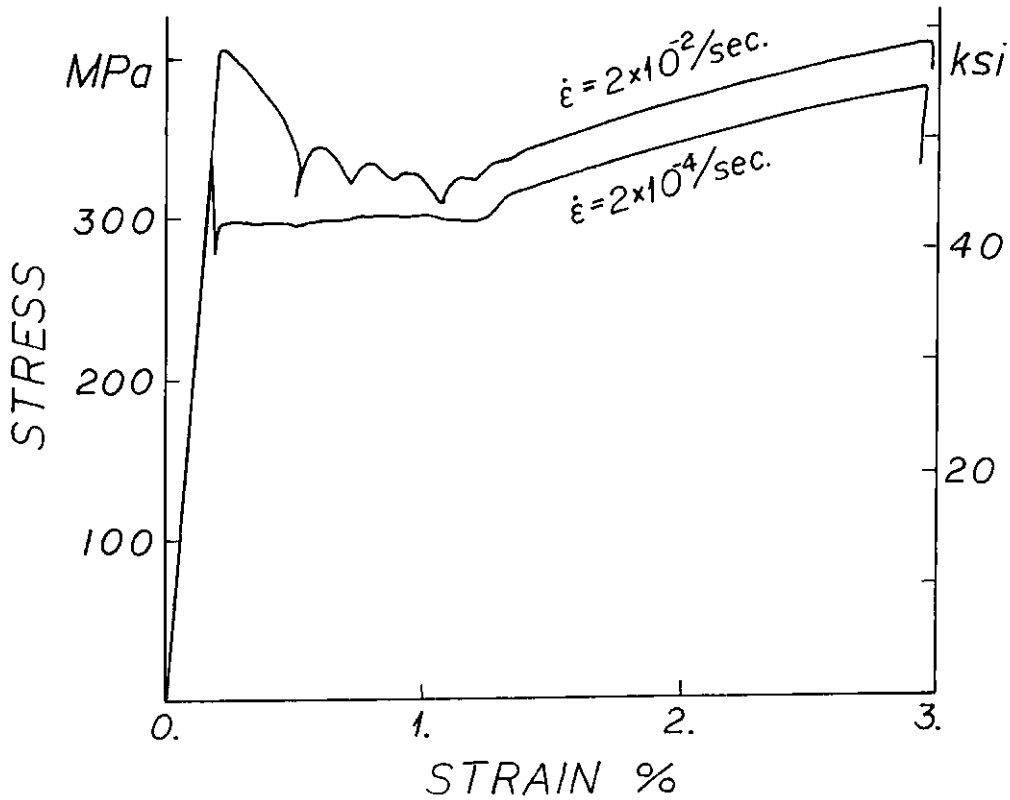

Figure 6.5 Tensile Stress-Strain Diagrams for Structural Steel Tested at Low and High Strain Rate

Table 6.3

Summary of Results for Strain Rate Effect on the Lower Yield Stress of Structural Steel

Strain Rate	No. of Specs.	Average Lower Yield Stress		Coefficient of Variation	Normalized Yield Stress
1/sec.	--	MPa	ksi	%	--
1×10^{-5}	3	300.6	43.60	0.5	0.981
1×10^{-4}	1	302.7	43.91	-	0.987
2×10^{-4}	3	306.5	44.46	0.4	1.
2×10^{-4}	4	297.9	43.21	1.2	1.
1×10^{-3}	3	310.8	45.08	1.5	1.043
5×10^{-3}	3	322.5	46.77	1.1	1.082
2×10^{-2}	2	333.0	48.30	0.1	1.118
1×10^{-1}	3	350.3	50.81	1.1	1.176

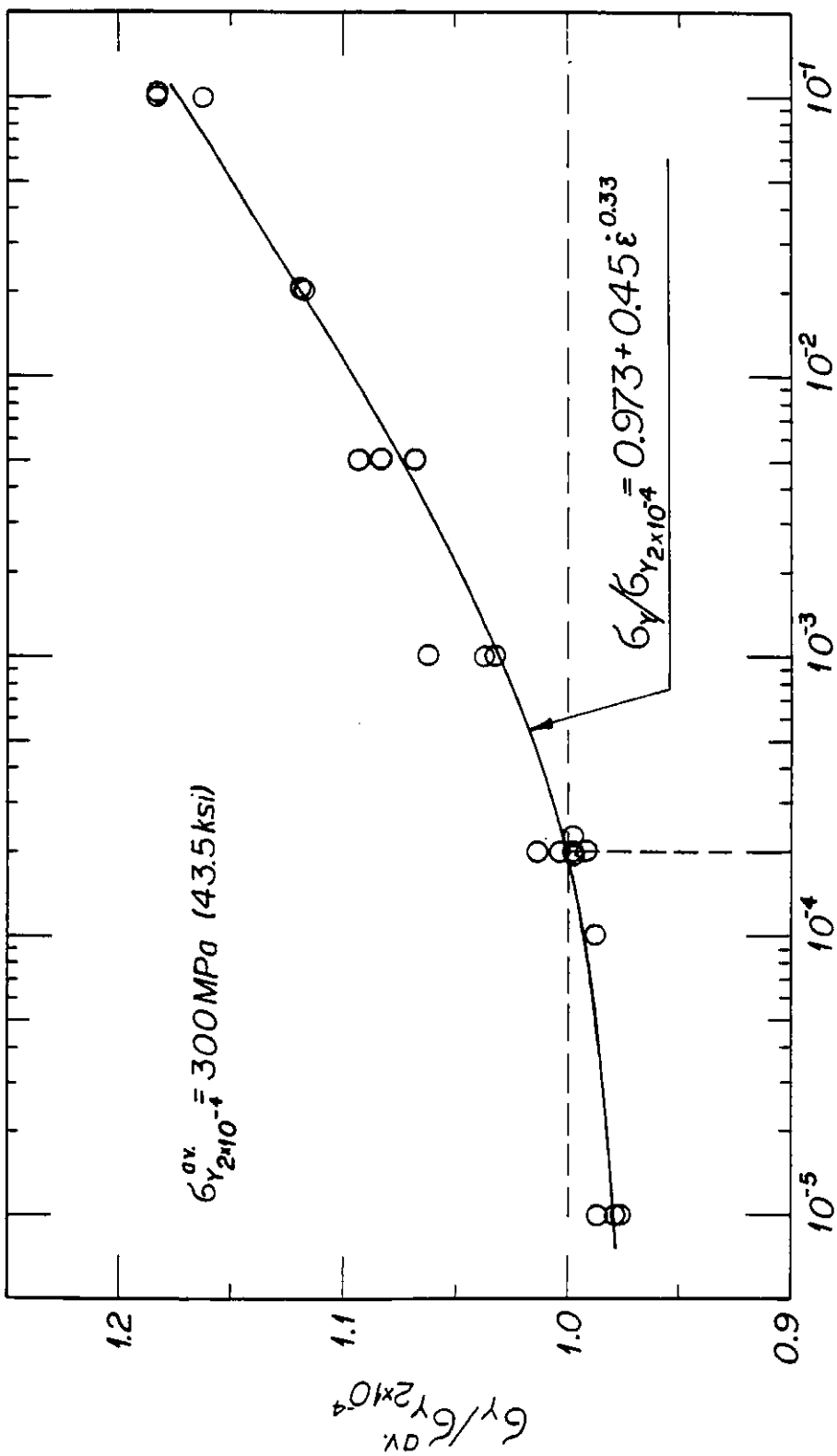

Figure 6.6 Strain Rate Effect on the Lower Yield Stress of Structural Steel

This curve and curves obtained by other researchers are plotted in Fig. 6.7. These curves show that in model studies, in which steel is used as model material, differences in the yield strength between the prototype and model can reach 3% of the value for 1:15 models with simulated gravity forces ($t_r = l_r^{-1/2}$), and up to about 6% for models in which gravity forces are neglected ($t_r = l_r$). Whether those relatively small differences in the initial yielding value are acceptable without adjustments has to be decided separately for each individual case.

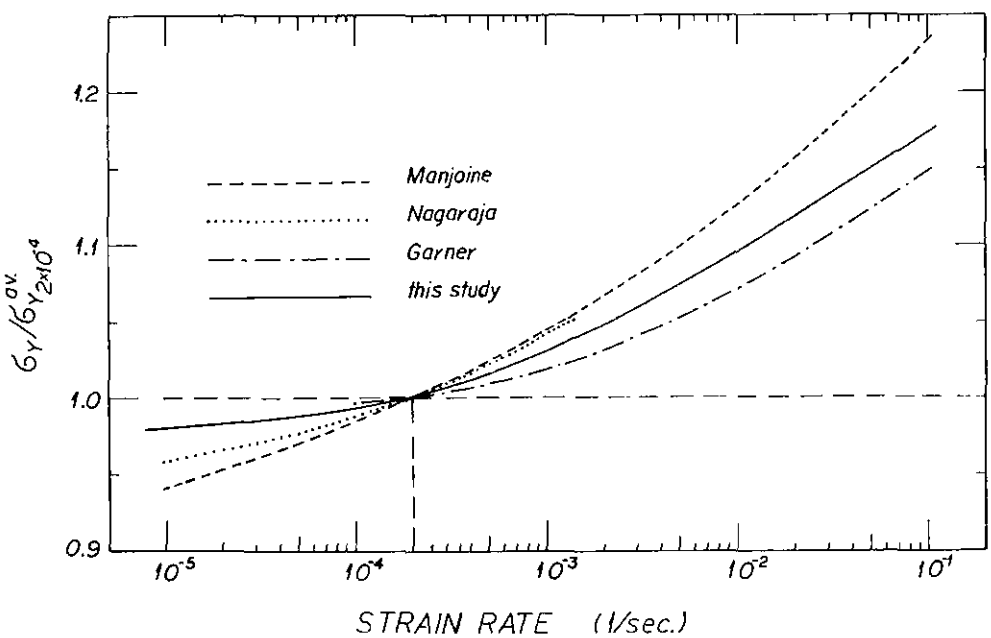

Figure 6.7 Results from Various Sources on the Strain Rate Effect on the Lower Yield Stress of Structural Steel

6.3.2.2 Size Effects

Conflicting opinions are expressed in the literature on size effects of mild steel and other materials. However, there is considerable experimental evidence of size effects on the yielding of mild steel (Refs. 154, 155). The effects are explained by the difference in stress gradients of large and small specimens. Richards recorded and evaluated statistically size effects in round steel bars subjected to axial tension

(Ref. 154) and rectangular steel beams subjected to pure bending (Ref. 155). He concluded that the yield stress can be related to the volume of the test specimens and can be expressed by the equation

$$\sigma_y = \frac{\sigma_{y1}}{V^{1/m}}$$

where V is the volume of the test specimen, σ_{y1} is the yield stress for a specimen of unit volume, and m is a material constant for the specific type of test. For the steel used in his investigation (a commercial quality killed structural mild steel with a carbon content of 0.18 percent) Richards found m to be equal to 58 for the tension tests and equal to 11.7 for the bending tests. Thus, it is evident that the size effect in bending is much more pronounced than in axial tension and may be significant for small scale models.

Size effects can be partially accounted for by the use of material specimens comparable in size to the smallest dimension of model structural element.

6.3.3 Copper Alloys

6.3.3.1 Introduction

Many copper alloys have mechanical properties which render them quite useful for model studies of steel structures. In addition, these alloys are readily available in bar and plate stock, can be easily machined into structural shapes, and permit joining of individual elements in a manner very similar to steel. However, it must be pointed out that heat effects from welding affect different alloys in different ways which make weldability the single most important criterion in the search for a suitable copper alloy for modeling of welded structures.

The E/ρ for most copper alloys is of the order of one half of that for steel, hence these alloys can be used for 1:2 scale true replica models. Probably more important is their application for models with artificial mass simulation since their elastic stiffness is approximately only half that of steel. Small scale steel models will often require excesssive amounts of additional mass which may either cause model fabrication problems or may place excessive demands on the weight and dynamic force requirements for small shake tables. When copper alloys are used as a model material, the weight requirements are cut in half and the dynamic force requirements are also reduced.

Although general information on mechanical properties of copper alloys can be found in many material handbooks (134 to 136), detailed data on stress-strain behavior and other relevant properties discussed in Section 5.2 were not available, which necessitated a testing program on several promising alloys. The alloys investigated in the course of this material study (copper alloys No. 260, 510, 614, and 655, see Table 6.4) exhibited quite different properties. However, all tested alloys originally had strength properties which were much too high to satisfy the similitude condition $(\sigma_y/E)_r = 1$. Thus, a trial and error annealing process had to be carried out to reduce the nominal yield strength to the desired value.

The results of high strain rate (3×10^{-2}/sec.) tension tests for three of these alloys in the non-annealed condition and for cartridge brass annealed at $408^{\circ}C$ are presented in Fig. 6.8. It is evident that AMPCO 8 and Everdue 1010 show undesirable stress-strain characteristics for a simulation of steel while cartridge brass and CA 510 appear to be well suited for this purpose.

Table 6.4

Copper Alloys Investigated Preliminarly in this Study

Commercial Name	Standard Designation	Chemical Composition	Form at Delivery
Cartridge Brass	CA 260	70% Cu, 30% Zn	6 mm (1/4 in.) half-hard plate
Ampco Grade 8	CA 614	91% Cu, 7% Al, 2% Fe	6 mm (1 4 in.) half-hard plate
Everdur 1010	CA 655	97% Cu, 3% Sn	12 mm (1/2 in.) half-hard rod
Phosphor Bronze	CA 510	94.8% Cu, 5% Sn, 0.2% P	12 mm (1/2 in.) half-hard rod

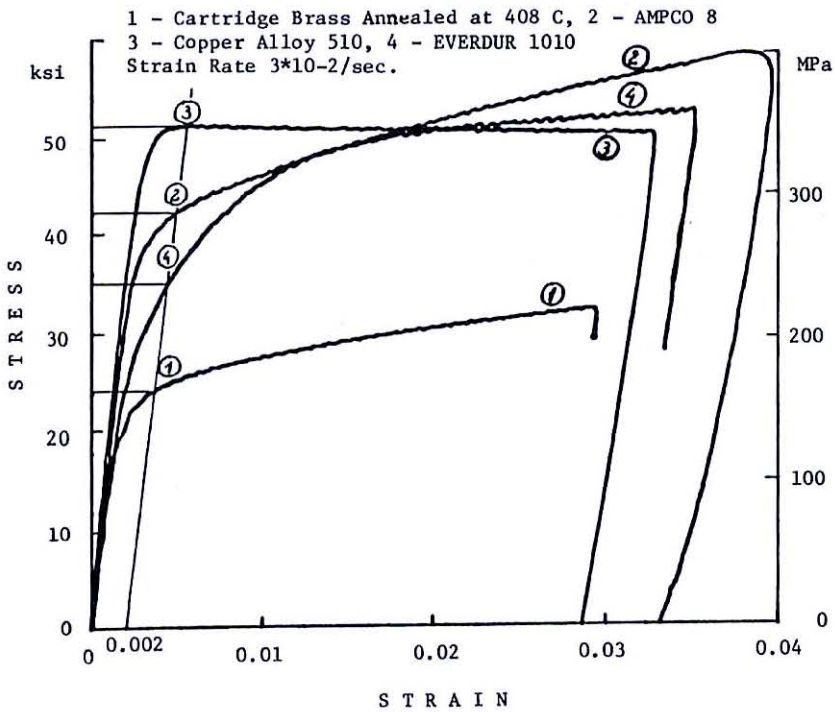

Figure 6.8 Stress-Strain Diagrams for Copper Alloys Tested at High Strain Rate ($\dot{\varepsilon} = 2.4 \times 10^{-2}$/sec.)

6.3.3.2 Preliminary Study on Cartridge Brass

This alloy attracted special attention because of its availability, reliable chemical composition (70% copper and 30% zinc with possible impurities of less than 0.1% lead and iron), and promising mechanical properties. The material was purchased in the form of half-hard, 1/4 in. thick plate. The properties of the delivered material were: $E = 1.12 \times 10^5$ MPa (16,300 ksi), σ_y = 386 MPa (56 ksi), and $\rho = 84$ kN/m^3 (0.31 lb/in.^{3}). Since this alloy was used to model structural steel with a measured yield strength of $(\sigma_y)_p$ = 293 MPa (42.5 ksi), it had to be annealed to $(\sigma_y)_m = E_r(\sigma_y)_p$ = 159 MPa (23 ksi). Guidelines for appropriate annealing temperatures were obtained from graphs presented in Ref. 177 and 178 which are reproduced for this alloy and for CA 510 in Fig. 6.9. Also shown in this figure are the yield strengths obtained in this study from a series of tension tests on cartridge brass specimens annealed for one hour at different temperatures. An annealing temperature of 408°C was found suitable to reduce the yield strength to the desired value. The test results obtained from low and high strain rate tension tests (2×10^{-4}/sec. and 3×10^{-2}/sec.) of cartridge brass annealed at 408°C are shown in Fig. 6.10. The following observations can be made from this figure:

(1) The material exhibits a large linear elastic range, but shows a gradual decrease of stiffness beyond the proportional limit until it stabilizes at a strain hardening stiffness of about 2.5 percent of the elastic stiffness. This transition range between proportional limit and "yield strength" was observed, to a lesser or larger degree, in all copper alloys investigated.

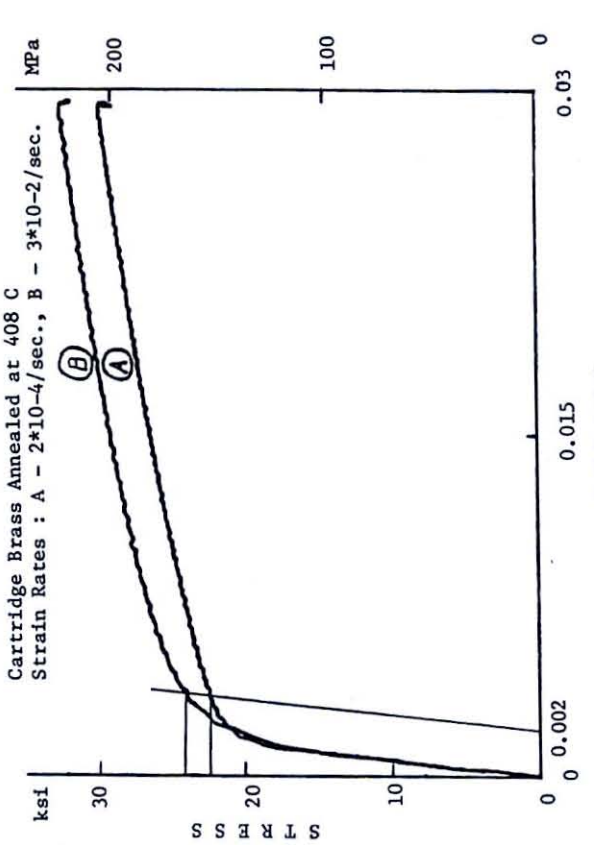

Figure 6.10 Tensile Stress-Strain Diagrams for Cartridge Brass Tested at Low and High Strain Rate

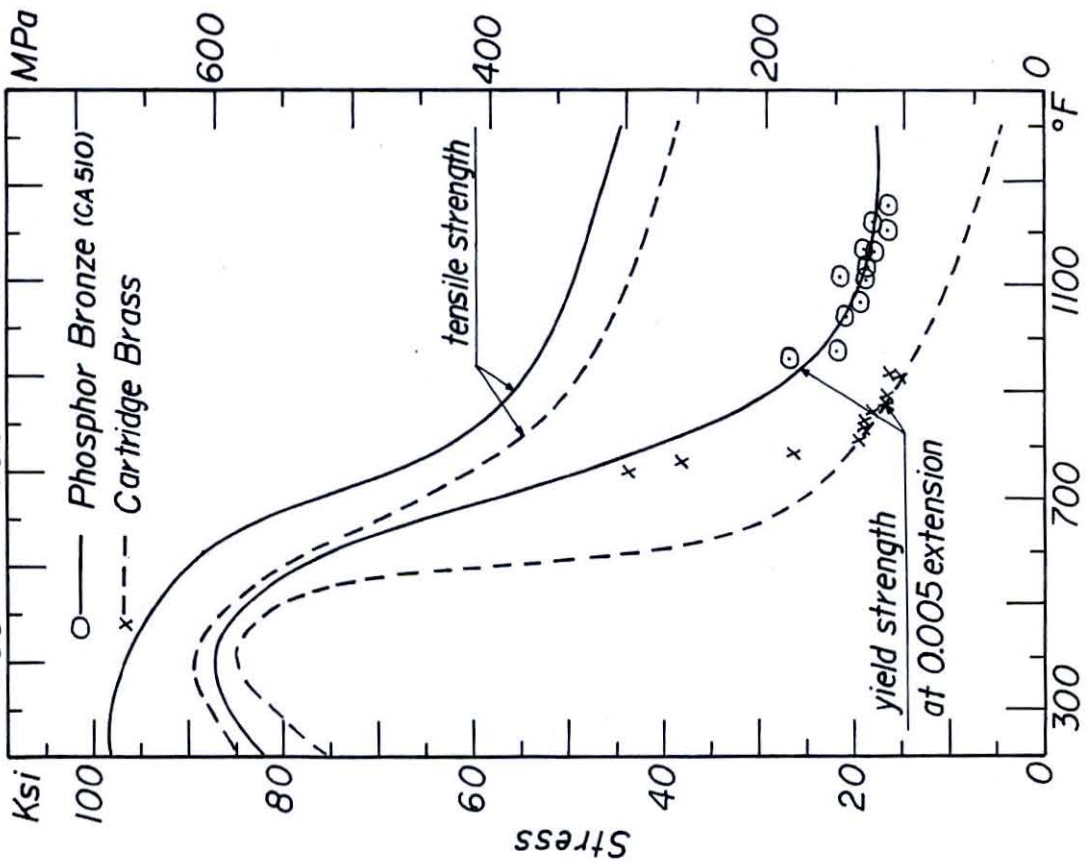

Figure 6.9 Annealing Curves for Phosphor Bronze and Cartridge Brass

(2) The strain hardening stiffness decreased very slowly below 2.5 percent in the strain range of interest. When compared to structural steel, this strain hardening causes a relatively higher strength beyond yielding under monotonic loading, promising even higher hardening under cyclic loading due to the highly annealed condition of the material.

(3) From the high strain rate test (curve B) it is evident that the strain rate effects are comparable to that of steel (see Fig. 6.5).

Thus, is can be concluded that annealed cartridge brass is a material that reproduces reasonably well the strength and stiffness properties of structural steel, at least under monotonic loading. However, unacceptable material properties developed in the heat-affected zones at welded connections. As can be seen from Fig. 6.9, continuous decrease in yield strength (grain growth) is associated with high temperature treatment. Even though the heat exposure due to welding is of short duration, over-annealing in a small region of the base material could not be prevented. Hence, cartridge brass should not be used for models of welded structures where yielding in the base material at welds is expected. Brazing may be an alternative in some cases, however, it would have to be done at temperatures below the desired annealing temperature which may not permit the attainment of sufficient strength, particularly at connections where high inelastic deformations have to be tolerated.

The problems associated with welding necessitated the investigation of copper alloy other than cartridge brass, and phosphor bronze was chosen for this purpose.

6.3.4 Phosphor Bronze (CA 510)

This alloy was selected mainly because of its specified excellent weldability (Ref. 179). CA 510 is very promising since its yield strength in the fully annealed condition is about 140 MPa (20 ksi) (see Fig. 6.9) which is in the range of the desired yield strength and, therefore, over-annealing due to welding should not pose a problem provided a too long exposure to the high welding heat can be avoided and thus large crystal growth can be prevented.

6.3.4.1 Stress-Strain Characteristics

Due to the content of interstitial atoms of phosphor in the crystalline structure, the general stress-strain behavior of phosphor bronze resembles that of structural steel where cool atoms fulfill a similar role. Not only does phosphor bronze exhibit a straight line behavior in its pre-yielding range but, as has been observed in several tests, also upper and lower yield can be identified in the tensile test diagram. Fig. 6.11 displays results of a tensile test of CA 510, annealed for 1 hr. at 520°C, and Fig. 6.12 provides a comparison between the stress-strain lines for structural steel and annealed phosphor bronze and cartridge brass. The similarity between the stress-strain diagrams for structural steel and CA 510 is noteworthy.

The modulus of elasticity of the annealed phosphor bronze is $E = 126.2 \times 10^3$ MPa (18.30×10^6 psi). The measured specific gravity is 8.8744. Thus, for the phosphor bronze and structural steel used in this study, the ratio of specific stiffnesses is $(E/\rho)_r = 1:1.92$, and the ratio of elastic stiffnesses is $E_r = 1:1.67$.

All the material tests on phosphor bronze were performed on

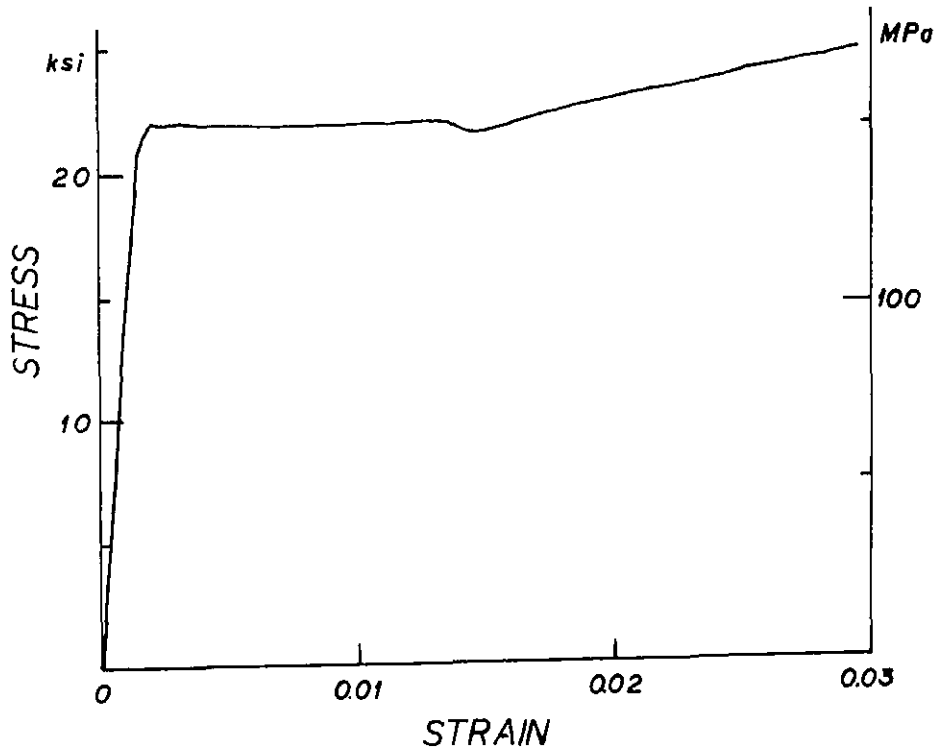

Figure 6.11 Tensile Stress-Strain Diagram for Half-Hard Phosphor Bronze (CA510) Annealed at 520°C/1 hr. and Tested at Low Strain Rate ($\dot{\varepsilon}$ = 2.4x10^{-4}/sec.)

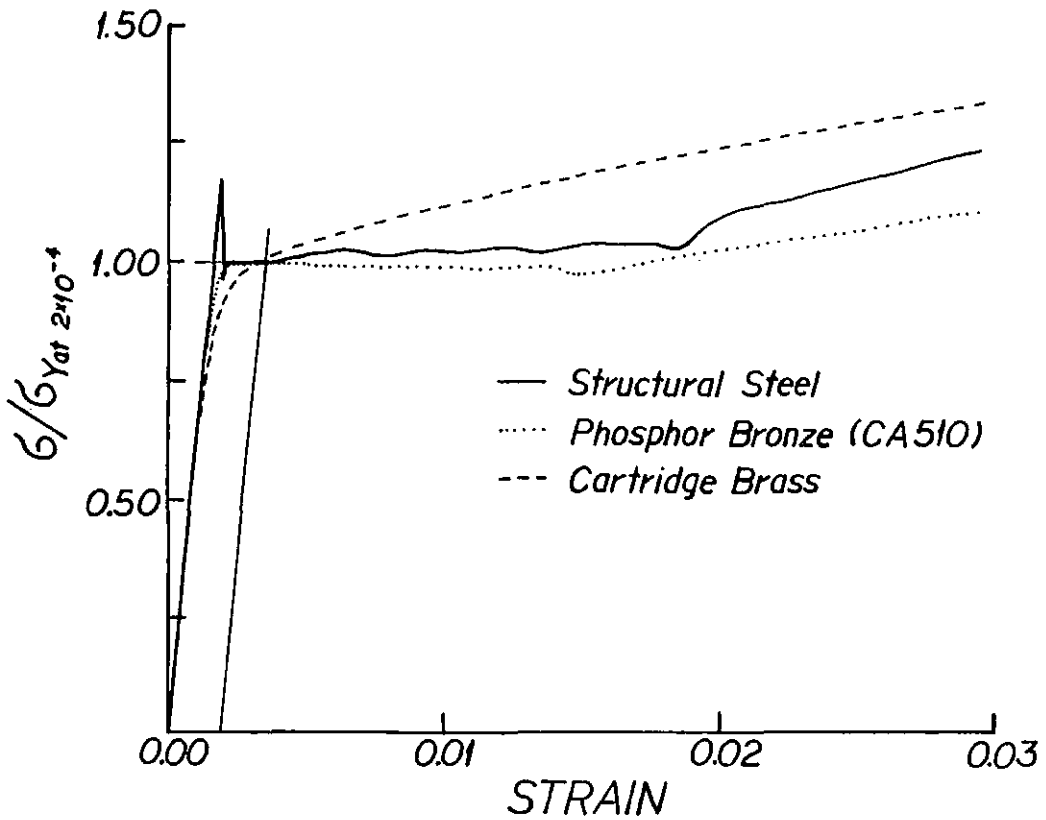

Figure 6.12 Tensile Stress-Strain Diagrams for Structural Steel, Annealed Phosphor Bronze and Annealed Cartridge Brass Normalized with Respect to their Individual Yield Stress

specimens scaled by l_r = 1:2 which approximately matches the E/ρ ratio of 1:1.92.

6.3.4.2 Annealing Results

Once the moduli of elasticity of the prototype and model materials are established the scale ratio for the yield stress can be derived from $(\sigma_y)_r = E_r$. For the CA 510 used in this study to model structural steel, the ratio $(\sigma_y)_r$ is 1:1.67 resulting in required σ_y of 171 MPa (25 ksi). A series of tensile specimens was annealed covering a range of annealing temperatures from 500°C to 675°C (930°F to 1250°F), and tested in tension on the MTS closed-loop system. Results of this study are shown in Fig. 6.9. An annealing temperature of 520°C (968°F) was chosen as appropriate for this study.

6.3.4.3 Strain Rate Effects

A study of the strain rate effect on the yield strength of phosphor bronze was performed to provide information allowing the correlation of static and dynamic test results, and to compare the magnitude of the effect in prototype and model materials.

A series of 15 annealed tension specimens was tested at strain rates varying from 1.4×10^{-5}/sec. to 1.4×10^{-1}/sec. The strain rates chosen for this study were based on applying a time scale factor t_r of $1:\sqrt{2}$ to the rates used in the steel study (see Table 6.3). This factor was based on the true replica scaling law correlating steel prototype and CA 510 model materials. The E/ρ ratio for these two materials is of the order of 1:2, hence $t_r = 1/\sqrt{2}$.

The results of this study are summarized in Table 6.5. Fig. 6.13 displays individual data points normalized with respect to the average value at strain rate 2.8×10^{-4}/sec. and a curve fitted between them. The equation of this curve is

$$(\sigma_y)_d/(\sigma_y)_{2.8\times10^{-4}} = 0.971 + 0.20\ \dot{\varepsilon}^{\,0.235} \qquad (6\text{-}4)$$

The obtained stress-strain results do not exhibit a noticeable change in the initial stiffness of the material, and exhibit only a minor decrease in the strain hardening stiffness, thus CA 510 behaves in a manner very similar to structural steel.

In order to provide a comparison between the curves for structural steel and for CA 510 both the curves are shown in Fig. 6.14. The lower strain rate effect exhibited by phosphor bronze will be partially accounted for by the higher strain rates occurring in the model. This is in particular true in the gravity neglected models for which $t_r = l_r$ and not $\sqrt{l_r}$ as for true replica models. Only for large-scale model studies of high strain rate phenomena (impact) the difference in yield strength may be significant since the time scale ratio is too small to provide a sufficient "shift" of the phosphor bronze curve to the left on the strain rate axis.

Table 6.5

Summary of Results for Strain Rate Effect

on the Yield Stress of Phosphor Bronze

Strain Rate	No. of Specs.	Average Yield Stress at 0.002		Coefficient of Variation	Normalized Yield Stress
1/sec.	--	MPa	ksi	%	--
1.4×10^{-5}	4	158.9	23.04	3.3	0.982
2.8×10^{-4}	5	161.9	23.48	1.6	1
6.9×10^{-3}	3	166.2	24.10	1.5	1.026
1.4×10^{-1}	3	178.2	25.85	2.1	1.101

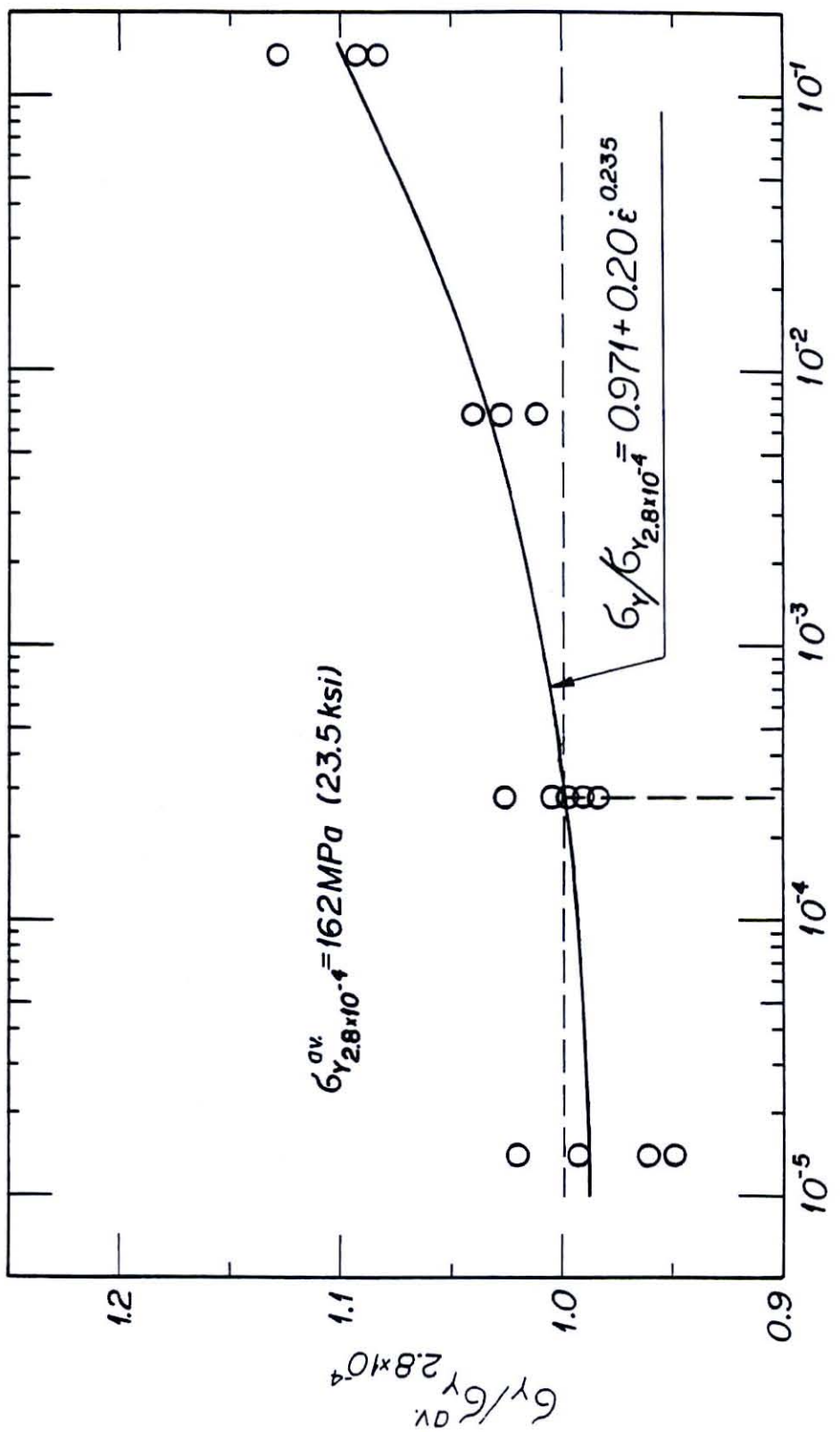

Figure 6.13 Strain Rate Effect on the Yield Stress of Phosphor Bronze (CA 510)

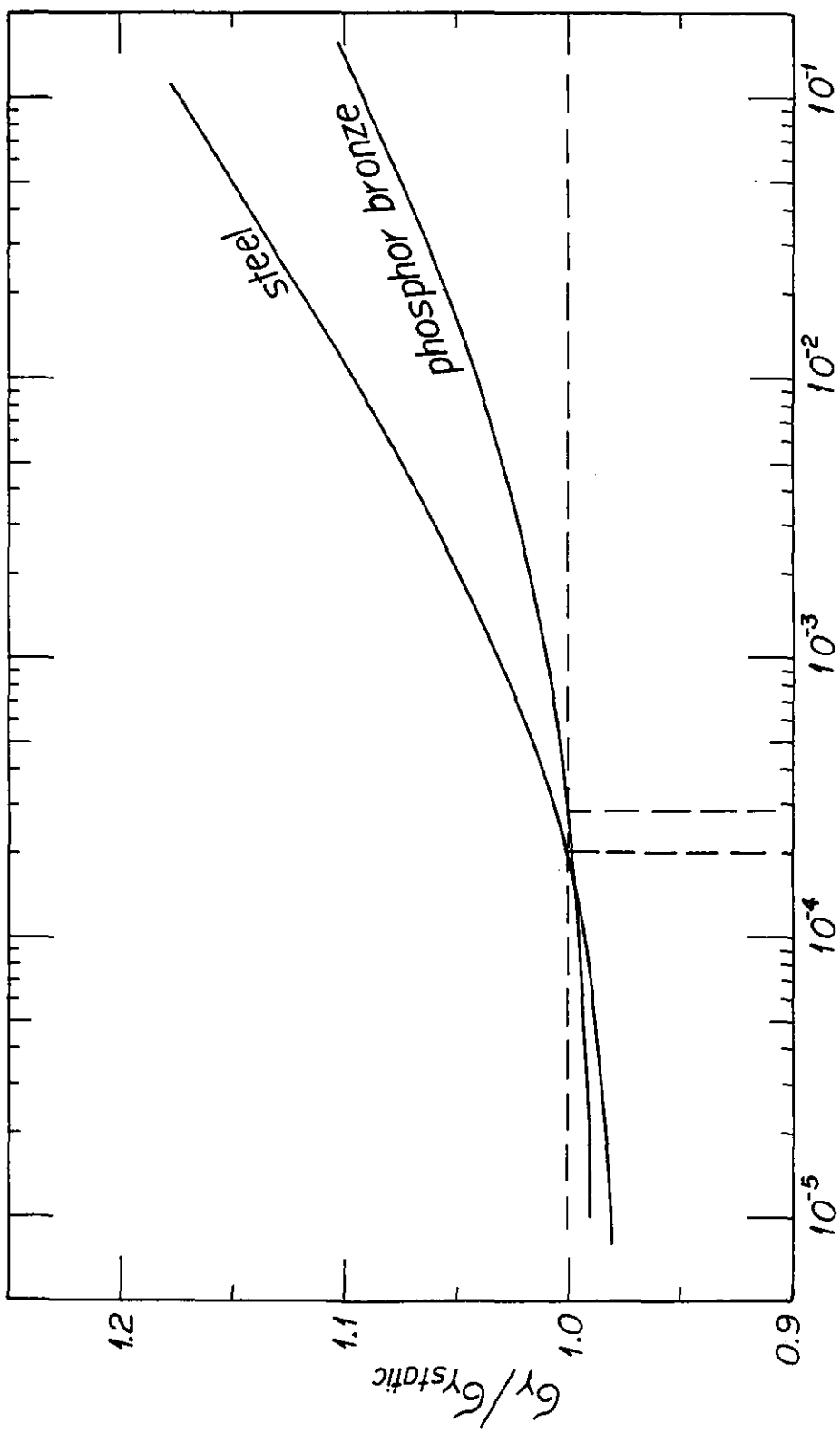

Figure 6.14 Comparison of Strain Rate Effect on the Yield Stress of Structural Steel and Phosphor Bronze

6.3.4.4 Cyclic Behavior

A series of cyclic tests was performed to provide comparison data for the simulation of cyclic behavior of structural steel.

The three loading histories used in cyclic tests of structural steel (see Table 6.1) were implemented using the same strain increments ($\varepsilon_{y,steel}$). It was found that, unlike the case for structural steel, three loops per amplitude did not lead to a stabilization of the hysteresis loops. Therefore, two additional load histories were carried out, namely load histories No. (2) and No. (3), but with twelve cycles per amplitude rather than with three. Even with this relatively large number of cycles the material, strongly softened by the annealing process, did not reach totally stable hysteresis loops although the peak stress difference between the last loops was very small. The first and last loops at various load amplitudes for three different load histories are presented in Fig. 6.15.

Fig. 6.16 shows cyclic stress-strain diagrams for structural steel and phosphor bronze for loading history No. 1 (Table 6.1). Both the diagrams are normalized with respect to the yield stress of the materials and with $\varepsilon_{y,steel}$, which was used to control the strain increments.

Comparing the two diagrams in Fig. 6.16 it is evident that the annealed phosphor bronze work-hardens considerably more than the structural steel. For strain amplitudes less than or equal to $7\varepsilon_{y,steel}$, the stress-strain hysteresis loops are similar in shape and enclosed area, but for larger strain amplitudes the similitude becomes rather unsatisfactory. The large and history dependent work-hardening of annealed phosphor bronze is more evident from Fig. 6.17 which shows skeleton curves for various deformation histories. For structural steel the

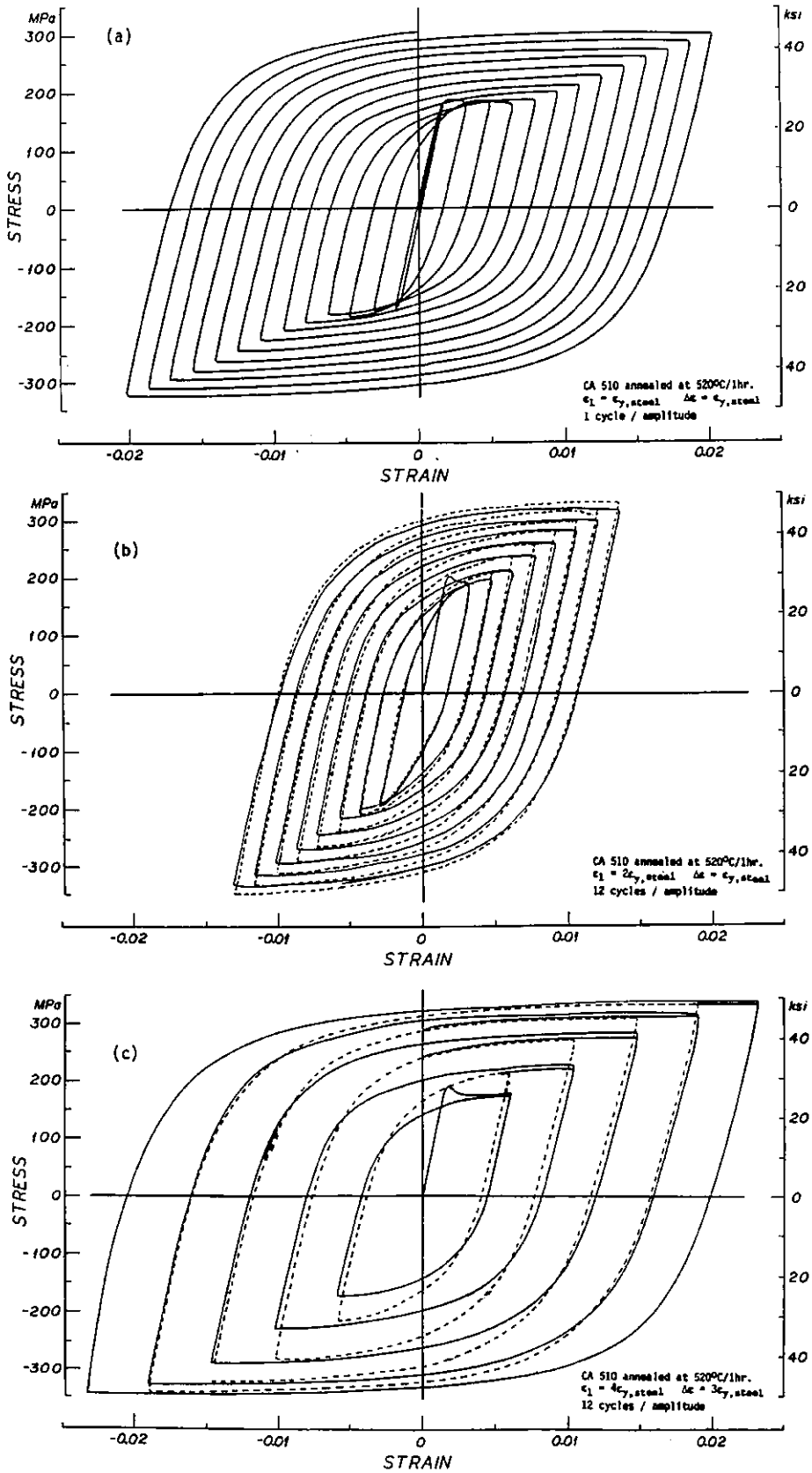

Figure 6.15 First and Last Loops at various Strain Amplitude from Cyclic Tests of Phosphor Bronze

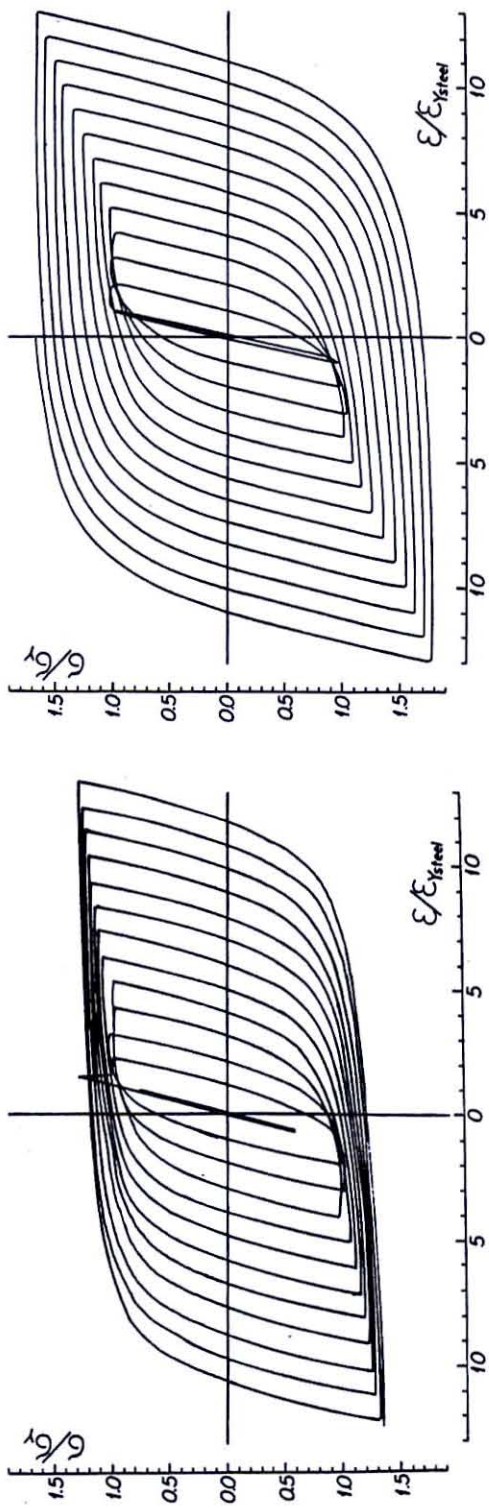

(a) Structural Steel (b) Annealed Phosphor Bronze

Figure 6.16 Comparison of Stress-Strain Hysteresis Loops of Structural Steel and Phosphor Bronze

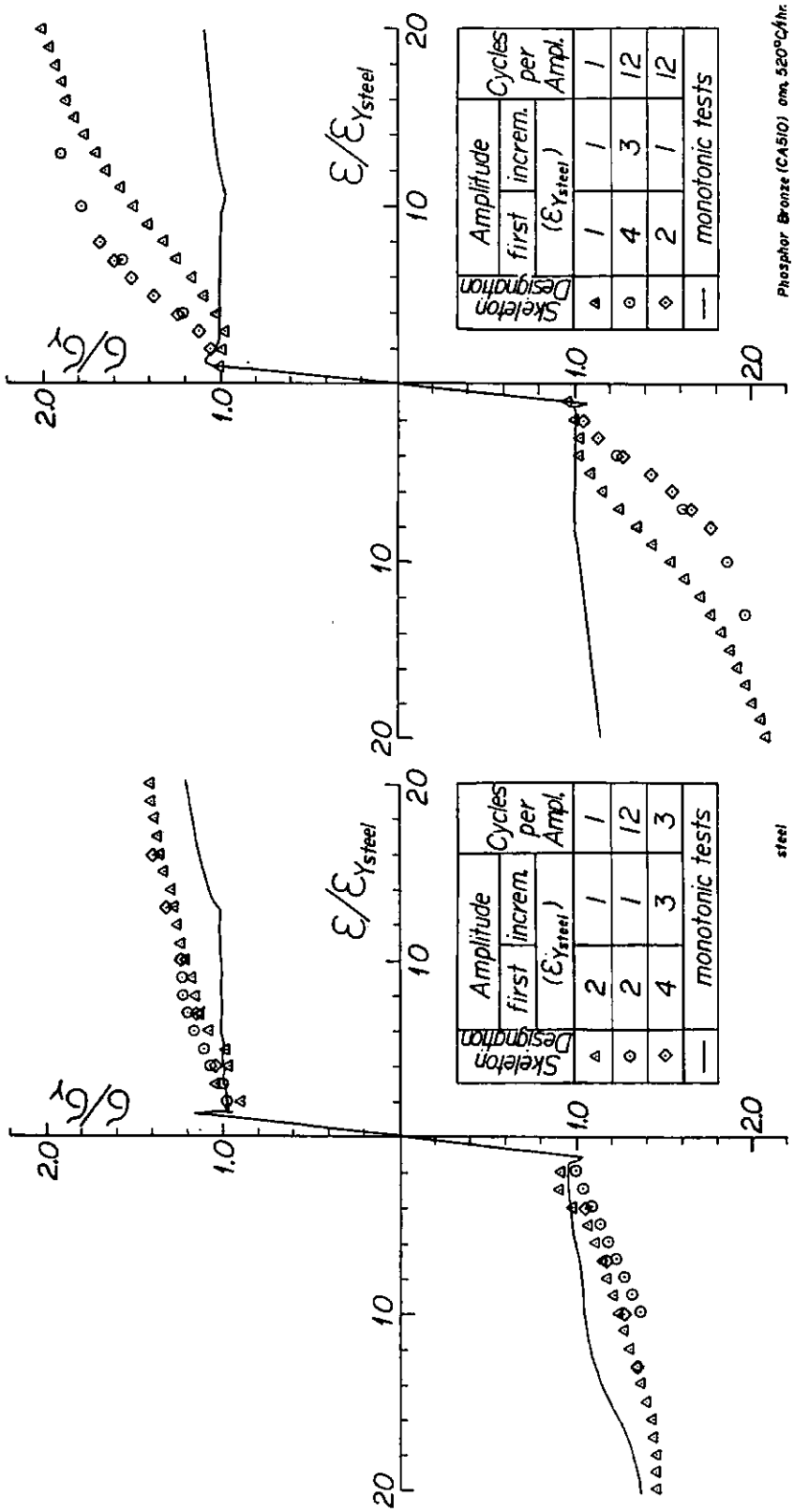

Figure 6.17 Skeleton Curves of Structural Steel and Phosphor Bronze for Various Cyclic Load Histories

skeleton curves are similar regardless of the number of cycles per amplitude, while annealed phosphor bronze exhibits significantly larger work-hardening for twelve cycles per amplitude than for one cycle.

The diagrams presented in Figs. 6.16 and 6.17 point out the limitations of the use of annealed phosphor bronze for simulation of the cyclic behavior of structural steel. Provided that the number of inelastic deformation cycles is small, satisfactory simulation appears to be possible. If the response history demands a large number of large deformation cycles, annealed phosphor bronze as model material may give misleading information on the energy dissipation capacity of structural steel due to its superior work-hardening properties. This simulation problem is discussed further in Section 8.1 and in Chapter 9 which present experimental data on pseudo-static component tests and shake table tests.

6.3.5 Lead and its Alloys

When it is desired to test a small scale replica model of a steel structure, and artificial mass simulation is not feasible, the choice of suitable model materials is very limited because of the requirement that $(E/\rho)_r = l_r$. In a review of available materials (see Table 6.2) only lead and its alloys showed some promise. These materials can easily be formed into structural shapes through casting or extruding but have certain material characteristics, such as high creep and damping, which pose difficulties in material simulation.

Chemical lead (99.9% Pb) has an E/ρ ratio less than one-twentieth that of steel. However,its stress-strain curve is very nonlinear at low

stresses, and the material is subjected to large creep deformations and high damping losses. Consequently, it has not been considered further in this studies.

Antimonial lead (94% Pb, 6% Sb) with E = 2.0×10^{10} Pa (2.9×10^{6} psi) and γ = 107 kN/m^3 (0.393 lb/in.^{3}) has an E/ρ of one-fourteenth that of steel. For the measured modulus, the desired yield strength to simulate A36 steel would be 24.8 MPa (3.6 ksi). The tension test on this material (see Fig. 6.18) showed too low a yield strength, but a suitable hardening or chemical treatments could be used to increase its yield strength to the desired level. More research on this material is needed to asses its feasibility as a model material.

Type metal (82.4% Pb, 5.9% Sn, 11.7% Sb) is a readily available material with an E/ρ of approximately one-tenth of that of steel. The measured E-modulus is 2.8×10^{10} Pa (4.0×10^{6} psi) which would require a yield strength of 34.5 MPa (5.0 ksi) to simulate A36 steel. The stress--strain diagram for this material (see Fig. 6.18) shows that the measured yield strength is somewhat too high, however annealing at 200°C did reduce the yield strength to approximately the desired value. However, the shape of the stress-strain diagram differs significantly from that of steel, and it will be extremely difficult to reconcile these differences to a satisfactory level through chemical treatment or mechanical hardening.

Material damping is another problem which must be considered in the use of type metal as a model material. This aspect was investigated through damping tests on a torsion pendulum apparatus. These tests have shown that damping in type metal is highly dependent on frequency, temperature and stress level. At 20°C it varied from 0.5% for high frequency

and low stress (cast material) to more than 2% for low frequency and high stress levels approaching yielding (rolled material). It was observed that the damping in rolled type metal was consistently higher than in cast material by an amount of 40 to 90% at different stress levels.

Due to the time dependent behavior of lead alloys and the early non-linearity in their stress-strain behavior, it was concluded that lead alloys cannot be recommended as model materials. Their use would necessitate complicated chemical or mechanical treatment which renders them unfeasible for most practical applications.

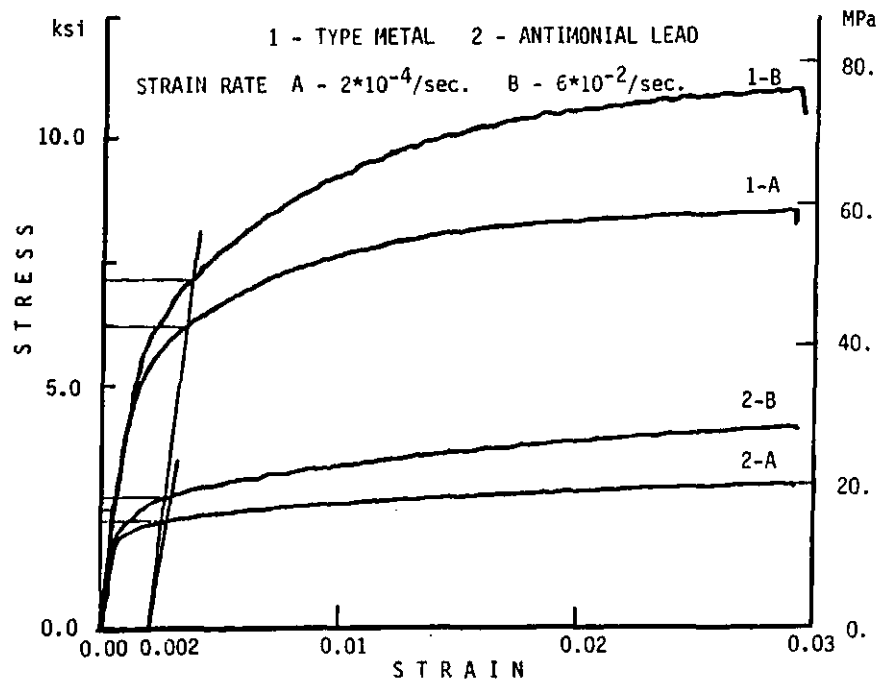

Figure 6.18 Stress-Strain Diagrams for Lead Alloys -- Low and High Strain Rates

CHAPTER 7

MATERIALS FOR MODELS OF REINFORCED CONCRETE STRUCTURES

7.1 SIMULATION OF CONCRETE

7.1.1 Introduction

Scale models of plain and reinforced concrete structures have gained acceptance as a tool of structural analysis, as has been shown in many publications and symposia devoted to this topic, e.g., Refs. 12, 13, 14.

As with other types of structural models, those of concrete structures can be divided into two fundamental groups : elastic models and ultimate strength models.

Elastic Models are constructed to study the overall structural behaviour and force distribution in the linear elastic regime. The materials used for elastic model tests must fulfill the basic requirements of the theory of elasticity, namely linear stress - strain relationship, invariant Poisson's ratio, and homogenity. Because of their high workability, the most commonly used materials are plastics, both thermosettting (epoxies, polyesters) and thermoplastic (acrylics, polivynyl chloride - PVC). Mirza (Ref. 14) provides a review of this type of models and a comprehensive list of specific references.

Ultimate Strength Models are constructed to provide not only information on the structure in its virgin stage, but also on its behaviour throughout the entire loading history till failure. The necessity of simulation of the behaviour of the prototype material in its entire

strength range significantly limits the number of potential model materials which will satisfactorily reproduce concrete behaviour. Gypsum plasters, cement mortars, and concrete made with aggregate of limited size known as microconcrete have been used with various degrees of success. Many reports of ISMES (e.g., Refs. 62 to 64 and 71) as well as Fumagalli in his book (Ref. 3) discuss the use of cement and pumice mortars in practical model analysis. Burggrabe (Ref. 117) gives a schematic presentation of the relation between the size of the model and the choice of the model material (Table 7.1).

Table 7.1

Size of Models and Suitable Model Materials

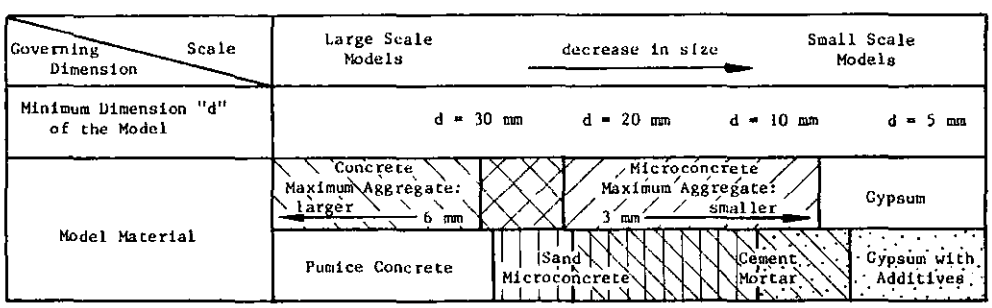

The minimum dimension of the model is by no means the only criterion in the decision on the model material, and such factors as the character of failure of the material (more brittle in mortar mixtures), creep for tests with sustained loadings, etc., can be of decisive importance.

Although gypsum has been used successfully for elastic model analysis because of its high workability, low Poisson's ratio and straight stress - strain relationship, its applicability to ultimate strength studies is limited. The reason is that the nonlinear stress - strain region exists in wet gypsum only, and the strength of wet gypsum is lower than that demanded for concrete modeling. Gypsum also possesses excessive tensile strength and low bond to the reinforcement in the case of reinforced gypsum models (Refs. 16,18,107).

Successful studies on gypsum-sand mixtures have been reported by White and Sabnis (Refs. 120,121), and by Zelman et. al. (Ref. 111).

Pumice mortars provide the often welcome low E modulus (Ref. 17) but the insufficient bond to the reinforcement causes considerable problems in small scale models (Ref. 107).

Microconcrete, made mainly of the same materials and with the same design philosophy as in the prototype concrete, has gained the widest acceptance of all the aforementioned model materials.

In the subsequent sections attention will be focused mainly on this material.

7.1.2 Design of Microconcrete Mixes

Several approaches to the design of microconcrete mixes have been developed, and their applicability depends on similitude requirements for the particular study, the model construction technique and other model design considerations. With the increase in the understanding of the properties of microconcrete and of their control, and with the development of new methods of quality control and evaluation of properties, the final goal, namely satisfactory fulfillment of similitude requirements, can be attempted more successfully than ever.

7.1.2.1 Basic Requirements Imposed on Microconcrete as Model Material

Modeling of plain, reinforced and prestressed concrete structures is subjected to the general laws of similitude which are presented in Chapter 4. In Refs. 15, 36, and 117 these laws are presented with particular

stress on modeling of concrete.

Similitude laws for uniaxial stress - strain relationship require affinity of the derivatives of stress with respect to strain, and of strain with respect to time (Chapt. 4). These criteria are subjected to modification according to the significance of a given material property to the studied problem.

The first goal in the most basic mix design is to achieve a prescribed compressive strength (f'_c) at a given age of the concrete. Full affinity of the stress - strain relationship for compressive tests is required next. Basic similitude laws for model materials demand that strains in the model be the same as in the prototype. It has been suggested (see Section 4.5.3) that this requirement could be relaxed ($\varepsilon_r \neq 1$) using appropriate modification factors.

Whenever tensile strength of concrete is of basic importance in the ultimate behaviour of the structure, the ratio of compressive over tensile strength should be equal in model and prototype.

The initial stiffness of a structure is strongly influenced by the elastic modulus of the material (E), demanding a proper simulation of this property. This would be achieved with full $f_c - \varepsilon$ line simulation.

Studies concerned with shear transfer in the post-cracking stage demand a closer look at the aggregate interlock mechanism which at this time is not understood fully even in the prototype domain. Since this mechanism depends on surface roughness and crack width, significant simulation problems have to be expected.

For structures for which long-time events are of significant importance, additional requirements are to be taken into account. This is true in particular when the prototype initial conditions need to be simu-

lated. In theory, simulation of initial conditions will require the tracing of all time history events affecting the prototype, from the time of construction to the time at which the dynamic event takes place. These events will include, amongst others, construction sequence, curing methods, time dependent material effects (creep, shrinkage, increase in compressive strength of concrete), as well as damage accumulation due to previous events.

Modeling of combined creep and shrinkage effects is a virtually impossible task because of incompatibilities in time scaling. Simulation of creep requires equal time in model and prototype ($t_r = 1$) while simulation of shrinkage requires large time scaling. Creep and shrinkage depend strongly also on the size and grading of the aggregates which are not reproduced at model scales. Considering these problems it is usually a futile exercise to attempt modeling of creep and shrinkage phenomena, particularly since they often have a reasonably small influence on the ultimate strength behavior under cyclic loading. It appears to be more appropriate to control the initial conditions in the model experiment by minimizing shrinkage and creep through sealing of the model structure (for instance, by applying coats of shellac) and avoiding long-time preloading prior to the dynamic test.

It is to be expected that, with the increasing understanding of constitutive relations for multi-axial strength of prototype concrete, an increasing effort will be made to accomodate this knowledge in microconcrete design and testing whenever justified.

7.1.2.2 Levels in the Simulation of Concrete Properties

Simulation of the properties of a heterogenous material such as con-

crete presents a particular difficulty due to the complexity of the influence factors. Studies of such a material can be performed at different levels:

a) atomic and molecular

b) inter-structural

c) macroscopic or phenomenological

It is seldom given to the designer to influence the atomar structure of microconcrete, except for the use of a specific cement type, aggregate and chemical additives, all of which influence the chemical reactions occurring in the gel formation and the gel-aggregate force development. Considering the complexity of hydration and hardening processes, it is not to be expected that intervention by the mix designer at the atomic and molecular level will be feasible.

Scaling of concrete properties at the inter-structural level would require not only the appropriate scaling of the aggregate size but also scaling of the pore sizes in the gel, and void sizes in the aggregate. Although the last requirement might be partly satisfied by the nature of small aggregates, the gel pore size can be only slightly influenced by the use of finer cements (i.e. Type III).

Gradeline design for the model aggregate based on length scale requirements is feasible only as far as the large aggregate size is concerned (Refs. 18, 39). Shifting of the entire sieve line according to the length scale of the model requires adjustments, as the lower limit of the aggregate size usually has to be increased from that dictated by similitude. It is customary (Refs. 13, 114) to limit the amount of aggregate passing U.S. No.100 sieve (0.15 mm) to less than 10%. Due to the high specific area of finer aggregate, the amount of water (A/W ratio) necessary to achieve desired workability increases rapidly with

the decrease of the average aggregate size, thus increasing the amount of cement (C/A) necessary to achieve the required compressive strength which in turn results in a too high tensile strength of the concrete.

The above speculations show that a phenomenological approach to the mix design, supported by the knowledge of the effects of inter-structural changes, might be the most appropriate, if not the only realistic one. In the design of prototype concrete one of the objectives is to find a grading which would result, for available aggregates, in the best workability at the lowest water content. This can be achieved, within limits, by minimizing the specific surface area. It has been found that, provided the specific surface area of the aggregate (coarse + fine) is kept constant, a wide difference in grading will not affect the workability appreciably, and this provides a means of designing a gap grading (Ref. 143). Abram's law (Ref. 144) suggests that, provided the concrete is fully compacted, the compressive strength is not affected considerably by the aggregate shape, surface texture and the aggregate grading. The above information does not imply that concrete properties are totally insensitive to aggregate grading, but that an extensive effort in the simulation of the grading curve of prototype mix might not be justified. On the other hand, for simulation of the concrete - reinforcement stress transformation zone, inter-structural similarity at this zone is important. This is shown by the schematic stress transfer diagram of Fig. 7.1 (from Ref. 119).

Line I - I represents the tensile crack, line II - II represents the shear crack, and line III - III either bond or compression failure. The development of crack line II-II and in particular crack line III - III depends strongly upon the structure of the aggregate matrix. Ferthermore

the bond failure III-III depends strongly upon the ratio of the size of reinforcement ribs to the size of the surrounding aggregate.

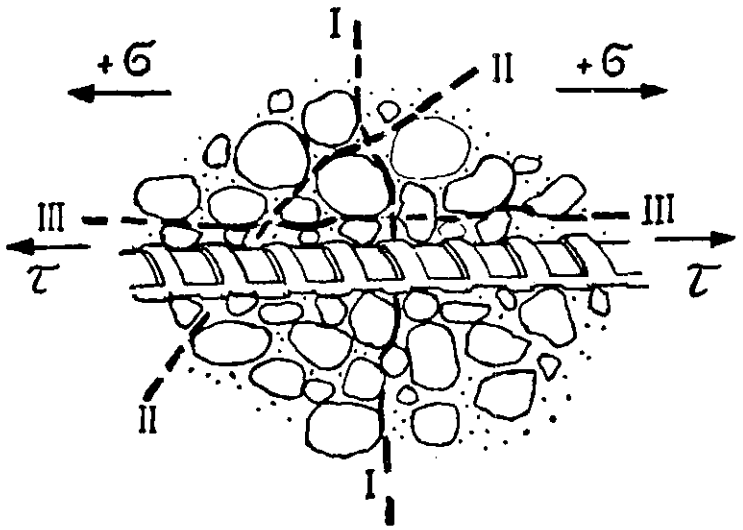

Figure 7.1 Stress Transfer in Reinforced Concrete (Ref. 119)

7.1.2.3 Control of Properties through Mix Proportioning and Use of Additives

Several attempts have been made to present definite guidelines for a mix with desired final strength properties (i.e. Refs. 14, 114). It has to be expected that, due to differences in the properties of the cement used, in the water absorption of the aggregate, in the compaction techniques and other mix design details, the properties of the final product may be quite different from the one predicted from the guidelines (Ref. 43). Nevertheless, these general guidelines can be very useful in the initial mix proportioning. Figure 7.2 presents sieve lines used by various investigators, and Table 7.2 lists mix proportions and the compressive strength of the concrete resulting from their application.

In this study the strength of microconcrete of a wide range of

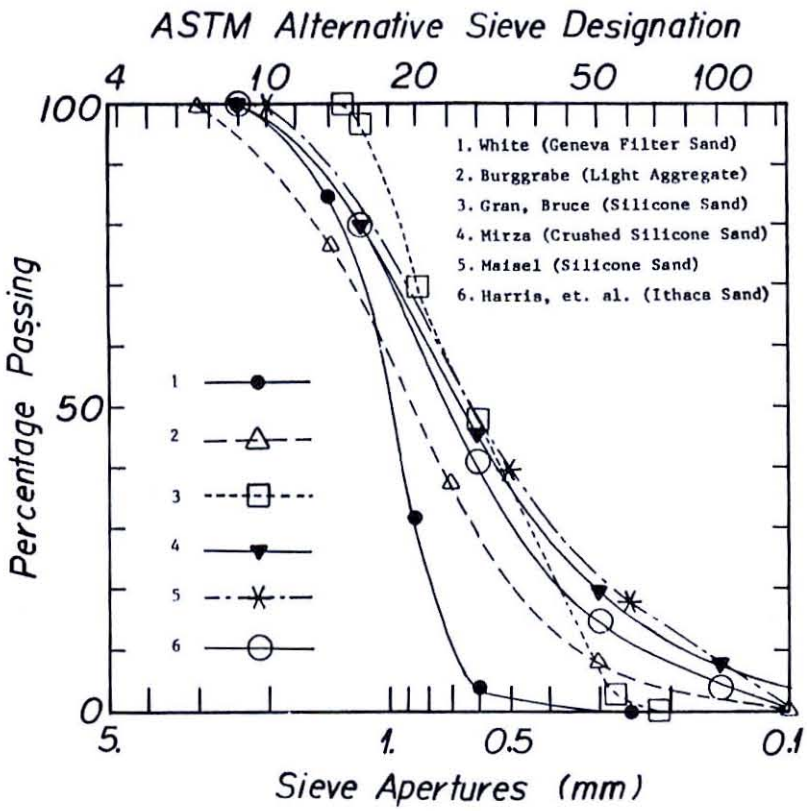

Figure 7.2 Sieve Lines Used by Various Researchers

Table 7.2

Microconcrete Mixes Used in Various Studies

C : A : W	Age	f'_c		Reference	C : A : W	Age	f'_c		Reference
	days	MPa	ksi			days	MPa	ksi	
1:4.0 :0.83	--	17	2.5	Mirza (Ref. 2)	1:5.0 :0.80	7	19	2.8	White (Ref. 43)
1:3.75:0.72	--	21	3.0			14	24	3.5	
1:3.25:0.60	--	28	4.0			28	29	4.2	
1:2.75:0.55	--	34	5.0		1:3.5 :0.60	7	32	4.6	
1:2.50:0.50	--	41	6.0			14	36	5.2	
1:2.25:0.40	--	48	7.0		1:3.0 :0.60	7	36	5.2	
1:3.75:0.72	14	38	5.5	Gran, Bruce (Ref. 23)		14	41	5.9	
1:3.25:0.60		39	5.7			28	47	6.8	
1:2.75:0.55		43	6.1						
1:2.50:0.50		51	7.4						
1:5.40:1.20	--	15	2.2	Fuss (Ref. 22)	1:4.4 :0.8	63	39	5.7	Harris, et. al., (Ref. 30)
1:4.32:1.00	--	20	2.9		1:3.6 :0.7	23	45	6.5	
1:3.40:0.83	--	28	4.1		1:3.6 :0.5	63	55	8.0	
1:2.68:0.70	--	36	5.2		1:2.4 :0.5	63	61	8.9	

aggregate to cement to water (A:C:W) ratios was investigated. This was done for two reasons. First, to evaluate the properties of microconcrete of different mix proportions, and second, to supplement the existing data on strain rate effects on the compressive strength of microconcrete.

All the material studies on microconcrete properties were performed on 50 x 100 mm (2 x 4 in.) cylinders, using Type 3 (High Early Strength) cement.

The maximum aggregate size (MAS) was established to be passing ASTM sieve #8 (2.4 mm), and the grading line for the aggregate was to match closely the grading line recommended by White in Ref. 25 (Fig. 7.3).

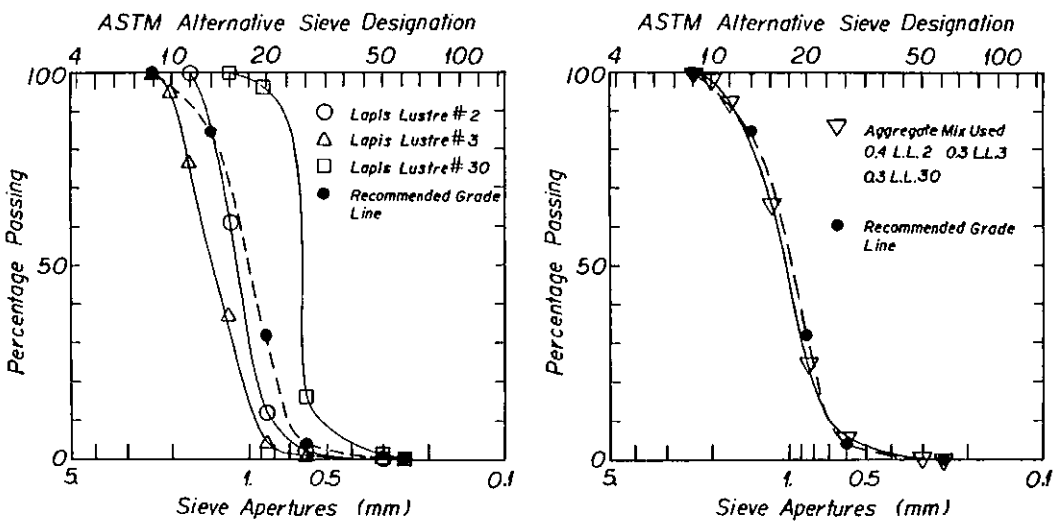

(a) Individual Sands (b) Final Grading Line

Figure 7.3 Sieve Line of Aggregate Used in This Study

Locally available (Lone Star, Monterey, California) sea sand (Lapis Lustre) was used as aggregate. The thoroughly washed sand is sold in sacks in narrow gradation ranges. Lapis Lustre #3 (MAS below 2.4 mm), #2 (MAS below 1.7 mm), and #30 (MAS below 0.84 mm) with individual grade lines as shown in Fig. 7.3a were mixed in proportions 0.4:03:03 to obtain a grade line as shown in Fig. 7.3b.

The mixing of the microconcrete was done manually by first combining the weighed aggregate and cement and then gradually adding of water. The mix was placed in the oiled steel cylinder molds in two layers, each of them compacted by 20 strokes of 12 mm (0.5 in.) rod. After smoothing of the upper surface of the concrete the molds were covered to prevent moisture loss and left undisturbed for 24 hours. Subsequently, the molds were stripped and the specimens were transfered to the fog room (95% RH at about 20°C).

At the age of approximately two weeks, the specimens were capped and then returned to the fog room. The capping was done using a melted sulphur capping compound and a precision jig (Fig. 7.4).

One day before testing, the specimens were submerged in lime-saturated water, and kept in this solution until about 45 minutes before the beginning of the actual test. This time span was needed for mounting of the specimen in the testing machine and attaching of the instrumentation.

The testing was performed on a closed-loop MTS testing machine, utilizing control of displacement rate. Because of the importance of the strain built-up in the testing system, displacement rates were controlled through an extensometer monitoring the distance between the plattens, rather then using conventional stroke control.

Average strains were obtained from displacement measurements at the central 50 mm (2 in.) of the specimen. The measurements were done with four clip extensometers attached at 90 degree angles to the specimen (Fig. 7.5). The four obtained strain-time records were averaged and the average was combined with the stress-time record resulting in one stress - average strain plot. The results obtained in this study are summarized in Table 7.3, Figs. 7.6 and 7.7.

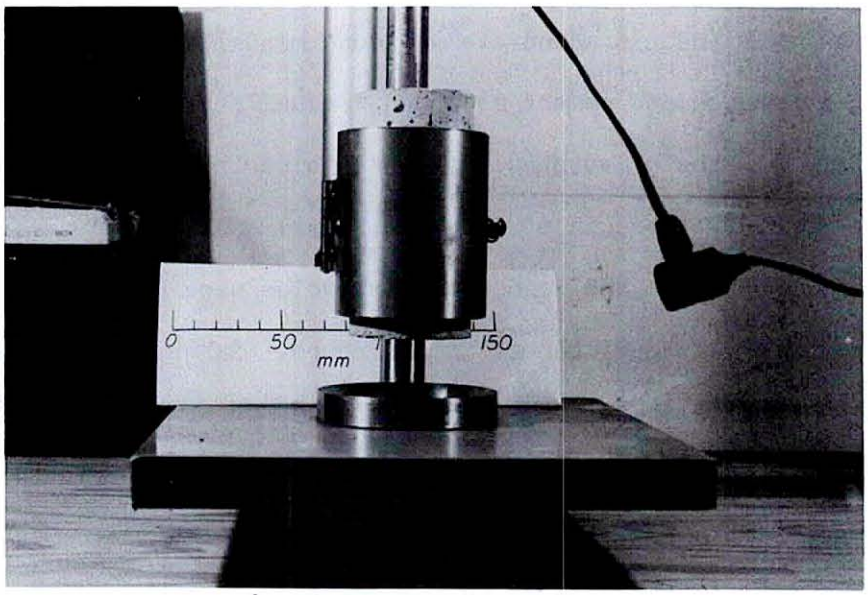

Figure 7.4 Capping Jig

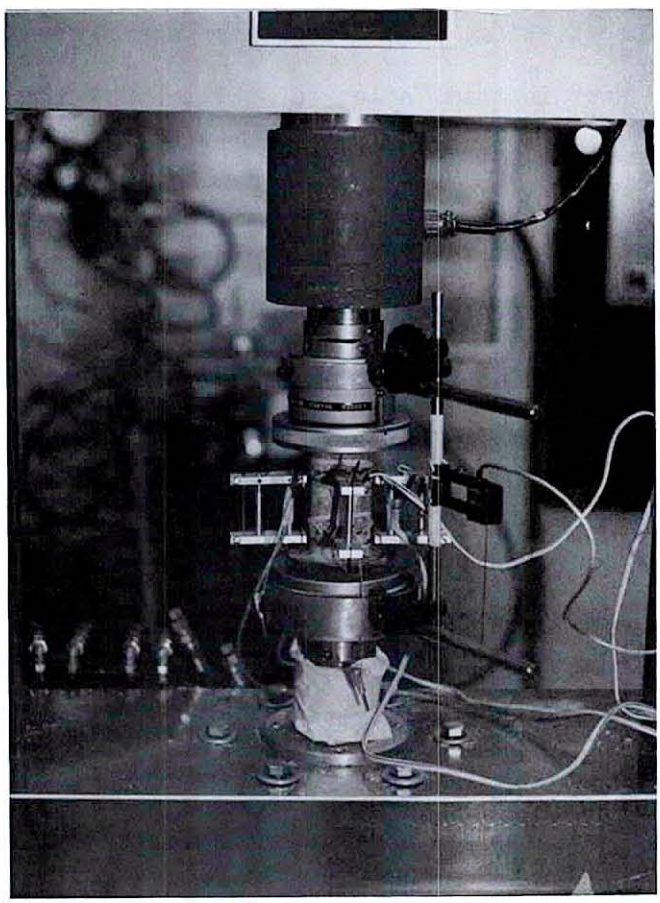

Figure 7.5 Compression Specimen with Attached Extensometers

Table 7.3 Microconcretes Used in This Study

Mix No.	C : A : W	Age	Compression				Split Cylinder		$\frac{f'_t}{f'_c}$ x100	$\frac{f'_t}{\sqrt{f'_c}}$
			No. of Specs.	f'_c		Coeff. of Var.	No. of Specs.	Coeff. of Var.		
		days	---	MPa	ksi	%	---	%	---	$\sqrt{ksi}$
I	1:5.0 :0.8	16	4	18.9	2.75	4.4				
		45	3	20.6	2.99	7.6				
1	1:5.0 :0.7	24	3	21.7	3.14	6.3				
2	1:5.0 :0.6	24	3	27.0	3.92	3.1				
3	1:4.0 :0.80	24	3	21.1	3.07	1.2				
4	1:4.0 :0.75	24	3	22.8	3.31	4.1				
5	1:4.0 :0.70	24	2	26.0	3.77	1.5				
6	1:4.0 :0.65	24	5	30.4	4.41	2.6	3	13.2	9.7	6.35
7	1:3.5 :0.75	17	3	27.0	3.91	3.8				
8	1:3.5 :0.70	17	3	30.1	4.37	0.9	4	10.0	8.8	5.99
9	1:3.5 :0.65	17	3	33.5	4.85	0.2				
10	1:3.25:0.8	14	3	36.1	5.23	2.8	4	4.7	9.6	6.85

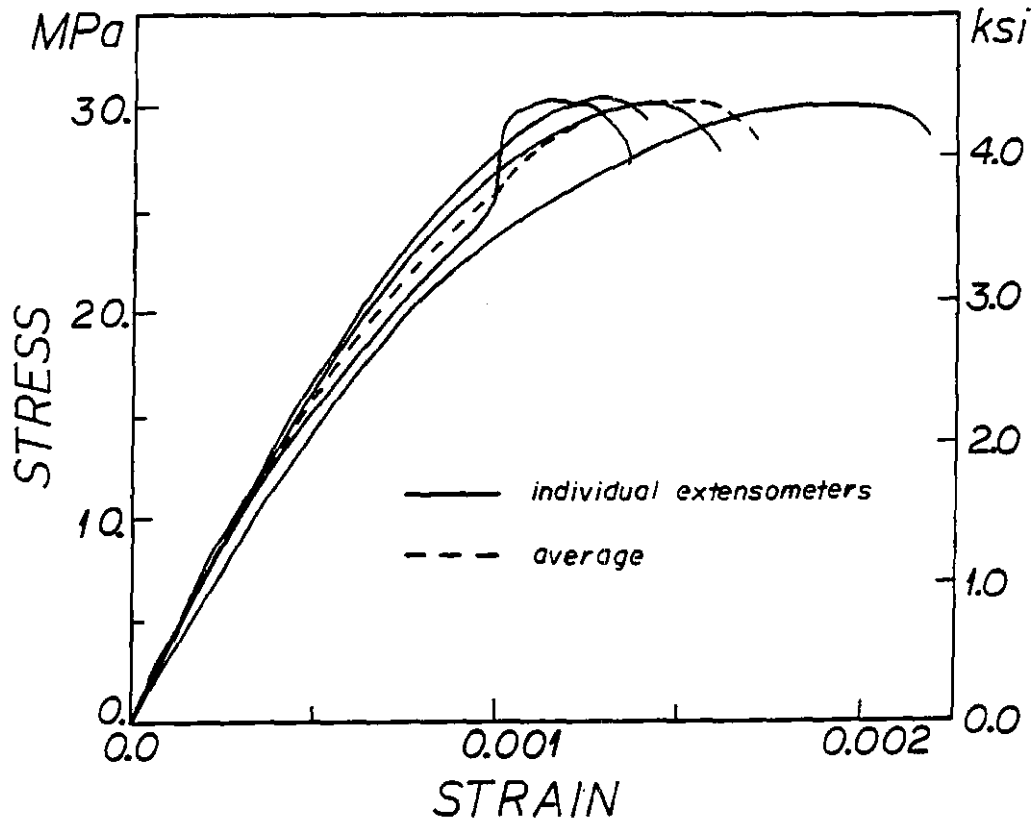

Figure 7.6 Four Stress-Strain Curves from Compression Test with Four Extensometers

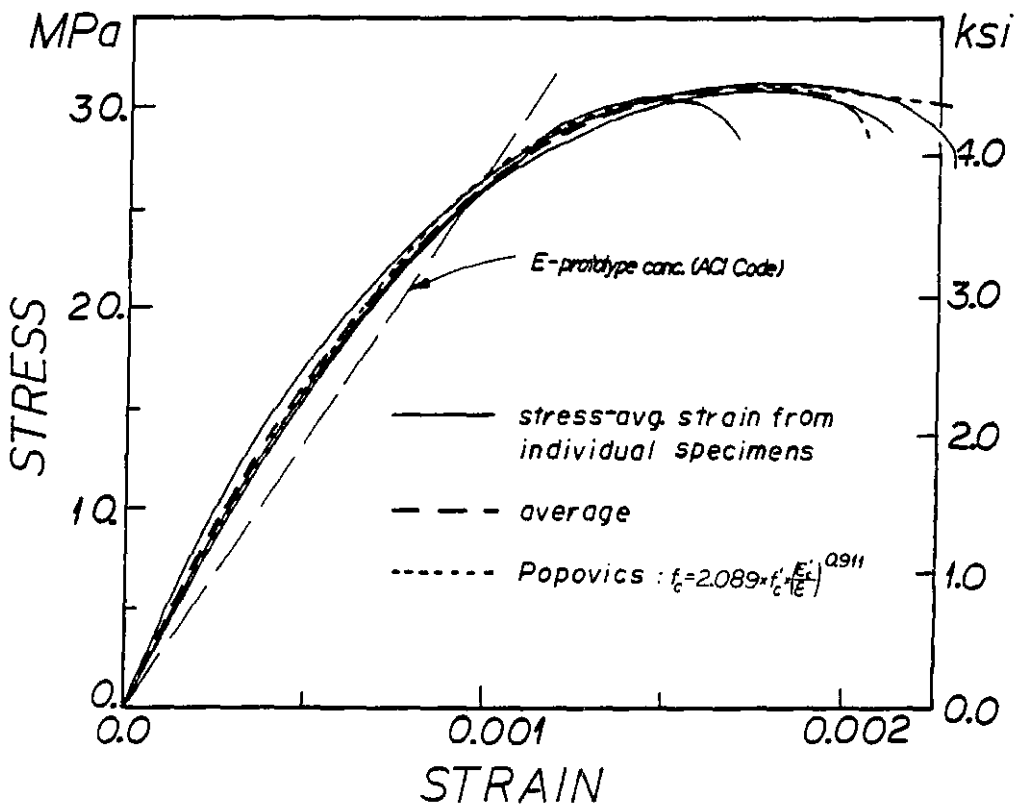

Figure 7.7 Average Stress-Strain Curves for Three Specimens Tested at the Same Speed

Figure 7.6 shows four individual stress-strain records which, when averaged, give the stress-average strain relationship for one test specimen (shown in dashed line in the figure). Figure 7.7 shows three stress-average strain curves for four individual specimens, the average stress--strain line derived from those curves (dashed line), and a stress-strain line based on the theoretical equation presented by Popovics in Ref. 188. The equation was developed for prototype concrete, and the stress-strain line is based on the compressive strength f'_c of the concrete.

All the tests summarized in Table 7.3, Figs. 7.6 and 7.7 were performed with an average strain rate of 6.3×10^{-5}/sec.

Fulfillment of the requirement of simultaneous similitude of f'_c and f'_t presents a much higher degree of difficulty (Refs. 14,18,39,114,118). As was discussed previously, the finer the aggregate used (smaller maximum aggregate size), the lower is the A/W ratio necessary to provide the desired workability. Low A/W ratios result in low A/C ratios (to retain the W/C ratio needed for desired f'_c), thus producing a mix with a sometimes much higher tensile/compressive strength ratio than in prototype concrete. Thus, it often may be necessary to reduce the tensile strength of microconcrete.

The schematic presentation of stress transfer in the composite material shown in Fig. 7.1 suggests that by decreasing the adhesion between the aggregate and the cement gel, the strength along the tensile crack line I - I will be influenced to a much higher degree than the compressive or direct shear strength. Maisel (Ref. 118) proved this observation by testing mixes with different aggregate types, namely relatively rough and porous light aggregate (inflated schist), relatively smooth sands of various origin, and aggregate coated with water-repellent, hard and

smooth silicon resin. It is deduced from the results presented that a change of the aggregate from porous schist to smooth sand caused a 25% decrease in the f'_t/f'_c ratio, a replacement of the porous schist by silicone resin impregnated schist caused a 44% decrease in that ratio and a replacement of the porous schist by silicone resin impregnated sand caused a 50% decrease of the f'_t/f'_c ratio. The above numbers suggest that smooth and non-porous materials should be used in microconcrete mixes, and when a particularly low f'_t/f'_c ratio is required, the impregnation of the aggregate with a silicone resin provides a practical solution.

Large size gaps in aggregate grading are also recommended for f'_t/f'_c reduction.

A summary of data presented by various researchers for the relation between split tensile strength and compressive strength is presented in Fig. 7.8 (from Ref. 29).

Maisel presents in Ref. 118 a table of a wide range of microconcrete mix design possibilities resulting in various strength properties. To supplement the data available in American literature, Table A2 (Appendix A) presents the translation of the summary of this work. The results presented in the Table are based on eight years (1971 - 1979) of experimental research done at the Institute for Model Mechanics at the University of Stuttgart, W. Germany. The characteristics of each test series are given through a code system (Table A1) informing the reader of the test conditions, mix proportions, aggregate type, aggregate treatment, type of cement and additives used. The table is arranged in such a way as to allow the entry with a specific f'_c and f'_t/f'_c in order to find an appropriate mix. Fig. A1 presents the sieve lines of various aggregates used in that study.

As was mentioned previously, this type of a table may be used as a guideline, and the agreement between the results will depend upon the similarity between the materials and the technique used in the study on which the table is based and those used in the current study.

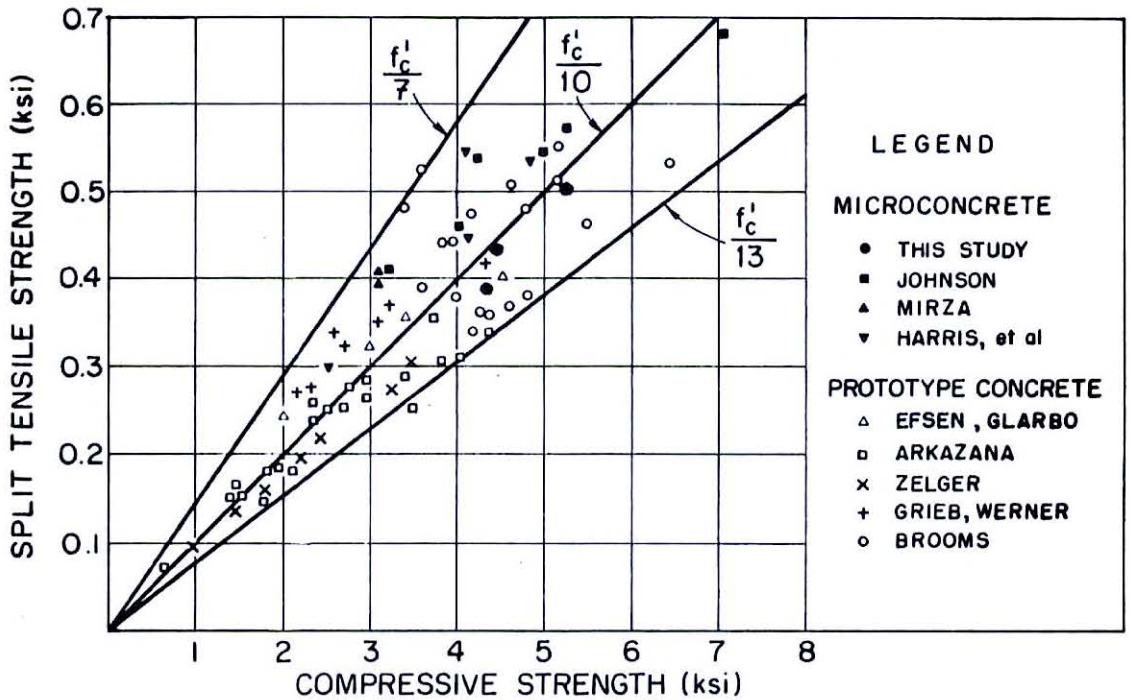

Figure 7.8 Split Tensile Strength vs. Compressive Strength from Various Studies (Ref. 29)

7.1.3 Scale Effects in Microconcrete

7.1.3.1 Size Effects

In general, size effect may be defined as a change in a characteristic material property of a specimen due to the change of its size.

Although there are a number of recognized sources of size effects in concrete, there is no general theory which includes them all. The theory of the failure of brittle materials through a propagation of cracks initiated at flaws explains size effects by assigning a constant flaw

to differential curing effect. The influence of the specific area of the aggregate on the magnitude of size effects was also studied by using mixes with different aggregate size. There was no noticeable difference in size effects observed between the finer and the coarser aggregate mixes.

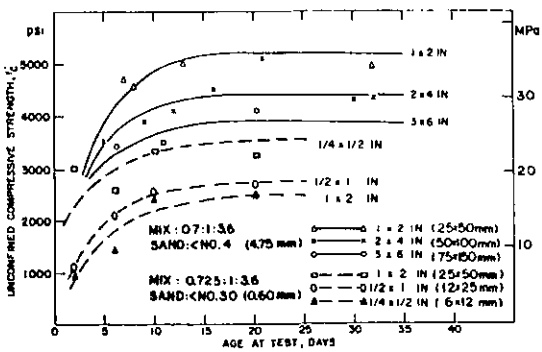

Figure 7.9 Influence of Specimen Size on the Compressive Strength (Ref. 118)

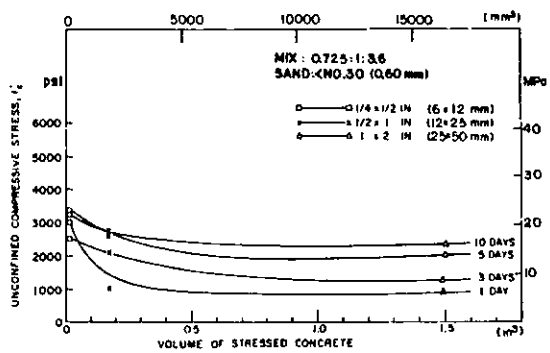

Figure 7.10 Unconfined Compressive Strength vs. Specimens Volume (Ref. 39)

In Ref. 18, Harris, Sabnis and White present a comparison between the size effect in prototype concrete and in microconcrete (Fig. 7.11). Although the trend of strength decrease with the increase of specimen size is evident for both the materials, it is much stronger for microconcrete as can be seen from curve A (prototype concrete) and the shifted curve M (microconcrete).

In a previously mentioned study (Ref. 39), third-point loaded beams of span to depth to width ratio of 12:2:1 were tested to study the size effects on the tensile strength in flexure. The results of these tests, summarized in Fig. 7.12 indicate that the flexural tensile strength is rather sensitive to specimen size, and is most sensitive to the change in the volume of the specimen.

In Ref. 21, Mirza presents results of a series of split cylinder tests using specimens of different dimensions but of otherwise identical

density per unit volume (volume effect). It cannot account for the influence of the specimen curing and testing conditions on the extent of the size effects. Other commonly quoted sources of size effects in microconcrete are differential drying throughout the volume of a specimen as a function of the distance from the surface, faster curing of smaller specimens (both effects often are referred to as the differential curing effects), increase of quality control with decreasing specimen size and changes in strain gradient in flexural tests.

Sabnis and Mirza present in Ref. 123 a review of the state-of-the--art on the question of size effects in microconcrete. The paper also includes an extensive list of literature concerned with this problem.

Selected results of important research in this area are discussed below.

In 1963 Harris et. al. (Ref. 39) presented the results of an extensive study on size effects in microconcrete. Compression cylinders of height to diameter ratio of 1:2 were used to study the influence of specimen size and curing age on the unconfined compressive strength f'_c. All the specimens were compacted manually by rodding and cured in a moist room (95% RH) until tested. Figure 7.9 shows the results obtained for two mixes with different aggregate sizes and for varying specimen sizes. For both mixes the smaller samples had a higher compressive strength and reached almost full strength in a shorter time than the larger ones (see individual points for the 1x2 in. specimens for W:C:A mix of 0.7:1:3.6 and along the 1/4x1/2 in. curve for 0.725:1:3.6 mix). The observed flattening of f'_c vs. volume of stressed concrete curves (Fig. 7.10), for all the concrete ages, indicates that part of the observed size effect is due

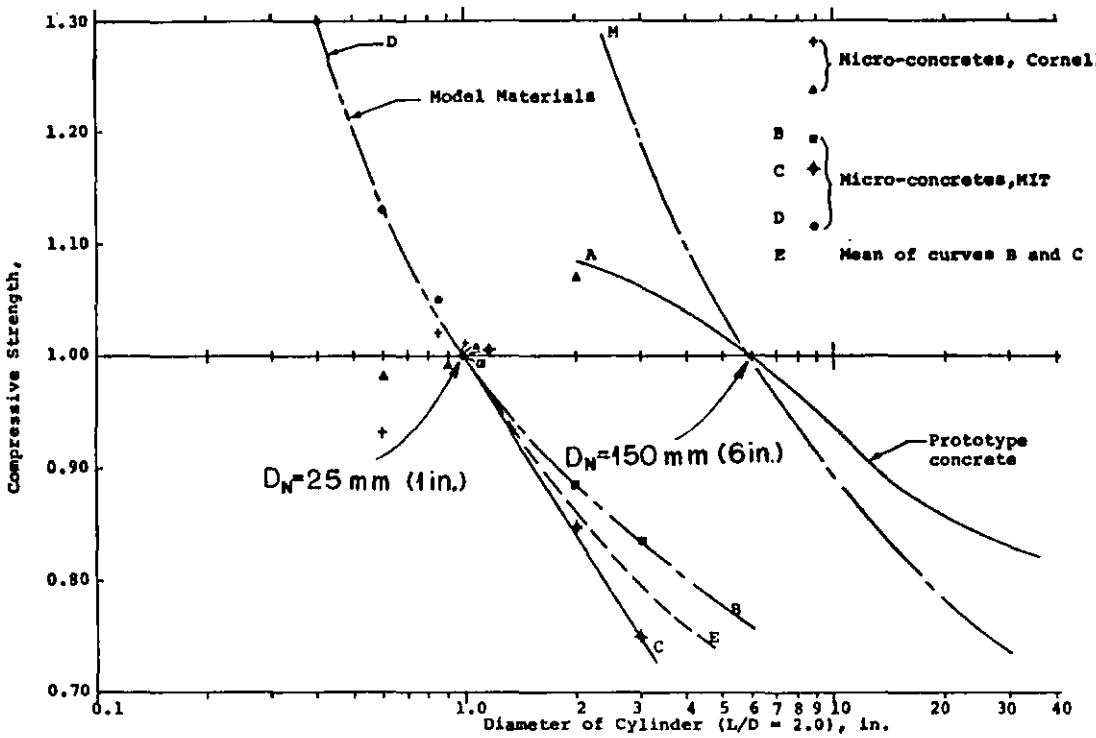

Figure 7.11 Size Effects on Compressive Strength of Prototype Concrete and Microconcrete (Ref. 18)

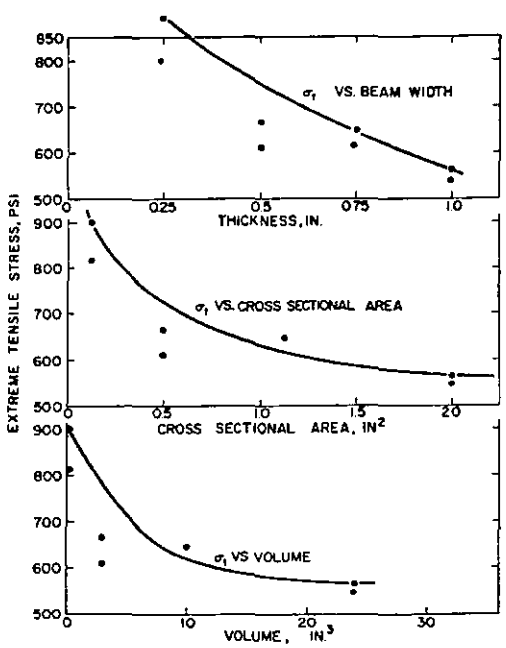

Figure 7.12 Variation of Flexural Tensile Strength with the Size of Specimen (Ref. 21)

properties. The mean strength and the standard deviation were found to decrease with an increase in size.

Based on current knowledge of the size effects in microconcrete, it is generally agreed that, to overcome partially the factor of uncertainty introduced into the results of small scale model test by the size effect, the design of the concrete mix should be based on material tests performed on specimens compatible in size with the smallest dimension of a structural element in the model. This will compensate for many of the aformentioned size effects but cannot account for strain gradient effects which may be encountered for instance in model studies of flexural response.

7.1.3.2 Strain Rate Effects

Many researchers have reported on quantitative evaluations of the effects of the rate of loading on the strength properties of both prototype concrete (Refs. 135 to 138 and 140 to 142) and microconcrete (Refs. 18, 33, 117, this study).

Jones and Richart (Ref. 141) performed a series of tests on prototype concrete cylinders at load rates "R" varying between 0.7 kPa/sec. $< R <$ 69 MPa/sec. (0.1 psi/sec. to 10 ksi/sec.), arriving at a relationship between loading rate and ultimate compressive strength of the form $f'_{cR}/f'_{cN} = 0.89 \times (1+0.08 \times \log R)$, where f'_{cN} is the strength at a loading rate of 24 kPa/sec. (35 psi/sec.), and f'_{cR} is the strength at loading rate "R" (in psi/sec.). Approximating the strain rates on the basis of load rates in the nearly elastic range of the material, the following change in ultimate strength with the change in strain rate is

predicted: $0.82 < f'_{cR} / f'_{cN} < 1.17$ for $3x10^{-8}$/sec. $< \dot{\varepsilon} < 3x10^{-3}$/sec.

Hatano and Tsutsumi (Ref. 142) performed a series of prototype concrete compression tests in which the time till failure was used as a measure of loading rate. The load was applied according to a time function of the form (1 - cos at) thus approaching a constant rate of machine head movement (stroke). The results are summarized in Fig. 7.13. The approximated strain rates vary from about $3x10^{-5}$/sec to $4x10^{-1}$/sec. Going from the slowest to the fastest rate, the increase in ultimate strength is about 43% and the increase in the modulus of elasticity is about 30%. Empirical formulas for f'_c and E_{secant} of a logarithmic form with respect to loading velocity (linear dependance) are reported in Ref. 142.

Both of the above studies used direct or indirect control of the load rate rather than control of the strain rate.

In Ref. 39 Harris et. al. present the results of a study of the strain rate effect on the unconfined compressive strength of microconcrete (Fig. 7.14). The specimens were 50x100 mm (2x4 in.) cylinders of microconcrete with an A:C:W ratio of 4.5:1:0.9. The tests were performed under stroke control, thus the strain rates were not constant (built-up of strain in the testing system) and can be estimated only approximately.

The curve for ordinary concrete presented in Fig. 7.14 seems to be somewhat low in comparison with the results of studies reported by others, thus perhaps overstressing the difference between micro- and prototype concrete sensitivity to strain rate effects.

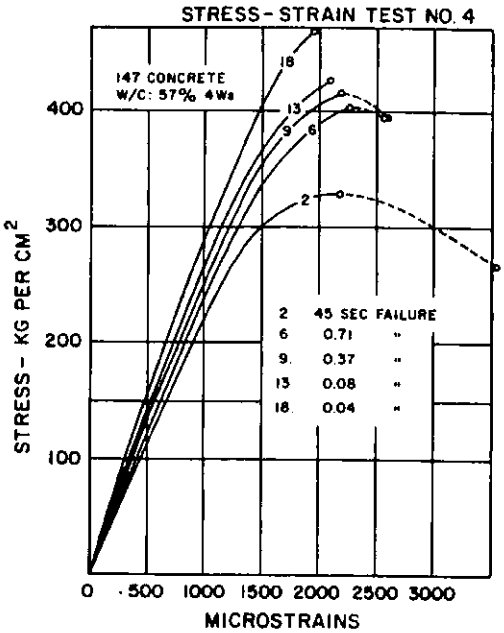

Figure 7.13 Effect of Loading Rate on Compressive Behavior of Prototype Concrete (Ref. 142)

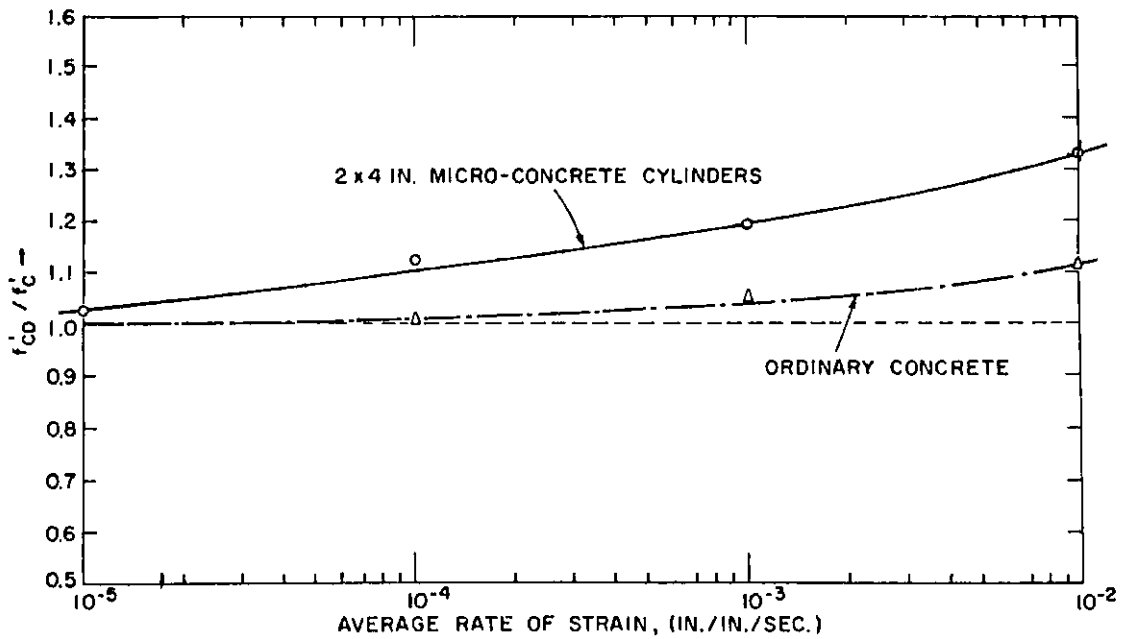

Figure 7.14 Strain Rate Effect on the Unconfined Compressive Strength of Concrete and Microconcrete (Ref. 39)

In this study the effects of strain rates on the strength of microconcrete were evaluated in a series of unconfined compression tests performed on 50x100 mm (2x4 in.) cylinders. Specimens cast from four microconcrete batches (Mixes 3, 6 and 8; see Table 7.3) were used. The strength of the microconcretes at a "static" strain rate ($2x10^{-4}$/sec.) varied from 28 to 41 MPa (4.1 to 5.9 ksi). Mix proportions, specimen preparation technique and testing procedure were described in detail in Section 7.1.2.3.

The matter of maintaining a constant strain rate throughout the test received considerable attention in this study. For this purpose, the differences between strain rates deduced from three displacement devices, namely, clip gages attached to the concrete, an extensometer attached to the loading plattens, and an LVDT used for stroke measurements were studied. In the latter two cases strains were obtained by dividing the measured displacement by the specimen height. It was found that $\varepsilon_{\text{plattens}} / \varepsilon_{\text{clip gages}} = 1.6$, and that this ratio remained almost constant for stresses up to f'_c. The ratio of strain rate assessed from stroke measurement to $\dot{\varepsilon}_{\text{extensometer}}$ varies from 15 to 25 depending upon whether the plattens were placed between the hydraulic grips (additional "soft" element in the testing system) or whether the grips were removed, and also depending upon the level of stress in the concrete. Thus, stroke control proved to be unsuitable for the study in question.

In the tests, a constant displacement rate was provided through the extensometer controlling the distance between the plattens. Since this displacement rate was shown to be linearly related to the average strain measured with the clip gages (by a factor of 1.6), the concrete specimen itself was subjected to constant strain rate for stresses up to f'_c, or

strains up to ε_c'. Once f_c' was exceeded, the strain energy release in the relatively soft testing machine could not be controlled through the extensometer feedback and a sudden increase in strain rate was evident. Thus, the decreasing branches of the recorded stress-strain curves could not be relied upon and are omitted in Fig. 7.15 which shows stress-strain curves obtained for various strain rates and for two mixes of different ultimate strength. The plots were obtained in the way described in Section 7.1.2.3. This figure clearly shows the expected increase in the ultimate strength (f_c') and in the initial stiffness (E), and the decrease in the strain value at the maximum stress (ε_c') with the increase in the strain rates.

The results of the study are summarized in Table 7.4.

The $f_c' - \dot{\varepsilon}$ data points for individual specimens are displayed in Figs. 7.16 a and b. From the curves fitted between the points the strength values at $\dot{\varepsilon} = 2\text{x}10^{-4}$/sec. were extracted. These values were used to normalize the average strength at each testing strain rate for all four test series (Fig. 7.17). The close correlation of these points obtained for concretes of different strength is noteworthy. A second order curve through the data points shown in this figure, derived from a regression analysis based on least square method, has the following form:

$$f_c' / f_{c_{2\text{x}10^{-4}}}' = 1.4776 + 0.1815 \log \dot{\varepsilon} + 0.0145 (\log \dot{\varepsilon})^2 \qquad (7\text{-}1)$$

Based on the more than one hundred strain rate tests carried out in this study, this empirical equation, which is independent of f_c', is best suited to describe the change in compressive strength with a change in strain rate.

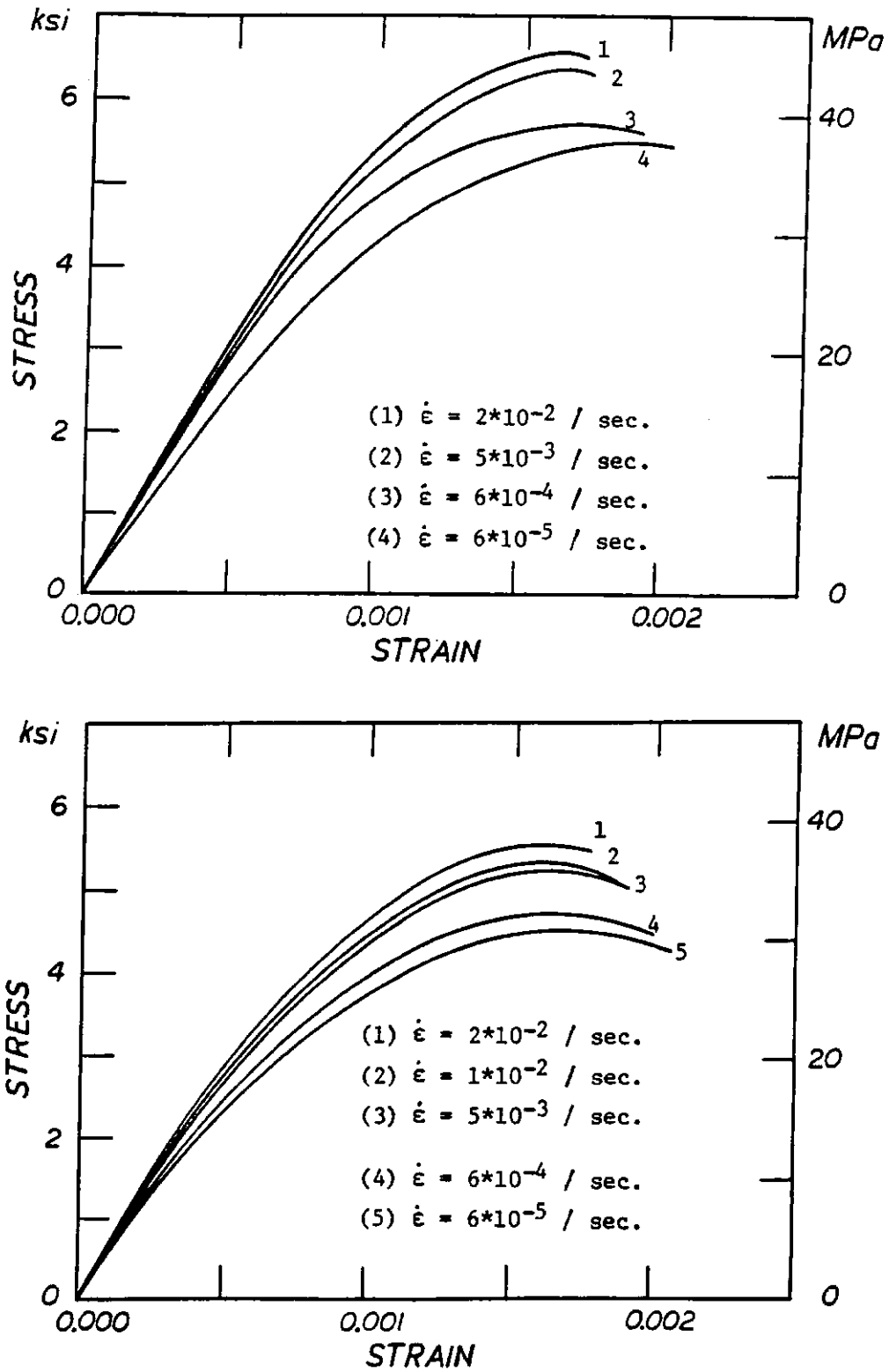

Figure 7.15 Stress-Strain Curves for Two Different Strength Microconcretes Compressed Under Various Strain Rates

Table 7.4

Results Summary for Strain Rate Effect

on Compressive Strength of Microconcrete

Mix No.	Strain Rate	No. of Specs.	f'_c avg.		Coeff. of Var.	f'_c avg. / f'_c norm.	Mix No.	Strain Rate	No. of Specs.	f'_c avg.		Coeff. of Var.	f'_c avg. / f'_c norm.
-	1/sec.	--	MPa	ksi	%	--	-	1/sec.	--	MPa	ksi	%	--
3	6.3×10^{-5}	5	28.8	4.17	9.8	0.96	6	1.0×10^{-5}	3	35.9	5.21	6.0	0.92
	1.5×10^{-4}	4	29.8	4.32	6.7	1.		6.3×10^{-5}	3	38.2	5.54	3.4	0.98
	6.3×10^{-4}	5	32.0	4.64	5.0	1.07		6.3×10^{-4}	4	40.5	5.87	10.0	1.04
	5.0×10^{-3}	5	34.0	4.93	5.9	1.14		5.0×10^{-3}	4	44.0	6.38	2.3	1.13
	1.0×10^{-2}	5	35.6	5.17	8.5	1.19		1.0×10^{-2}	3	45.6	6.61	2.1	1.17
	2.0×10^{-2}	5	35.9	5.20	6.3	1.20		2.0×10^{-2}	2	47.9	6.95	0.5	1.23
	f'_c norm. =		29.9	4.33	--	--		f'_c norm. =		38.9	5.64	--	--
3	2.5×10^{-6}	5	26.2	3.80	5.6	0.92	8	2.5×10^{-6}	3	37.4	5.42	2.6	0.91
	1.0×10^{-5}	6	27.0	3.91	6.3	0.95		6.3×10^{-5}	9	39.9	5.79	6.9	0.975
	6.3×10^{-5}	9	27.4	3.98	4.5	0.97		1.5×10^{-4}	6	40.2	5.83	7.2	0.98
	1.5×10^{-4}	7	28.3	4.11	7.1	0.997		6.3×10^{-3}	3	45.9	6.65	5.6	1.12
	5.0×10^{-3}	7	32.3	4.68	9.4	1.14		1.0×10^{-2}	4	47.8	6.94	1.6	1.17
	f'_c norm. =		28.4	4.12	--	--		f'_c norm. =		40.9	5.94	--	--

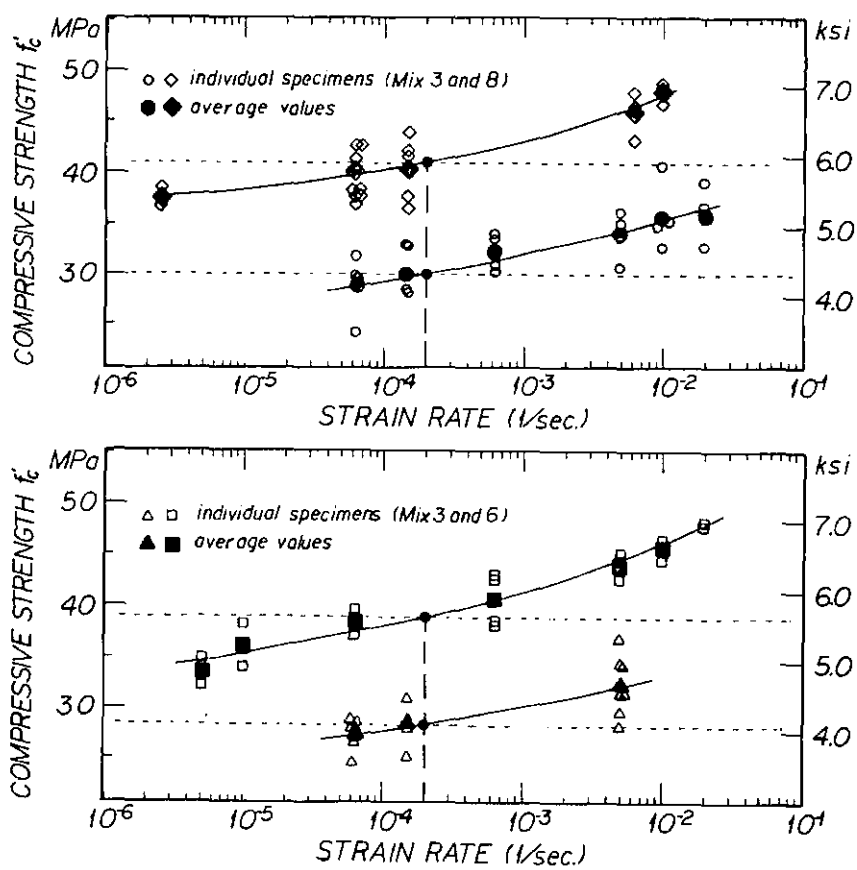

Figure 7.16 Results of the Study of Strain Rate Effect on Compressive Strength of Four Different Strength Microconcretes

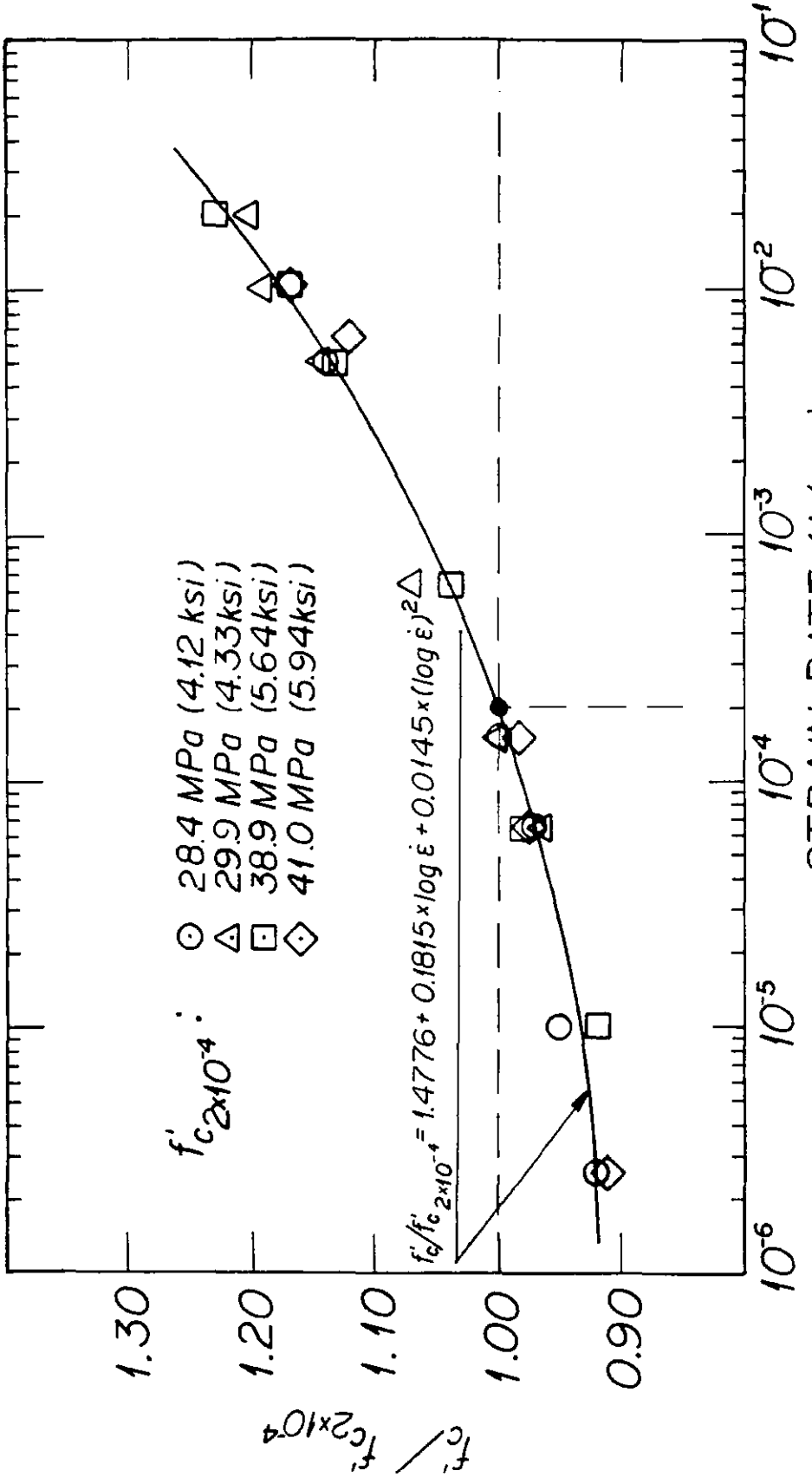

Figure 7.17 Normalized Compressive Strength of Microconcrete vs. Strain Rate

Figure 7.18 provides a summary of the results of several studies on the effect of strain rates on the compressive strength of microconcrete (Harris, et. al., Ref. 39; this study), and prototype concrete (Jones and Richart, Ref. 141; Hatano and Tsutsumi, Ref. 142). A comparison of the results obtained by Harris and the results obtained in this study provides additional confidence that the regression line expressed with Eq. (7-1) is representative for microconcretes of various origins and strength. The strain rate effect on the compressive strength of prototype concrete is of similar magnitude as for microconcrete. Quantitative statements cannot be made due to the fact that data on truly strain rate controlled tests of prototype concrete was not found.

7.2 SIMULATION OF REINFORCEMENT

7.2.1 Introduction

The modeling of concrete reinforcement has attracted a considerable amount of attention, and techniques allowing the manipulation of reinforcement strength and ductility have been presented by many researchers. This section summarizes the most widely accepted methods of fabrication and control of properties of model reinforcement and discusses the reinforcement used in this study.

The wide acceptance of microconcrete as modeling material, having strength properties close to those of the prototype concrete, limits the choice of model reinforcement to those material with strength similar to the strength of prototype reinforcement, thus to steel. In the cases where the strength of concrete is subjected to scaling, materials other than steel can be considered. Copper alloys provide wire of lower

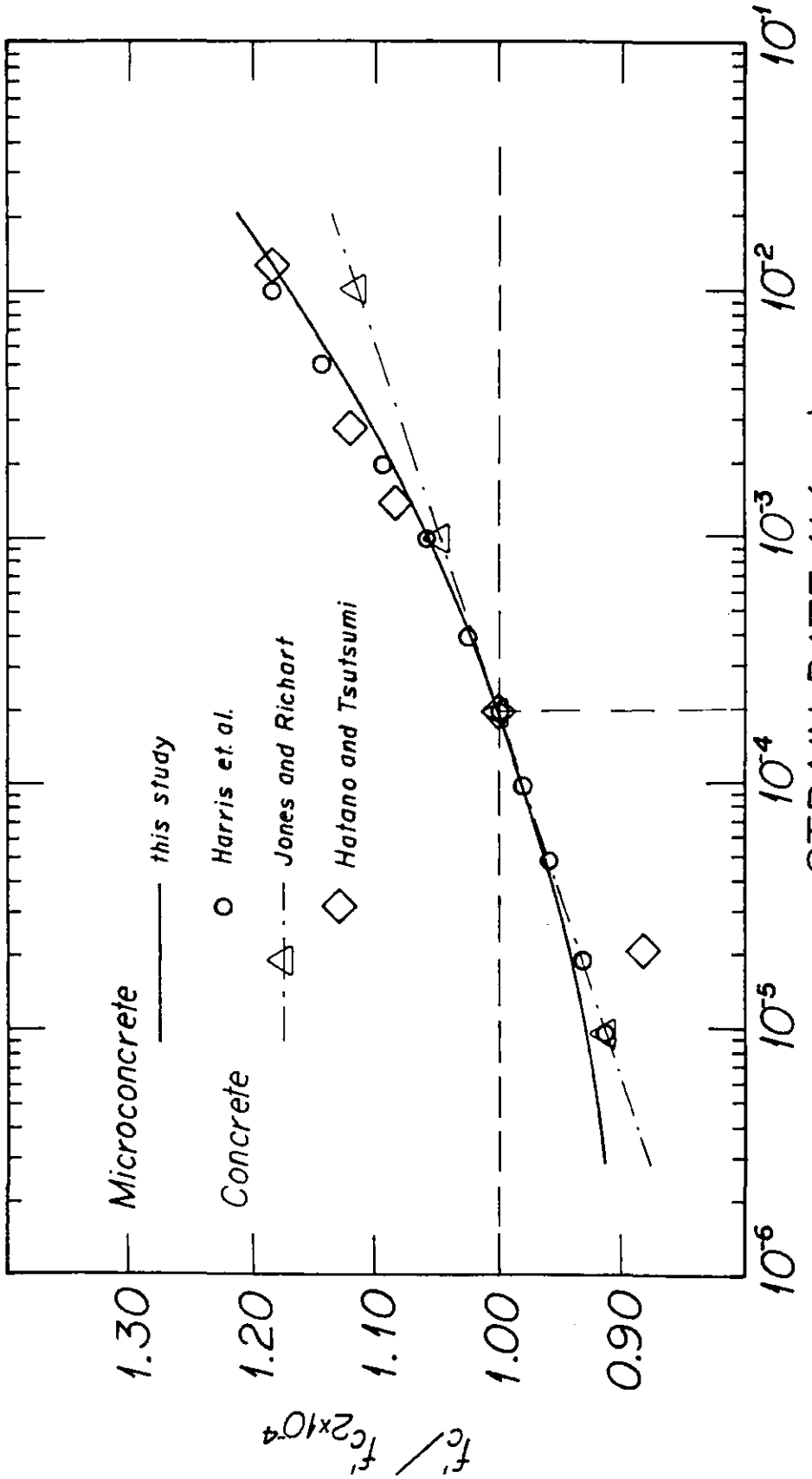

Figure 7.18 Summary of Results from Various Sources on Strain Rate Effects on Compressive Strength of Concrete and Microconcrete

E-modulus if so desired. However, caution should be exercised in the use of these materials as the adhesive forces between concrete and copper alloys are negligible (Ref. 117).

The subsequent discussion will be devoted to steel wires, due to the predominant use of this material as model reinforcement.

7.2.2 Fabrication of Model Reinforcement

The concrete - reinforcement bond simulation imposes special requirements on the surface characteristic of the wire used.

Bond stress development may be assured either through adhesive forces or through wire surface deformation achieved either through chemical treatment or, more commonly and with higher reliability, through mechanical deformation of the wire.

Burggrabe (Ref. 117) presents results obtained with zinc-galvanized wire. He found that the use of zinc plating in the case of chrome rich cement (0.1% Cr) results in a strong chemical bond between the wire and the cement. In the case of cement with much lower content of chrome, a thin film of zincoxide can develop, providing a viscous layer between the steel and the concrete.

A simple and reliable method of providing and controlling bond strength is to deform soft steel wire through cold-rolling. The deformation may be applied by pulling the wire through a set of knurling wheels (Fig. 7.19). A detailed description of a knurling apparatus can be found in Refs. 18 and 40. Types of deformations and their effect on bond simulation are discussed in Section 7.3.

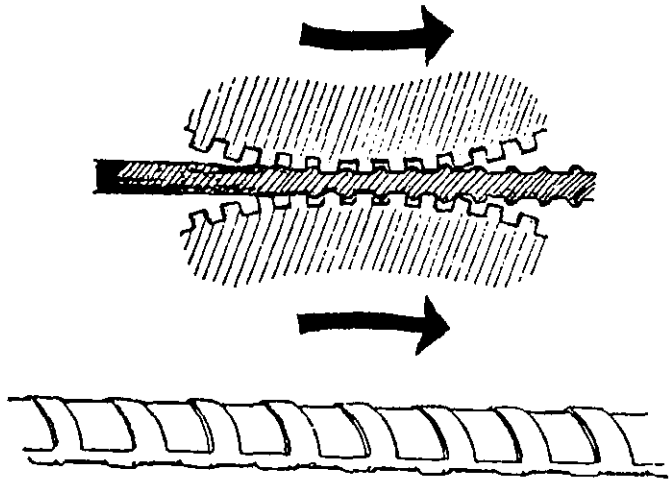

Figure 7.19 Knurling Mechanism

After the cold-rolling process the wire tends to assume a curvature due to built up residual stresses resulting from local bending which later makes the assemblage of the reinforcing cage cumbersome. This problem can be reduced by using knurling wheels of sufficiently large radius. Maisel (Ref. 118) reports good success with the use of wheels of diameter 75 times the diameter of the deformed wire. Heat treatment of the deformed wire in tight sleaves also has been used successfully to eliminate curvatures (Ref. 43).

The cold rolling causes work hardening of the steel resulting in increased yield strength without a well defined yield-point and in significantly decreased ductility. The yield strength and, to some degree, the shape of the stress-strain diagram can be controlled through subsequent annealing as shown with the curves of Figs. 7.20 a b and c.

The annealing temperature at constant annealing time, or annealing time at constant annealing temperature, necessary to lower the yield strength of the cold rolled material to a desired value depends upon the

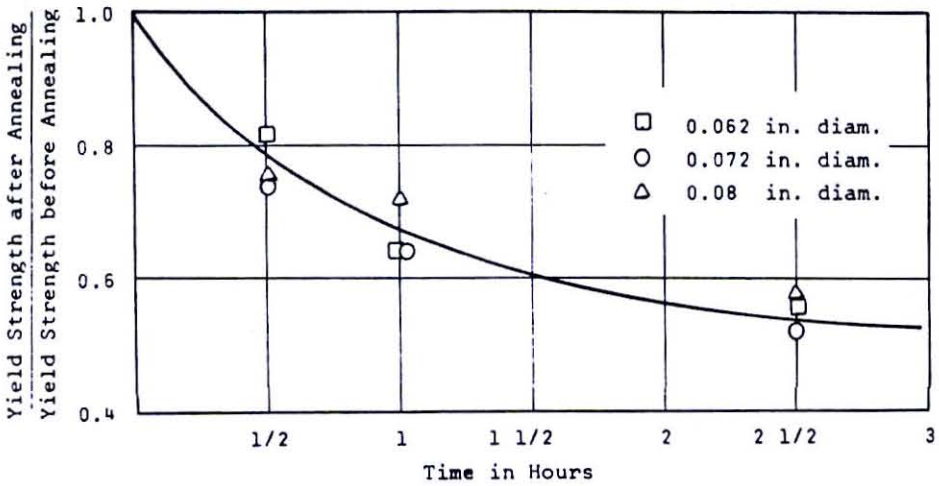

(a) Relative Yield Strength vs. Annealing Time at 538°C (1000°F) (Ref. 18)

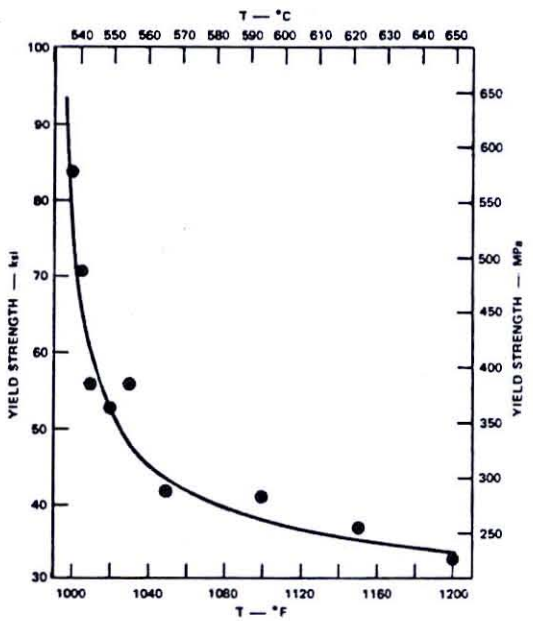

(b) Yield Strength vs. Annealing Temperature (t = 1 hr.) for Cold Drawn 1020 Steel Wire (Ref. 43)

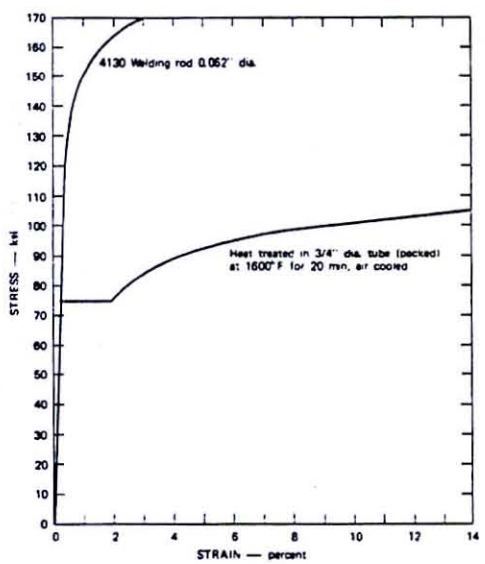

(c) Change in Stress-Strain Curve Through Heat Treatment (Ref. 43)

Figure 7.20 Effects of Heat Treatment on the Strength of Small Scale Reinforcement

amount of cold work applied to the specimen and on the diameter of the specimen. Thus, a trial annealing by varying temperature or time has to be performed. Gran and Bruce (Ref. 43) used quenching followed by tempering of the wire at various temperatures (quenching: heat beyond A_3 temperature equal about 910°C, cool rapidly to obtain brittle hard martensite structure; tempering: heat the specimen to temperature in the range of 200°C to 360°C and cool slowly to obtain ferrite-cementite composition of relatively high strength and high ductility). They report that the yield strength manipulated in this way ranges between 410 MPa (59 ksi) and 620 MPa (90 ksi) depending upon the tempering temperature.

In this study soft steel wire of diameter 2.0 mm (0.08 in; Gauge 14) was used to simulate the main reinforcement consisting of No. 9 rebars (28.6 mm). The wire was purchased in a black annealed form in coils of about 2000 m (6000 ft) length.

The yield strength of the wire as delivered was 255 MPa (37 ksi), whereas the desired yield strength was above 414 MPa (60 ksi, Grade 60 reinforcement). The increase in strength to 440 MPa (63.7 ksi, Fig. 7.21) was achieved through cold rolling of the wire with a set of knurls, producing two orthogonal sets of indentations. The ultimate strain of the deformed wire was between 0.08 and 0.12. The resulting effective diameter of the wire "d" was 1.98 mm (0.078 in.) with an indentation depth "w" of about 0.13 mm (0.005 in.), and indentation spacing "s" of 0.74 mm (0.029 in.). The ratios $w/d = 0.06$ and $s/d = 0.37$ satisfy the minimum protrusion height and maximum protrusion spacing specified by ASTM Standards, Section A615 (Ref. 187). A microscope enlargement of the deformed wire is shown in Fig. 7.22. Heat treatment of the deformed wire was omitted since the strength was close to the desired one. In

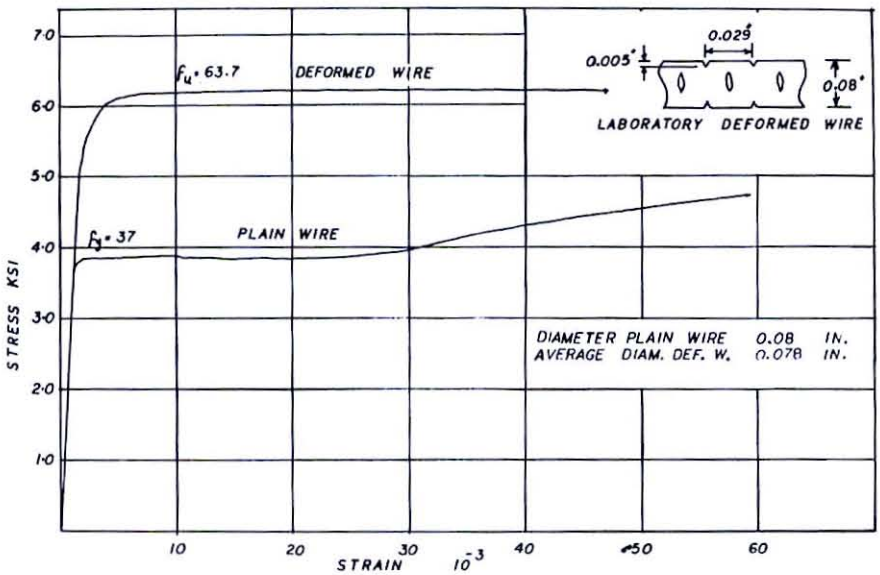

Figure 7.21 Effect of Deformation on Stress-Strain Behavior of Reinforcing Wire Used in this Study

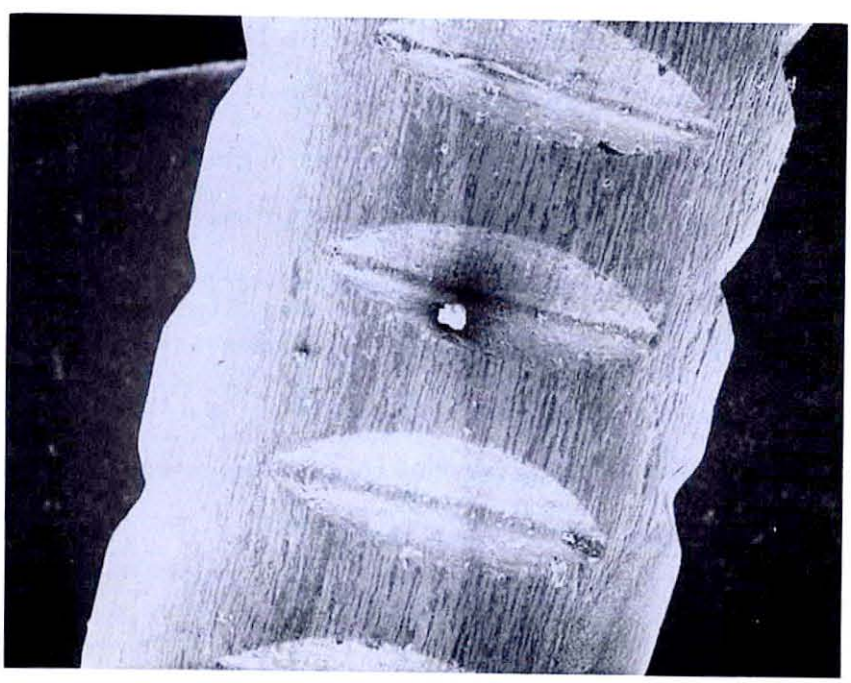

Figure 7.22 Deformed Wire Gage 14 (d = 2mm; 0.078 in.) (SEM 44X)

retrospect, it must be said that quenching and tempering would have been desirable to improve the strain hardening characteristics of the deformed wire.

To simulate the shear reinforcement, which consisted of stirrups of No. 4 bars (12.7 mm), black annealed Gauge 20 wire (0.88 mm = 0.035 in.), available in small coils in hardware stores under the commercial name of Handi-Wire, was used. The wire, as purchased, has a shiny smooth black scale on its surface, thus promising a very low bond to the concrete. Due to the very small diameter of the wire, chemical surface roughening was chosen rather than mechanical deformation. The following treatment procedure was employed:

- o immerse the wire for 2 minutes in 10 % HCL solution to remove the smooth scale present on its surface,
- o subsequently immerse the wire for 45 seconds in 30% H_2SO_4 solution to roughen the surface of the wire, and
- o wash the wire thoroughly under a stream of tap water.

The procedure resulted in lowering of the strength of the wire by 6% thus indicating a change in the effective area by that amount. Test of four treated wires resulted in a coefficient of variation of the ultimate strength of 0.015, hence the process results in a uniform area decrease.

No noticeable change was observed either in the wire ductility or its stress-strain characteristics due to the above treatment.

Fig. 7.23 presents microscope enlargements of the wire surface before and after the treatment.

7.2.3 Size and Strain Rate Effects in Model Reinforcement

Despite extensive studies on the yield and ultimate strength of

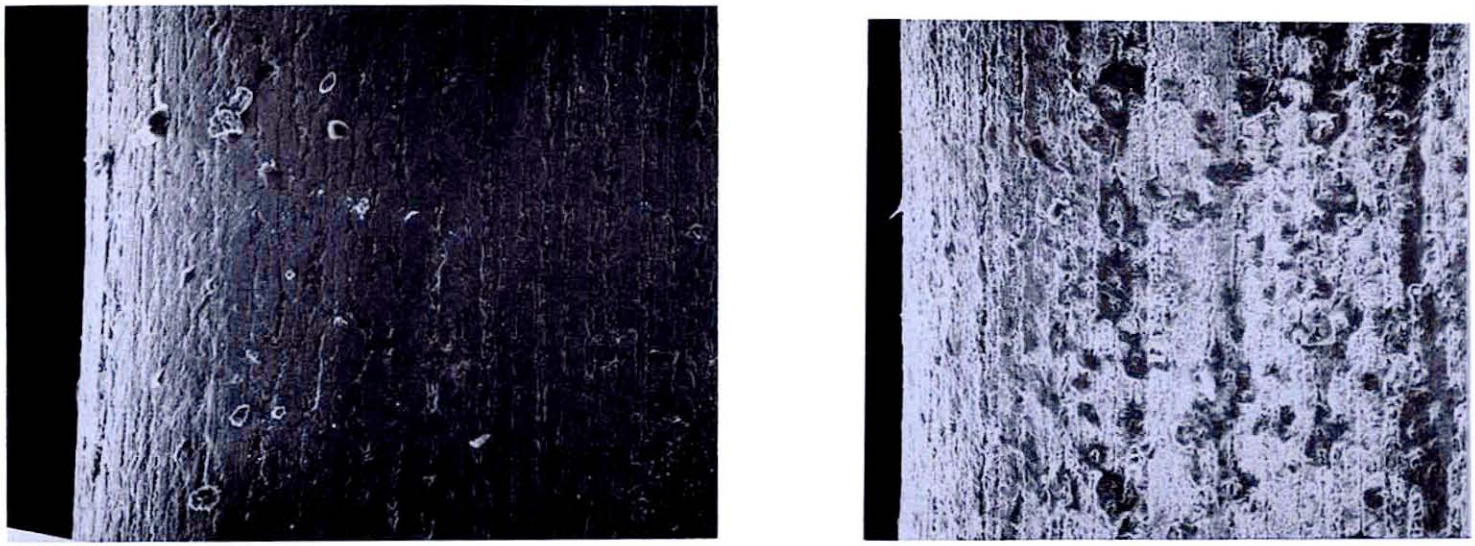

Untreated

Chemically Roughened

Gauge 20 Steel Black
Annealed Wire
(SEM 200 X)

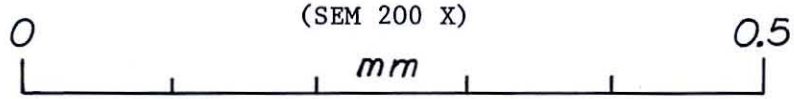

Figure 7.23 Surface of Stirrup Wire (Gage 20; d = 0.88mm = 0.035 in.) Before and After Chemical Treatment (SEM 200X)

wires subjected to various treatments, little attention has been paid in the literature to the effect of the wire diameter on its properties. This is justified as the strength of the wire used in each individual study is manipulated separately to obtain the desired values.

Very limited information is available on the elastic stiffness of small wires. Maisel (Ref. 118) observed a modulus of elasticity of about 20% lower for 2 mm wire than could be expected from the base material properties. A survey of data presented by Harris et. al. (Ref. 18), and Staffier and Sozen (Ref. 146) shows also a decrease in the stiffness value. Maisel suggests that a major portion of this decrease should be attributed to the initial bends formed along the wire which act as arch springs.

Strain rate effects in model reinforcement were extensively studied by Staffier and Sozen (Ref. 146). Results for two sizes of laboratory deformed and heat treated wires are summarized in Fig. 7.24. The increase in yield stress at higher strain rates is very similar to that reported in Section 6.2.1 for structural steel. Comparing Fig. 7.24 with Fig. 7.17, it can be seen that the strain rate effects are lower for model reinforcement than for microconcrete.

7.3 BOND SIMULATION

Proper simulation of the force transfer between concrete and the reinforcement poses a major problem at model scales. The force transfer will affect not only the resistance against pull-out but also the spacing between direct tension cracks and the occurence of secondary failure mechanisms such as longitudinal splitting along bars close to the surface. In this section, only those aspects of force transfer will be discussed

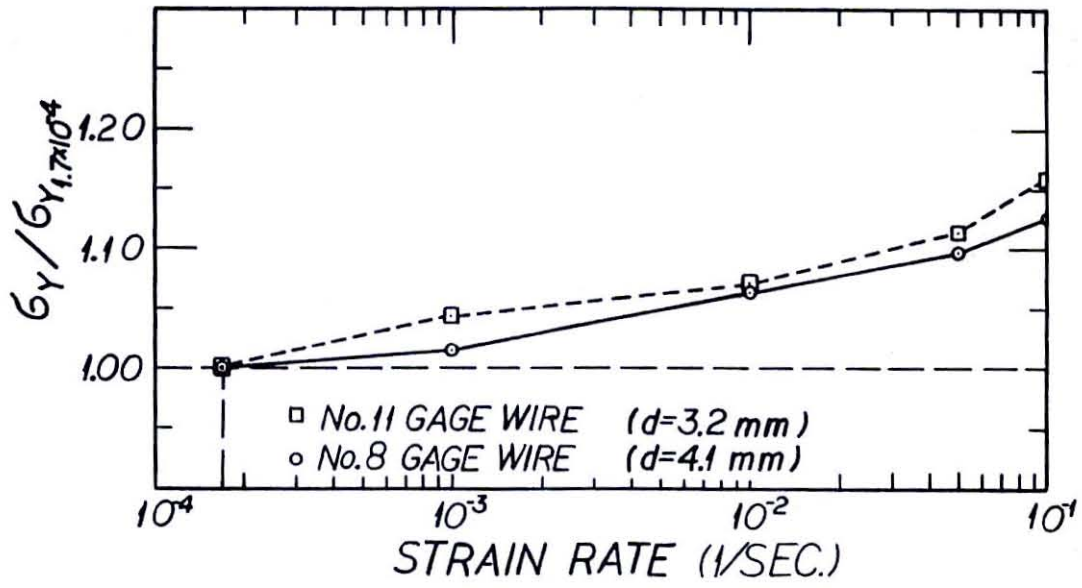

Figure 7.24 Strain Rate Effect on the Lower Yield Strength of Model Reinforcement (Ref. 146)

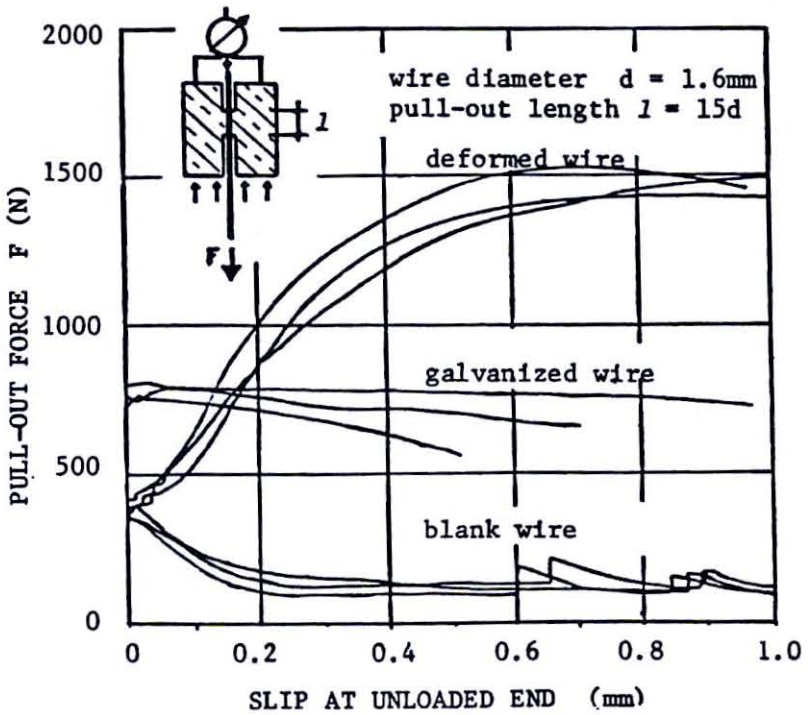

Figure 7.25 Effect of Surface Preparation on the Bond Characteristics of Reinforcement Wire (Ref. 118)

which are concerned with resistance against pull-out as determined from simple pull-out tests.

The surface preparation of the reinforcement, together with the embedment length, will determine the bond characteristics of the wire. This is illustrated in Fig. 7.25, in which results of pull-out tests of smooth, galvanized, and deformed wire are displayed (from Ref. 118).

Smooth wire can provide only a small amount of bond based mainly on adhesion between the steel and the wire.

Zinc-galvanized wire permits the development of relatively high bond stresses, however, once a maximum bond-stress is reached, a deterioration of the composite action occurs.

Deformed wire presents the most realistic and reliable solution to the bond problem. Even then, certain compromises are necessary since a perfect affinity between the prototype and model bond layer cannot be achieved in practice.

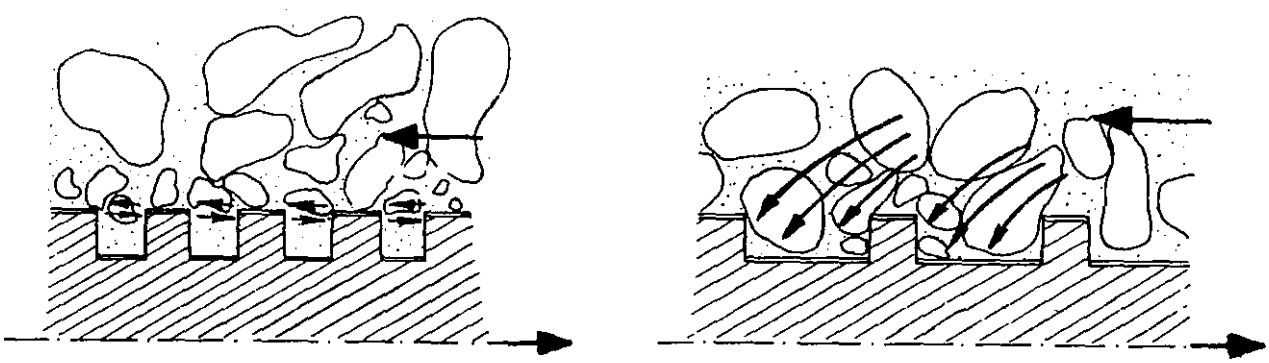

(a) short indentations -- gel shear action

(b) long indentations -- compressive arch action

Figure 7.26 Influence of Shape and Spacing of Wire Deformations on Bond Mechanism (Ref. 117)

The shape and spacing of the surface deformation significantly influences the bond behavior (Fig. 7.26). Burggrabe (Ref. 117) found that,

using 3 mm diameter wire, the bond strength was 2.8 times higher for 1 mm wide ribs spaced 1 mm apart than for a threaded rod with the same depth of thread, and 1.5 times higher for ribs spaced 3 mm apart rather than 1 mm. Harris et. al. (Ref. 18) stressed the major differences between the surface character of most laboratory deformed wires and of prototype reinforcement, the first of which usually has a surface with indented internal valleys, whereas the second has external protrusions. The importance of these differences can be diminished, however, by a proper spacing and shape of the knurls. Nevertheless, it can be expected that a better simulation of all characteristics of the force transfer between reinforcement and concrete will be achieved through protrusions on the wire rather than indentations. Actual cold-rolling of wires which produced protrusions of the type shown in Fig. 7.19 was used sucsessfully at the University of Stuttgart (Ref. 118).

A limited study on the bond characteristics of the model reinforcement used in this study was performed by Bader (Ref. 29). The results of pull-out tests on wires with different embedment length are shown in Fig. 7.27. The corresponding ultimate bond stresses are shown in Fig. 7.28 together with the results obtained by other researchers for model and prototype reinforcement. The comparison shows satisfactory bond strength of the reinforcement used.

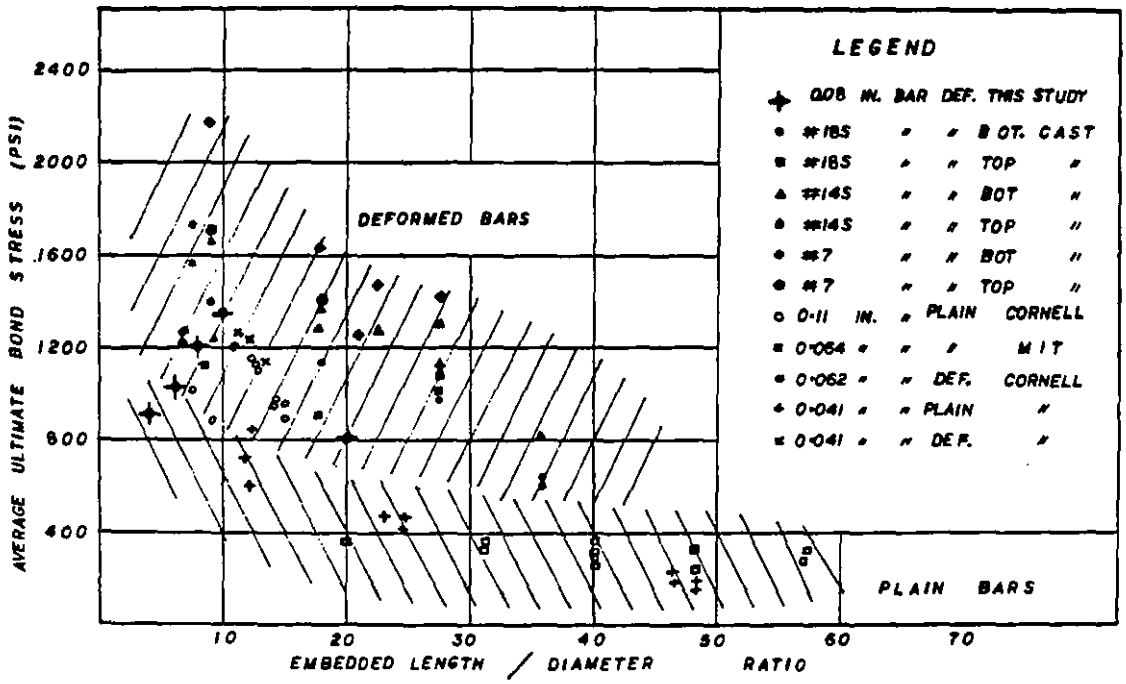

Figure 7.26 Bond Strength for Reinforcement Used in This and Other Studies (Refs. 29 and 39)

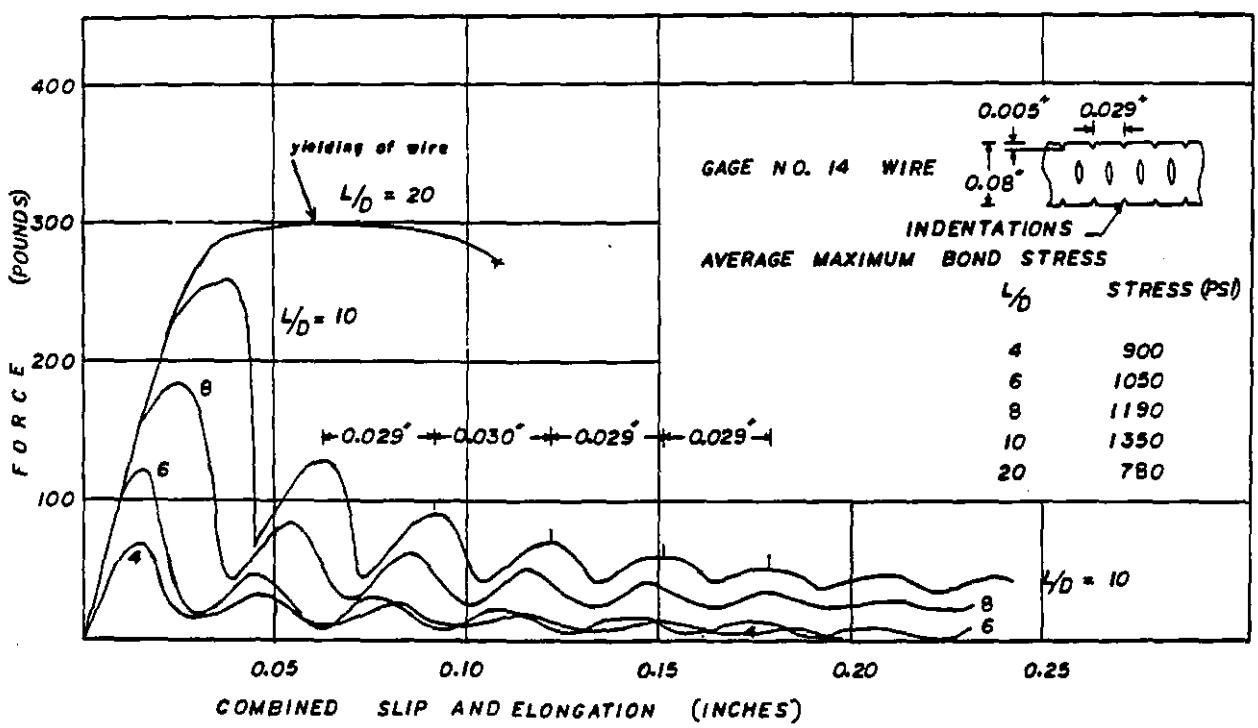

Figure 7.27 Results of Pull-Out Test of Wire Used in This Study (Ref. 29)

CHAPTER 8

MODEL COMPONENT TESTING

8.1 INTRODUCTION

The material studies described in Chapters 6 and 7 provide information on the material (metal or concrete) behavior under various load histories. Understanding of the behavior of a complete structure or structural model requires additional information on the behavior of structural elements and structural subassemblies. This, in particular, is true for complicated structural details such as beam-to-column connections in steel structures or concrete - reinforcement interaction in joints and members of reinforced concrete structures. Tests of structural components also provide a direct calibration of structural component response to the applied load. Phenomena which can be detected neither at the material test level nor through a complete dynamic test of the structure can be studied through component tests. Detection of crack initiation and study of the subsequent change in strength of the component, post-yield component behavior and localized yield effects are examples of such phenomena.

In this study, tests were performed on reinforced microconcrete, steel and phosphor bronze cantilever beams.

8.2 MODELS OF REINFORCED CONCRETE CANTILEVER BEAMS

8.2.1 Introduction

To evaluate the adequacy of material simulation in the case of composite materials, testing of structural elements is necessary. This, in particular, is true for reinforced concrete models because of the complicated nature of the concrete - reinforcement interaction. It is an unfortunate fact that even the tightest material control does not assure similitude of all possible failure modes. These modes may be affected by crack and bond similitude, cyclic loading effects, confinement and multiaxial states of stresses in concrete, stress and strain gradient effects, fabrication accuracy and many other considerations. Several of these aspects are not fully understood in prototype structures and even to a lesser degree in models.

In this study, the simulation of inelastic cyclic response characteristics and cycling rate effects for beam elements were investigated. For this purpose eighteen 1:14.4 scale models of a previously tested cantilever beam (Ref. 186) were tested. The first test series (2 beams) was concerned with the simulation of the prototype response using its properly scaled load history. The prototype failed in a combined flexure and shear mode. The second series (12 beams) was tested to study the effects of different cycling frequencies on the strength, stiffness and hysteresis behavior of beams subjected to high bending moments and small shears. The third series (4 beams) was concerned with the simulation of failure modes controlled primarily by shear rather then flexure.

The model beams for the three test series had identical material and geometrical properties and differed only in the shear span to depth ratio

l/d indicated in Part 1 of Table 8.1.

8.2.2 Specimens

To permit a direct comparison of model and prototype response, the choice of a prototype was limited to an element for which the material properties and the cyclic response characteristics were well documented. Beam No. 46 of a study reported in Ref. 186 was chosen for this purpose. The prototype is shown in Fig. 8.1, and a summary of its geometry and material properties is presented in the third column of Table 8.1.

The geometric scale ratio of l_r = 1:14.4 was established on the basis of the diameter of the available main reinforcement wire used in previous studies performed at Stanford (see Pragraph 7.7.2). Figs. 8.2 and 8.3 show the external dimensions of a model specimen, which consisted of two beams joining into a column stub, and details of the reinforcement layout, respectively. The fifth column of Table 8.1 provides a summary of these data. Figs. 8.4 and 8.5 show assembled cages and casting forms, respectively.

The model reinforcement cage was made of three types of wire whose properties are summarized in Table 8.1 :

1) main reinforcement - Gauge 14 black annealed wire, deformed in the laboratory by cold-knurling (see Paragraph 7.2)
2) beam and column stirrups - black annealed Gauge 20 and 18 wire was used for beam and column stirrups, respectively (Handi-Wire, available in hardware stores). The wire was annealed and chemically roughened after stirrup fabrication.

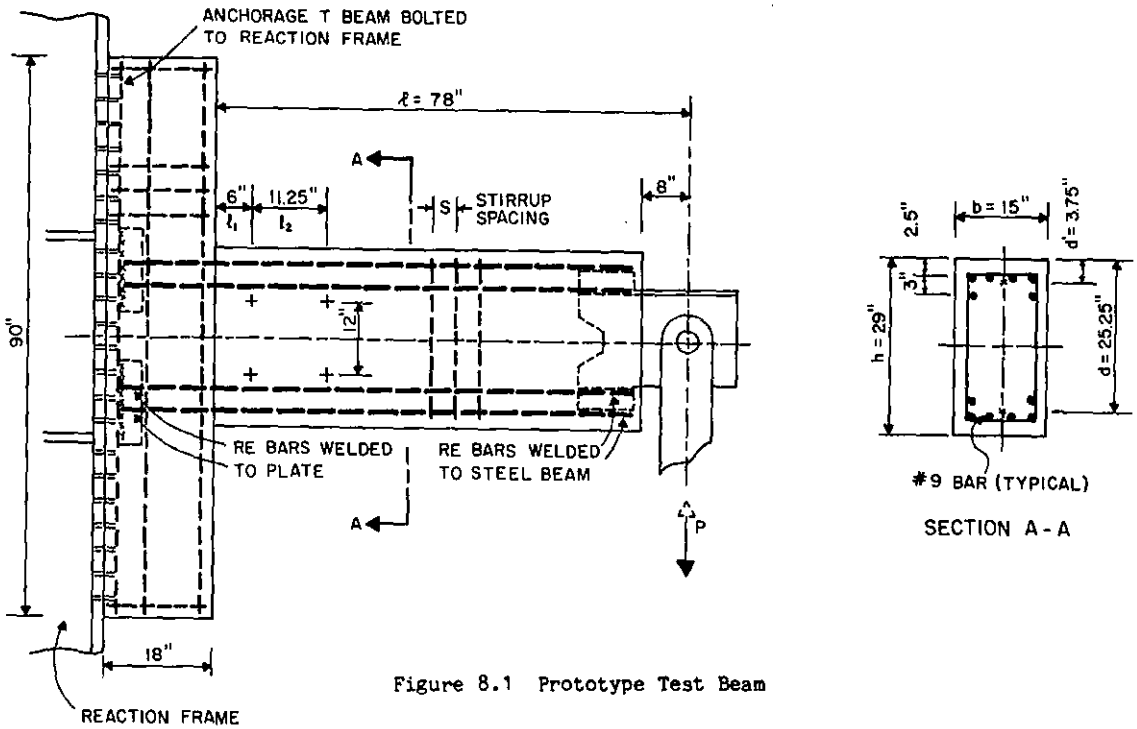

Figure 8.1 Prototype Test Beam

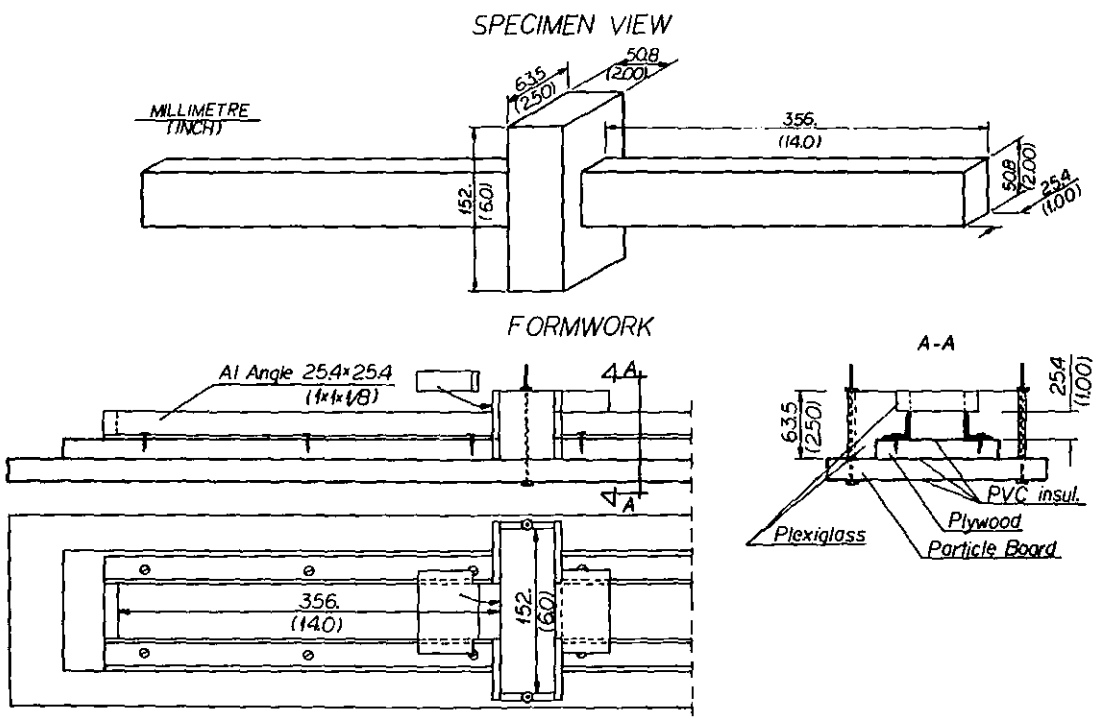

Figure 8.2 Model Geometry and Formwork

Table 8.1 Summary of Prototype and Model Properties

	PARAMETERS	PROTOTYPE	MODEL	
			Prototype Domain	Model Domain
1	geometry			
	l mm (in.)			
	l/d = 6.9		4419 (174.0)	306.9 (12.08)
	l/d = 3.1	1981 (78.0)	1981 (78.0)	137.6 (5.42)
	l/d = 2.24		1439 (56.6)	99.9 (3.93)
	l/d = 2.0		1316 (51.8)	91.4 (3.60)
	h mm (in.)	737 (29.0)	731 (28.8)	50.8 (2.00)
	b mm (in.)	381 (15.0)	366 (14.4)	25.4 (1.00)
	d mm (in.)	641 (25.25)	642 (25.28)	44.6 (1.76)
	d' mm (in.)	95 (3.75)	89 (3.52)	6.2 (0.24)
	$A_s = A'_s$ mm^2 ($in.^2$)	3871 (6.00)	3835 (5.95)[x]	19 (0.029)[x]
2	main reinforcement	#9 bars		Gauge 14 knurled wire
	ø mm (in.)	28.6 (1.12)	28.5 (1.12)	1.98 (0.078)
	f_Y MPa (ksi)	461.9 (67.0)	413 (59.9)[x]	
	f_u MPa (ksi)	710.2 (103.2)	439 (63.7)[x]	
	P_Y kN (kips)	265.3 (59.6)	263.8 (59.3)	1.27 (0.29)
	P_u kN (kips)	407.8 (102.4)	280.4 (63.0)	1.35 (0.30)
3	stirrup ties	#4 bars		Gauge 20 chemically roughened wire
	ø mm (in.)	12.7 (0.5)	12.0 (0.5)	0.88 (0.033)[xx]
	f_Y MPa (ksi)	413.7 (60.0)	345 (50.0)[x]	
	f_u MPa (ksi)	661.9 (96.0)	413 (59.9)[x]	
	P_Y kN (kips)	52.4 (11.78)	39.3 (8.8)	0.189 (0.042)
	P_u kN (kips)	83.8 (18.85)	46.4 (10.4)	0.224 (0.050)
	s mm (in.)	152 (6.00)	114 (4.5)	7.9 (0.31)
	$2P_Y/s$ kN/mm (kips/in.)	0.689 (3.927)	0.692 (3.952)	0.048 (0.275)
	$2P_u/s$ kN/mm (kips/in.)	1.103 (6.283)	0.815 (4.651)	0.057 (0.323)
4	concrete			microconcrete
	f'_c MPa (ksi)	27.5 (3.99)	37.9 (5.50)	
	f'_t MPa (ksi)	3.1 (0.45)	4.4 (0.63)	
	f'_t/f'_c x 100	11.3	11.6	

[x] values based on approximate diameter of the wire

[xx] diameter after chemical treatment

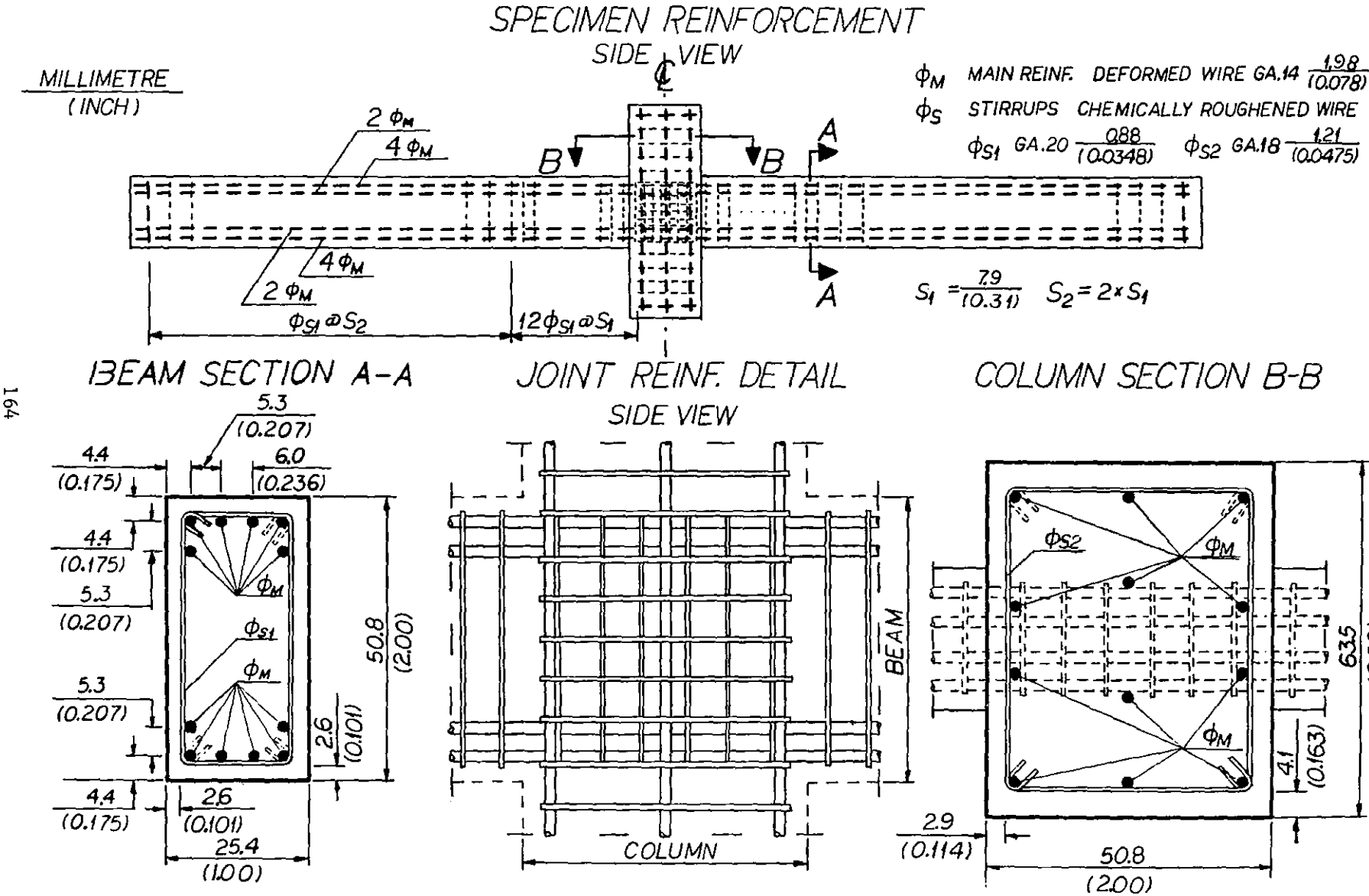

Figure 8.3 Model Reinforcement

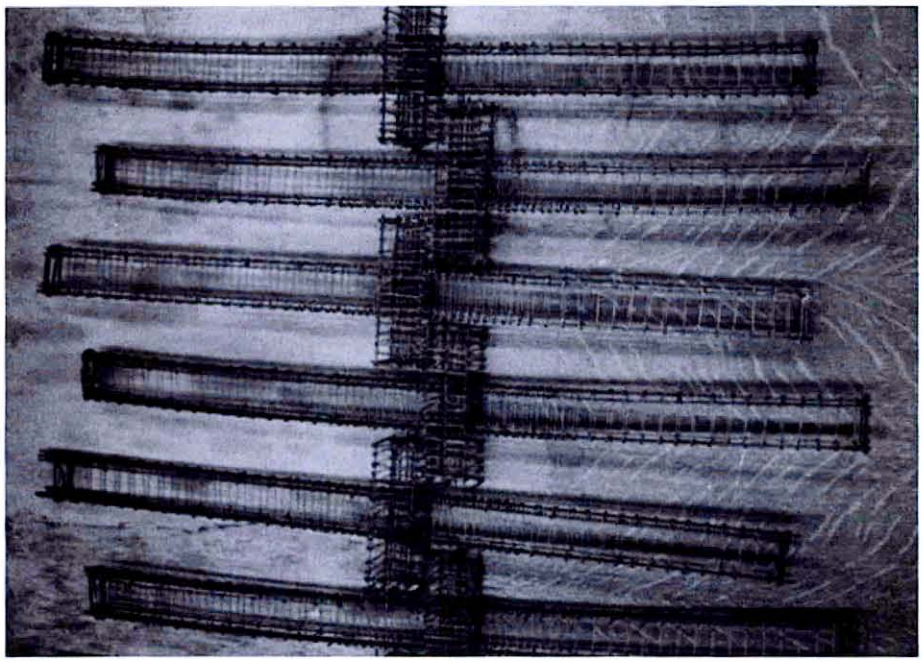

Figure 8.4 Assembled Reinforcement Cages

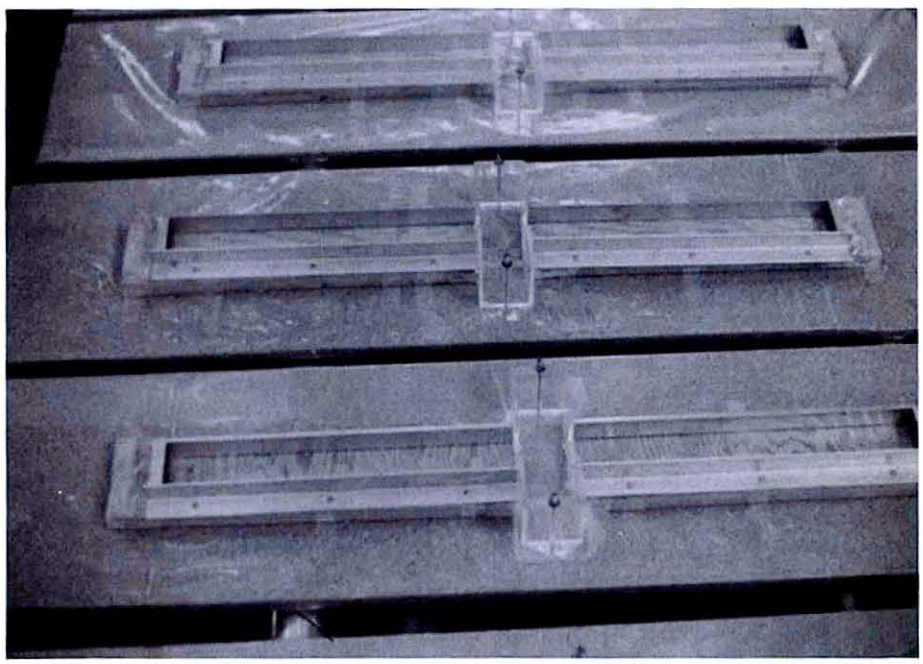

Figure 8.5 Casting Forms

8.2.2.1 Specimen Fabrication

Due to the cold-knurling process, the main reinforcement was assuming a curvature of a radius of about 5 m, which required a special arrangement for the assembly of the reinforcement cage. The wires were threaded through templets with precisely located holes, anchored at one end, and tensioned to about 1/3 of their yield strength at the other end by means of turn buckles as shown in Fig. 8.6. The spacing of the wires was also controlled by intermediate spacers (see Fig. 8.7). Details of reinforcement cages, with all longitidunal and transverse reinforcement in place, are shown in the photographs of Fig. 8.8.

The beam stirrups were fabricated in the following steps:

1) spooling the wire tightly on a machined steel bar of a cross section equal to the internal stirrup dimensions,
2) stress relieving of residual stresses (600°C (1112°F) for 2 hrs.) built up during the unwinding of the coil of the wire and during the rewinding around the steel core,
3) sliding the wire off the steel core and cutting it into individual stirrups while accounting for the hooks still to be formed, and
4) chemically treating the stirrups to remove the shiny and smooth scale and to roughen the wire surface (see Paragraph 7.2).

The main beam and column reinforcement was threaded through the closed stirrups except in the joint area, where the column stirrups had to be opened and reclosed after being positioned.

Since the strength of the stirrup wire was lower than that required by the scaling of the prototype properties (Table 8.1), the spacing of the stirrups was altered to provide an equivalent amount of shear rein-

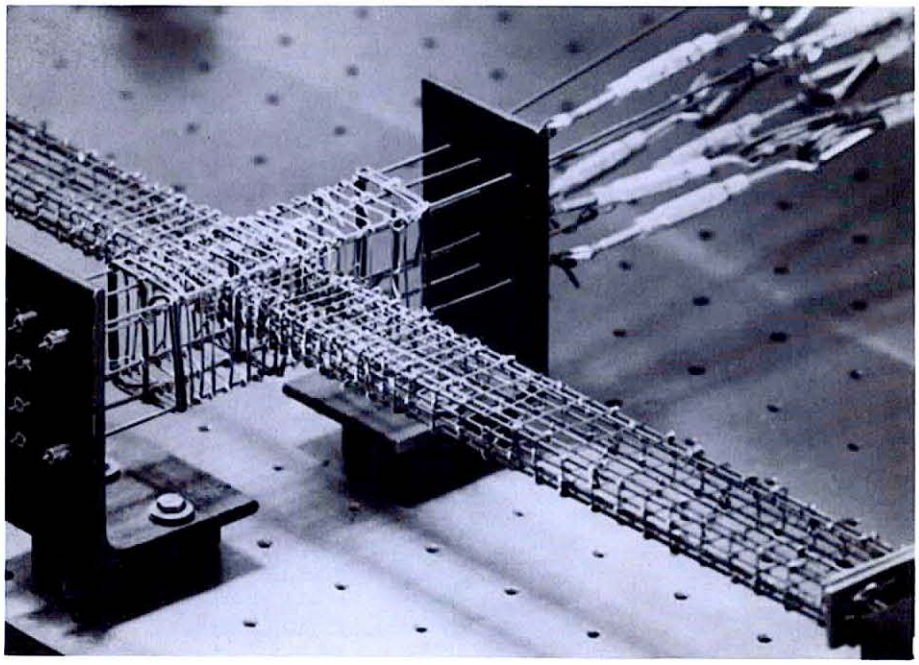

Figure 8.6 Setup for Reinforcement Cage Assemblage

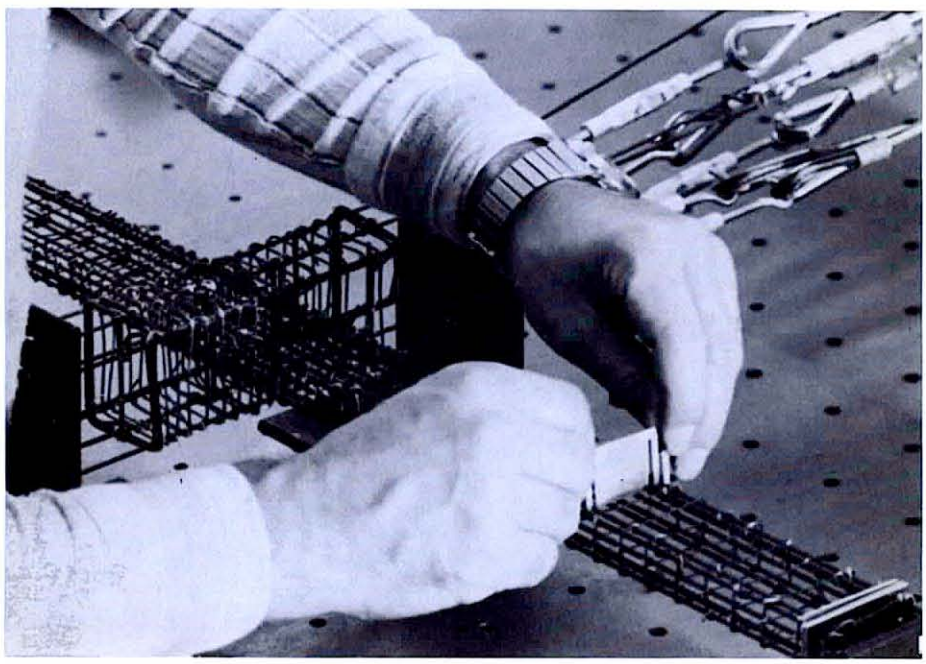

Figure 8.7 Control of Wire Location in Reinforcement Cage

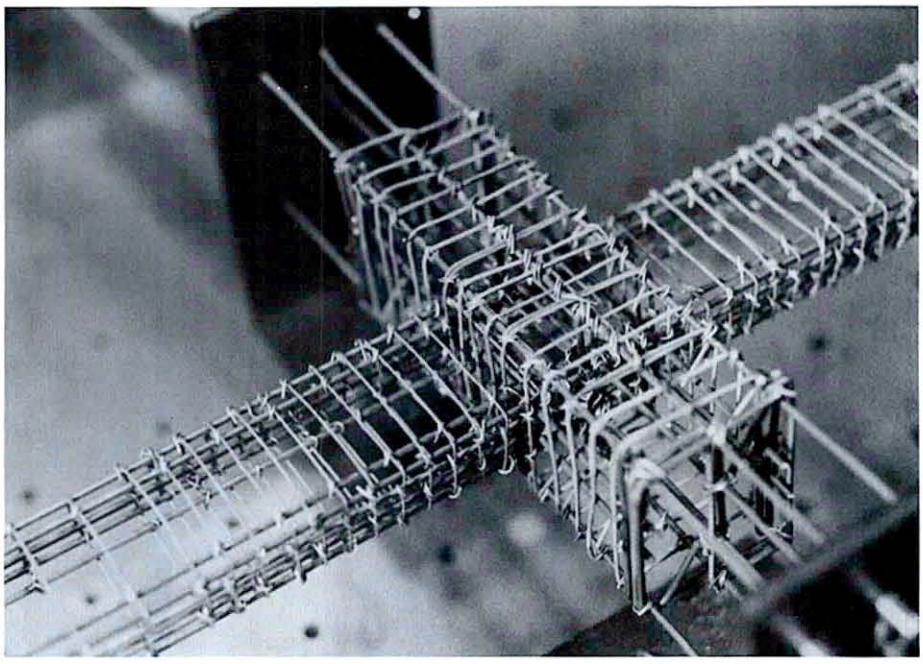

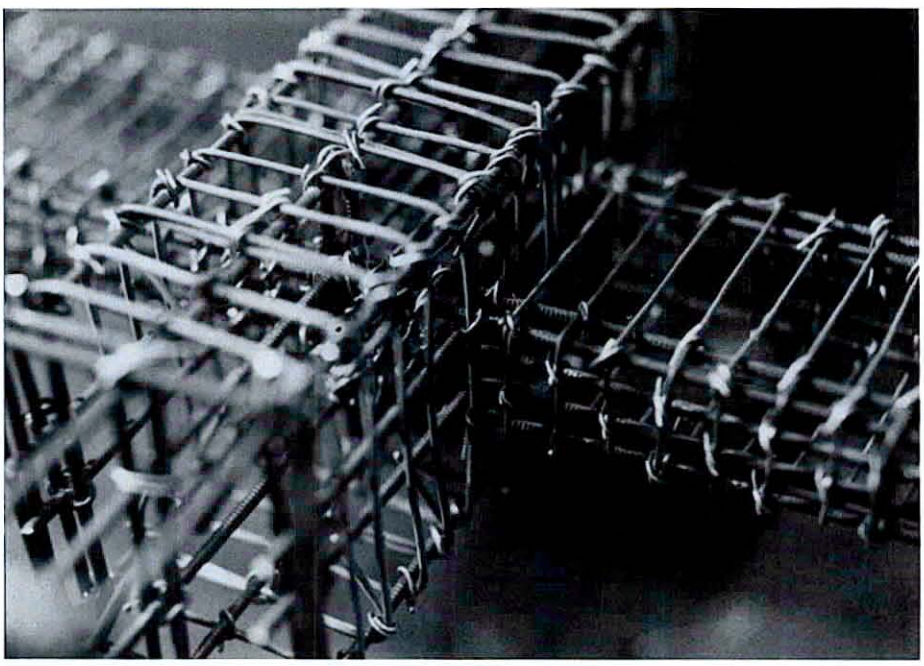

Figure 8.8 Details of Reinforcement Cage

forcement per unit length:

$$s_m = s_p l_r (P_{Ym}/P_{Yp}) l_r^{-2}$$

where s is the stirrup spacing, l_r the length scale ratio (1:14.4), and P_Y the yield force of the stirrup.

The stirrups were spaced at the calculated spacing s_m for a beam length equal to twice the beam depth and at $2s_m$ thereafter to reduce the fabrication effort. Machined plexiglass combs were used to control the spacing.

The stirrups were attached to the main reinforcement by tightening them together with Gauge 24 wire at every third crossing along the main reinforcement (Figs. 8.7, 8.8). The tightening required some practice in order not to bend the relatively weak stirrups. Finally, at each such node a very small amount of adhesive (GR-R-1P, Alpha Cyanocrylate adhesive by GC Electronics) was applied, which resulted in a slip-free connection between the stirrups and main reinforcement, thus providing the rigidity of the cage necessary for further handling after removal from assembling table.

In average, it took less than three working days to assemble one reinforcement cage.

The forms for casting of the specimens were made out of wood covered with PVC foil to prevent wood warping and adhesion between the forms and the concrete, and out of aluminum angles of depth equal to the width of the beam (Figs. 8.2 and 8.5). The beams were cast horizontally as in the case of the prototype. The cages were positioned in the forms using spacers and stiff horizontal stainless steel wires passing through the aluminum angles.

The microconcrete used for the specimens had a C:A:W ratio of 1:3.5:0.72, with aggregate grading and cement type as reported in Section 7.1.2.3 for mixes used in this study.

All the specimens were cast together using a single batch of concrete. A total of 35 accompanying 50x100 mm (2x4 in.) cylinders were cast at the same time.

The mixing was done using a two-speed 0.5 $ft.^3$ (0.003 m^3) mechanical mixer. The procedure used (as recommended in Ref. 18) was as follows:

1. Place the entire quantity of mix water in the bowl of the mixer.
2. Add cement, mix for 30 seconds at slow speed, add aggregate, mix for 30 seconds.
3. Stop mixer for 50 seconds. Scrape any mortar stuck to the sides down into the batch.
4. Mix for 60 seconds at slow speed.

The concrete was poured into the forms and vibrated into place by touching the forms with a pneumatic hand vibrator. Once the concrete reached the upper edge of the beam form, a plexiglass stopper (Fig. 8.1) was placed in position to prevent the flow of the concrete during the casting of the higher located portion of the column.

After the casting was completed the forms were covered with PVC foil to prevent moisture loss, and left undisturbed for 24 hours. Then the forms were stripped (by dismantling the formwork which was connected by screws) and the specimens were placed in a fog room (20°C, 95% RH).

To assure equal moisture content in all specimens at the time of testing, as well as to prevent shrinkage cracking, all specimens were sealed using clear shellac spray, as it was recommended in Ref. 18. The coating is water proof, transparent and highly brittle, thus providing

the possibility of crack observation during the test. The sealing was accomplished by removing the test beams and accompanying cylinder specimens from the fog room after 5 weaks, allowing their surface to dry for about 40 minutes and then spraying the surface with the first coat of shellac. Subsequently, two additional coats were applied. The coated specimens were then stored in a constant temperature room ($20^{o}C$) till the day of testing.

8.2.2.2 Test Setup and Instrumentation

The tests were performed using the MTS closed-loop testing machine with the adjustable testing frame shown in Fig. 5.4.

The test setup and part of the instrumentation are shown in Figs. 8.9 and in the photos of Fig. 8.10. The cyclic loads were applied to the column stub by means of the MTS hydraulic actuator. In order to avoid force redistribution between the two beams of a test specimen, the column stub was rigidly connected to the hydraulic actuator.

The supports of the beams were provided by linkages consisting of two spherical rod-end bearings with a load cell mounted between them (Fig. 8.10). A turn-buckle in each of the two linkages allowed precise adjustment of the length of the linkages.

The ends of both beams were braced against lateral out-of-plane movement. The bracing was provided through teflon-lined, rigidly supported plates (not shown in Fig. 8.9). A very small gap was left between the teflon and beam faces. Closing of this gap was not observed in any test, thus out-of-plane bending did not occur.

The instrumentation of the test consisted of the following:

1. LVDT of the hydraulic actuator measuring the column displacement. In

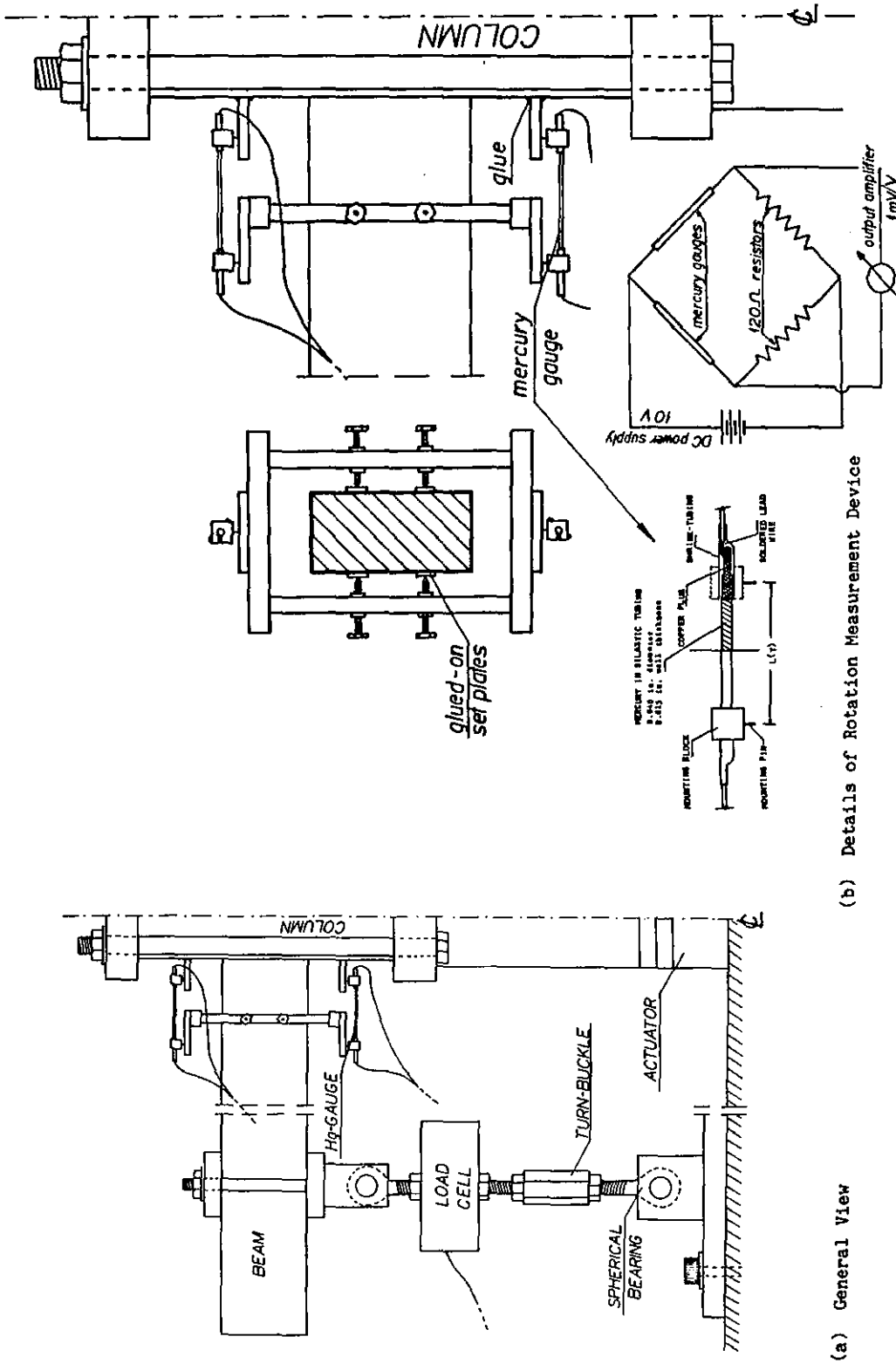

(b) Details of Rotation Measurement Device

(a) General View

Figure 8.9 Experimental Setup and Instumentation

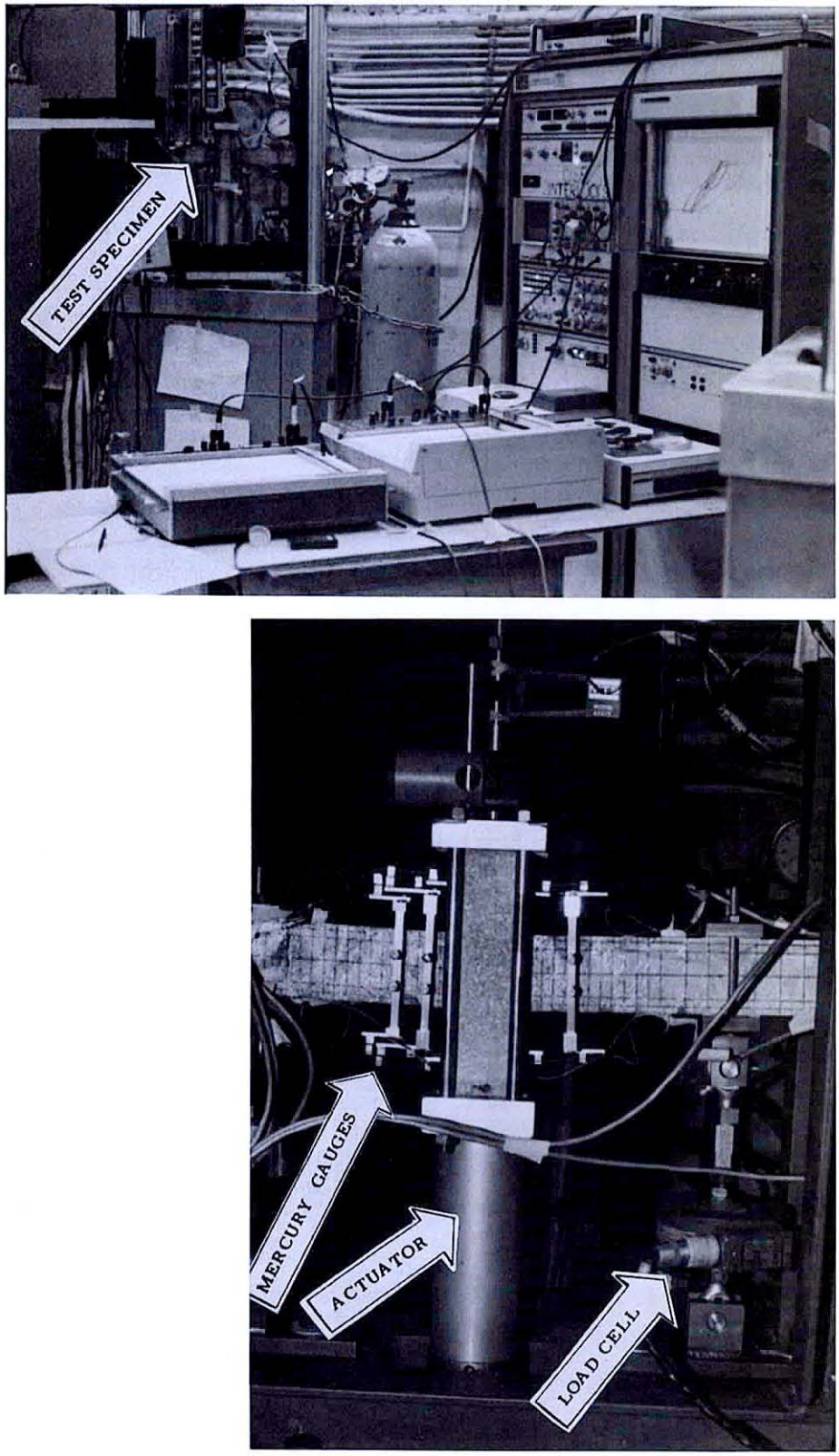

Figure 8.10 Views of Experimental Setup and Instrumentation

most of the cases the actuator stroke was also used for test control. In this manner, both beams were subjected to equal displacement histories but were permitted to undergo different load histories when unequal strength properties existed in the two beams.

2. Two load cells measuring the force at the end of each beam independently. One of the load cells was used for the test control in the sub-yielding cycles of the high shear tests.
3. Two or three pairs of mercury gauges for the measurement of displacements at the top and bottom sides of rectangular rigid frames which were attached to the beam as shown in Figs. 8.9 and 8.10. From the displacement measurements the rotations and average curvatures over a predetermined distance were deduced. The use of mercury gauges is discussed in Chapter 5. Average curvatures were measured between the column face and two sections located at 10.5 mm (0.41 in.) and 30.5 mm (1.20 in.) from the column face.

Signals of all the instruments were recorded in digitized form by a minicomputer. Several X-Y recorders registering the load-deflection and load-average curvature measurements were also used in the low frequency tests to allow visual control of the test. In the high frequency tests, load-displacement histories were registered on oscilloscope screens.

All the beams were coated with shellac (see previous section) on which a grid identifying the location of the main reinforcement and stirrups was drawn with a felt pen.

The cracks were observed with the help of a magnifying glass, marked with a felt pen, and recorded photographically.

8.2.3 Simulation of Prototype Response (l/d = 3.1)

In order to evaluate the adequacy of a small-scale model of a beam element subjected to bending and high shear, two beams (one specimen) were subjected to the properly scaled prototype loading history (Ref. 186). The loading history of the prototype beam is shown schematically in Fig. 8.11.

The loading velocity was controlled through a ramp function with the speed of loading based on the assumption that the time of first loading to yielding is 100 seconds.

Load-displacement response of the prototype is reproduced from Ref. 186 and presented in Figs. 8.12 , with the load points corresponding to the ones marked in Fig. 8.11.

In order to compare these results on a one-to-one basis with the results obtained for the model beams, appropriate scale factors were applied to the measured model response values. Comparisons of several load-displacement hysteresis loops of the prototype and model response are presented in Figs. 8.13 and 8.14. Table 8.2 provides a comparison of tangent stiffnesses in different cycles in the prototype and model beams.

For the cycles below and slightly beyond yielding of the main reinforcement, the shapes of the hysteresis loops are similar in model and prototype and an accurate simulation of the prototype response was achieved with the small-scale model. However, at the first large amplitude reversal (Point 26) and thereafter, a significant strength deterioration is evident in the model response which did not occur in the prototype. This phenomenon must be attributed largely to the lack of strain hardening in the main reinforcement of the model beam. It is

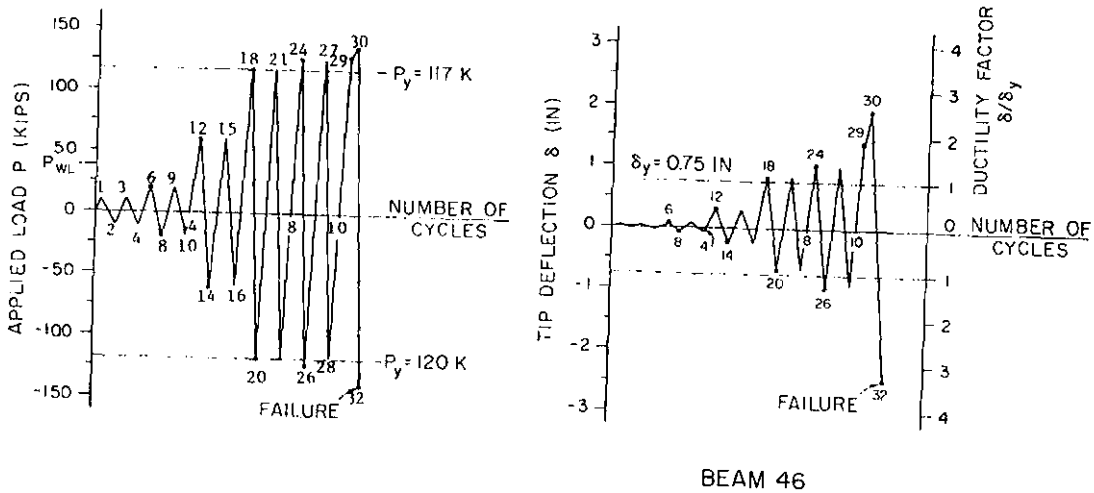

Figure 8.11 Prototype Loading History

Table 8.2 Tangent Stiffness of Prototype and Model Beams

Cycle	Load Point	Prototype		Model+		Prototype / Model
		kN/mm	(kips/in.)	kN/mm	(kips/in.)	
2		61.3	(350)	63.9	(364)	0.96
4	12	29.8	(170)	34.7	(198)	0.86
7	18	23.5	(134)	23.7	(135)	0.99

+ Prototype Domain

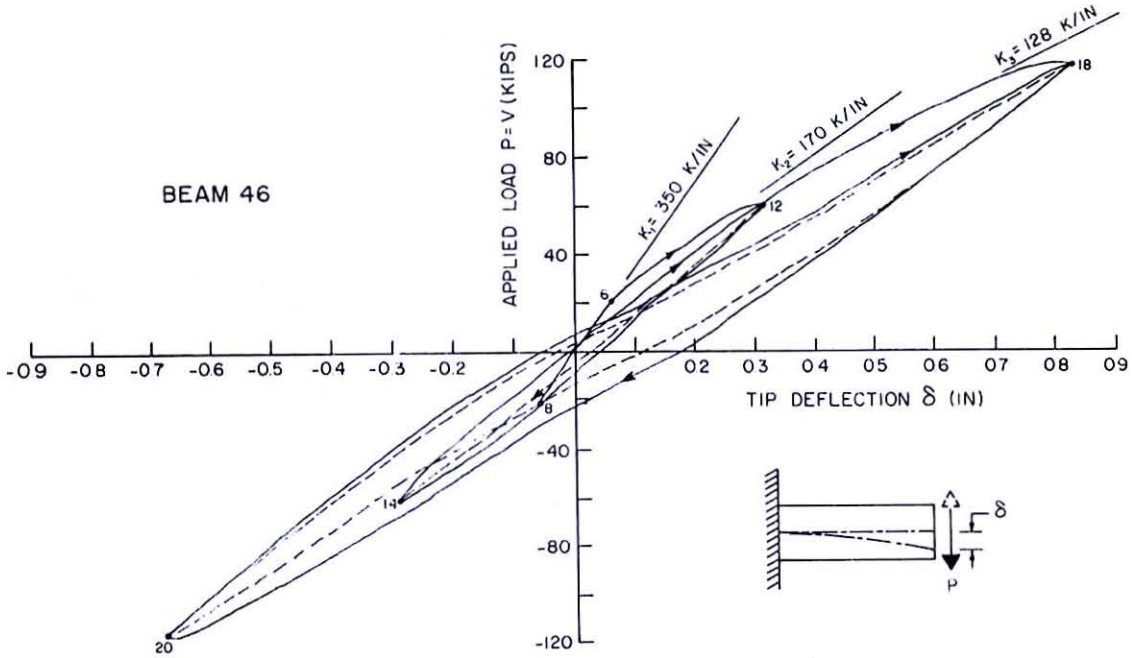

(a) Up to Yielding of Reinforcement

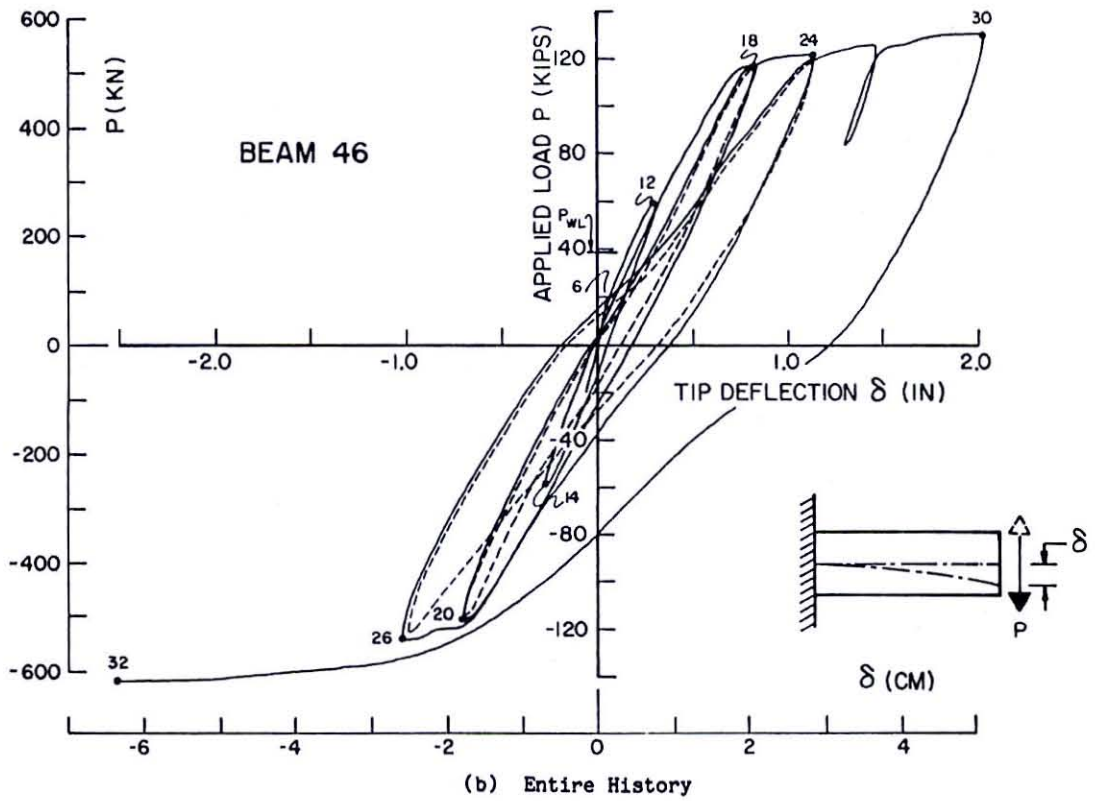

(b) Entire History

Figure 8.12 Prototype Load Displacement Response

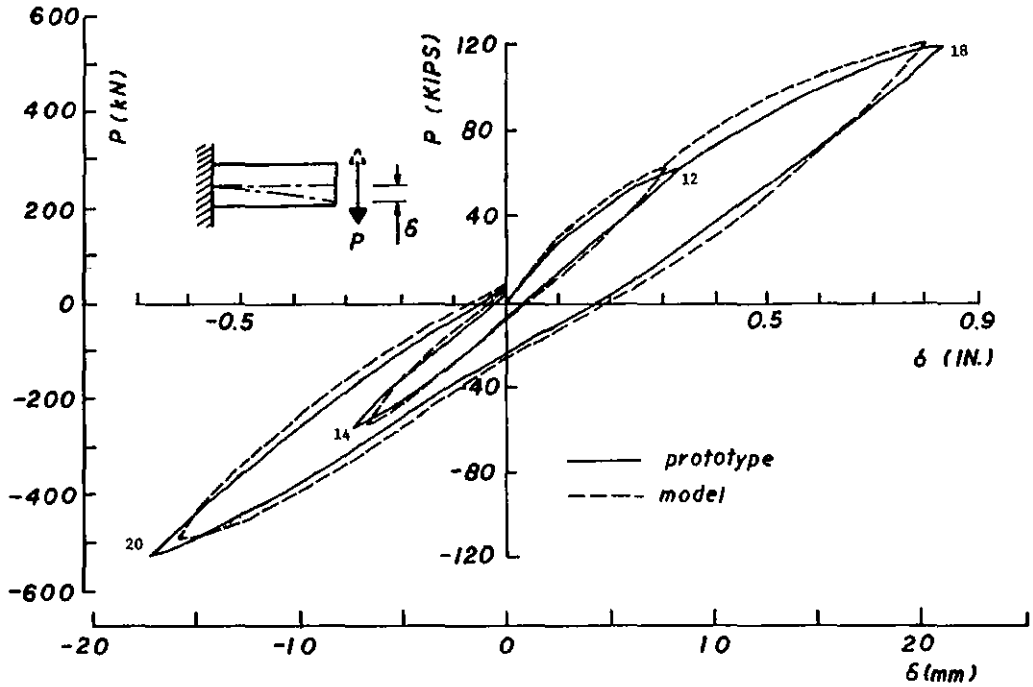

Figure 8.13 Comparison of Model and Prototype Load-Displacement Response for Cycles up to Yielding of Reinforcement (Prototype Domain)

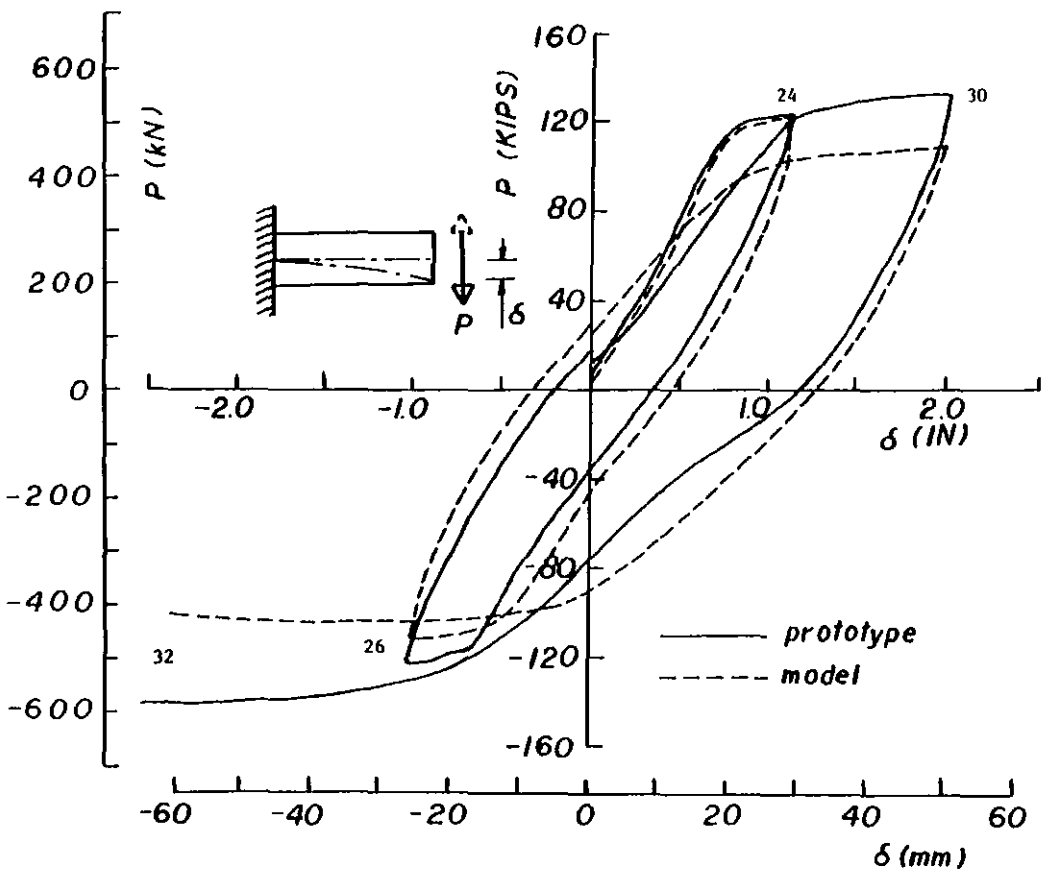

Figure 8.14 Comparison of Model and Prototype Load-Displacement Response for Cycles beyond Yielding of Reinforcement (Prototype Domain)

believed that, with reinforcement which is heat-treated to develop the necessary strain hardening ability, also the larger amplitude loops could be successfully reproduced.

Figure 8.15 presents the load-average curvature (or moment-curvature after multyplying of the vertical axis by a constant) response of the model over a length of 438 mm (17.3 in.) (prototype domain). The curvature record shows a symmetrical behavior corresponding to the symmetrical displacement history. This indicates that the inelastic tip deflection is caused primarily by a symmetric pattern of cracks concentrated in the close vicinity of the column. Figure 8.16 shows the load-curvature relationship over a length of 152 mm (6 in.) for the prototype. Superimposed are the peak values of the curvatures measured at the same location in the model. It can be seen that the peak values differ considerably between model and prototype. The unsymmetric peaks in the prototype are attributed to the strain hardening in the prototype reinforcement which led to a redistribution of strains which had no counterpart in the model due to lack of strain hardening.

In retrospect, the importance of simulating the strain hardening characteristics in model reinforcement cannot be overemphasized. It is well established that the post-yielding cyclic response characteristics of flexural elements are largely controlled by the mechanical properties of the reinforcement. Strain hardening will permit an increase in the bending resistance and will also cause a spreading of flexural (and also shear) cracks into the beam proper.

Figures 8.17 a and 8.17 b present the crack pattern in the prototype and in the model, respectively. Here again the lack of strain hardening

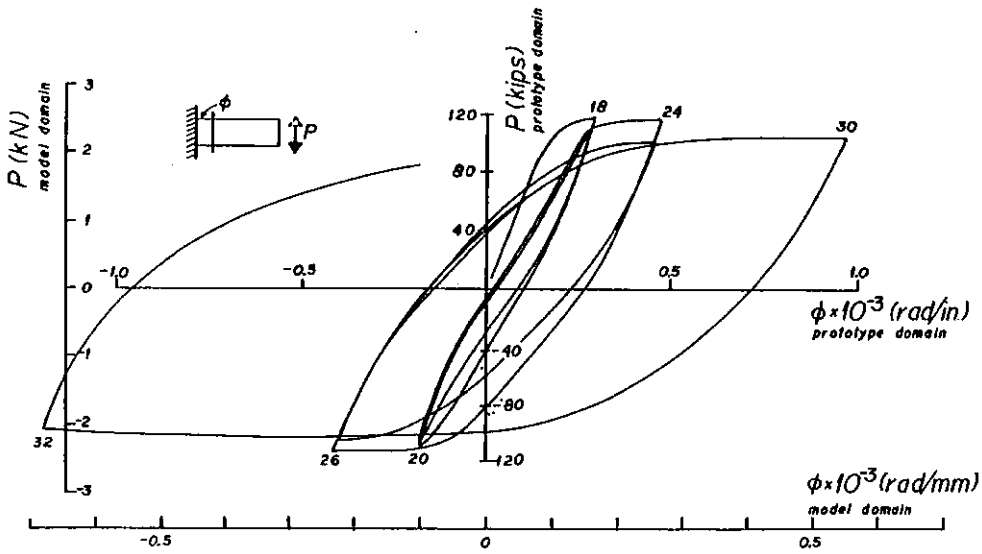

Figure 8.15 Model Moment-Curvature Response

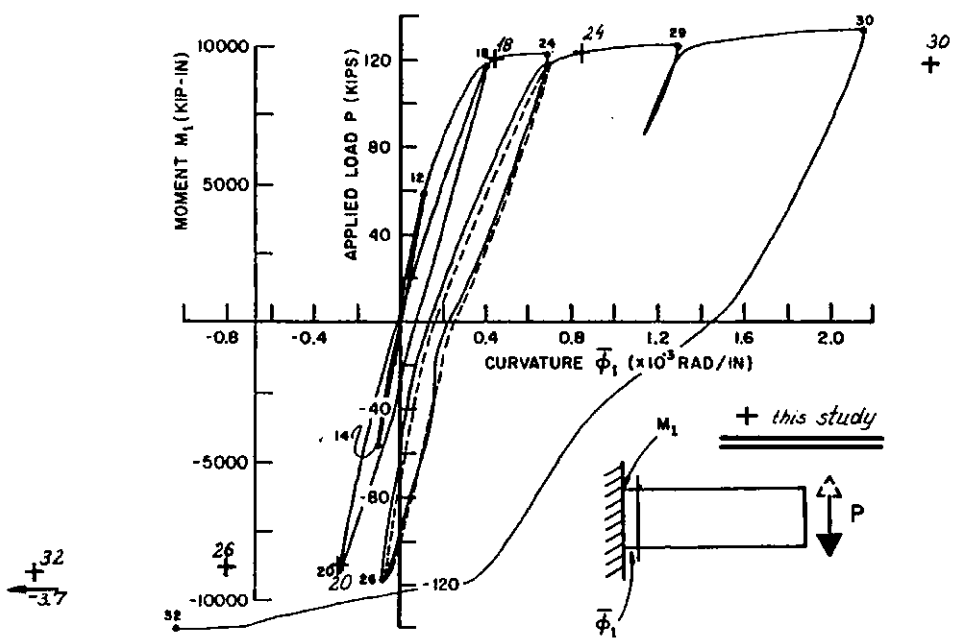

Figure 8.16 Comparison of Model and Prototype Moment-Curvature Response

(a) Prototype

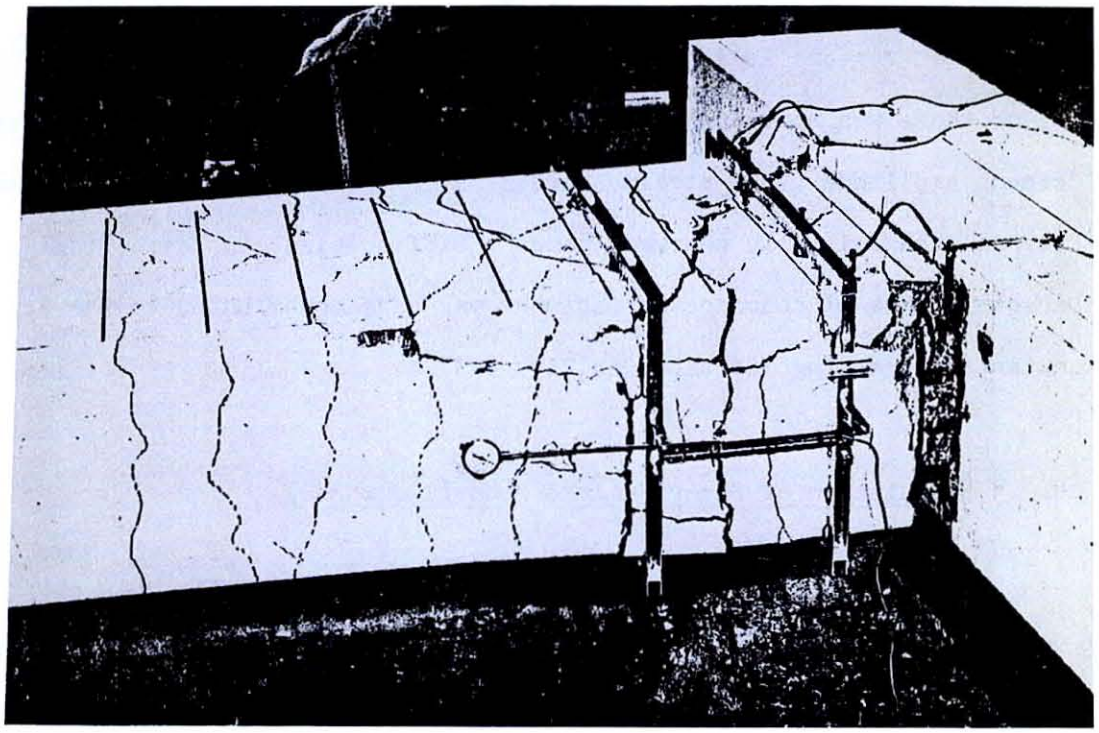

(b) Model

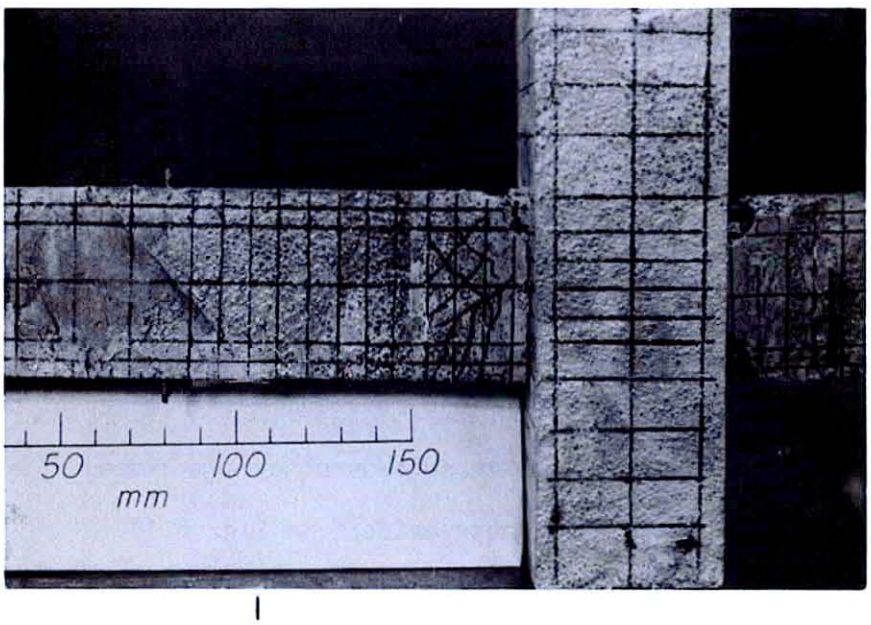

Figure 8.17 Views of Prototype and Model Crack Patterns

in the model reinforcement is of a visible influence. Although the cracks in the vicinity of the column are similar, no cracking in the model beam regions located further away from the column was observed. Since there was no increase in the beam capacity with increasing displacement amplitude (no strain hardening), the cracks did not propagate beyond the initially cracked zone. Difficulties in detecting small cracks in the microconcrete specimens may have contributed to the limited extent of cracking indicated in Fig. 8.17 b.

8.2.4 Simulation of Shear Failure Mode ($l/d = 2.0$)

Four of the beams were tested with very small shear span to depth ratios to examine the feasibility of small-scale model tests of beams failing in a mode controlled primarily by shear. Two of the cantilever beams were loaded at a distance of 2.0d from the column face and two at a distance of 2.24d.

Figure 8.18 shows the load-displacement hysteresis loops for one of the beams with $l/d = 2.0$. The applied load history consisted of three cycles at a displacement amplitude slightly beyond yielding of the reinforcement and three subsequent cycles of twice this amplitude. Prototype test data are not available for a direct comparison of response behavior, but the model test results exhibit all the characteristics expected from a high shear test. The first load reversal led to a set of nearly orthogonal diagonal cracks which in subsequent cycles caused the well-known pinching of the hysteresis loops evident in Fig. 8.18.

At the large displacement amplitude, the second and third cycles led to a rapid deterioration in strength and stiffness. This deterioration was caused primarily by a decrease in the aggregate interlock along the

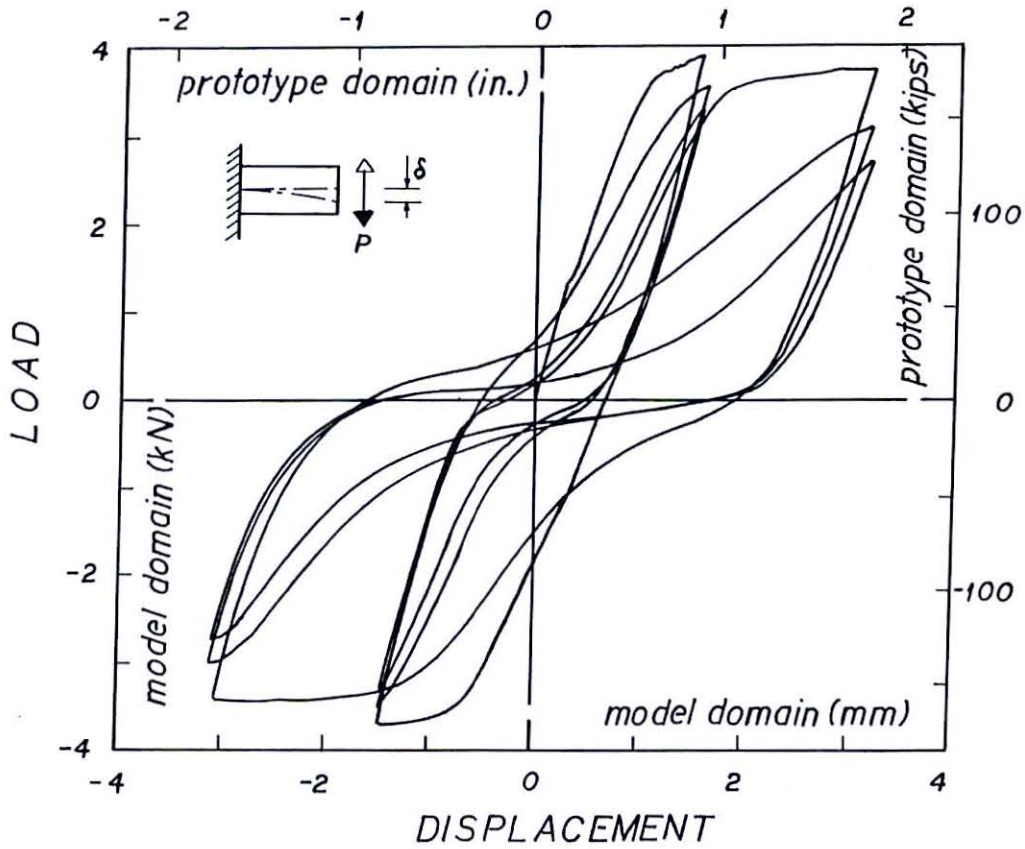

Figure 8.18 Load-Displacement Response from Test with l/d = 2.0

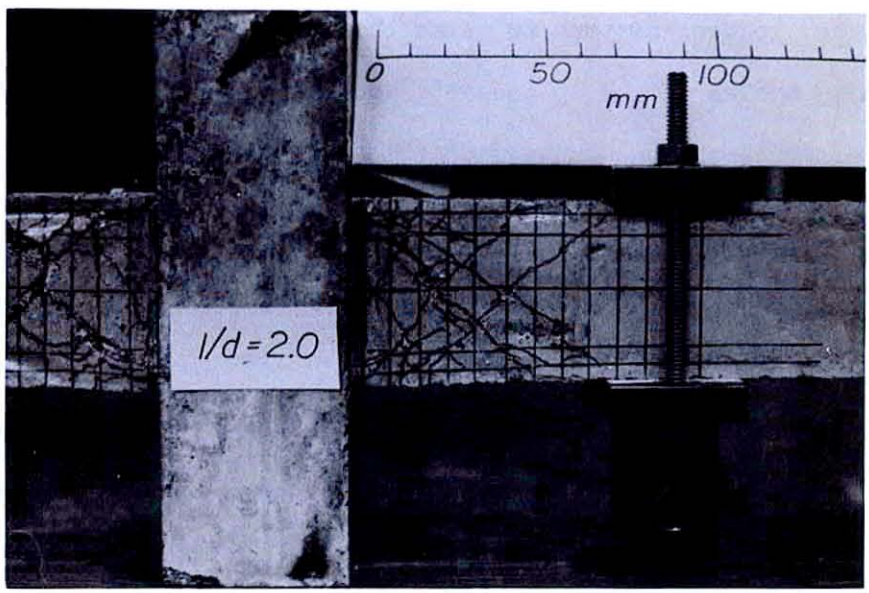

Figure 8.19 View of Crack Pattern from High Shear Test

major diagonal cracks. Considerable crushing of the concrete occurred along these cracks, as can be seen in Fig. 8.19 which shows the crack pattern at the end of the applied load history. This crack pattern appears to be representative of prototype cracking although the spacing of the major shear cracks probably is larger than that of a prototype. The spacing of shear cracks in a prototype of the dimensions shown in Fig. 8.1, but with different l/d and shear reinforcement (Ref. 186) than that used in the model beams, is approximately equal to one-fifth of the beam height whereas it is on the average one-quarter of the beam height in the model beam.

8.2.5 Simulation of Flexural Failure Mode (l/d = 6.9)

In order to explore the feasibility of simulation of a predominantly flexural mode of failure a couple of cantilever beams was tested with shear span to depth ratio equal to 6.9.

The loading history to which the cantilevers were subjected consisted of 3 cycles at a displacement amplitude slightly beyond yielding of the reinforcement and subsequently 3 cycles at twice this amplitude.

Figure 8.20 shows load-displacement hysteresis loops obtained in this test. There is no shear pinching effect, and the observed strength deterioration can be attributed entirely to the lack of work hardening exhibited by the main reinforcement. The crack pattern developed in the beams (Fig. 8.21) was entirely of flexural nature, although, as in the previous tests, all the cracks of visible size were concentrated in the region relatively close to the column stub.

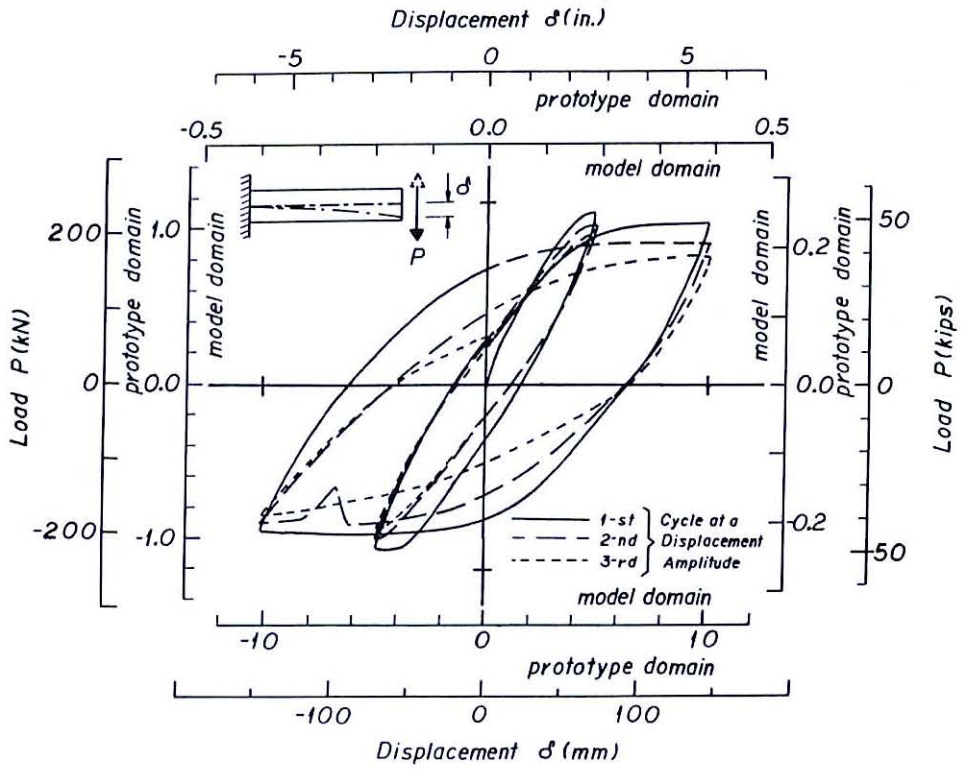

Figure 8.20 Load-Displacement Response from Test with l/d = 6.9

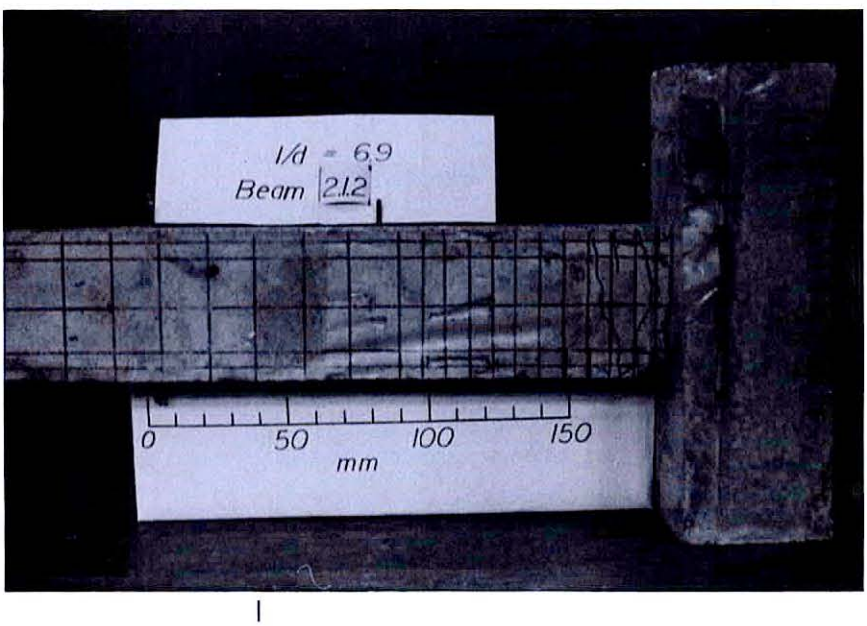

Figure 8.21 View of Crack Pattern from High Flexure Test

8.2.6 Effects of Cycling Frequencies

Most experimental studies performed on structural subassemblies are executed through pseudo-static load application. This is not necessarily due to the limitations of the loading equipment, but mainly to permit measurements with conventional monitoring equipment and to permit visual observations during the test. It remains to be seen whether the behavior under slow pseudo-static load application is fully representative of the dynamic response characteristics of components under earthquake excitations. For this reason a series of tests was performed on the previously described cantilever beam specimens with shear span to depth ratio of 6.9. All the beams were subjected to an identical displacement history consisting of three cycles at an amplitude slightly beyond the yield level of the main reinforcement, and three cycles at twice this amplitude. Three cycling frequencies were adopted and 4 beams (2 pairs) were tested at each frequency. The selected frequencies were 2.5×10^{-3} Hz which may be representative of a pseudo-static test, and 2 Hz and 10 Hz, which may be representative for the frequencies of prototype and model components in structures under earthquake excitations.

Figures 8.22 a and 8.22 b display hysteresis loops for beams tested at a cycling frequency of 2.5×10^{-3} Hz and 10 Hz, respectively. Figure 8.23 provides a comparison of the first hysteresis loops at two displacement amplitudes obtained from three beams cycled at different frequencies. The loads are normalized with respect to the average maximum load from four beams tested at a frequency of 2 Hz and the displacements are normalized with respect to the average maximum displacement at the first cycle of all twelve beams. The intent was to keep the displacement amplitudes the same for all tests but difficulties in the MTS stroke

(a) Cycling Frequency 0.0025 Hz

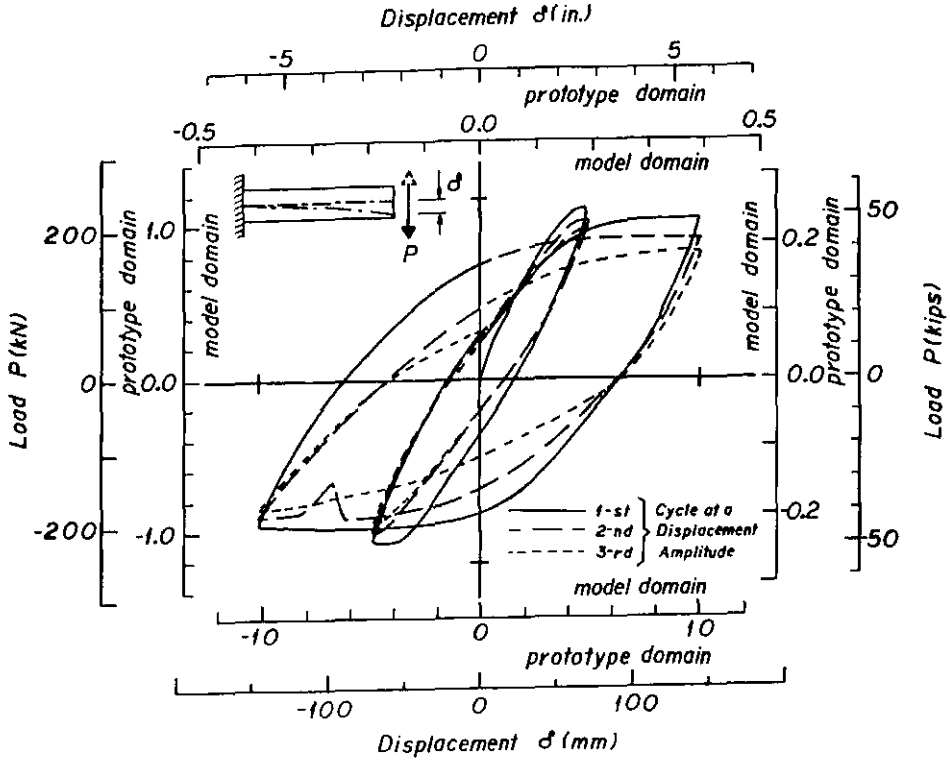

(b) Cycling Frequency 10 Hz

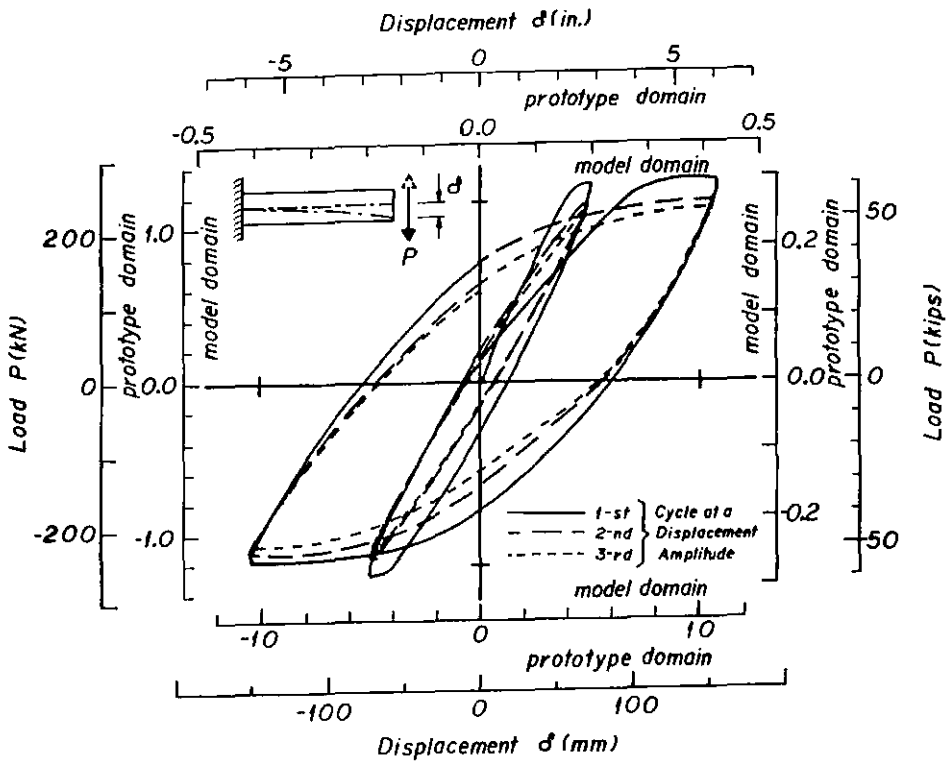

Figure 8.22 Comparison of Load-Displacement Responsefor Beams Tested at Different Frequencies

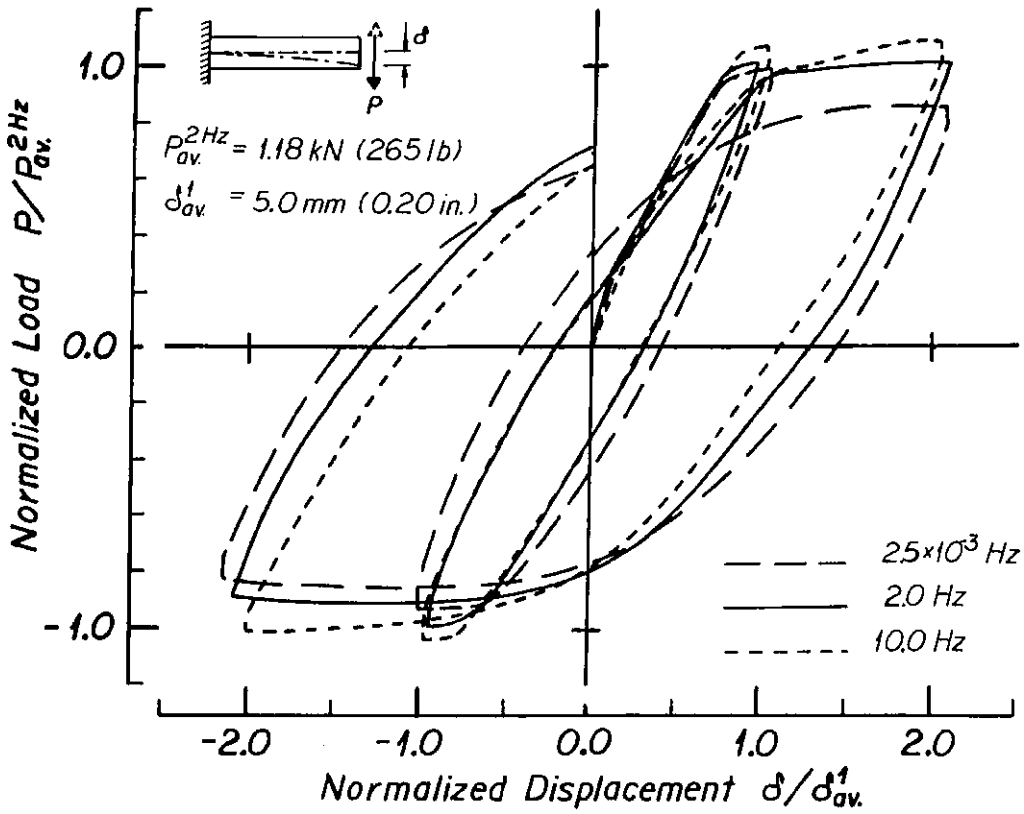

Figure 8.23 Load-Displacement Response for Three Different Cycling Frequencies

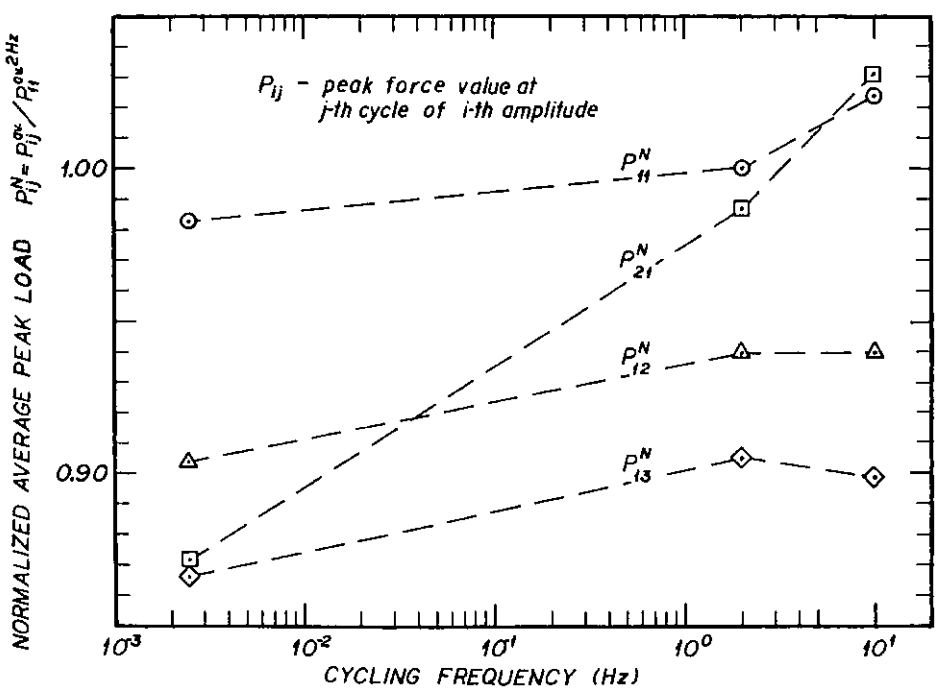

Figure 8.24 Influence of Cycling Frequency on the Peak Load at a Displacement Amplitude

control at high frequencies did cause some differences.

All the hysteresis loops obtained from the measurements performed during the tests of the twelve beams are presented in Appendix B. For each beam a normalized load-displacement history, and a normalized bending moment-average curvature history are presented. Table B.1 summarizes the measured maximum load values vs. displacement amplitude.

Figure 8.24 presents the quantification of the influence of cycling frequency on the average peak loads at the two displacement amplitudes. The average load values are normalized with respect to the average peak load obtained in the first cycle of the 2 Hz tests. Three of the presented lines, P^N_{11}, P^N_{12} and P^N_{13}, represent the change in the peak load values in the first, second and third cycle of the first amplitude. The fourth line (P^N_{21}) reflects the change for the first cycle of the second amplitude. Lines P^N_{11} and P^N_{21} indicate the significant difference in the strength of the beams tested at the static frequency (0.0025 Hz) and at dynamic frequencies (2 Hz and 10 Hz). The difference between the two lines shows a loss of strength, from the smaller to the larger amplitude of approximately 13% for the lowest frequency, about 1% for the second frequency and some minimal gain for the highest frequency. There is no significant difference between the strength deterioration rate for cycles of the same amplitude carried out at different frequency levels.

The crack patterns of the beams described for the lowest frequency in Section 8.2.5 were also studied for the higher frequencies. It was observed that, although the crack pattern was basically independent of the cycling frequency, there was a difference in crack sizes. In the low frequency test, pieces of concrete around the major crack at the column

face spalled off whereas in the high frequency tests the crushed concrete pieces did not fall out. This may explain the large difference between the peak load values for the first cycle of the small and the large amplitude in a low frequency test, and the relatively small difference in the high frequency tests. Line P^{N}_{11} indicates that the effect of material strain rate accounts for a 5% strength increase by increasing the cycling frequency from 0.0025 Hz to 10 Hz, and thus is small relatively to the effect of cycling frequency on the post-cracking behavior of concrete particles located in the cracked area.

8.2.7 Conclusions

Because of the lack of strain hardening in the model reinforcement, only a limited assessment of the simulation of the various failure modes (flexure, flexure-shear, and shear) can be made from this study. Also, prototype test results are available only for the beam failing in a flexure-shear mode. For this case, the stiffnesses in the various cycles are closely simulated at model scales and the strength values are adequately reproduced in the early post-yield range. The tests on specimens with small l/d ratios show the characteristic pinching of hysteresis loops while the tests on specimens with large l/d exhibit the expected fat hysteresis loops controlled by the stress-strain characteristics of the reinforcement. Considering the complex mechanisms that are involved in shear transfer (aggregate interlock, dowel action, contribution of shear reinforcement, etc.), the results of this limited test series are not fully conclusive but are indicative that most of these complex mechanisms can be simulated with reasonable success at small model scales. In all cases, strength deterioration in the inelastic range

occurred at a rate which exceeds that expected in the prototype. It is likely, although it cannot be proven at this time, that much or all of this discrepancy is caused by the lack of strain hardening in the model reinforcement used in this study. Further research with more accurately scaled stress-strain characteristics of the reinforcement is needed to verify this conclusion.

The study of the cycyling frequency effect indicated that the material strain rate effects, as discussed in Sections 7.1.3 and 7.2.3, appear to have relatively little effect on the strength of the specimens. Of larger importance seems to be the effect of deformation rate on the post-cracking behavior of the concrete which restrains dislocation of concrete particles in high frequency tests. This phenomenon causes doubts in the accuracy of dymamic response prediction from psuedo-static load tests.

8.3 MODELS OF STEEL CANTILEVER BEAMS

In this study, tests were carried out on two metal cantilevers, an A36 structural steel cantilever and a 1:1.92 model of it made of CA 510 annealed phosphor bronze. The tests were performed to provide information on the load-deformation behavior of columns of two single-degree of freedom models tested on the shake table. This information was needed particularly for the phosphor bronze model, in which temperature effects due to the column welding process were of particular concern. The study was also performed to investigate the effect of cycling frequency on the load-deformation behavior of the specimens.

For ease of fabrication, rectangular cross sections were selected for the specimens. The dimensions of the cantilevers were based on the dimensions of columns of single-degree of freedom models studied subsequently on the shake table. The steel columns were fabricated from a 13x19 mm (1/2x3/4 in.) hot rolled flat bar. The mill scale was machined off, and the final dimensions of the cantilever were: hxbxl = 12.3x18.3x279 mm (0.484x0.719x11.0 in.), l being the distance from the face of the column to the point of load application corresponding to one half of the column height. The phosphor bronze columns were machined from 13 mm (1/2 in.) diameter half-hard rod. The scaling ratio from the steel columns to the phosphor bronze columns is based on true replica model rules demanding that $l_r = (E/\rho)_r$. In this study, the ratio was 1:1.92. Thus, the dimensions of the phosphor bronze cantilever were: hxbxl = 6.4x3.5x145 mm (0.252x0.374x5.7 in.).

The cantilever beams were welded to a rigid steel column. In the case of the phosphor bronze, a small alumnimum bronze plate was welded first to the face of the column, and then the cantilever was welded to

that plate. This procedure was chosen to minimize the heat input to the cantilever, and thus to minimize the over-annealing of the material. The welding was done using tungsten innert gas (TIG) technique.

The cantilevers were tested in the test frame described in Section 5.3.1.2 and shown in Figs. 5.3 and 5.4. Figure 8.25 shows schematically the test setup. The instrumentation consisted of a load cell measuring the tip force applied to the cantilever, a LVDT measuring the vertical displacement at the force application point, and two pairs of strain gages measuring strains on the top and bottom surface of a cross section. The first pair was positioned at a minimal distance from the welded joint, and the second at a position where no material yielding was expected. The measurements from the latter pair were used to obtain a reliable moment-strain calibration for the shake table study.

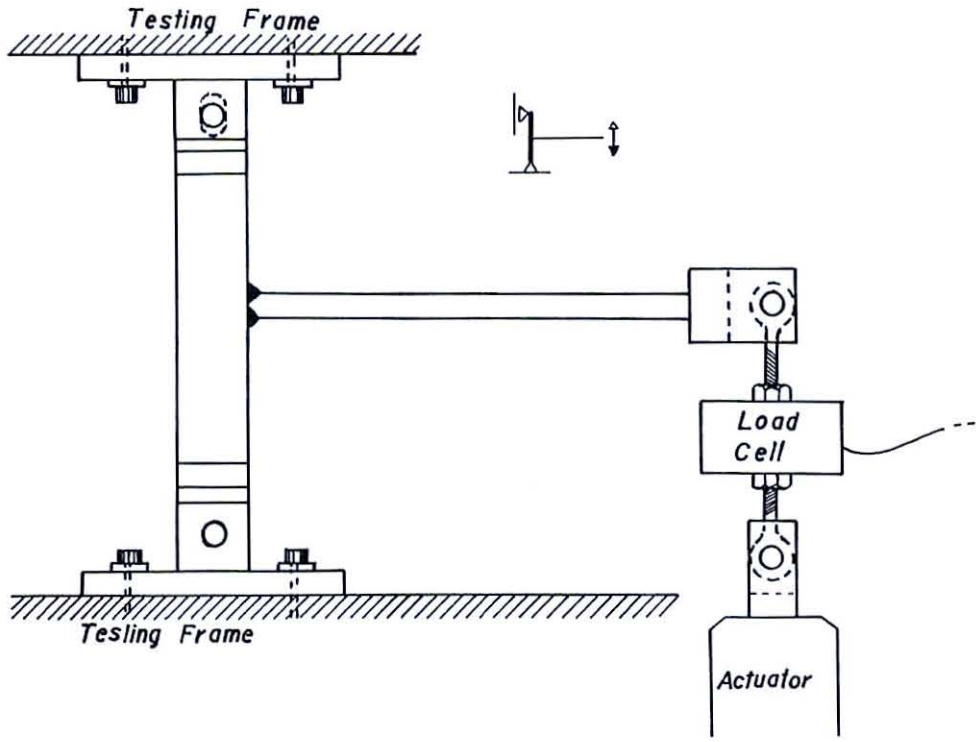

Figure 8.25 Experimental Setup for Cantilever Test

The testing was performed under stroke control with symmetric excursions for positive and negative displacements. The displacement history consisted of the following steps:

Step 1: 1/2 δ_y - 3 cycles at a low frequency

Step 2: 2 δ_y - 5 cycles at a low frequency, 3 cycles at a high frequency and 2 cycles at a low frequency

Steps 3 and 4 as in Step 2 with 3 δ_y and 4 δ_y displacement amplitude, respectively

Step 5: 5 δ_y - as in Step 2 followed by repeated sequences of 98 high frequency and 2 low frequency cycles till failure.

The results of the study are discussed in two following sections, the first concentrating on the comparison of the behavior of the steel pseudo-prototype and the phosphor bronze model cantilever, the second concentrating on the effect of cyclic frequency on the load-displacement response.

8.3.1 Steel vs. Phosphor Bronze Cantilevers

One of the major objectives of this test was to evaluate the feasibility of simulation of the behavior of a welded steel cantilever with a scale model made of phosphor bronze.

Figure 8.26 presents a comparison of hysteresis loops of the two cantilevers at amplitutde levels of 2 δ_y and 3 δ_y. The value of δ_y corresponds aproximately to the yield displacement of the steel cantilever. The response of the phosphor bronze beam is scaled to the prototype domain through division by $E_r l_r^2$ on the vertical axis and by l_r on the horizontal axis. It is noticeable that the lower amplitude cycles

resulted in very slim hysteresis loops for the steel, whereas the phosphor bronze loops exhibited a significant amount of plastic deformation. These discrepancies must be attributed to the effect of overheating near the welds of the phosphor bronze specimen. The welding process caused a loss of strength in excess of the desired reduction in strength which was controlled through subsequent annealing.

With the exception of the first few post yielding cycles, the peak forces at the different displacement amplitudes and also the hysteresis loops for the two specimens matched rather closely. This can be attributed to the high work hardenings of the phosphor bronze which first lessened and later eliminated the effect of the lower yield strength. Nevertheless, in dynamic response studies the lower yield strength and fatter hysteresis loops of phosphor bronze will lead to dissimilarities in the response, at least for the first few inelastic cycles. These dissimilarities may not be large, however, since the premature yielding in phosphor bronze is partially counterbalanced by the greater energy dissipation capacity represented by the fatter hysteresis loops.

These simple cantilever tests as well as the material tests indicate that phosphor bronze is not an ideal material for models of welded steel structures. The major problems are represented by the excessive work hardening of annealed phosphor bronze (see Section 6.3.4.4) and by the excessive loss of strength in the heat affected zones at weldments. It is fortunate that these two effects counteract each other to a degreee which may make phosphor bronze an acceptable model material. This is demonstrated by the shake table study of a simple steel structure and its phosphor bronze model discussed in Chapter 9.

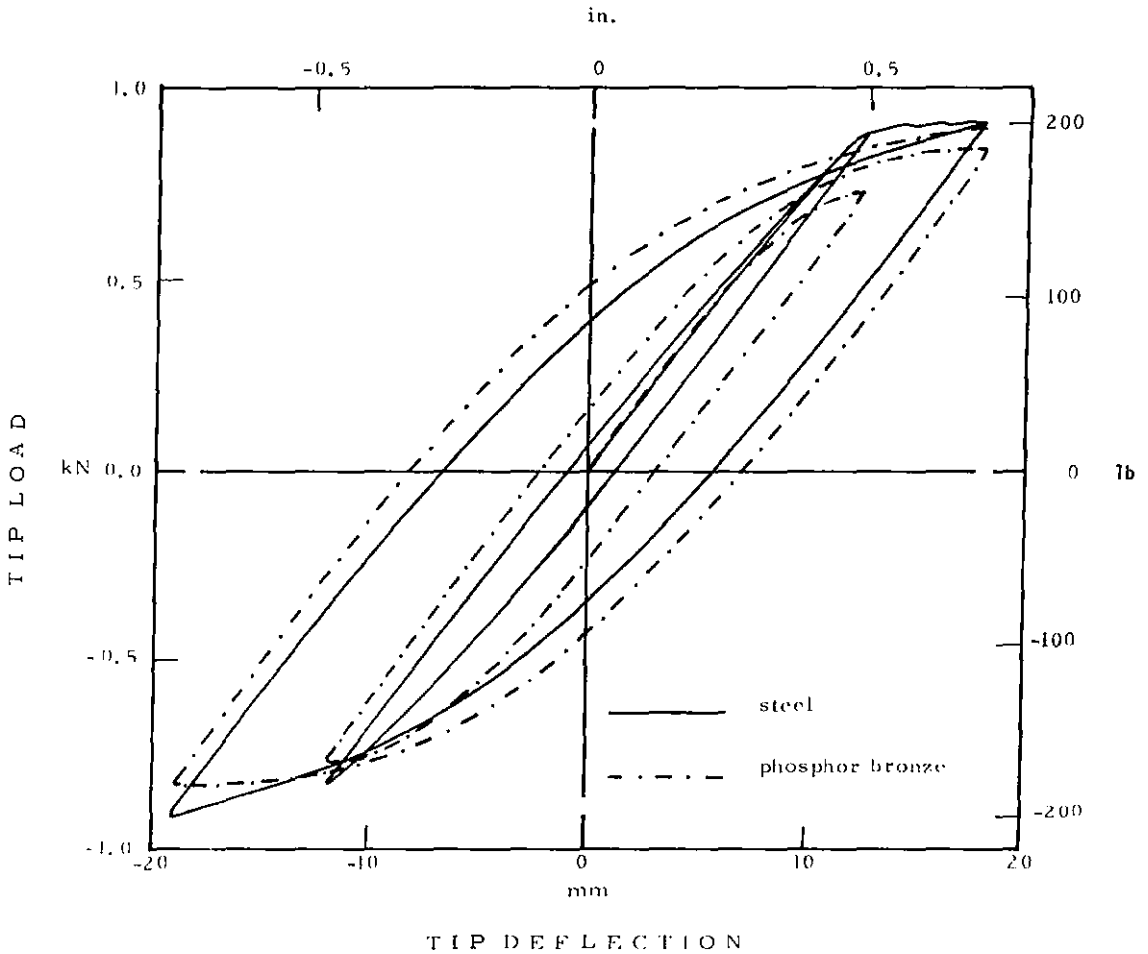

Figure 8.26 Comparison of Load-Displacement Response of Steel and Annealed Phosphor Bronze Cantilevers (Steel Cantilever Domain)

8.3.2 Effect of Cycling Frequency

The effect of the frequency at which the component is tested or, rather, at which it is acting within the structure requires consideration in the case of dynamically loaded structures. The questions which have to be answered are: what is the shape of the hysteresis loops for various testing frequencies, and what is the influence of the cycling frequency on the fatigue life of the component?

The first question is answered by including alternate slow and fast cycles in the testing program, thus providing a basis of numerical

comparison between the responses. Figure 8.27 shows hysteresis loops from static and dynamic cycles of the phosphor bronze cantilever. The static cycles were conducted at 0.01 Hz corresponding to the average strain rate of 2.4×10^{-4}/sec. The dynamic tests were conducted at 2.8 Hz corresponding to the average strain rate of 7.5×10^{-2}/sec.

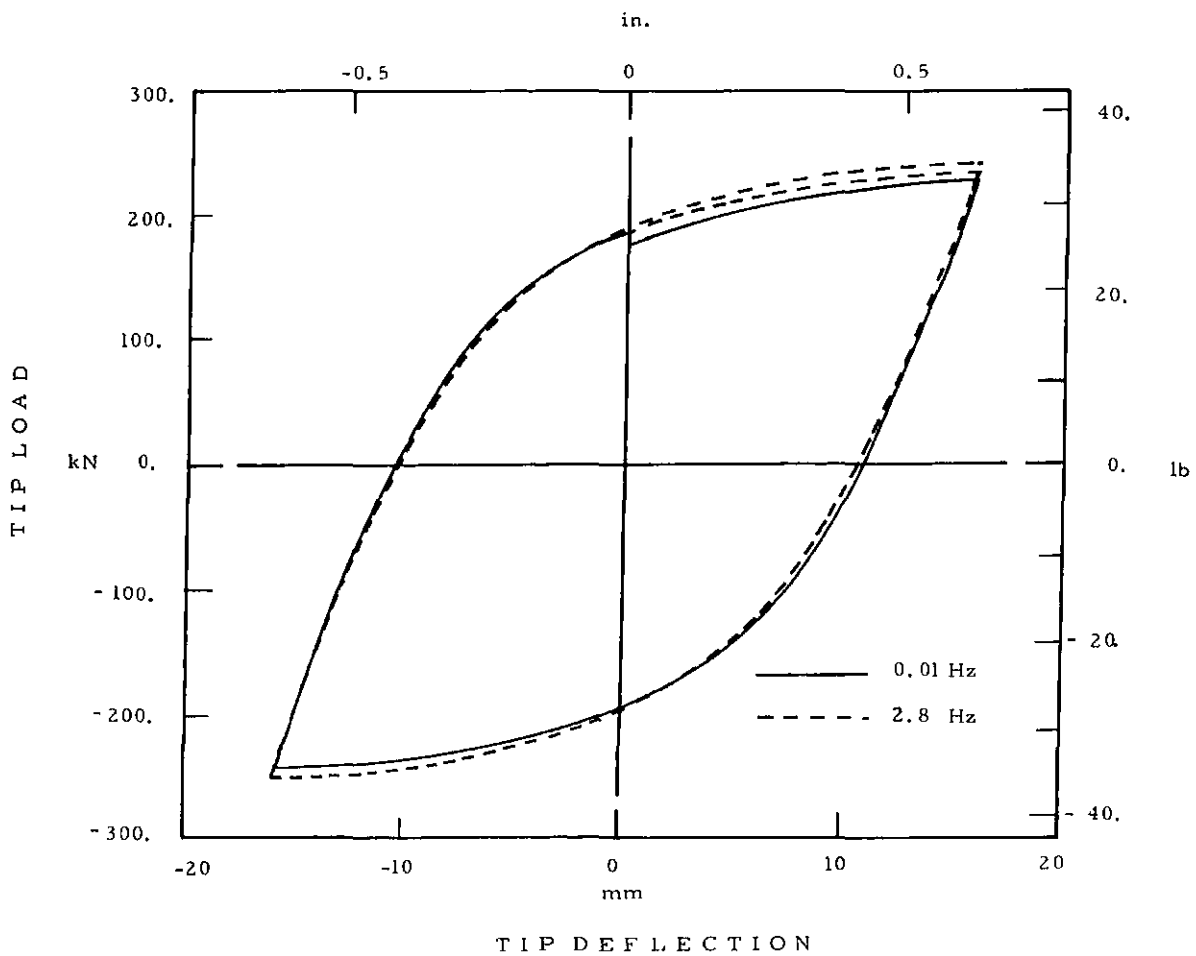

Figure 8.27 Comparison of Hysteresis Loops for Static and Dynamic Cycles of Annealed Phosphor Bronze Cantilevers

The loops are nearly identical except of the somewhat higher peak value exhibited by the high frequency loop. This can be accounted for almost entirely by the high work hardening of the material. The hysteresis loops for the steel cantilever showed virtually identical strength values in low and high frequency loops. It should be noted, however, that the

tests were carried out with sinusoidal displacement control. Thus, the strain rates close to the peak force and displacement values are approaching zero, regardless of the cycling frequency. The lack of influence of the cycling frequency on the response of the cantilevers is in an agreement with the findings by Almuti (Ref. 191).

The effect of cycling frequency on the fatigue-crack-growth rate has been studied by others in conjunction with the material toughness and fatigue behavior. In Fig. 8.28, Rolfe and Barsom (Ref. 201) present a summary of cyclic studies performed on A36 steel at frequencies from 0.1 to 100 Hz. The figure indicates that the cycling frequency does not influence the fatigue behavior of the material (in benign environment). Figure 8.29 (Ref. 201) indicates the independance of the fatigue behavior of the shape of load function used to control the test.

It should be noted, however, that the data presented in Figs. 8.28 and 8.29 were obtained in the range of elastic nominal stress cycles and it is not known whether the conclusion drawn from this set of data can be extended to the regime of plastic fracture mechanics.

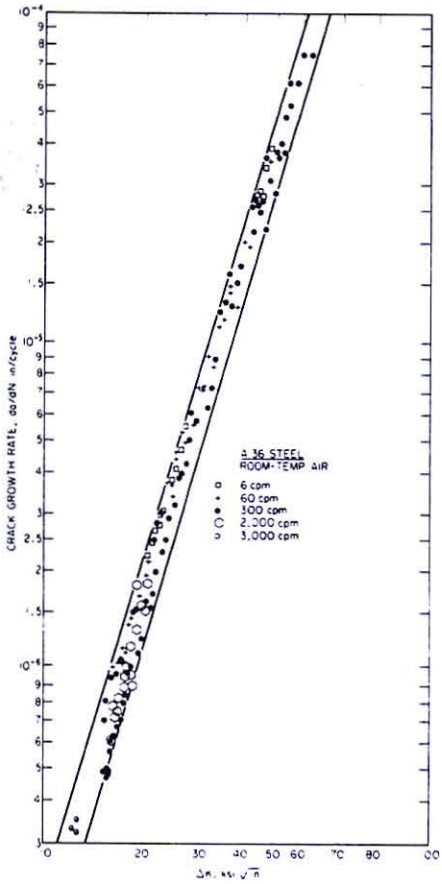

Figure 8.28 Effect of Cycling Frequency on Crack Growth Rates (from Ref. 201)

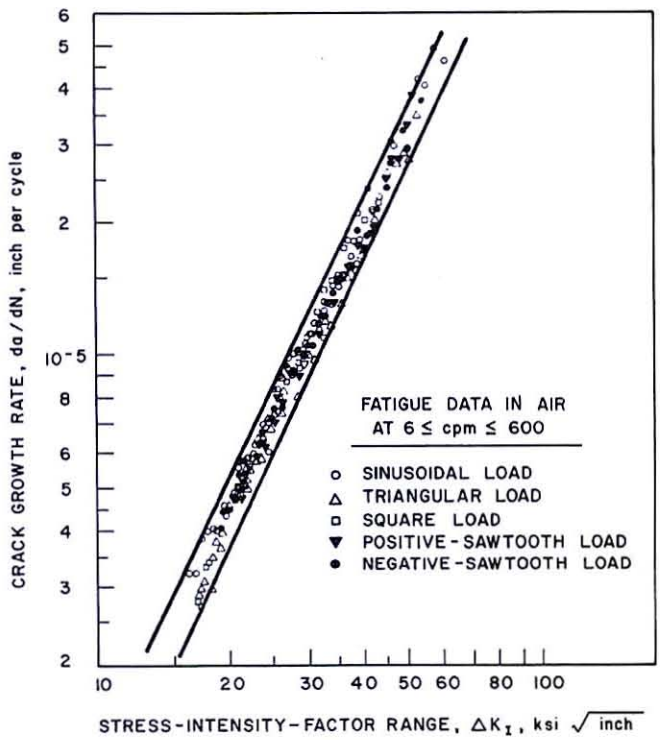

Figure 8.29 Effect of the Shape of Load Function on Crack Growth Rates (from Ref. 201)

CHAPTER 9

TRUE REPLICA MODEL STUDY OF A STEEL STRUCTURE

A study on a simple structure subjected to earthquake excitation was necessary to evaluate experimentally the laws presented in Section 4.5.1 for true replica models, and to subject the steel and phosphor bronze studied at the material level (Chapter 6) and component level (Chapter 8) to a true earthquake test.

9.1 MODEL DESCRIPTION, INSTRUMENTATION AND TESTING PROGRAM

For simplicity, a single degree of freedom system was selected as a test structure. The tested structures consisted of four rectangular columns connected by welding to a rigid top plate and to base plates rigidly attached to the shake table (Fig. 9.1). The columns are stronger in the direction orthogonal to the uniaxial motion and are braced at mid-height to prevent motion in that direction. Two structures were tested on a shake table, one made of steel and one made of phosphor bronze.

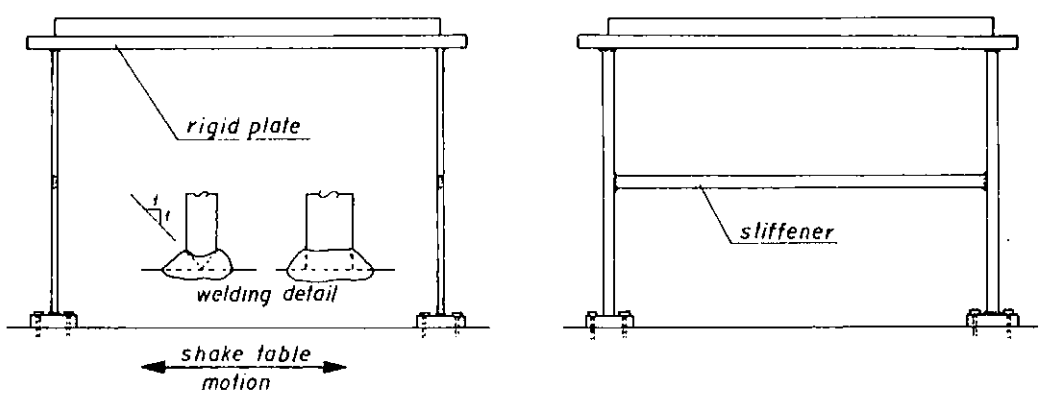

Figure 9.1 Longitidunal and Transverse View of The Model

The steel model is used as a pseudo-prototype structure for the phosphor bronze model, thus allowing numerical comparison of the results

obtained from tests on both the models. The overall dimensions of the pseudo-prototype are based on the size of the shake table available at Stanford, and on cost considerations. The steel model can be viewed as a 1:4 scale model (with artificial mass simulation) of an actual structure with the dimensions as specified in Table 9.1. This structure was designed to resist the N-S component of the 1940 El Centro acceleration record at a level close to the yield of the columns. The material properties of the steel used in the pseudo-prototype and of the phosphor bronze (CA 510) used in the true replica model are summarized in Table 9.2. The dimensions of the phosphor bronze model are derived by applying the scaling rules for true replica models (Section 4.5.1) to the pseudo-prototype dimensions. The following are the inverse values of the scaling factors:

$l_r^{-1} = (E/\ )_r^{-1} = (210.3/7.6930) \ / \ (126.2/8.8744) = 1.92$

$(\sigma_y)_r^{-1} = E_r^{-1} = 210.3 \ / \ 126.2 = 1.67$

$W_r^{-1} = (E_r l_r^2)^{-1} = 1.67 \times 1.92^2 = 6.16$

The instrumentation used in the experiment is shown in Fig. 9.2. The shake table accelerometer and LVDT provide a record of the input motion, the accelerometers and LVDT's attached to the top plate of the model provide a record of the model response. The accelerometer oriented in the direction transverse to the direction of shake table motion provides information as to whether any significant transverse movement takes place. The two relative motion LVDT's permit an estimate of any rotational motion. Strain gages attached to the columns within their elastic range provide a strain history record thus allowing the calculation of shear forces experienced by the columns. This is done using the formula $V = (M_1 + M_2) \ / \ h$, in which h is the distance between the instrumented

Table 9.1

Dimensions of the Prototype,
the Steel and Phosphor Bronze Models

	prototype	steel model	phosphor bronze model
column height l	2235 mm (88 in.)	559 mm (22 in.)	291.0 mm (11.46 in.)
bay width	3251 mm (128 in.)	813 mm (32 in.)	423 mm (16.7 in.)
cross section bxh	47x73 mm (1.8x2.9 in.)	12.3x18.2 mm (0.46x0.72 in.)	6.40x9.50 mm (0.252x0.374 in.)
story weight W	28.8 kN (6.46 kips)	1797 N (404 lb.)	292.5 N (65.7 lb.)

Table 9.2

Properties of Model Materials

	steel	annealed phosphor bronze
modulus of elasticity	210×10^3 MPa (30.5×10^3 ksi)	126×10^3 MPa (18.3×10^3 ksi)
yield at 0.002 offset	286 MPa (41.4 ksi)	171 MPa (24.8 ksi)

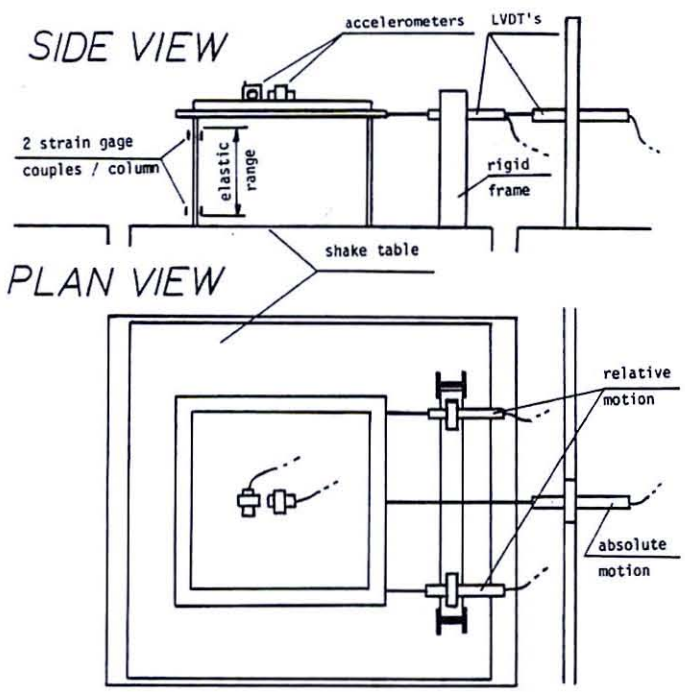

Figure 9.2 Schematic View of the Instrumentation

cross section, and M_1 and M_2 are the moments recorded at the two cross sections. The moments were recorded directly by using the moment-strain calibrations obtained from the cantilever tests (Section 8.3).

The testing program was designed to provide maximum information on the correlation of the behavior of the pseudo-prototype and its model at various levels of dynamic excitation. The N-S component of the 1940 El Centro earthquake was chosen as a basic input motion. The record was scaled for the pseudo-prototype using a length scale of $l_r = 1:4$ and a time scale of $t_r = \sqrt{l_r} = 1:2$, and for the CA 510 model using $l_r = 1:(4x1.92) = 1:7.68$ and $t_r = 1:\sqrt{7.68} = 1:2.77$. For both the structures, $a_r = 1$. The models were subjected to two time histories, consisting of 60% and 177% (shake table limitation) of the displacements obtained from the 1940 El Centro record.

To establish the dynamic elastic characteristics of the structure free vibration tests were performed prior to the shake table tests. The natural frequencies and damping values of the models are established from the free vibration time record and from the mean spectral density function obtained from Fourier analysis of the record. The free vibration tests were repeated after the entire testing history to evaluate the changes in the dynamic elastic characteristics of the structure.

9.2 RESULTS AND CONCLUSIONS

9.2.1 Elastic Tests

The free vibration tests for the pseudo-prototype and its model yielded the following results (in the pseudo-prototype domain) :

	pseudo-prototype	model
natural frequency	4.45 Hz.	4.60 Hz.
percent of critical damping	0.134%	0.137%

The slight discrepancy (3%) between the natural frequencies of the pseudo-prototype and the model is mainly attributed to the difference in column stiffnesses due to the different height of the weld. A difference of this order of magnitude may have already some effect on the elastic response and makes directly overlaid time histories more difficult to review.

Figure 9.3 shows the first 20 seconds of the shake table displacement response to 60% of the El Centro record scaled for the pseudo-prototype and the model and represented in the pseudo-prototype domain. Although the records are very close, some dissimilarities can be observed at the peaks of the displacements, where the very small displacement fluctuations are not reproduced at the model level. These dissimilarities, which are caused by stiction problem at the shake table bearings, are a source of discrepancies in the response of the two test structures.

Figures 9.4 and 9.5 show a comparison of the story displacement and acceleration response between the steel pseudo-prototype and the phosphor bronze model. The plots represent the response to the 60% El Central motion in the pseudo-prototype domain. For the time window shown (4 seconds in the pseudo-prototype domain, i.e., 8 seconds in the prototype domain), the responses are rather similar except that the peak responses are consistently larger, by a few percent, for the phosphor bronze model. Considering that the two structures respond elastically and that the measured damping is almost identical, this discrepancy must be attributed primarily to problems in reproducing the input motion at the two model

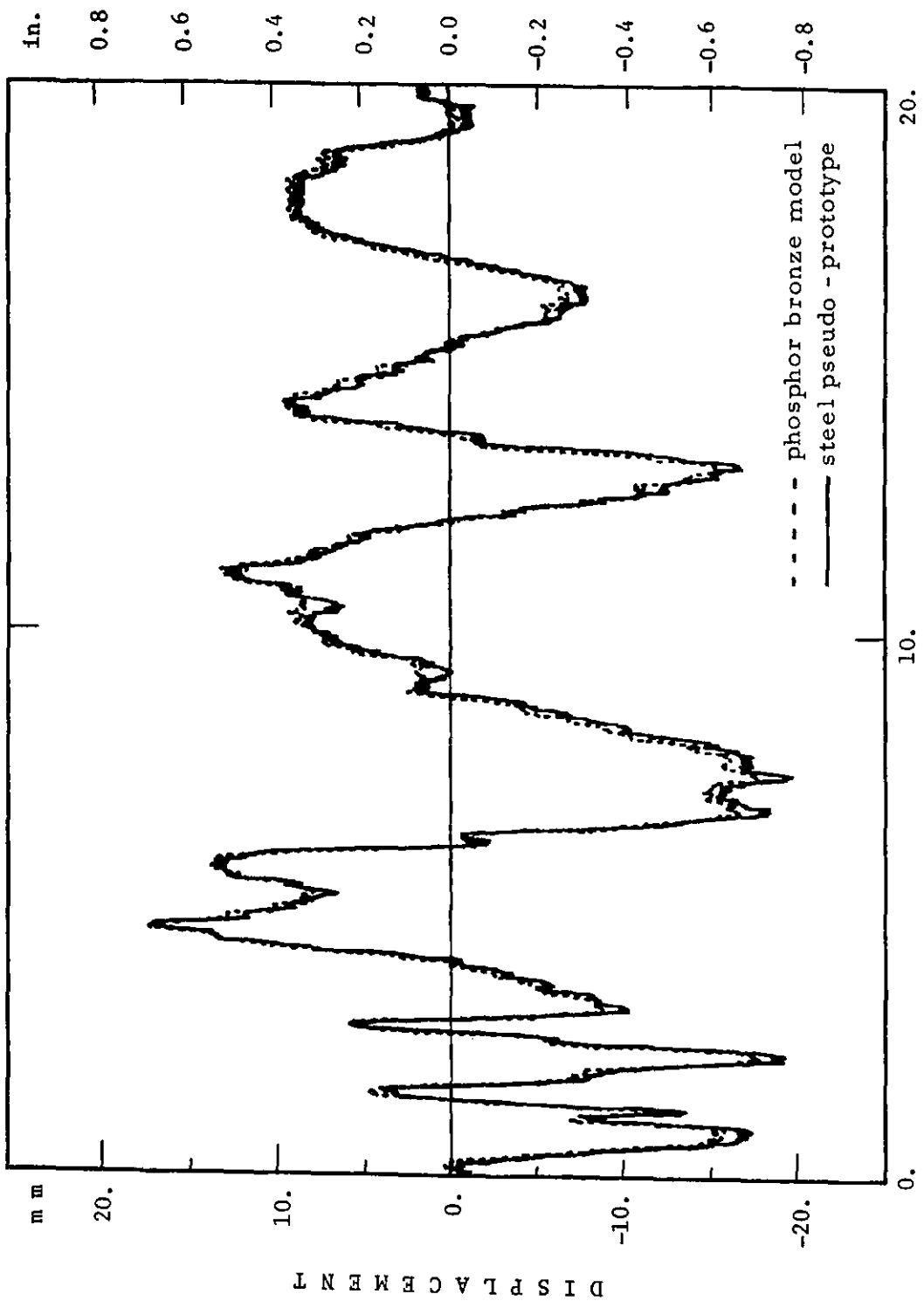

Figure 9.3 Shake Table Displacement Record for 63% El Centro Motion Input (Pseudo-Prototype Domain)

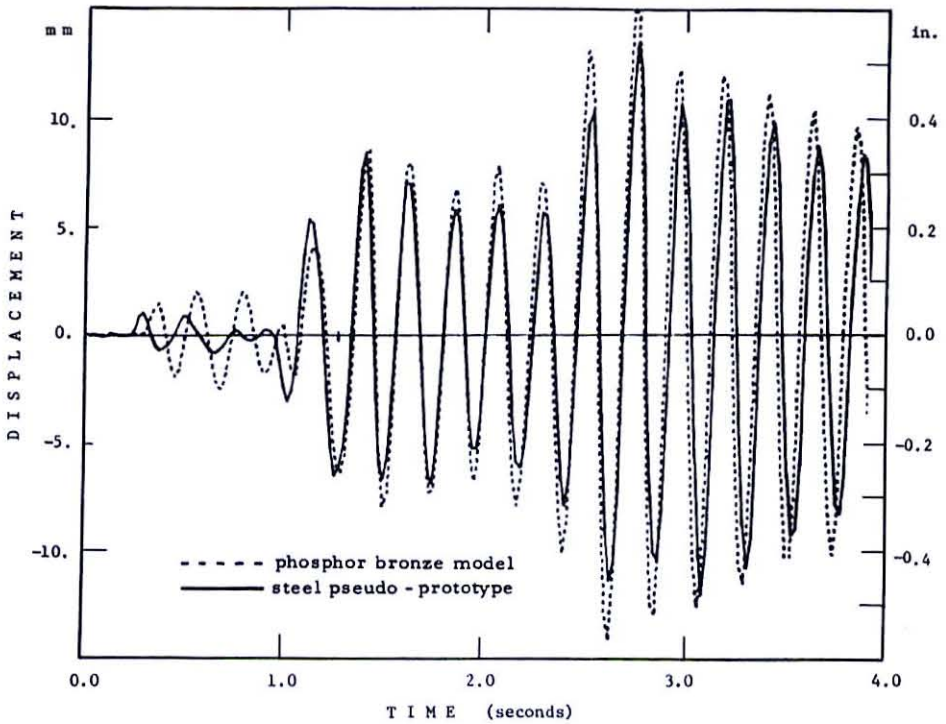

Figure 9.4 Displacement Response of the Structures to 63% El Centro Motion (Pseudo-Prototype Domain)

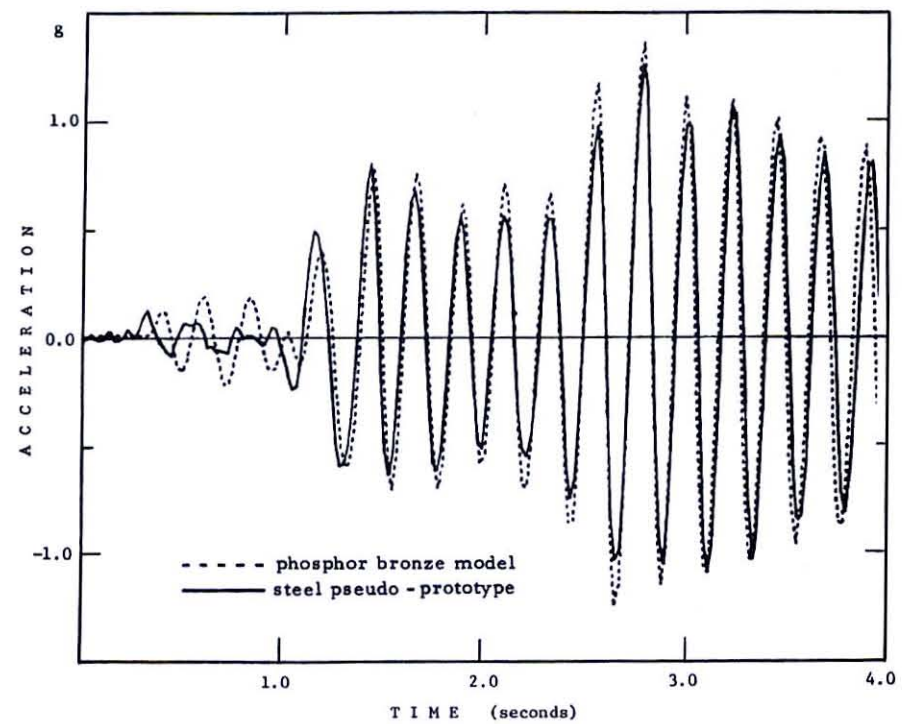

Figure 9.5 Acceleration Response of the Structures to 63% El Centro Motion (Pseudo-Prototype Domain)

scales. This conclusion is substantiated further by larger discrepancies in the respnoses in later stages of the motion (not shown in the figures) which must have been caused by spurious signals in the shake table motion.

9.2.2 Inelastic Tests

Figure 9.6 presents the first 20 seconds of the shake table displacement response to 177% of the El Centro record scaled for the steel pseudo-prototype and phosphor bronze models. The discrepancies between the two records are smaller than these observed in the lower amplitude test (Fig. 9.3).

Figures 9.7 and 9.8 provide the comparison of the displacement and acceleration responses of the pseudo-prototype and its model for the first four seconds in the pseudo-prototype domain. In the time domain, the displacements compare well for the first three seconds while the maximum floor acceleration are in general lower for the inelastic cycles in the phosphor bronze model. The differences in the response are more evident from Fig. 9.9 which shows the column shear vs. story displacement response for the first four seconds. As was expected from the material and component tests (Chapters 6 and 8) the yield strength of the phosphor bronze model is smaller and its hysteresis loops are fatter than in the steel structure. Nevertheless, the comparison of the column shear--story displacement response is quite satisfactory as for the number of major inelastic excursions and their force and displacement amplitudes.

The low amplitude response after the first three seconds and the subsequent inelastic response did, however, exhibit considerable discre-

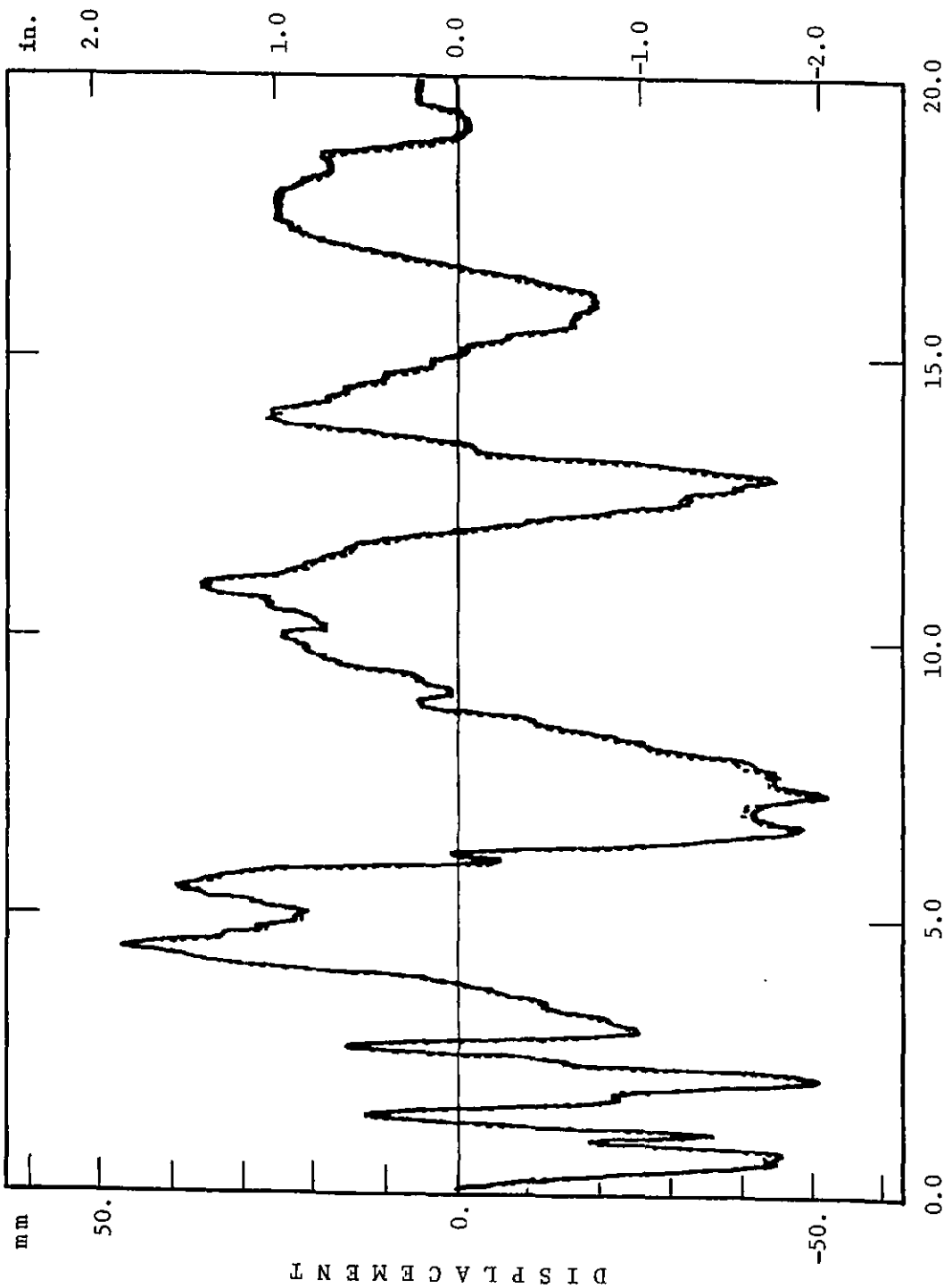

Figure 9.6 Shake Table Displacement Record for 177% El Centro Motion Input (Pseudo-Prototype Domain)

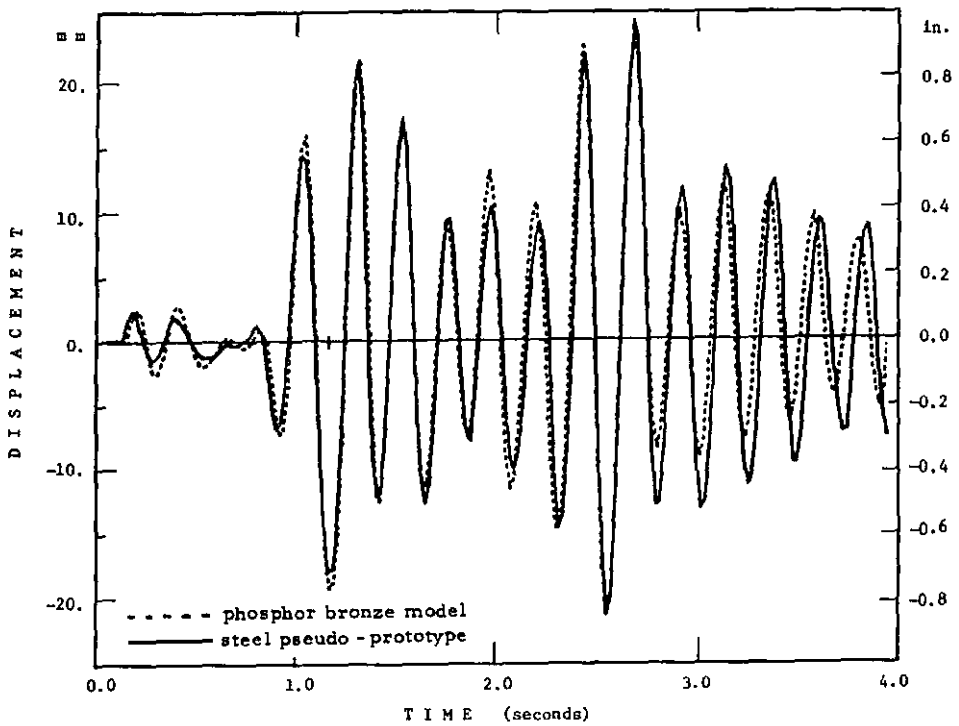

Figure 9.7 Displacement Response of the Structures to 177% El Centro Motion (Pseudo-Prototype Domain)

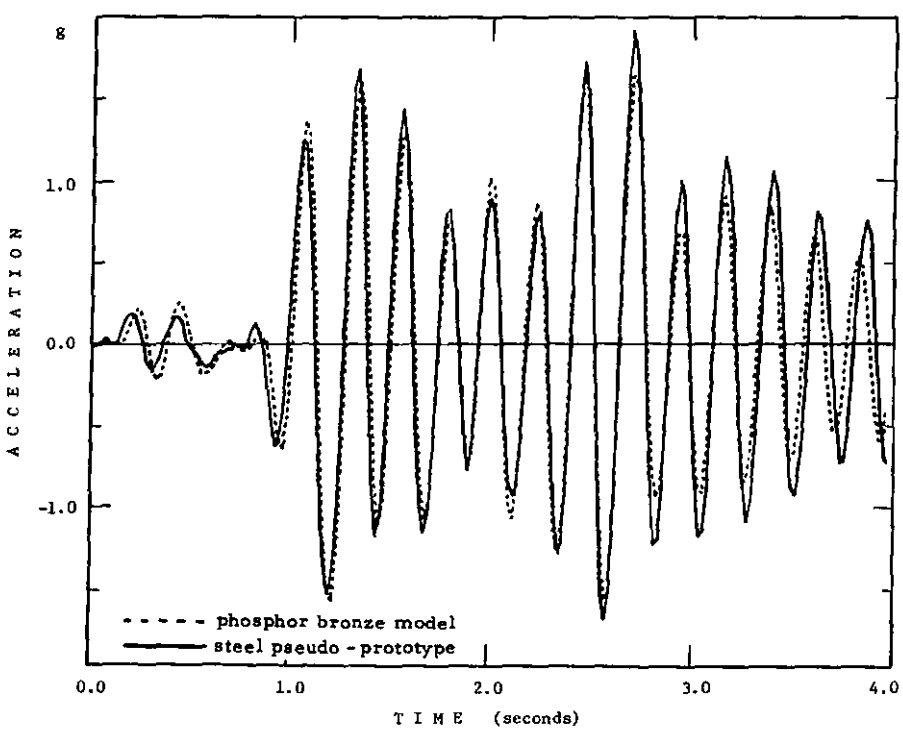

Figure 9.8 Acceleration Response of the Structures to 177% El Centro Motion (Pseudo-Prototype Domain)

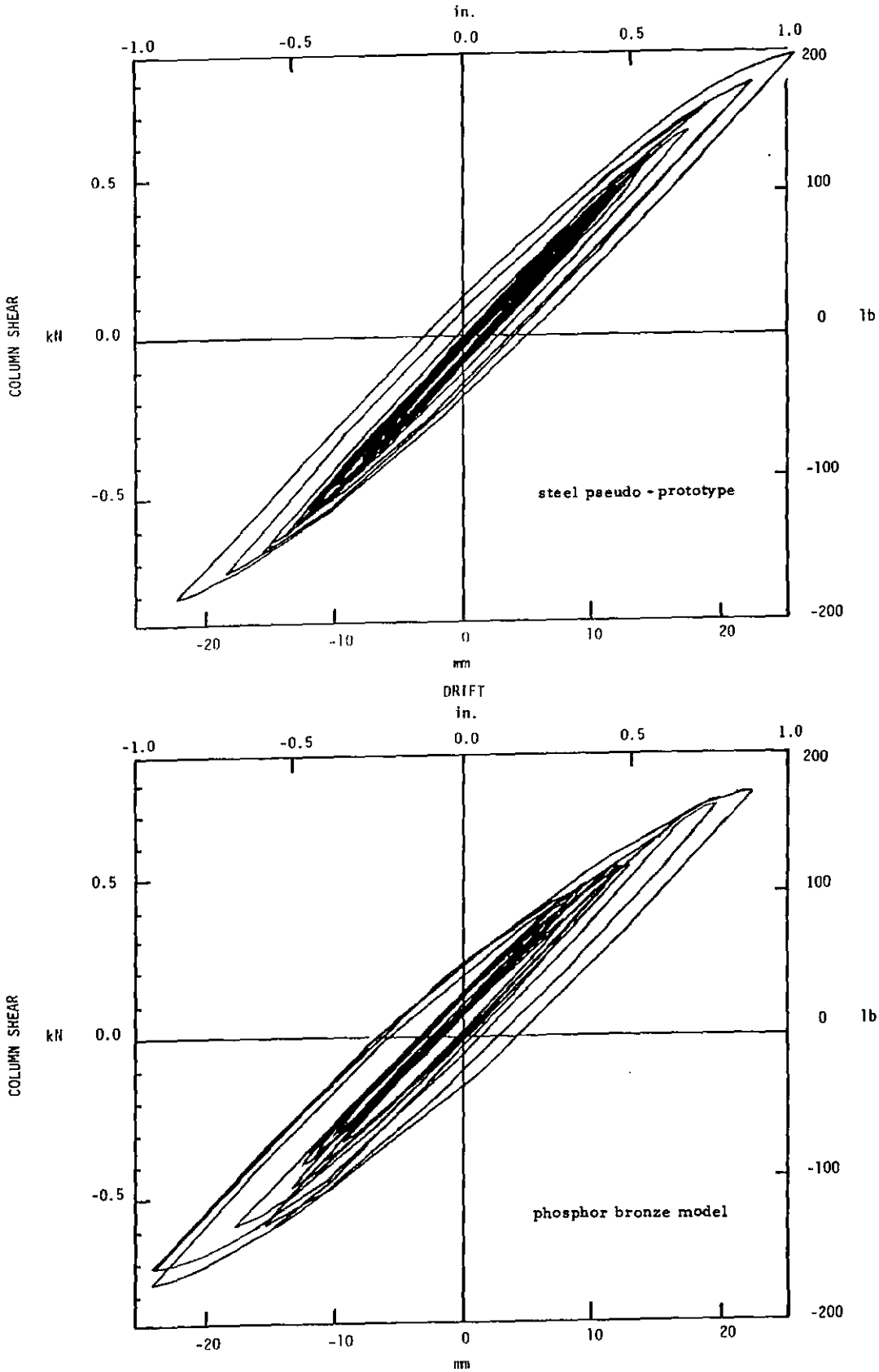

Figure 9.9 Shear-Displacement Response of One Column to 177% El Centro Motion
(Approximately First Four Seconds of the Motion; Pseudo-Prototype Domain)

pancies. In part, these discrepancies must be attributed to the aforementioned differences in the material behavior but, more likely, much of the response difference is caused by difficulties in reproducing the input motion at different model scales. This statement is supported by the observation that similar response discrepancies did occur at similar times in the elastic test.

In conclusion, this series of shake table tests demonstrated that phosphor bronze is an adequate but not ideal material for models of steel structures. Based on the results obtained within the first four seconds of the inelastic shake table test, it appears that good simulation of overall response characteristics can be obtained from phosphor bronze models. The major problem encountered in such models is the decrease in yield strength in heat affected zones at weldments. A closer simulation of the inelastic response can be expected when welding is not required or when inelastic deformations occur in regions removed from weldments.

CHAPTER 10

FEASIBILITY AND LIMITATIONS OF MODEL TESTING IN EARTHQUAKE ENGINEERING

The results of the study presented in this report and in the previous report by Mills et. al. (Ref. 58), together with research performed by others permit an assessment of model analysis as a tool in earthquake engineering.

Tests carried out at Stanford and other places have demonstrated that the dynamic response of structural building systems (frames, shear wall structures, etc.) can be simulated quite accurately at model scales. However, the quality of response prediction depends strongly on the accuracy of material simulation (particularly in reinforced concrete), suitable fabrication techniques that properly simulate initial and boundary conditions, accuracy in simulating important details, reproducibility of dynamic input (performance spectrum of earthquake simulator), resolution of instrumentation system and speed of data acquisition system. It must also be recognized that model tests may not be feasible when damage or failure is initiated by certain localized phenomena such as weld fracture in steel structures or bond failure in reinforced concrete structures.

Although no experience exists at this time, it appears quite feasible to incorporate realistic floor slab systems and nonstructural elements (partitions, walls, stair cases, elevator shafts, etc.) in carefully designed models. Model studies may also be utilized to study specific problems in earthquake engineering, such as overturning and uplift, dynamic instability and effects of stiffness and mass irregularities.

Experiments with true replica models (column 1 of Table 4.2) have

proven feasible for dynamic studies on steel structures, using certain copper alloys which permit approximately a 1:2 scale ratio. Copper alloy 510 (a phosphor bronze) was found to be a suitable material which permits satisfactory welding and, with appropriate heat treatment, reproduces within certain limits the desired stress-strain properties. Experiments on simple welded models have shown that true replica models predict rather accurately the maximum response. Welding in critical region poses a problem since the strength of phosphor bronze in the heat affected zone may be reduced to a value less than that dictated by model similitude.

Lead alloys which possess specific stiffnesses ($E/\ $) allowing scaling in the order of 1:10 to 1:20 have been found in the initial study to be of limited use because of several undesirable material properties (early nonlinearity, excessive damping, high creep).

Although the usefulness of a true replica copper alloy scale model is debatable due to the scale limitation to a 1:2 ratio, the utilization of such an alloy, which has a much smaller stiffness than steel, is of much value when combined with artificial mass simulation since it permits a significant reduction of the weights which have to be added to the model ($M_r = E_r l_r^2$). This idea is particularly attractive for structures in which the mass distribution along linear members is of importance. Space trusses, transmission towers and antennas, long span and cable stayed bridges can serve as an example of this type of structures.

Models with artificial mass simulation are the obvious choice when gravity effects cannot be neglected and prototype material is used in the model. A detailed shake table study has been carried out at Stanford on a 34 in. high 1:6 scale model (Ref. 58) of a steel frame prototype tested previously at U.C. Berkeley. The structural shapes were machined from

A36 bar stock and all primary frame connections were fully welded using the TIG heliarc process. Subsequent heat treatment of the finished model frame was performed to relieve initial stresses and to satisfy scaled prototype construction tolerances. The model structure was subjected to scaled versions of the prototype input motions and the measured model response quantities were then scaled back to the prototype domain for prototype response prediction.

A detailed comparison was carried out between true prototype response and the response predicted from the model test. This comparison was done for strains, joint distortions, story displacements and accelerations and integrated energy terms (input energy vs. dissipated energy). In all cases very good agreement was observed between model and prototype test results. Some local differences between the results are attributable primarily to discrepancies in table input motions and an unavoidable oversizing of welds in the model.

The study not only proved the possibility of reliable prediction of prototype response with tests performed on small scale models, but also gave an insight into the relative cost and effort involved in both the studies. The major cost difference is in the size of the required testing facilities. Also, the saving in material is very significant, although the benefit of it is decreased by the rather high cost of custom-made structural shapes. The cost of instrumentation and data acquisition is about equal in prototype and model tests since the larger effort in developing more sensitive instrumentation for model tests is balanced by its smaller size and the reduced cost of instrument support frames.

Shake table experimentation on a variety of small scale models of reinforced concrete structures, utilizing artificial mass simulation with

lumped masses of the floor levels, has been carried out for several years at the University of Illinois (Refs. 46, 48). Although these model structures did not simulate specific prototypes, they have resulted in a wealth of detailed information on the seismic response of reinforced concrete structures. Much of the presented data are in good agreement with mathematical models used for prototype structures. Other tests (Ref. 23) have demonstrated that even localized crack patterns can be simulated in small scale models. Strain rate effects in model concrete and structural components were investigated in this study and are discussed in Chapters 7 and 8.

Discretely distributed additive masses, rather than lumped masses, will be required in models of structures where mass distribution in space is of importance. This is the case in problems of frame-floor slab interaction, walls subjected to transverse excitations and in many towers and antennas. Caution must be used in separating the added masses from the structural material in such a way that they will not influence the stiffness characteristics of the material.

Scale model investigations are of much interest for the verification of the seismic safety and integrity of large man-made structures whose failure would be of severe consequences. Components of nuclear reactors and containment vessels are appropriate examples. For the latter, the gravity effects are often negligible compared to effects of internal pressurization and severe ground motion. Thus, the modeling requirements of column (3) of Table 4.3 may be utilized. In this case the major problem is in the reproduction of the scaled seismic input which requires an earthquake simulator with high frequency reproducibility (since $t_r = l_r$) and large dynamic force capacity (since $a_r = l_r^{-1}$). Piping systems can be

modeled through artificial mass simulation, by adding lumped masses to the structural components of the reactor and discretely distributed masses to the piping system.

Dynamic model studies on bridge structures have been performed for some time, more recently also on shake tables (Ref. 57). Because of the importance of gravity effects, artificial mass simulation is usually required. However, where possible the use of model material of reduced stiffness ($E_r < 1$) is recommended to reduce the weight requirements for the model. The experiment discussed in Ref. 57 is an example of a model test in which strength properties were intentionally only simulated in regions where damage was anticipated while the design was simplified in other regions. Clearly, this simplification must be done with due regard to simulation of dynamic characteristics to transmit the proper effects to the regions of potential damage. The simulation of boundary conditions will often pose a significant problem and, when small scale models are used, it may be difficult to reproduce the pertinent seismic frequency range on conventional earthquake simulator.

The need for model studies is well established in the field of dam engineering. Ideally, this requires the modeling of the dam (concrete or embankment), the reservoir water and the geomechanical boundary conditions. Practical considerations make the use of water desirable as model fluid which in turn requires model materials of very low stiffness and strength for the dam (since $E_r = \sigma_r = l_r$ for $\rho_r = 1$). It is possible to develop suitable materials for small scale models of concrete dams but not for earth dams.

Niwa and Clough (Ref. 192) have performed a shake table study of 1:150 models of segments of arch and gravity dams. They used a mixture

of casting plaster, celite, water and sand as model material for concrete. For the arch model lead weights were used to simulate the density of the concrete while for the gravity dam model lead powder was mixed into the plaster to increase its density. The properties of the model materials used in this study depended strongly on the water to plaster ratio and varied considerably with the amount of added sand and lead powder. For some of the mixes the measured E_r and $_r$ did approach the desired ratio of 1:150 and limited reproduction of the stress-strain characteristics of concrete was observed. The ratio of compressive strength to tensile strength was approximately equal to nine. The study addressed two major problems associated with the performance of arch dams during earthquakes, namely the opening of vertical joints existing between the concrete monoliths and horizontal cracking of vertical monoliths. Both the phenomena are highly nonlinear and most difficult to simulate in a reliable fashion with computer analysis. The report concludes that shake table testing of a complete arch dam model is feasible and can provide insight into the nonlinear earthquake response and failure mechanism of concrete arch dams.

Model testing of earth and rockfill dams poses considerable problems since it is virtually impossible to find a model material which permits the proper scaling of all physical quantities entering a dynamic problem. In this case, the reliabililty of prototype response prediction depends on the ingenuity placed in the model design and the ability to evaluate the effects of model distortions. One way to evaluate these effects is to test several models at different scales and extrapolate the distortions to the prototype domain. Also, the results of the model tests can be utilized to gain an understanding of the physical phenomenon and to develop analytical models which may then be used to improve the response

prediction.

One major problem requires consideration in all model studies regardless of scale, namely the simulation of boundary conditions. In dynamic model studies a proper simulation of boundary conditions may be even more essential than in static model studies. Taking seismic response studies on shake tables as an example, supporting the model structure rigidily on the table will not allow for the rocking and translational motion at the foundation-soil interface and for the energy dissipation by hysteretic action and radiation of waves in the supporting medium. It is quite feasible to support model structures on a medium that simulates these phenomena to various degrees (Ref.193). The largest difficulty will be encountered in simulating wave radiation which depends on the wave propagation velocity, v and requires a scaling of $v_r = \sqrt{l_r} = \sqrt{(E/\rho)_r}$ for a true model. Since the stiffness of the supporting medium must be scaled in the same manner as the stiffness of structural material (usually $E_r = 1$) this will necessitate a very high density medium.

Within the limitations discussed in this chapter, it can be concluded that testing of small scale models of steel and reinforced concrete structures can result in a reliable prediction of the overall response of prototypes, provided that:

1) Similitude laws are satisfied in the design of the model, in the choice of the model material, and in the scaling of the input motion.
2) Care is exercised in the fabrication of the model, in particular in areas of special importance such as joints and weldments.

3) The testing facility is capable of precise reproduction of the prescribed motion, the instrumentation is sensitive enough to monitor the measured values, and the data acquisition system is capable of registration of the output of the measuring devices without introduction of data distortions.

A simulation of localized failure modes can be achieved in some cases but not in others (e.g., crack propagation of weldments). When doubts exist regarding the simulation of localized failure modes, the model study should be complemented with prototype component tests. The response history of the component, as obtained from a shake table test of the model structure, can serve as the loading history applied in the prototype component test.

CHAPTER 11

SUMMARY AND CONCLUSIONS

The major goal of this research project was to develop a methodology for small scale modeling of structures in earthquake engineering studies, and to evaluate the feasibility and limitations of model analysis in dynamic response studies.

Dimensional analysis can be utilized to derive similitude laws for dynamic models. In studies involving material and/or geometric nonlinearities, the simultaneous simulation of gravity and inertia effects poses a major problem. If both effects have to be simulated fully, similitude requires the use of model materials with specific stiffnesses (E/ρ) which scale in the same proportion as the length. An alternative, which permits the use of prototype material for many practical cases, is provided by adding lumped masses to the structure. These lumped masses must be structurally ineffective and should be distributed in a fashion that permits adequate simulation of all important gravitational and inertial effects. In linear elastic model studies and in other cases in which gravity effects can be neglected, a different set of similitude laws can be derived which permits the use of prototype materials without the addition of lumped masses. The use of distorted models may provide acceptable response predictions in some cases but necessitates either several model studies at different scales or considerable insight into the physical phenomena to permit an evaluation of the response distortion.

Adequate simulation of material properties was found to be the most difficult and important aspect of small scale modeling. Similitude of the monotonic stress-strain behavior alone is insufficient for dynamic

response studies. Cyclic response properties, strain rate and size effects, damping characteristics and other time and temperature dependent effects must be considered. Laboratory testing programs suitable for an evaluation of these properties are proposed in this report and the test facilities and instrumentation used in this study for a comprehensive material testing program are discussed in detail.

Modeling of steel structures can be performed using either ferrous or non-ferrous materials. Material tests on structural steel and copper and lead alloys were performed as part of this study. Monotonic and cyclic load tests were carried out as well as a series of strain rate tests. The monotonic stress-strain curves of steel and annealed phosphor bronze show a remarkable similarity. In the cyclic tests, phosphor bronze reveals a higher work hardening than structural steel. Considerably more cycles are needed to obtain stable cycles in phosphor bronze than in steel. Thus, the peak stress reached by phosphor bronze at a prescribed strain amplitude depends strongly on the previous cyclic history, as revealed by cyclic tests with various histories. This phenomenon occurs also in structural steel, but to a much smaller degree. It is concluded that in earthquake studies, where usually only a small number of cycles extends into the inelastic range, this phenomenon should not have a major effect on the model response unless the deformation history leads to a very unsymmetric cyclic response.

The strain rate tests revealed that an increase in strain rate leads to an increase in the yield strength but has no noticeable effect on the elastic and post-elastic stiffness properties of the monotonic stress--strain curve. Empirical curves and their analytical equations are developed which give the relationship between strain rate and yield strength

for A36 steel and annealed phosphor bronze. Annealed phosphor bronze shows considerably less sensitivity to the change in the strain rate. However, in small scale models made of phosphor bronze, this difference will be at least partly accounted for by the increased strain rates due to the scaling of time.

For small-scale models of concrete structures, microconcrete offers the possibility of a close simulation of concrete properties using prototype-like material. It was found that a wide range of compressive strengths and of tensile/compressive strength ratios can be achieved with appropriate mix proportioning. This report discusses mix design practices and presents strength data for a large number of mix designs used in this study and in model studies by other investigators.

An extensive study involving close to 200 cylinder specimens was performed to evaluate the stress-strain behavior of various mixes of microconcrete and the effect of strain rate on the compressive strength and the stress-strain diagram. The tests were performed using a close control over the speed of platten movement, thus allowing reduction of the data without having to account for the effect of relative stiffnesses of the testing machine and the specimen. Average strain measurements were obtained from four clip extensometers developed for this purpose. The strain rate study revealed that the relative magnitude of the strain rate effect on the compressive strength of microconcrete is essentially independent of the strength of the material. It was found that the strain rate effect in microconcrete is of a similar magnitude as in prototype concrete. A second order logarithmic equation for strain rate effect on the compressive strength of microconcrete is derived.

Reinforcement for model studies of reinforced concrete structures

requires particular attention as the behavior of the composite material largely depends upon the force transfer between the two materials. Techniques for surface deformation of steel wire through cold rolling or knurling are presented. Chemical treatment can be used for small diameter wires to roughen the surface sufficiently for bond simulation. Pull-out tests on the knurled wire showed a satisfactory bond strength. Knurling raises the yield strength of wires but severely decreases the strain hardening. In order to simulate the strain hardening present in prototype reinforcement, it will be necessary to cold work (through knurling or rolling) the wire sufficiently to raise the yield strength above the desired value and subsequently subject the wire to annealing which lowers the yield strength but recreates the strain hardening characteristics. Guidelines for annealing are discussed in this report.

Model tests on structural components and subassemblies are an essential aspect of model studies on complete structures. Such tests provide information on the adequacy of model construction techniques, on the material behavior under stress distributions similar to those prevailing in the complete structure, and on material interaction in the case of composite materials such as reinforced concrete. These tests may also be used to develop calibration curves for load-deformation quantities which have to be monitored during the dynamic test of the complete structure.

A series of tests on reinforced microconcrete cantilever beams was carried out to study the accuracy of simulation of various failure modes from flexural to shear and the sensitivity of the response to cycling frequency. A comparison of available prototype results with the results obtained for the model beams reveals a very good simulation of the response in the pre-yielding cycles. Cycles of higher displacement

amplitude show the importance of proper simulation of post-yield characteristics of the reinforcement. The lack of strain hardening in the model reinforcement used in this study resulted in a faster strength deterioration in the model than in the prototype beam.

The tests with varying shear span to depth ratios have shown that response characteristics (load-dispacement hysteresis loops, crack pattern) for various failure modes can be reproduced satisfactorily with small scale models. The spacing of major cracks in flexure and in shear is somewhat larger in models than in prototypes, but the crack patterns in critical regions are of similar configuration in both domains. However, the lack of strain hardening in the model reinforcement has a considerable effect on the size and on the distribution of cracks away from the critical region.

Tests at various cycling frequencies were carried out to evaluate the differences in the structural response of elements subjected to pseudo-static and elements subjected to dynamic cycling histories. It was found that the material strain rate effects have a relatively small influence on the component behavior. However, the spalling out of the crushed concrete is much smaller in high frequency tests, thus reducing the strength deterioration as compared to pseudo-static tests. This phenomenon affects the reliability of dynamic response prediction based on the results of pseudo-static tests. The relatively small difference in cycling frequency between dynamically tested prototypes and their scale models ($t_r = \sqrt{l_r}$ or $t_r = l_r$) should have a negligible effect on response prediction.

The feasibility of simulation of the behavior of welded steel structural element with scale models made of phosphor bronze was studied through a series of tests of steel and annealed phosphor bronze canti-

levers. The large heat sensitivity of phosphor bronze presents a major problem in the welding heat affected zone. In these zones the yield strength of the base material may be reduced to a value less than that required by material similitude. However, this effect is counteracted by the large work hardening of annealed phosphor bronze. Thus, in the early inelastic cycles phosphor bronze cantilevers exhibited smaller strength values but in the latter cycles rather similar loops were obtained. Response to cycling under different frequencies revealed a negligible difference between static and dynamic cycles for both structural steel and annealed phosphor bronze. Thus, the effects of material strain rates on the structural response response of metal structures is shown to be of negligible importance in seismic response studies.

A shake table study of a simple steel pseudo-prototype structure and its annealed phosphor bronze model was carried out to assess the applicability of annealed phosphor to modelling of welded structures. Within the limitations discussed in the previous paragraph, the simulation of the inelastic response (story shear and displacement) was quite satisfactory. It can be expected that results of similar quality will be obtained with more complex model structures. Thus, phosphor bronze models can provide satisfactory simulation of overall response characteristics but will result in distortions in the prediction of local stress--strain histories.

The experience gained from this study can be summarized as follows. The most important aspects of model research are a thorough knowledge of modeling theory, a comprehensive material study, much diligence and patience in faithfully reproducing all pertinent details and characteristics of the prototype and, last but not least, the recognition of the

shortcomings and limitations of model research. It is an unfortunate fact that very few inelastic dynamic response phenomena can be reproduced "precisely" at model scales. True replica models require materials with specific stiffnesses (E/ρ) which are much less than those of the prototype materials, but no two materials in nature are exactly alike. Artificial mass simulation permits the use of prototype material but introduces distortions in the force simulations. Thus, there is no ideal model test but there are many adequate model tests, provided that their "distortions" are recognized, evaluated and found to be acceptable. In order to make this judgement, much experience in model research and a thorough understanding of the physical phenomenon under study is needed. If a model test is performed without due regard to its limitations, it may easily lead to erroneous information and may discredit an otherwise quite reliable experimental analysis technique.

REFERENCES

1. Hossdorf, H., Model Analysis of Structures, Van Nostrand Reinhold Co., New York, 1971.

2. Muller, R. K., Handbuch der Modellstatik, Springer Verlag, Berlin, Heidelberg, New York, 1971.

3. Fumagalli, E., Statical and Geomechanical Models, Springer Verlag, Berlin, New York, 1973.

4. "Models of Structures--RILEM Symposium," Bulletin RILEM, No. 12, 1961.

5. Oberti, G., "Large Scale Model Testing of Structures Outside the Elastic Limit," Bulletin RILEM, No. 7, July 1960.

6. Rocha, M., "Structural Model Techniques--Some Recent Developments," Chapter 16 in Stress Analysis, edited by O. C. Zienkiewicz and G. S. Holister, John Wiley and Sons Ltd., 1965.

7. Oberti, G. and Castoldi, A., "New Trends in Model Research on Large Structures," ISMES Publication No. 53, Bergamo, Italy, 1977.

8. Oberti, G., "Model Contribution to the Design and Safety Control of Large Structures," ISMES Publication No. 89, Bergamo, Italy, 1977.

9. Litle, W. A. and Hansen, R. J., "Use of Models in Structural Design," Journal of Boston Society Of Civil Engrs., Vol. 50, No. 2, April 1963.

10. Breen, J. E., "Fabrication and Tests of Structural Models," Proceedings, ASCE, V. 94, ST 6, June 1968.

11. Zia, P., White, R. N. and Van Horn, D. A., "Principles of Model Analysis," Models for Concrete Structures, Special Publication #24, ACI, 1970.

12. Models for Concrete Structures, Special Publication #24, ACI, 1970.

13. Proceedings of Symposium on "Models in Structural Engineering," Canadian Chapter of the ACI, Montreal, Oct. 1972.

14. "Structural Concrete Models--A State-of-the-Art Report," compiled and edited by M. S. Mirza, Dept. of Civil Engineering, McGill University, Montreal, Oct. 1972.

15. ACI Committee 444, "Models of Concrete Structures--State-of-the--Art," Report No. ACI 444R-79, Concrete International, Jan. 1979.

16. Brock, G., "Direct Models as an Aid to Reinforced Concrete Design," Engineering 187, No. 4857, pp. 468, 470, 1959.

17. Fumagalli, E., "The Use of Models of Reinforced Concrete Structures," Magazin of Concrete Research, No. 12/35, 1960.

18. Harris, H. G., Sabnis, G. M. and White, R. N., "Small Scale Direct Models of Reinforced and Prestressed Concrete Structures," Dept. of Structural Engineering Report 326, Cornell University, Sept. 1966.

19. Magura, D. D., "Structural Model Testing - Reinforced and Prestressed Mortar Beams," PCA Journal, Vol. 9, No. 1, Jan. 1967.

20. Harris, H. G., Sabnis, G. M. and White, R. N., "Small Scale Ultimate-Strength Models for Concrete Structures," paper presented at SESA Annual Meeting, Oct. 1967.

21. Mirza, M. S., "An Investigation of Combined Stresses in Reinforced Concrete Beams," Thesis presented to McGill University in partial fulfillment of the Ph.D. requirements, Montreal, Canada, 1967.

22. Sabnis, G. M. and White, R. N., "Behavior of Reinforced Concrete Frames Under Cyclic Loads Using Small Scale Models," Journal of the American Concrete Institute, Sept. 1969.

23. Chowdhury, A. H. and White, R. N., "Inelastic Behavior of Small Scale Reinforced Concrete Beam-Column Joints Under Severe Reversing Loads," Report No. 342, Department of Structural Engineering, Cornell University, Ithaca, New York, Oct. 1971.

24. White, R. N. and Chowdhury, A. H., "Behaviour of Multi-Storey Reinforced Concrete Frames Subjected to Severe Reversing Loads," Symposium on the Resistance and Ultimate Deformability of Structures Acted on by Well Defined Repeated Loads, International Assoc. for Bridge and Structural Engineering, Lisbon, 1973.

25. White, R. N., "Modeling Techniques for Reinforced Concrete Structures," Department of Structural Engineering, Cornell University, Ithaca, New York, March 1976.

26. Chowdhury, A. H., White, R. N. and Scott, N. R., "Small Scale Models for Reinforced Concrete Structures," ASAE Transactions, Vol. 20, No. 1, Nov. 1976.

27. Harris, H. G. and Mushivitch, J. C., "Study of joints and Sub-Assemblies - Validation of Small Scale Direct Modeling Techniques," Department of Civil Engineering, Drexel University, Oct. 1977.

28. Godden, W. G., "Model Analysis and Design of Prestressed Concrete Nuclear Reactor Structures," Nuclear Engineering and Design, North-Holland Publishing Company, Amsterdam, 1969.

29. Bader, M. A., "Shear and Moment Transfer in Thick-Walled Reinforced Concrete Cylinders," Ph.D. Dissertation, Stanford University, Stanford, California, Sept. 1980.

30. Becica, I. Y. and Harris, H. G., "Evaluation of Techniques in the Modeling of Masonry Structures," Department of Civil Engineering, Structural Model Laboratory, Report No. M77-1, Drexel University, Philadelphia, June 1977.

31. Little, W. A., Foster, D. C., Oakes, D., Falcone, P. A., Reiner, R. B., "Structural Behavior of Small-Scale Models," Steel Research for Construction, Bulletin No. 10, AISI, April 1968.

32. Ruge, A. C., "The Determination of Earthquake Stresses in Elastic Structures by Means of Models," Bulletin of Seismological Society of America, Vol. 24, 1934.

33. Ruge, A. C., "Earthquake Resistance of Elevated Water-Tanks," Transaction ASCE, Vol. 103, 1938.

34. Jacobsen, L.S., "Vibration Research at Stanford University," Bulletin of the Seismological Society of America, Vol. 19, No. 1, March 1929.

35. Jacobsen, L. S., "Dynamics of Structural Models in U.S.A.," Proceedings, I Modelli Nella Tecnica, Academia Nazionale Dei Lincei, Rome, Italy, 1956.

36. Antebi, J., Smith, H. D., Sharma, S. D., Harris, H. G., "Evaluation of Techniques for Constructing Model Structural Elements," Research Report R-62-15, Department of Civil Engineering, Massachusetts Institute of Technology, May 1962.

37. Smith, H. D., Clark, R. P. and Mayor, R. P., "Evaluation of Model Techniques for the Investigation of Structural Response to Blast Loads," Report No. R63-16, Massachusetts Institute of Technology, Feb. 1963.

38. Harris, H.G., Pahl, P. J. and Sharma, S. D., "Dynamic Studies of Structures by Means of Models," Research Report R-63-23, Department of Civil Engineering, Massachusetts Institute of Technology, Sept. 1962.

39. Harris, H. G., Schwindt, P.C., Taher, I., Werner, S. D., "Techniques and Materials in the Modeling of Reinforced Concrete Structures Under Dynamic Loads," Research Report R63-24, Department of Civil Engineering, Massachusetts Institute of Technology, Dec.1963.

40. Murphy, G. and Young, D. F., "A Study of the Use of Models to Simulate Dynamically Loaded Underground Structures," TDR 62-2, Air Force Special Weapon Center, 1962.

41. Young, D. F. and Murphy, G., "Dynamic Similitude of Underground Structures," Proceedings, ASCE, Vol. 90, EM3, June 1964.

42. Dobbs, N. and Cohen, E., "Model Techniques and Response Tests of Reinforced Concrete Structures Subjected to Blast Loads," ACI, SP-24, Models for Concrete Structures, 1970.

43. Gran, J. K. and Bruce, J. R., "Scale Modeling Techniques for MX Vertical Shelter Structures," Project Report, SRI International, Menlo Park, California, June 1979.

44. Sozen, M. A., "Earthquake Simulation in the Laboratory," Preprints of the NSF Workshop on Earthquake Resistant Reinforced Concrete Building Construction, Berkeley, July 1977.

45. Otani, S. and Sozen, M. A., "Behavior of Multi-Story Reinforced Concrete Frames During Earthquakes," Civil Engineering Studies, Structural Research Series No. 392, University of Illinois, Urbana, Nov. 1972.

46. Otani, S. and Sozen, M. A., "Simulating Earthquake Tests of R/C Frames," Journal of the Structural Division, ASCE, Vol. 100, ST3, Proc. Paper 10435, Mar. 1974.

47. Sozen, M. A., Aristozabal, J. D. and Lybas, Y. M., "Multi-Story Walls Subjected to Simulated Earthquakes," Proceedings, 6th World Conference on Earthquake Engineering, New Delhi, India, Jan. 1977.

48. Aristozabal, J. D. and Sozen, M. A., "Behavior of Ten-Story Reinforced Concrete Walls Subjected to Earthquake Motions," Civil Engineering Studies, Structural Research Series No. 431, University of Illinois, Urbana, Oct. 1976.

49. Lybas, J. M., "Response of Reinforced Concrete Coupled-Wall Systems to Earthquakes," Ph.D. Thesis submitted to the Graduate College, University of Illinois, Urbana, June 1977.

50. Chowdhury, A. H., and White, R. N., "Multi-Story Reinforced Concrete Frames Under Simulated Seismic Loads", Vibration of Concrete Structures, ACI Special Publication SP-60, 1980.

51. Clough, R. W., Rea, D., Tang, D. and Watabe, M., "Earthquake Simulator Test for a Three Story Steel Frame Structure," Proceedings, 5th World Conference on Earthquake Engineering, Vol. I, Rome, Italy, June 1973.

52. Clough, R. W. and Tang, D. T., "Earthquake Simulator Study of a Steel Frame Structure, Vol. I: Experimental Results, EERC Report No. 75-6, Berkeley, California, 1975.

53. Clough, R. W. and Hidalgo, P., "Design of a Shaking Table Test for a Reinforced Concrete Frame Structure," Proceedings, 5th World Conference on Earthquake Engineering, Vol. I, Rome, Italy, June, 1973.

54. Hidalgo, P. and Clough, R. W., "Earthquake Simulator Study of a Reinforced Concrete Frame," EERC Report No. 74-13, Berkeley, California, 1974.

55. Clough, R. W. and Huckelbridge, A. A., "Preliminary Experimental Study of Seismic Uplift of a Steel Frame," EERC Report No. 77-22, Berkeley, California, 1977.

56. Clough, D. and Clough, R. W., "Earthquake Simulator Study of Cylindrical Liquid Storage Tanks," presented at the ASCE Annual Convention, San Francisco, October, 1977.

57. Williams, D. and Godden, W. G., "Experimental Model Studies on Seismic Response of High Curved Overcrossings," EERC Report No. 76-18, Berkeley, California, 1976.

58. Mills, R. S., Krawinkler, H. and Gere, J. M., "Model Tests on Earthquake Simulators-Development and Implementation of Experimental Procedures, Report No. 39, The John A. Blume Earthquake Engineering Center, Department of Civil Engineering, Stanford University, Stanford, California, June, 1979.

59. Colloquium on "Use of Models and Scaling in Shock and Vibration," ASME Winter Meeting, Philadelphia, Pennsylvania, Nov. 1963.

60. Proceedings of the Symposium on Aeroelastic and Dynamic Modeling Technology, U.S. Air Force RTD-TDR-63-4197, Part I, 1964.

61. Bannister, R. L. and Aneja, I. K., "Before-the-Fact Modeling Solves Turbomachinery-Foundation Problems," Power, August, 1980.

62. Lauretta, E., "Dynamic Behavior of Large Structures Studied by Means of Models," Prelim. Publication, 7th Congress, IABSE, Rio de Janeiro, August, 1964.

63. Castoldi, A., "New Techniques of Model Investigation of the Seismic Behavior of Large Structures," presented at the ASCE National Structural Engineering Meeting, San Francisco, April 1973.

64. Oberti, G. and Lauretta, E., "Structural Models for the Study of Dam Earthquake Resistance," Transactions, 9th International Congress on Large Dams, Vol. 4, 1967.

65. Oberti, G., "Development of Aseismic Design and Construction in Italy by Means of Research on Large Model Test," ISMES Publication No. 6, Bergamo, Italy, June 1957.

66. Oberti, G. and Lauretta, E., "Dynamic Tests on Models of Structures," ISMES Publication No. 19, Bergamo, Italy, June 1962.

67. Lauretta, E., "Dynamic Features of a Recent Italian Arch Dam," ISMES Publication No. 24, Bergamo, Italy, October 1964.

68. Lauretta, E., "Theoretical Considerations and Experimental Research on the Behavior of Tall Buildings During Earthquakes," ISMES Publication No. 28, Bergamo, Italy, January 1965.

69. Oberti, G., "Results and Interpretation of Measurements Made on Large Dams of All Types, Including Earthquake Observations," ISMES Publication No. 29, Bergamo, Italy, Jan. 1965.

70. Oberti, G. and Lauretta, E., "Structural Models for the Study of Dam Earthquake Resistance," ISMES Publication No. 33, Bergamo, Italy, Aug. 1967.

71. Lauretta, E. and Castoldi, A., "Dynamic Tests on Models of PEC Nuclear Reactor Containment Building," ISMES Report, Bergamo, Italy, 1968.

72. Castoldi, A., "New Techniques of Model Investigation of the Seismic Behavior of Large Structures," ISMES Publication No. 56, Bergamo, Italy, April 1973.

73. Castoldi, A. and Casirati, M., "Experimental Techniques for the Dynamic Analysis of Complex Structures," ISMES Publication No. 74, Bergamo, Italy, 1976.

74. Bastellani, A., Castoldi, A. and Ionita, M., "Numerical Analysis Compared to Model Analysis for a Dam Subjected to Earthquakes," ISMES Publication No. 83, Bergamo, Italy, Sept. 1976.

75. Baglietto, E., Casirati, M., Castoldi, A., Miranda, F. and Sammartino, R., "Mathematical and Structural Models of Zarate-Brazo Largo Bridges," ISMES Publication No. 85, Bergamo, Italy, Sept. 1976.

76. Borges, F. J. and Pereira, J., "Dynamic Model Studies for Designing Concrete Structures," ACI, SP-24, Models for Concrete Structures, 1970.

77. Borges, J. F., "Dynamic Structural Studies on Models," Final Report, IABSE 7th Congress, 1964.

78. Borges, F. J. and Ravara, A., "Structural Behavior of Panel Structures under Earthquake Actions," Proceedings, RILEM Symposium of the Effects of Repeated Loading of Materials and Structures, Mexico, 1966.

79. Bostjancic, J., "Model Materials Suitable for Dynamic Tests of Models in the Plastic Range," Preprints, Vol. No. 9, 6th World Conference on Earthquake Engineering, New Dehli, India, Jan. 1977.

80. Mihai, C., et al., "On the Static and Seismic Behavior of a Structural Model of an Industrial Storied Hall," Preprints, Vol. 9, 6th World Conference on Earthquake Engineering, New Dehli, India, Jan. 1977.

81. Barkov, Y. V. and Glina, Y. V., "Theoretical and Experimental Investigations of Precast and Monolithic Frameless Buildings on Large-Scale Reinforced Concrete Models," Proceedings, 5th World Conference on Earthquake Engineering, Rome, Italy, June 1973.

82. Shaishmelashvili, V. N. and Edisherashvili, N. A., "Experimental Studies of Dynamic Characteristics of Multy-Story Steel Frame Buildings Large-Scale Models with Difference Vertical Bracings," Preprints, 5th World Conference on Earthquake Engineering, Rome, Italy, June 1973.

83. Irwin, A. W., "Static and Dynamic Tests on a Model Shear Wall Structure," The Institution of Civil Engineers, Proceedings, 51, Paper No. 7486, April 1972.

84. Berriaud, C. and Tigeot, Y., "Paraseismic Testing of Model Structures," Closed Loop, 3, 6, 1973.

85. Okada, H., Takeda, T., Yoshiaka, K., Omote, Y. and Nakagawa, K., "Experiment and Research on the Response of Steel Model Structures Subjected to Impact Horizontal Loading and to Simulated Earthquakes, Proceedings, 5th World Conference on Earthquake Engineering, Rome, Italy, June 1973.

86. Kato, B. et. al., "Dynamic Collapse Tests of Steel Structural Models," Preprints, 5th World Conference on Earthquake Engineering, Rome, Italy, 1973.

87. Suzuki, T. et al., "Experimental Study on PCRV-Support Sructures Under Simulated Earthquake Motion," Preprints, 2nd International Conference on Structural Mechanics in Reactor Technology, Vol. 4.

88. Takeda, T. and Yamaguchi, T., "Dynamic Model Test and Analysis for Prestressed Concrete Containment Vessel," Report of the Technical Research Institute, Ohbayashi-Gumi, Ltd., 6, Ohbayashi-Gumi, Ltd., Tokyo, 1972.

89. Bridgman, P. W., Dimensional Analysis, Yale University Press, 1920, 2nd Edition, 1931.

90. Murphy, G., Similitude in Engineering, Ronald Press, New York, 1950.

91. Langhaar, H. L., Dimensional Analysis and Theory of Models, Wiley, New York, 1951.

92. Huntley, H. E., Dimensional Analysis, McDonald, London, Dover, New York, 1967.

93. Sedov, L. I., Similarity and Dimensional Methods in Mechanics, Translation of 4th Russian Edition of 1956, Academic Press, New York, 1959.

94. Birkhoff, G., Hydrodynamics: A Study in Logic, Fact and Similitude, Princeton University Press, 1950, 1960.

95. Ipsen, D. C., Units, Dimensions and Dimensionless Numbers, McGraw-Hill, New York, 1960.

96. Hudson, D. E., "Scale-Model Principles," Chapter 27, Shock and Vibration Handbook, McGraw-Hill, 1967.

97. Pankhurst, R. C., Dimensional Analysis and Scale Factors, Reinhold, New York, 1964.

98. Skoglund, V. Y., Similitude, Theory and Applications, International Textbook Company, 1967.

99. Buckingham, E., "On Physically Similar Systems," Phys. Review 4, 1914.

100. Rayleigh, Lord, "The Principles of Similitude," Nature 95, 1915, Preprint in Scientific Papers 6, Dover, New York, 1964.

101. Ashley, H., "General Considerations on Scaling," National Academy of Engineering Workshop on Simulation of Earthquake Effects on Structures, Proceedings, San Francisco, Ca., Sept. 1973,

102. Goodier, J. N. and Thomson, W. T., "Application of Similarity Principles to Structural Models," NACA, Technical Note No. 933, July 1944.

103. Rocha, M., "Dimensionnement Experimental des Constructions," Annales de 1'I.T.B.P., 1952.

104. Borges, J. F., "Statistical Theories of Structural Similitude," RILEM international Colloquium on Models of Structures, Madrid, June 1959.

105. Beaujoint, N., "Similitude and Theory of Models," Bulletin RILEM No. 7, June 1960.

106. Fumagalli, E., "Materials for Scale Models and Devices of Loading," Bulletin RILEM No. 8, Sept. 1960.

107. Roll, F., "Materials for Structural Models," Proceedings, ASCE, Vol 94, ST 6, June 1968.

108. Mirza, M. S., White, R. N., Roll, F. and Batchelor, B. de V., "Materials for Dircet and Indirect Structural Models," State-of-the-Art Report on Structural Concrete Models, edited by M.S. Mirza, Department of Civil Engineering, McGill University, Montreal, October 1972.

109. Mirza, M.S., White, R. N., and Roll, F., "Materials for Structural Models," Proceedings, ACI Symposium on Models of Concrete Structures, Dallas, March 1972.

110. Carpenter, J. E., Roll, F., and Zelman, M. I., "Techniques and Materials for Structural Models," Models for Concrete Structures, Special Publication No. 24, ACI, 1970.

111. Zelman, M. I., Heidebrecht, A. C., Tso, W. K. and Johnston, W. A., "Practical Problems and Costs of Fabricating Multi-Story Models," Models for Concrete Structures, Special Publication No. 24, ACI, 1970.

112. Chowdhury, A. H. and White, R. N., "Materials and Modeling Techniques for Reinforced Concrete Frames," ACI Journal, Vol. 79, No. 11, Nov. 1977.

113. Ferrito, J. M., "An Evaluation of the Accuracy of Material Model Representation of Reinforced Concrete," 1979 SESA Spring Meeting, Paper No. A-4, San Francisco, California, May 1973.

114. Fuss, D. S., "Mix Design for Small-Scale Models of Concrete Structures," Technical Report R564, Naval Civil Engineering Laboratory, Port Hueneme, California, Feb. 1968.

115. Johnson, R. P., "Strength Tests on Scaled-Down Concretes Suitable for Models, With a Note on Mix Design," Magazine of Concrete Research, Vol. 14, No. 40, March 1962.

116. Tsui, S. H. and Mirza, M. S., "Model Microconcrete Mixes," Structural Concrete Series, No. 23, McGill Univeristy, Montreal, November 1969.

117. Burgrabe, A. H., "Mikrobeton fuer Modellstatische Untersuchungen," Berichte des Institutes fuer Modellstatik der Universitaet Stuttgart, Heft Nr. 1, 1972.

118. Maisel, E., "Mikrobeton fuer modelstatische Untersuchungen II," Berichte des institutes fuer Modellstatik der Universitaet Stuttgart, 1979.

119. Steffens, K., "Entwicklung eines Kunstharzmoertels zur Nachbildung des Werkstoffes Beton bei Modellversuchen fuer Stahlbeton-tragwerke," Lehrstuhl fuer Massivbau, TU Hannover.

120. Sabnis, G. M. and White, R. N., "A Gypsum Mortar for Small-Scale Models," ACI Journal, Vol. 64, No. 11, Nove. 1976.

121. White, R. N. and Sabnis, G. M., "Size Effects in Gypsum Mortars," Journal of Materials, V. 3, No. 1, March 1968.

122. Ferrito, J., "Dynamic Tests of Model Concrete." Technical Report R-650, Naval Civil Engineering Laboratory, Port Hueneme, California, Nov. 1969.

123. Sabnis, G. M., Mirza, S. M., "Size Effects in Model Concretes?," ASCE Journal of the Structural Division, June 1979.

124. Litle, W. A. and Paparoni, M., "Size Effects in Small-Scale Models of Reinforced Concrete Beams," ACI Journal, Vol. 63, No. 11, Nov. 1966.

125. Wang, P. T., Shah, S. P. and Norman, A. E., "Stress-Strain Curves of Normal and Lightweight Concrete in Compression," ACI Journal, Proceedings, Vol. 75, No. 11, Title No. 75-62, Nov. 1978, pp. 603-611.

126. Brock, G., "Concrete: Complete Stress-Strain Curves," Engineering (London), Vol. 133, No. 5011, May 1962, p. 602.

127. Barnard, P. R., "Researches into the Complete Stress-Strain Curve for Concrete," Magazine of Concrete Research (London), Vol. 16, No. 49, Dec. 1969, pp. 203-210.

128. Turner, P. W. and P. R. Barnard, "Stiff Constant Strain Rate Testing Machine," The Engineer (London), Vol. 214, No. 5557, July 1962, pp. 146-148.

129. Sangha, C. M. and Dhir, R. K., "Strength and Complete Stress-Strain" Relationships for Concrete Tested in Uniaxial Compression Under Different Test Conditions," Materials and Structures/Research and Testing (Paris), Vol. 5, No. 30, Nov.-Dec. 1972, pp. 361-370.

130. Popovics, S. and Sandor, "A Review of Stress-Strain Relationship for Concrete," ACI Journal, Proceedings, Vol. 67, No. 3, Mar. 1970, pp. 243-248.

131. Kaar, P. H., Hanson, N. W. and Capell, H. T., "Stress-Strain Characteristic of High Strength Concrete," Douglas McHenry International Symposium on Concrete and Concrete Structures, Sp-55, ACI, Detroit, 1978, pp. 161-185.

132. Sinha, B. P., Gerstle, K. H. and Tulin, L. G., "Stress-Strain Relations for Concrete Under Cyclic Loading," ACI Journal, Vol. 61, No. 2, Feb. 1964.

133. Ramsley, D. and McHenry, D., "Stress-Strain Curves for Concrete Strained Beyond the Ultimate Load," Laboratory Report No. SP-12, U.S. Interior Department, Bureau of Reclamation, Denver, March 1947.

134. Hughes, B. P. and Chapman, G. P., "The complete Stress-Strain Curve for Concrete in Direct Tension," Bulletin RILEM, No. 30, March 1966.

135. Rusch, H., "Physikalische Fragen der Betonpruefung," Zement - Kalk - Gips, Vol. 12, No. 1, 1959.

136. Rusch, H., "Research Toward a General Flexural Theory for Structural Concrete," ACI Journal, Proceedings, Vol. 32, No. 1, July 1972.

137. Raphael, J. M., "Big Tujunga Dam Strength and Elasticity of Concrete in Dam," Structural Research Laboratory, University of California, Berkeley, June 1975.

138. Raphael, J. M., "The Nature of Mass Concrete in Dams," Douglas McHenry International Symposium on Concrete and Concrete Structures, ACI Publication SP-55, Detroit, 1978.

139. "Recomended Practice for Evaluation of Compression Test Results of Concrete," ACI Committee 214, ACI, Detroit, 1965.

140. Mirza, S. A., Hatzinikolas, M. and MacGreor, J. G., "Statistical Description of Strength of Concrete," Journal of the Structural Division ASCE, June 1979.

141. Jones, P. G. and Richart, F. E., "The Effect of Testing Speed on Strength and Elastical Properties of Concrete," Proceedings ASTM, Vol. 36, Part II, 1936, pp. 380-391.

142. Hatano, T. and Tsutsumi, H., "Dynamic Compression and Failure of Concrete Under Earthquake Load," Technical Report C-5904, Technical Laboratory of the Central Research Institute of the Electric Power Industry, Tokyo, Sept. 1959.

143. Orchard, D. F., "Concrete Technology," Vol. 1, 3rd Ed., Applied Science Publishers Ltd., June 1979.

144. Abrams, D. A., "Design of Concrete Mixtures," Structural Materials Research Laboratory, Lewis Institute, Bulletin No. 1, Chicago, 1918.

145. Harris, H. G., Sabnis, G. M. and White, R. N., "Reinforcement for Small Scale Direct Models of Concrete Structures," Models for Concrete Structures, Special Publication No. 24, ACI, 1970.

146. Staffier, S. R. and Sozen, M. A., "Effect of Strain Rate on Yield Stress of Model Reinforcement," University of Illinois, Civil Engineering Studies, Structural Research Series No. 415, Urbana, February 1975.

147. Borges, J. F. and Arga e Lima, J., "Crack and Deformation Similitude in Reinforced Concrete," Proceedings, RILEM Symposium on Models of Structures, (Madrid, 1959), First Session RILEM Bulletin, No. 7, Paris, June 1960.

148. Mahin, S. Bertero, V. V., Rea, D. and Ataley, M., "Rate of Loading Effects on Uncracked and Repaired Reinforced Concrete Members," EERC Report No. 72-9, Berkeley, California, 1972.

149. Sabnis, G. M. and White, R. N., "Small Scale Models of Concrete Structures Subjected to Dynamic Loads," Preprints, 6th World Conference on Earthquake Engineering, Vol. 9, New Delhi, India, Jan. 1977.

150. Mayerjak, R. J., "A Study of the Resistance of Model Frames to Dynamic Lateral Load," University of Illinois Publication No. 108, Aug. 1955.

151. Nagaraja Rao, N. R., Lohrmann, M. and Tall, L., "Effect of Strain Rate on the Yield Stress of Structural Steels," Journal of Materials, Vol. 1, No. 1, March 1966.

152. Manjoine, M. J., "Influence of Rate of Strain and Temperature on Yield Stresses of Mild Steel," Journal of Applied Mechanics, Dec. 1944.

153. Garner, R. R., "Behavior of Yield and Ultimate Strength of Steel Under Dynamic Loading," Journal of Materials, JMLSA, Vol. 5, No. 3, Sept. 1970, pp. 618-632.

154. Richards, C. W., "Size Effect in the Tension Test of Mild Steel," Proceedings, ASTM, 1954.

155. Richards, C. W., "Effect of Size on the Yielding of Mild Steel Beams," Proceedings, ASTM, 1958.

156. Zohrei, M., "Cyclic Stress-Strain Behavior of A36 Steel," Engineering Thesis, Civil Engineering Department, Stanford University, Stanford, California, Dec. 1978.

157. Hayden, H. W., Moffatt, W. G. and Wulff, J., The Structure and Properties of Materials, Vol. III, "Mechanical Behavior," John Willey & Sons, Inc. New York, London, Sydney, 1965.

158. Dove, R. C. and Adams, P. H., Experimental Stress Analysis and Motion Measurement, Charles E. Merrill Publishing Co., Columbus, Ohio, 1964.

159. Sabnis, G. M., "Instrumentation in Structural Models," State-=-of-the-Art Report on Structural Concrete Models, edited by M. S. Mirza, Department of Civil Engineering, McGill University, Montreal, Oct. 1972.

160. Mills, R. S. and Krawinkler, H., "The Use of Minicomputers for Control and Data Handling in Dynamic Tests," Proceedings, International Instrument Society of America, Anaheim, California, May 1979.

161. Selander, C. E. and Carpenter, L. R., "Application of the Minicomputer in Measurement, Analysis and Control of Structural Testing by BUREC," Preprint No. 2950, ASCE Convention, San Francisco, Oct. 1977.

162. Ives, K. D., "Considerations for Instrumentation of Typical Dynamic Tests," Experimental Mechanics, 13, May 1973.

163. "Earthquake Environment Simulation," Final Report and Proceedings of a Workshop on Simulation of Earthquake Effects on Structures, in San Francisco, Sept. 1973, published by National Academy of Engineering, 1974.

164. Penzien, J. Bouwkamp, J. G., Clough, R. W. and Rea, D., "Feasibility Study of Large-Scale Earthquake Facility," EERC Report No. 67-1, Berkeley, California, 1967.

165. Stephen, R. M., Bouwkamp, J. G., Clough, R. W. and Penzien, J., "Structural Dynamics Testing Facilities at the University of California, Berkeley," EERC Report No. 69-8, Berkeley, California, 1969.

166. Rea, D. and Penzien, J., "Dynamic Response of a 20 x 20-ft Shaking Table," Paper No. 180, Proceedings, 5th World Conference on Earthquake Engineering, Rome, Italy, June 1973.

167. Takahashi, Y., Rea, D. and Abedi-Hayati, S., "Effects of Test Specimen Reaction Loads of Shaking Tables," Preprints, 5th World Conference on Earthquake Engineering, Rome, Italy, June 1973.

168. Lauretta, E. and Castoldi, A., "Earthquake Simulation by a Shake Table," 4th World Conference on Earthquake Engineering, Santiago, Chile, 1969.

169. Tsutsumi, H., "Vibration Research in CRIEPI by Means of Shaking Table, Some Recent Earthquake Engineering Research and Practice in Japan, Japanese National Committee, International Assn. for Earthquake Engineering, Tokyo, May 1973.

170. Lazan, B. J., "Energy Dissipation in Structures, with Particular Reference to Material Dumping," Colloquium on Structural Damping, ASME, Atlantic City, N.Y., Dec. 1959.

171. Sherby, O. D., "Anelastic Properties of Solids," Department of Material Science, Stanford University, California, 1973.

172. Manual on Low Cycle Fatigue Testing, ASTM STP 465, ASTM, 1969.

173. Richards, C. W., Engineering Material Science, Brooks/Cole, Belmont, California, 1961.

174. Jacobsen, L. S., "Damping in Composite Structures," Proceedings, 2nd World Conference on Earthquake Engineering, Tokyo, Japan, 1960.

175. Internal Friction, Damping, and Cyclic Plasticity,""Internal Friction, Damping, and Cyclic Plasticity," ASTM Symposium, Chicago, June 1964, Special Technical Publication No. 378, ASTM, 1964.

176. Kircher, C. A., "Ambient and Forced Vibration Analysis of Full Scale Structures," John A. Blume Earthquake Engineering Center Report No. 27, Stanford University, No. 1977.

177. ASM Metals Handbook, Vol. 1, ASM, 1973.

178. Alloy Digest, Engineering Alloys Digest, Inc., Upper Montclair, New Jersey.

179. "Standards Handbook, Wrought Copper and Copper Alloy Mill Products, Part 2--Alloy Data," Copper Development Association Inc., N.Y., 1973.

180. Crandall, S., ed., Random Vibrations, Massachusetts Institute of Technology Press, 1958.

181. Newland, D., An Introduction to Random Vibrations and Spectral Analysis, Longman, 1975.

182. Housner, G. and P. Jennings, "Generation of Artificial Earthquakes," Proceedings, ASCE, Engr. Mech. Div., Vol. 90, EM1, Feb. 1964.

183. Scanlan, R. and Sachs, K., "Earthquake Time Histories and Response Spectra," Proceedings, ASCE, Engr. Mech. Div., Vol. 100, EM4, Aug. 1974.

184. Tsai, N., "Spectrum--Compatible Motins for Design Purposes," Proceedings, ASCE, Engr. Mech. Div., Vol. 98, EM2, April 1972.

185. Tang. D. T., "Earthquake Simulator Study of a Steel Frame Structure," Vol. II: "Analytical Results," EERC Report No. 75-36, University of California, Berkeley, California, 1975.

186. Popov, E. P., Bertero, V. V. and Krawinkler, H., "Cyclic Behavior of Three R. C. Flexural Members with High Shear," Report No. EERC 72-5, Earthquake Engineering Research Center, College of Engineering, University of California, Berkeley, California, Oct. 1972.

187. 1978 Annual Book of ASTM Standards, Part 14, "Concrete and Mineral Aggregates".

188. Popovics, S., "A Numerical Approach to the Complete Stress-Strain Curve of Concrete", University of Arizona, Cement and Concrete Research, Vol. 3, 1973.

189. Pirotin, S. D. and East, G. H. Jr., "Large Deflections, Elastic--Plastic Response of Piping : Experiment, Analysis and Application", Transactions of the 4th International Conference on Structural Mechanics in Reactor Technology, vol. F, Paper F3/1, San Francisco, California, 1977.

190. Rolfe, S. T. and Barsom, J. M., Fracture and Fatigue Control in Structures, Prentice-Hall, Inc., Englewood Cliffs, New Jersey.

191. Almuti, A. M., "Post-Elastic Response of Mild Steel Beams to Static and Dynamic Loading", University of Michigan, Civil Engineering Department.

192. Niwa, A. and Clough, R. W., "Shaking Table Research on Concrete Dam Models", EERC Report No. 80-05, University of California, Berkeley, California, Sept. 1980.

193 Kinoshita, K. and Kushida H., "Experimental Study on Vibrational Characteristics of The Structures with Embeded Foundations", Proceedings, 5th World Conference on Earthquake Engineering, Rome, Italy, June 1973.

APPENDIX A

CONTROL OF MICROCONCRETE STRENGTH PROPERTIES

This appendix presents a summary of results of an experimental study on microconcretes whose strength properties were controlled through different mix ingredients, chemical additives, and through aggregate treatment resulting in smooth and moisture sealed aggregate. The study from which the results are reproduced was performed at the Institute for Model Mechanics at the University of Stuttgart, W. Germany (Ref. 118).

The summary is presented in Table A.2. The results are ordered with declining compressive stength f'_c for each specimen age. The compressive strength is obtained from tests on prismatic specimens and the tensile strength is obtained from flexural tests. The modulus of elasticity is based on initial specimen stiffness.

Each specimen series is characterized by code designations providing information on the specimen age, mix proportions, ingredients, and aggregate treatment. The key to the code is given in Table A.1, and the various aggregate sieve lines are shown in Fig. A.1.

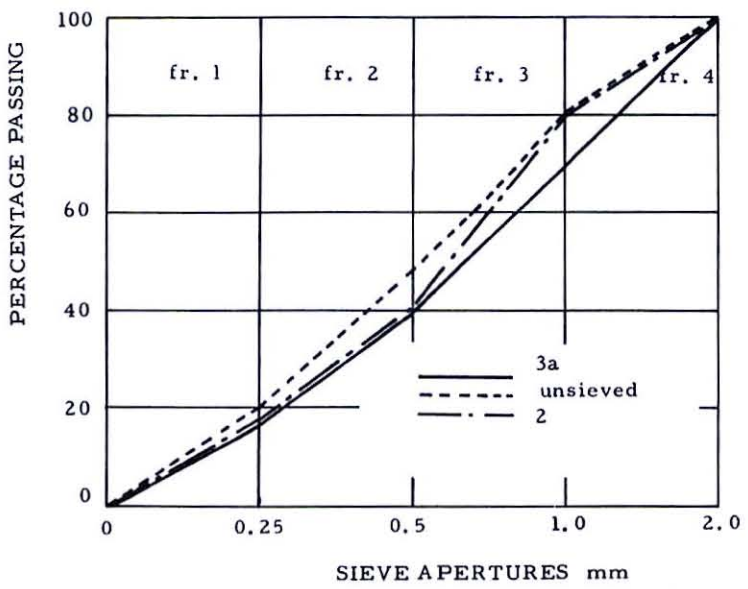

Figure A.1 Sieve Lines of Aggregates Used

Table A.1 Key to Specimen Designation Code Used in Table A.2

Note:
1) Aggregate/Cement Ratio is constant for all the specimens and equals A/C = 2
2) The largest aggregate size is 2 mm unless specified differently
3) Compression tests were performed on prismatic specimens of width to height ratio of 1:4
4) Tensile strength was obtained from bending tests
5) Aggregate sieve lines are given in Fig. A.1 and are identified in code designation C
6) The code key consists of code designations ABCDE

Code Designation A	Age of Tested Specimens (days)
1	7
2	14
3	21
4	28
5	42
6a	47
6b	68

Code Designation B	W/C Ratio
1	0.55
2	0.60
3	0.65
4	0.70
5	0.75
6a	0.50
6b	0.61
6c	0.67

Code Designation C	Aggregate Type
1	Sand
2	Light aggregate (inflated shist) not sieved
3	Light aggregate; sieve lines 2 and 3a
4	Light aggregate (fraction 1), sand (frs. 2,3,4)
5	Light aggregate (fr. 1), sand (frs. 2,3), river sand (fr. 4)
6a	No frs. 1 and 2, sand or mixture of light aggregate and sand (fr. 3), sand or light aggregate (fr. 4)
6b	Light aggregate (fr. 1), light aggregate or sand (fr. 2), sand (frs. 3,4)
6c	Light aggregate (frs. 1-4), sand (fr. 5; 2-3 mm)

Table A.1 Continuation

Code Designation C	Aggregate Type
6d	Sand (frs. 1,2), light aggregate (frs. 3,4)
6e	Light aggregate (fr.1), blast furnace clincker (frs. 2,3,4)
6f	Light aggregate (frs. 1,2), light aggregate or blast furnace clincker (fr. 3), blast furnace clincker (fr. 4)

Code Designation D	Aggregate Treatement
0	Non-treated
1	Coated with silicon resin solution+ 108.4 g/kg cement
6a	As 1 but with 216.8 g/kg cement
6b	As 1 but with 54.2 g/kg cement

Code Designation E	Cement type, additives
0	Portland cement, no additives
1	Hydro-cement, no additives
2	Hydro-cement with air entrainment :
2a	92 mm^3/kg cement
2b	110 mm^3/kg cement
2c	115 mm^3/kg cement
2d	130 mm^3/kg cement
2e	55 mm^3/kg cement
2f	30 mm^3/kg cement
	with a minimal amount of oil coating on aggregate fractions 2,3,4 :
2g	55 mm^3/kg cement
2h	80 mm^3/kg cement
3	Hydro-cement with retarder
4	Hydro-cement with workability improving additives
4a	50 mm^3 liguefier /kg cement
4b	70 mm^3 liquefier /kg cement
4c	90 mm^3 liquefier /kg cement
4d	110 mm^3 liquefier /kg cement
5	With oil coated aggregate

+ resin used for impregnation of concrete formework; in W. Germany known under the commercial name of Pluvoil

Table A.2

	Age at Test	f'_c		f'_t/f'_c	E x 10^3		No. of Specs.	Code Key
	days	MPa	ksi	--	MPa	ksi	--	--
1	14	53.8	7.80	0.128	41.0	5.95	9	21100
2		49.4	7.17	0.130	--	--	6	21303
3		49.4	7.17	0.174	--	--	2	26c200
4		46.9	6.80	0.120	23.7	3.44	6	3246b0
5		45.9	6.66	0.128	23.0 (12)	3.34	21	22200
6		45.0	6.53	0.137	19.5	2.83	12	22300
7		44.3	6.43	0.150	--	--	12	23303
8		41.7	6.05	0.142	20.3 (8)	2.94	24	23200
9		41.1	5.36	0.154	18.5 (12)	2.68	18	23300
10		39.7	5.76	0.125	24.8	3.60	3	236b00
11		38.3	5.64	0.160	17.6 (12)	2.55	45	24300
12		38.8	5.63	0.136	23.9	3.47	3	23100
13		38.5	5.58	0.148	23.5	3.41	3	236b00
14		37.7	5.47	0.163	20.3	2.94	3	236d00
15		35.0	5.08	0.201	27.3	3.96	6	26a410
16		34.4	4.33	0.153	18.1 (24)	2.62	59	24200
17		33.0	4.73	0.171	16.7	2.92	3	23304a
18		32.5	4.71	0.181	22.1	3.20	6	3246a0
19		31.7	4.60	0.177	22.1	3.20	6	23412b
20		30.5	4.42	0.127	26.3	3.81	12	23110
21		30.5	4.42	0.174	16.8	2.44	3	236b02e
22		30.5	4.42	0.206	15.8	2.29	3	23306c
23		30.4	4.44	0.146	21.4	3.10	6	25400
24		30.4	4.41	0.163	13.4	1.34	3	23304d
25		30.7	4.38	1.039	22.1	3.20	3	25100
26		23.5	4.28	0.166	14.0	2.03	3	23304b
27		27.1	3.33	0.146	17.0	2.47	3	236c05g
28		27.0	3.32	0.133	19.6	2.84	24	23410
29		26.7	3.87	0.129	18.5	2.68	3	236b10
30		26.6	3.86	0.163	13.7	1.99	12	23305b
31		24.4	3.54	0.157	21.2	3.07	48	25410
32		24.4	3.54	0.240	13.0	1.89	3	23304c
33		24.1	3.50	0.163	12.9	1.87	6	23310
34		23.9	3.47	0.168	22.8	3.31	6	25510
35		23.2	3.37	0.140	18.0	2.61	12	24410
37		22.7	3.29	0.167	17.8	2.58	3	236b05g
38		22.3	3.23	0.211	14.4	2.09	3	236b02f
39		22.1	3.20	0.209	16.3	2.36	3	236b02g
40		21.9	3.18	0.211	11.7	1.70	6	23302e
41		21.4	3.10	0.167	19.4	2.81	24	25517a
42		21.1	3.06	0.179	19.2	2.78	3	236b0b
43		20.8	3.02	0.177	19.6	2.84	6	25417a
44		20.6	2.99	0.223	11.9	1.73	3	23302a
45		20.5	2.97	0.157	12.9	1.87	3	23305a
46		19.9	2.89	0.209	13.7	1.99	3	236b02h
48		19.6	2.84	0.189	14.3	2.07	3	236b06b
50		19.4	2.81	0.185	14.6	2.12	3	236d05i

Table A.2 Continuation

	Age at Test	f'_c		f'_t/f'_c	E x 10^3		No. of Specs.	Code Key
	days	MPa	ksi	--	MPa	ksi	--	--
51		19.3	2.80	0.186	16.1	2.34	3	236b05i
52		19.2	2.79	0.183	17.6	2.55	3	236a06e
53		19.2	2.79	0.207	10.0	1.45	3	23302d
54		19.1	2.77	0.169	17.9	2.60	6	25517b
55		18.9	2.74	0.131	11.5	1.67	3	23302b
56		18.8	2.73	0.183	13.2	2.73	6	25417b
57		18.7	2.71	0.196	14.5	2.10	3	236f05i
59		18.0	2.61	0.191	16.2	2.35	3	236a05f
60		17.6	2.55	0.186	11.6	1.68	3	236e05i
61		17.4	2.52	0.200	18.3	2.65	6	25417c
62		17.1	2.48	0.230	13.9	1.44	3	23302c
63		16.4	2.38	0.195	11.9	1.73	3	236e05g
64		16.1	2.34	0.271	10.4	1.51	6	23306a
65		16.0	2.32	0.214	13.6	1.37	3	236a05d
66		15.3	2.22	0.204	13.5	1.96	3	236a02g
67		15.1	2.19	0.184	13.0	1.88	3	236b06a
68		14.5	2.10	0.227	13.3	1.93	3	236a06b
69		13.5	1.36	0.250	11.0	1.60	3	236b06a
70		12.5	1.81	0.230	12.2	1.77	3	236a060
71		12.4	1.80	0.215	12.3	1.78	6	23411
72		10.0	1.45	0.164	27.7 (1)	4.02	6	25110
73		5.8	0.84	0.307	7.5	1.09	6	32416d
1	21	42.6	6.18	0.157	16.5	2.39	6	33200
2		40.7	5.90	0.180	27.7	4.02	3	33100
3		40.5	5.87	0.191	19.5	2.83	6	36b200
4		38.7	5.61	0.177	29.8	3.60	6	33110
5		32.8	4.76	0.205	23.4	3.39	6	35400
6		32.1	4.66	0.216	23.7 (1)	3.44	3	35100
7		31.0	4.50	0.188	21.7	3.15	6	34410
8		28.5	4.13	0.208	20.8	3.02	6	35410
1	28	50.7	7.35	0.140	18.6	2.70	12	42300
2		43.0	6.24	0.170	17.3	2.51	3	43300
3		42.8	6.21	0.162	16.4	2.38	6	43200
4		41.6	6.03	0.180	25.8	3.74	6	43100
5		38.5	5.58	0.196	16.4	2.38	6	431101
6		34.7	5.03	0.176	22.4	3.25	3	45100
7		34.7	5.03	0.224	22.0	3.19	6	45400
8		33.5	4.86	0.225	21.1	3.06	3	44410
9		32.0	4.64	0.209	19.2	2.79	6	45410
10		27.5	3.99	0.239	18.6	2.70	6	436b05i
11		19.1	2.77	0.264	15.0	2.18	6	436a05e
12		18.5	2.68	0.257	--	--	6	436b06a
13		13.5	1.96	0.274	12.0	1.79	6	436a06a

APPENDIX B

HYSTERESIS LOOPS OF REINFORCED MICROCONCRETE BEAMS

This appendix presents load-displacement and moment-average curvature response curves of beams tested in the study of the cycling frequency effects (Section 8.2.6).

Table B.1 summarizes the results of this study in terms of relative peak load at each cycle for each of the specimens tested. The load value used for normalizing of the results was taken as the average peak load of the first excurssion of the beams tested at a frequency of 2 Hz. The normalizing values for the displacements and curvatures are the average of the peak values for all the beams at the first amplitude. The specimens are identified in the table and in the figures by a set of three digits, the first of which denotes the testing frequency (0.0025 Hz, 2 Hz and 10 Hz), the second denotes the specimen number at a frequency, and the third the beam number in the specimen.

Table B.1

Summary of Normalized Peak Response Values

for Beams Tested at Various Cycling Frequencies

TEST. FREQ.	SPEC. NO.	BEAM NO.	FIRST AMPLITUDE							SECOND AMPLITUDE						
			DISPL.	PEAK FORCES						DISPL.	PEAK FORCES					
				+P1	+P2	+P3	-P1	-P2	-P3		+P1	+P2	+P3	-P1	-P2	-P3
1	1.1	1.1.1	1.07	1.015	.976	.934	.942	.773	.730	2.12	.866	.781	0.000	.798	0.000	0.000
		1.1.2		.982	.857	.824	.915	.844	.811		.853	.774	0.000	.832	.661	0.000
	1.2	1.2.1	.98	1.000	.915	.862	.930	.886	.836	2.02	.889	.765	0.000	.805	0.000	0.000
		1.2.2		.933	.869	.834	.906	.830	.794		.879	.781	.705	.823	.763	.719
	MEAN VALUE			.983	.904	.863	.923	.833	.793		.872	.775	.705	.814	.712	.719
	ST. DEV.			.036	.054	.050	.016	.047	.045		.016	.008	0.000	.016	.072	0.000
2	2.1	2.1.1	.94	1.029	1.010	.959	.985	.934	.891	2.04	1.019	.917	.747	.917	.866	.764
		2.1.2		1.009	.959	.934	1.002	.934	.917		1.019	.908	.840	.917	.857	.756
	2.2	2.2.1	1.05	.985	.895	.869	.979	.908	.875	2.13	.976	.877	.816	.900	.850	.775
		2.2.2		.977	.896	.859	.971	.890	.853		.935	.865	.806	.904	.845	.763
	MEAN VALUE			1.000	.940	.905	.984	.916	.884		.987	.892	.802	.909	.855	.764
	ST. DEV.			.023	.055	.049	.013	.021	.027		.040	.025	.040	.009	.009	.008
3	3.1	3.1.1	1.00	1.005	.925	.885	.973	.893	.861	2.05	1.029	.909	.877	.901	.861	.829
		3.1.2		1.037	.951	.908	1.002	.917	.883		1.036	.908	.866	.917	.866	.832
	3.2	3.2.1	.98	1.024	.914	.887	1.002	.941	.915	2.01	1.040	1.010	.981	.983	.956	.903
		3.2.2		1.031	.969	.917	.977	.931	.884		1.018	.934	.915	.947	.889	.843
	MEAN VALUE			1.024	.940	.899	.989	.921	.886		1.031	.940	.910	.937	.893	.852
	ST. DEV.			.014	.025	.016	.015	.021	.022		.009	.048	.052	.036	.044	.034

Normalizing Values : P_N = 1.18 kN δ_N = 5.03 mm M_N = 359.5 kN:mm $\phi_N = 0.231 \times 10^{-3}$ rad/mm

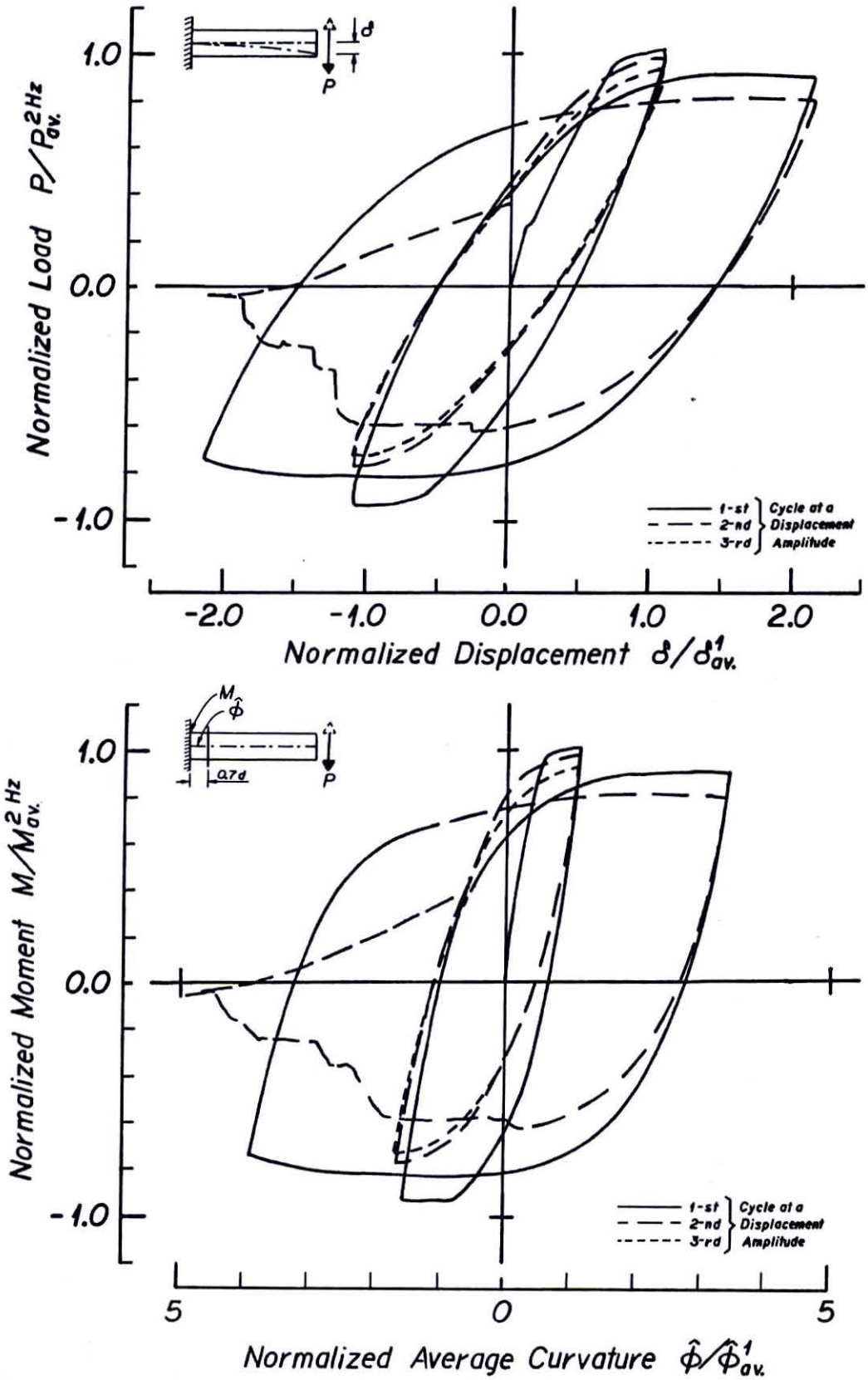

Figure B.1 Normalized Load-Displacement and Moment Curvature Response of Beam Tested under Frequency 0.0025 Hz (Specimen 1.1.1)

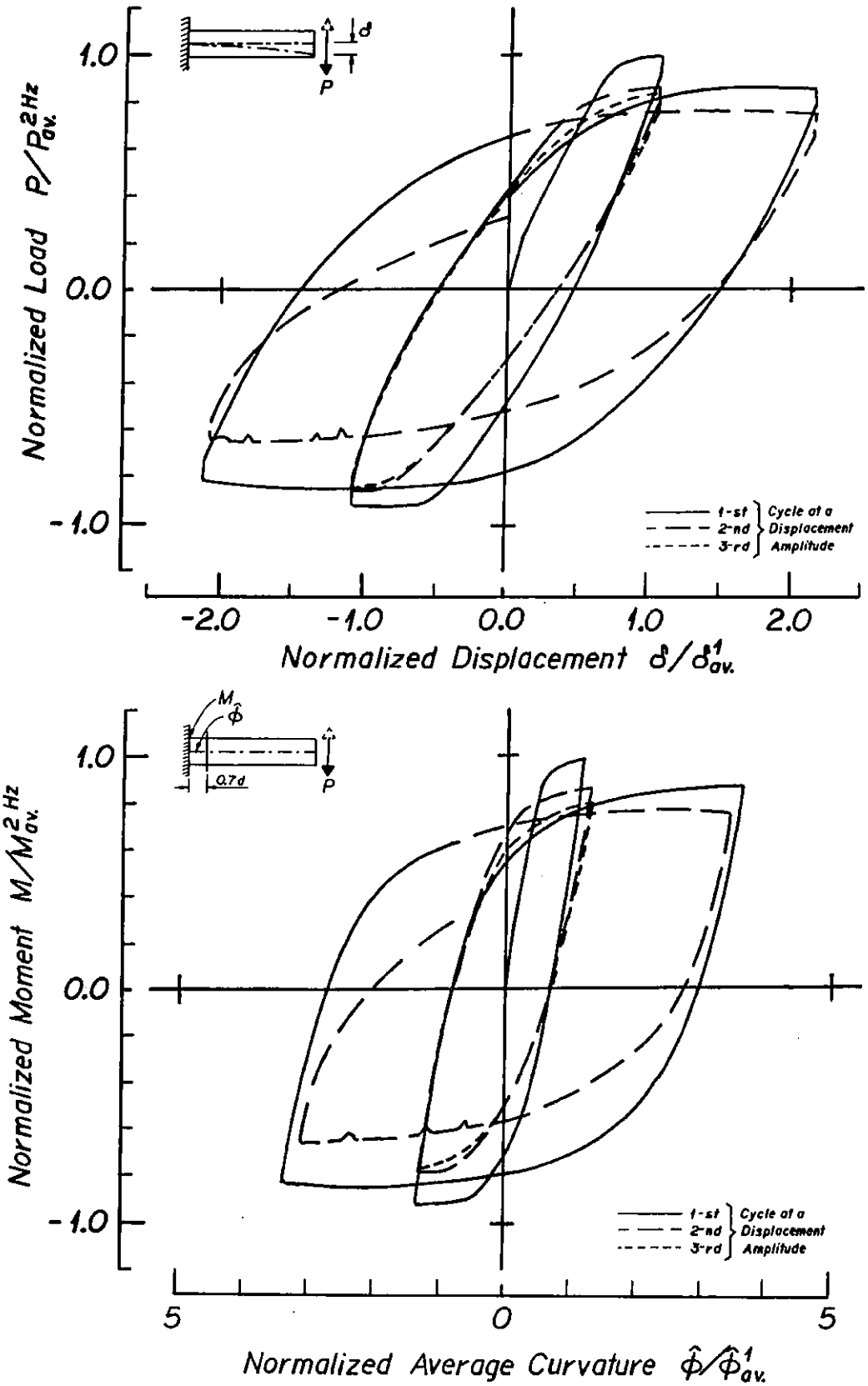

Figure B.2 Normalized Load-Displacement and Moment Curvature Response of Beam Tested under Frequency 0.0025 Hz (Specimen 1.1.2)

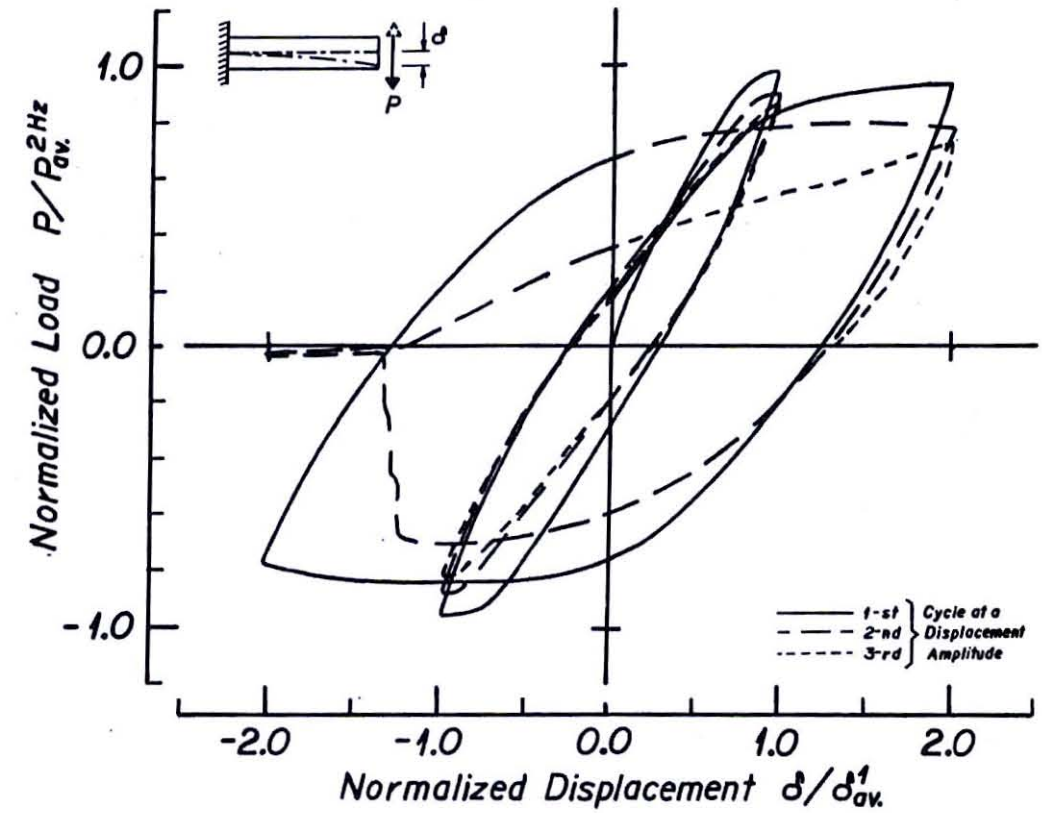

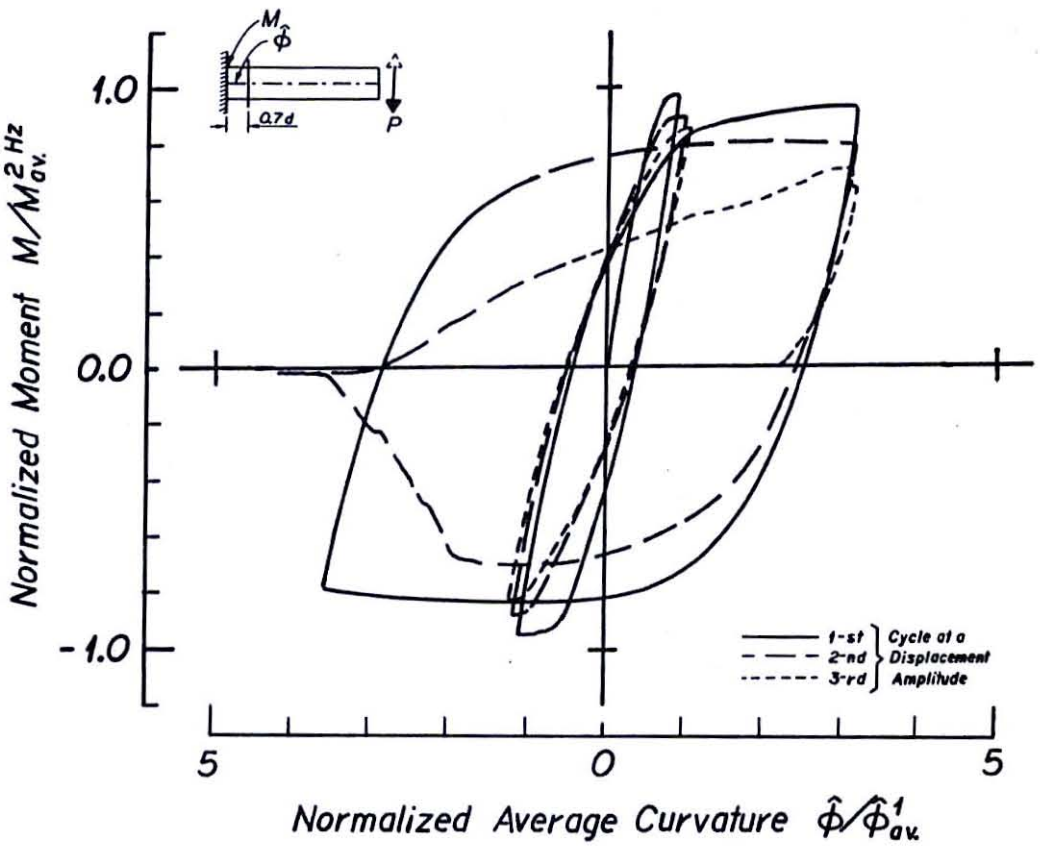

Figure B.3 Normalized Load-Displacement and Moment Curvature Response of Beam Tested under Frequency 0.0025 Hz (Specimen 1.2.1)

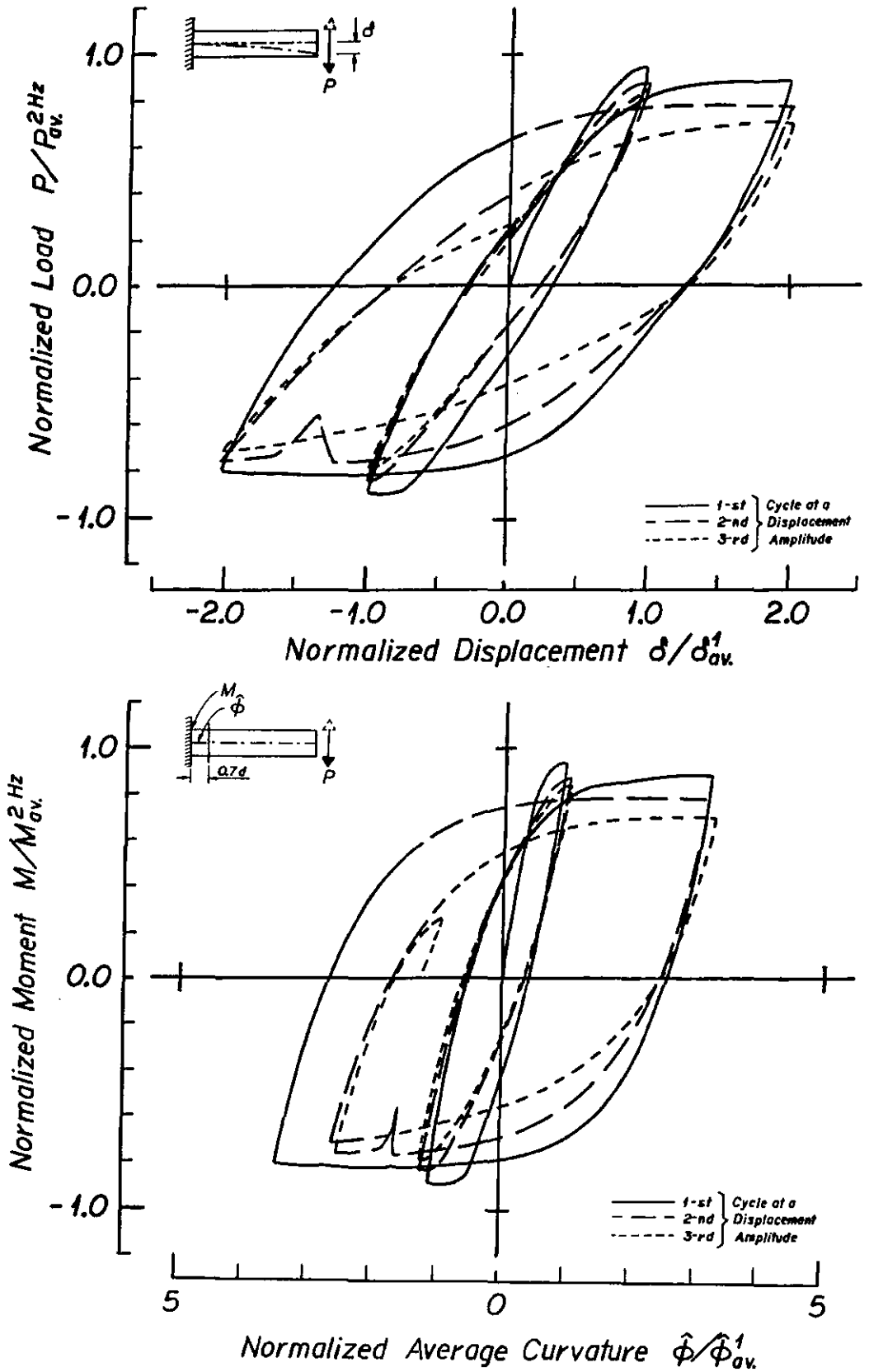

Figure B.4 Normalized Load-Displacement and Moment Curvature Response of Beam Tested under Frequency 0.0025 Hz (Specimen 1.2.2)

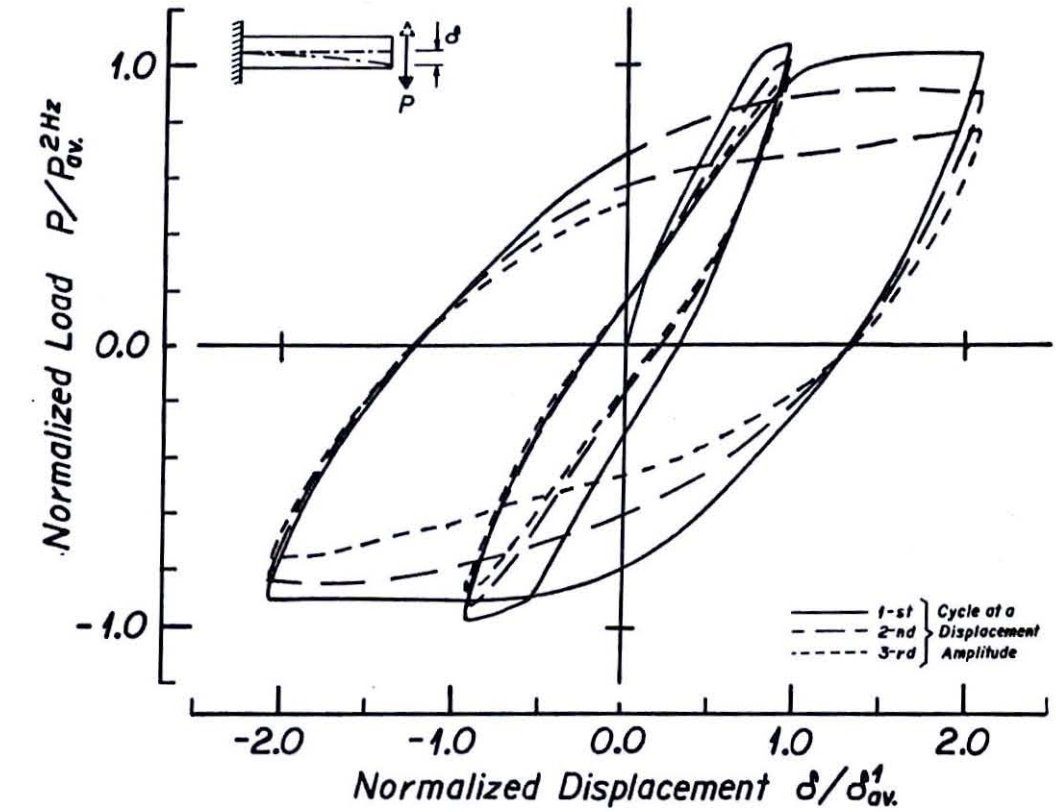

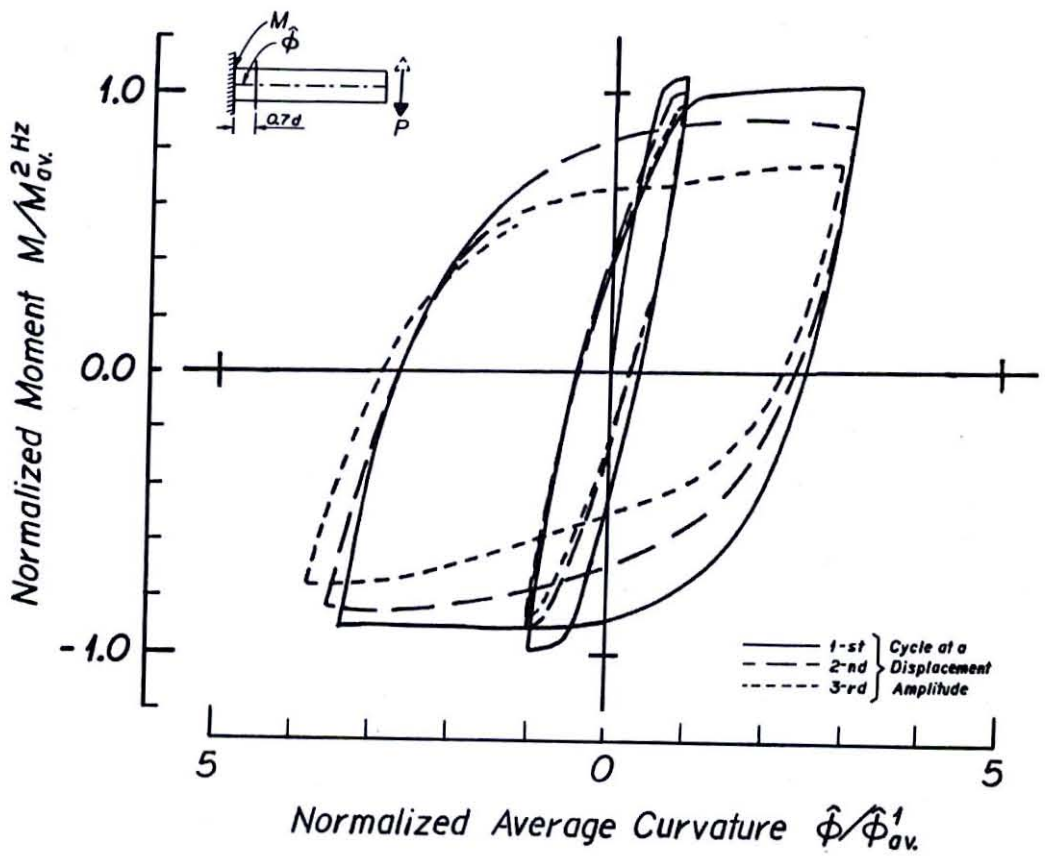

Figure B.5 Normalized Load-Displacement and Moment Curvature Response of Beam Tested under Frequency 2 HZ (Specimen 2.1.1)

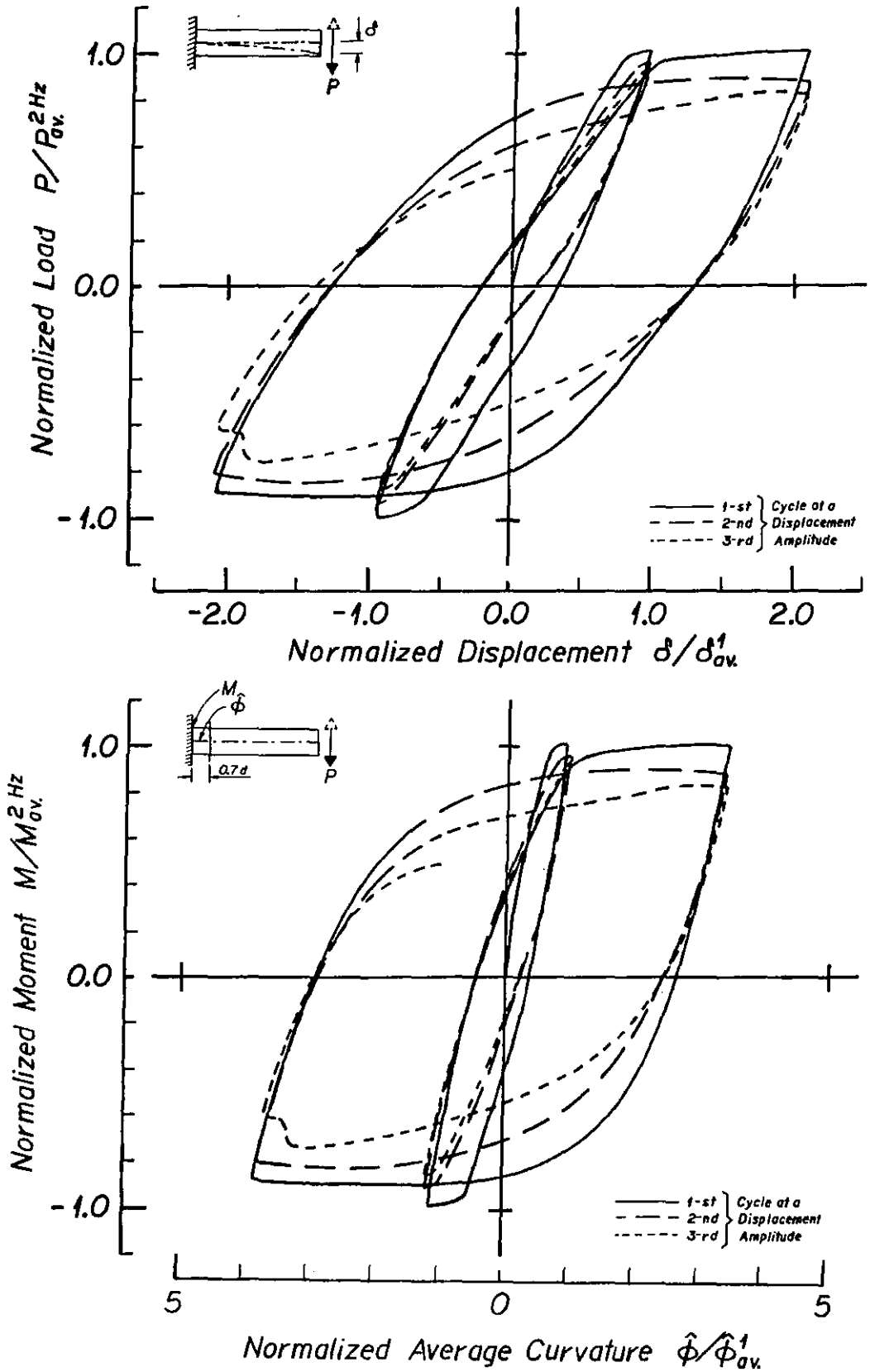

Figure B.6 Normalized Load-Displacement and Moment Curvature Response of Beam Tested under Frequency 2 Hz (Specimen 2.1.2)

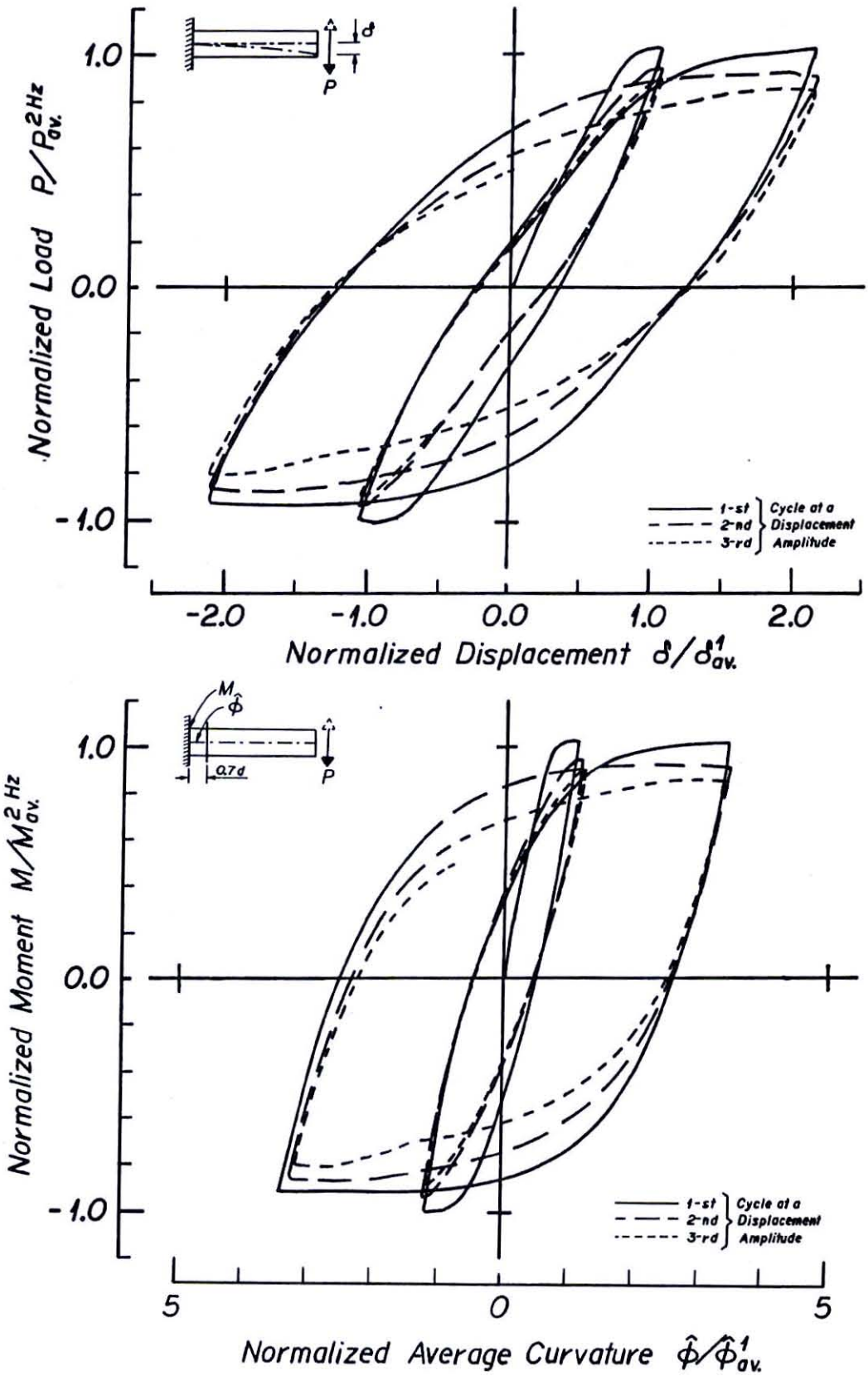

Figure B.7 Normalized Load-Displacement and Moment Curvature Response of Beam Tested under Frequency 2 Hz (Specimen 2.2.1)

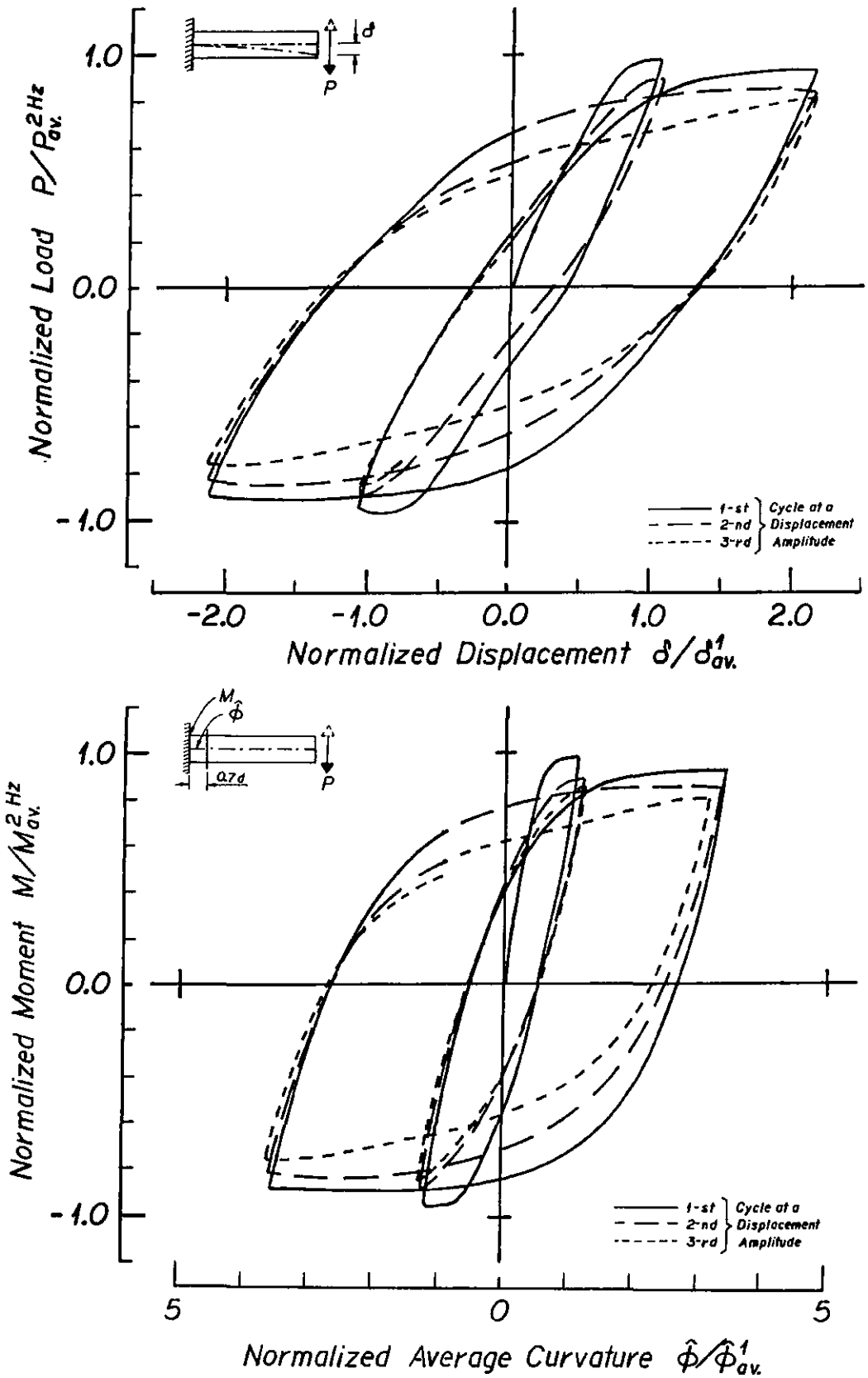

Figure B.8 Normalized Load-Displacement and Moment Curvature Response of Beam Tested under Freqdency 2 Hz (Specimen 2.2.2)

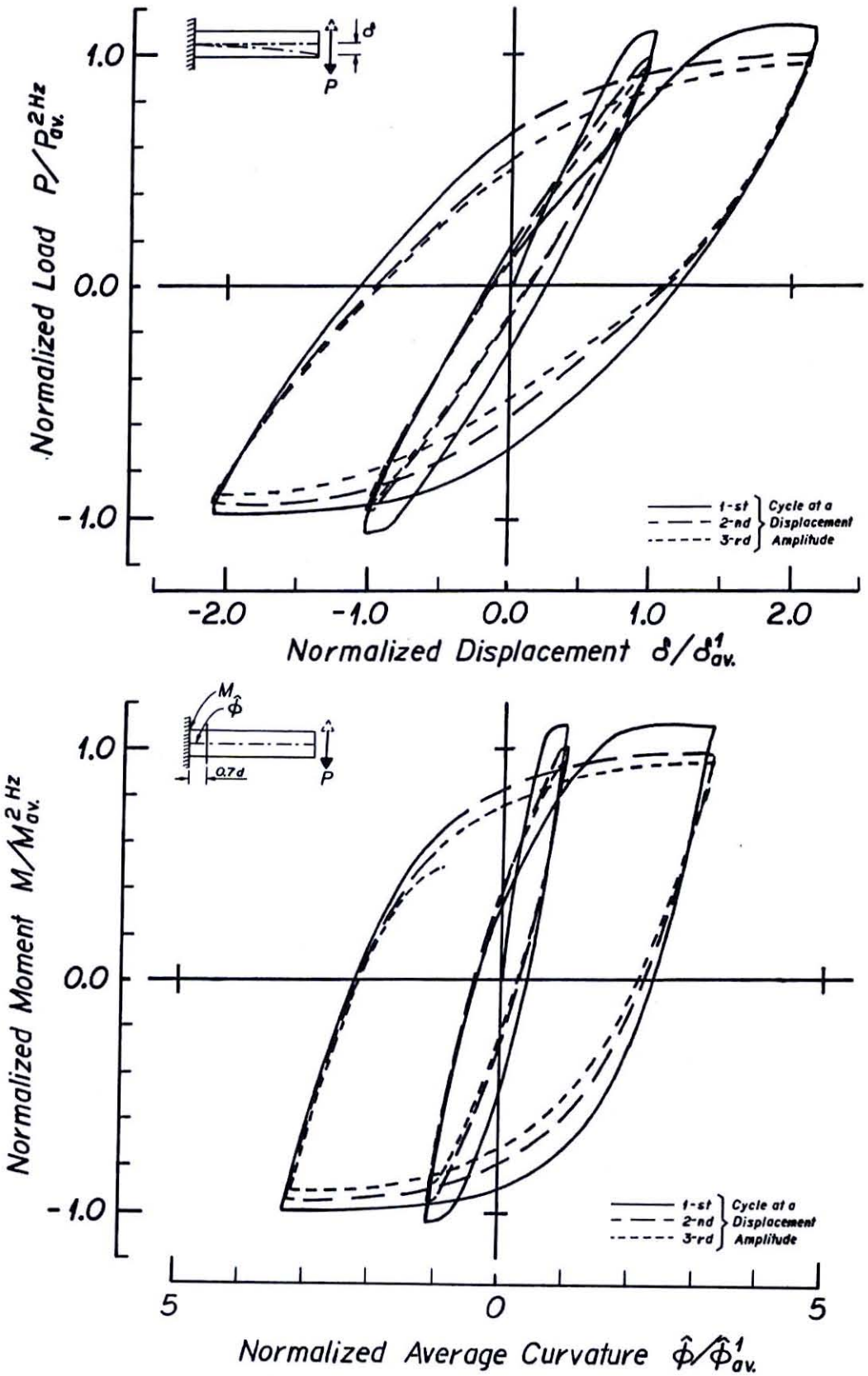

Figure B.9 Normalized Load-Displacement and Moment Curvature Response of Beam Tested under Frequency 10 Hz (Specimen 3.1.1)

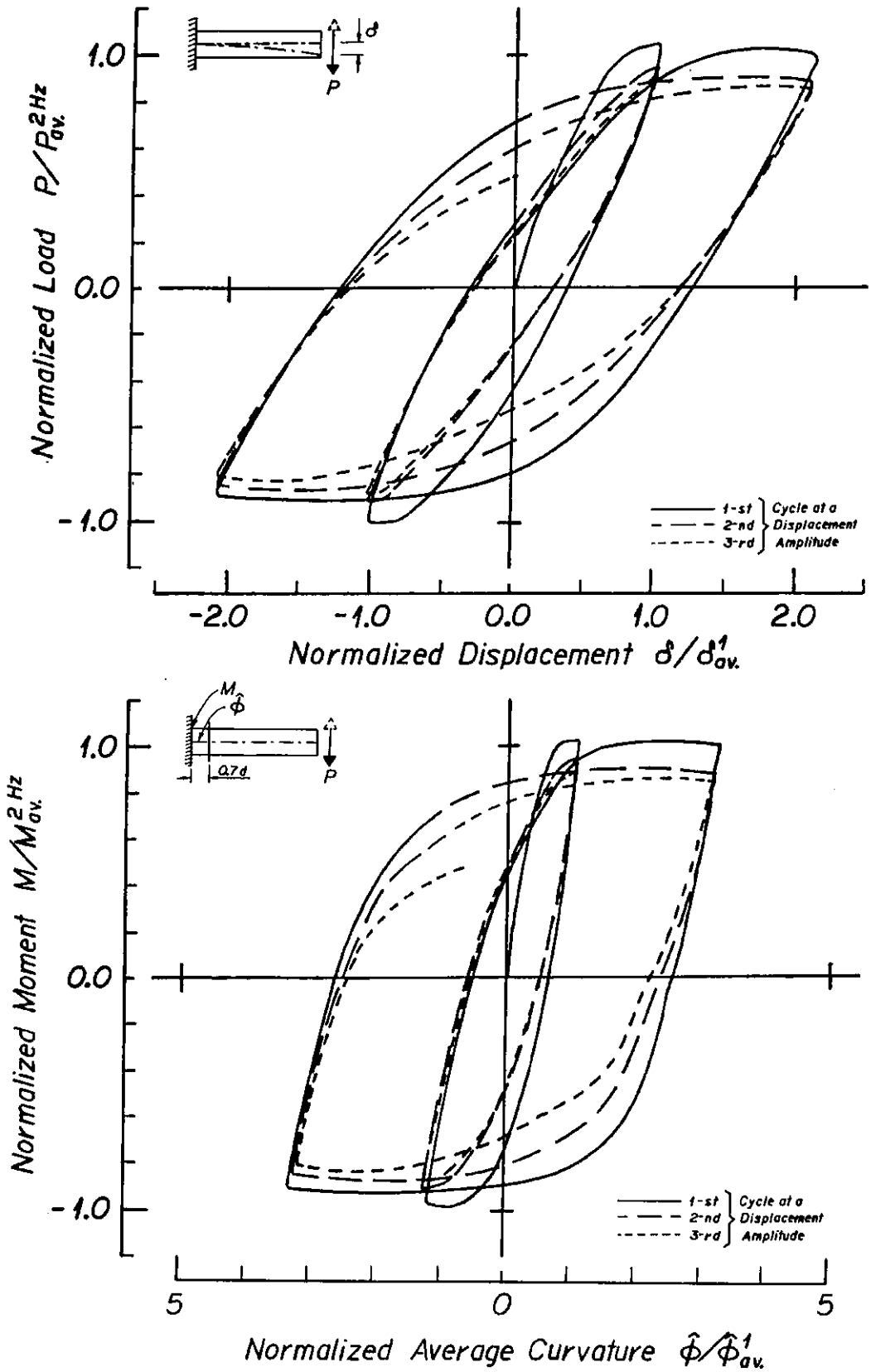

Figure B.10 Normalized Load-Displacement and Moment Curvature Response of Beam Tested under Frequency 10 Hz (Specimen 3.1.2)

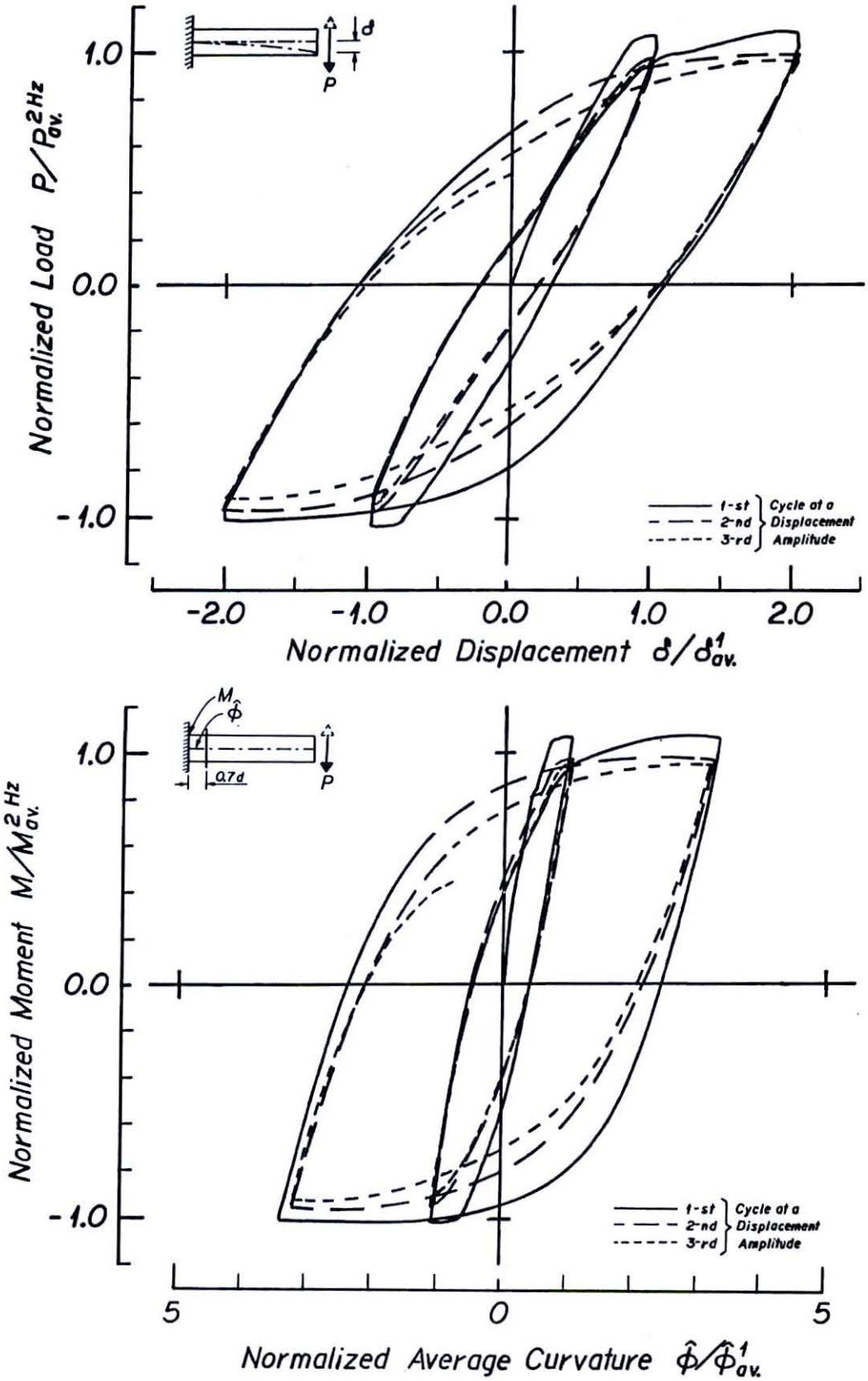

Figure B.11 Normalized Load-Displacement and Moment Curvature Response of Beam Tested under Frequency 10 Hz (Specimen 3.2.1)

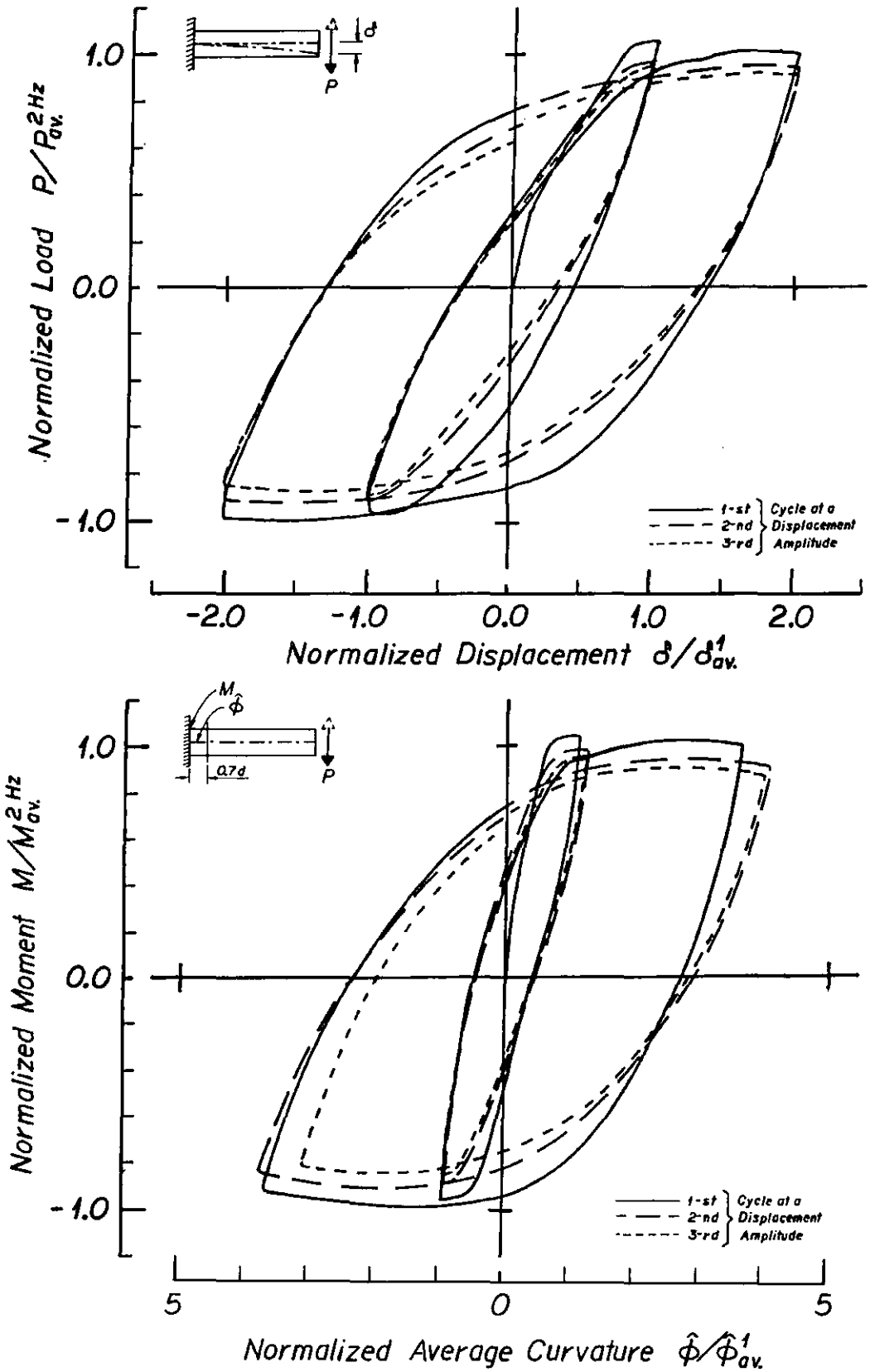

Figure B.12 Normalized Load-Displacement and Moment Curvature Response of Beam Tested under Frequency 10 Hz (Specimen 3.2.2)